

The effect of molecular bend on the
properties of bimesogenic materials

Craig Thomas Archbold

Doctor of Philosophy

University of York

Chemistry

September 2017

Abstract

A series of compounds were synthesised belonging to two families of unusually shaped liquid-crystals, a series of dimers, also called bimesogens, with varying molecular architecture, as well as a series of so-called “pseudo bent-core” materials, wherein the molecule is in possession of a mostly rigid core, with one possible site of flexibility in the central unit.

The properties of the pseudo bent core materials were found to be strongly dependent on the shape of the central unit, ranging from non-mesogenic for those materials with sterically bulky central cores, to nematic for cores with a group that promotes linearity, to lamellar and even the relatively uncommon dark conglomerate phase in materials that are more bent.

For the flexible bimesogens the behaviour was much more consistent, with all of the phase behaviour displayed being nematic in nature, with some exhibiting the hotly debated twist-bend nematic (N_{TB}) phase. It was found that the phase behaviour, particularly the occurrence of the N_{TB} phase was strongly dependent on both the terminal unit; conjugating polar groups gave more stable phases than non-conjugating, and the nature and length of the spacer. With methylene spacer providing a more stable N_{TB} phase, and the stability of the phase behaviour generally increasing with spacer length. Mixture studies indicated that the primary barrier to ether linked compounds forming the N_{TB} phase was their high melting point. Mixtures with a chiral dopant also provided some insight into the N_{TB} phase, and allowed for the observation of the first direct isotropic- N_{TB} transition.

This thesis is concluded with a discussion on the relationship between molecular bend and flexibility and the phase behaviour of these materials, relating the phase behaviour of both the bimesogens and the “pseudo bent-cores” to their ability to twist and reshape to effectively pack into certain mesophases.

Table of Contents

Abstract	2
Table of Contents	3
Acknowledgements	5
Declaration	6
Chapter 1: Introduction	7
1.1. Introduction to liquid crystals.....	8
1.2. Thermotropic liquid crystals.....	9
1.3. Calamitic phases formed by rod like molecules.....	10
1.4. Liquid crystals of unusual shape.....	13
1.4.1. Bent core liquid crystals.....	
1.4.2. Liquid crystal dimers.....	14
1.5. The nematic phase.....	16
1.6. The chiral nematic phase.....	17
1.7. The smectic A phase.....	18
1.8. The smectic C phase.....	20
1.9. Blue phases.....	22
1.10. Liquid crystal bimesogens.....	23
1.11. Terminal liquid crystal bimesogens.....	25
1.11.1. The nature of the flexible spacer.....	
1.11.2. The nature of the terminal group.....	28
1.11.3. Unsymmetrical bimesogens.....	29
1.12. The twist-bend nematic (N_{TB}) phase.....	31
1.12.1. Occurrence of the N_{TB} phase in liquid crystal bimesogens.....	32
1.13. The dark conglomerate phase.....	33
1.14. Phase identification techniques.....	34
1.14.1. Polarised optical microscopy.....	35
1.14.1.1. Textures and defects of the nematic phase.....	36
1.14.1.2. Textures and defects of the smectic A phase.....	39
1.14.2. Differential scanning calorimetry.....	41
1.14.3. X-ray diffraction.....	43
Chapter 2: Aims	48
2. Aims.....	49
2.1. Synthetic targets.....	
2.1.1. Pseudo bent-core materials.....	
2.1.2. Target bimesogens.....	50
Chapter 3: Synthetic Methods	53
3.1 Synthetic and analytical methods.....	54
3.1.1 Reagents.....	
3.1.2. TLC and column chromatography.....	
3.1.3. Nuclear magnetic resonance spectroscopy.....	
3.1.4. Mass spectrometry.....	
3.1.5. Infra-red Spectroscopy.....	
3.1.6. High performance liquid chromatography.....	55
3.1.7. Polarised optical microscopy.....	
3.1.8. Electro-optic measurements.....	
3.1.9. Differential scanning calorimetry.....	56
3.1.10. X-ray diffraction.....	
3.1.11. Computational chemistry.....	

3.1.12. Preparation of liquid crystal mixtures.....	57
3.2. Synthetic procedures.....	57
3.2.1. Preparation of pseudo bent-core materials (compounds 12-41).....	
3.2.2. Preparation of hepta- and nonamethylene linked bimesogens (compounds 42-52 and 66-76).....	58
3.2.3. Preparation of ether linked bimesogens (compounds 55-65).....	59
3.2.4. Preparation of unsymmetrical bimesogens (compounds 77-84).....	61
3.3. Synthetic discussion.....	63
3.3.1. Steglich esterification.....	
3.3.2. Williamson ether synthesis.....	64
3.3.3. Hydrogenation.....	65
Chapter 4: Results and discussion.....	66
4.1. Pseudo bent-core materials.....	67
4.1.1. Synthetic procedures.....	87
4.2. Bimesogens with a 7-unit spacer.....	116
4.2.1. Bimesogens with a heptamethylene spacer.....	
4.2.2. Bimesogens with an ether linked pentamethylene spacer.....	122
4.2.3. Synthetic procedures.....	126
4.3. Nonamethylene spaced bimesogens.....	141
4.3.1. Synthetic procedures.....	149
4.4. Unsymmetrical bimesogens.....	157
4.4.1. Synthetic procedures.....	162
4.5. Mixture studies.....	171
4.5.1. Mixture studies of compounds 44-52 and 55-65 with CB9CB.....	
4.5.2. Mixture studies of compound 76 with a high HTP dopant.....	177
Chapter 5: Conclusions.....	192
References.....	200
Glossary.....	208
Appendices.....	212
Appendix 1: Binary phase diagrams of compounds 44-65 with CB9CB.....	213
Appendix 2: Transitional behaviour of mixtures of compound 76 with CD-1 as presented in Figure 73.....	229

Acknowledgements

To my parents, who's unceasing belief and support is the only reason I have managed to get this far, I hope this massive lump of paper shows it was a good investment, even if you're 90% sure I've made up most of the words I've used.

To John Goodby, who has had to put up with my nonsense since I set foot in the university. You went above and beyond to get me this opportunity when I was finishing my Masters and have always made me feel like a valued member of your long list of students. I will be eternally grateful for everything you've done.

To Stephen Cowling, thank you for all your help over the years, with both training, emotional support, and generally putting up with my scatter-brained approach to things. I can imagine how frustrating I have been due to my tendency to do things last minute. But you've always been willing to help regardless.

To Edward Davis and Richard Mandle, without the two of you I would likely still be wandering wide-eyed around the lab with no idea what I was doing. Your heroic patience dealing with my constant questions and confusion, through both my Masters and PhD definitely helped to keep me sane.

To the rest of the Materials group at York from 2012-2017, thank you for making what could have been the most frustrating, stressful 5 years of my life some of the most enjoyable, I'll always treasure the memories I have from my time with you all.

To the University of York I am grateful for making this PhD even possible thanks to the Teaching Scholarship I was granted.

To the entire Teaching Lab team at York, especially David Pugh, thank you for making the 4 years of demonstrating both an immensely enjoyable and educational experience, and showing me how rewarding teaching can be.

Thank you to all of you, if it weren't for all the support I've received from you, and others I doubt I'd have made it this far.

Declaration

I declare that this thesis is a presentation of original work and I am the sole author. This work has not previously been presented for an award at this, or any other, University. All sources are acknowledged as References.

Several starting materials were provided by Dr. Richard Mandle of the Liquid Crystals and Advanced Materials Group at the University of York. Compound 35 was synthesised by Dr. Edward Davis of the Liquid Crystals and Advanced Materials Group at the University of York but phase analysis was carried out by myself. Resonant Soft X-Ray scattering experiments were carried out by Chenhui Zhu and Mirosław Salamończyk of the Lawrence Berkeley National Laboratory Advanced Light Source.

Some work presented in this thesis has been previously published in peer-reviewed articles of which I am the primary author or a credited co-author, a list of references to these works follows;

Archbold, C. *et al.* Chiral dopants and the twist-bend nematic phase- induction of novel mesomorphic behaviour in an apolar bimesogen. *Soft Matter*, **38**, 7547-7557 (2015)

Archbold, C. *et al.* Effect of the linking unit on the twist-bend nematic phase in liquid crystal dimers: a comparative study of two homologous series of methylene- and ether-linked dimers. *Liquid Crystals*, **44**, 84-92 (2017)

Mandle, R.J. *et al.* The relationship between molecular structure and the incidence of the N_{TB} phase. *Liquid Crystals*, **42**, 688-703 (2014)

Mandle, R.J. *et al.* Apolar Bimesogens and the Incidence of the Twist-Bend Nematic Phase. *Chemistry- A European Journal*, **21**, 8158-8167 (2015)

Chapter 1: Introduction

1. Introduction

1.1. Introduction to liquid crystals

Liquid crystals are a state of matter that fall between the solid and the isotropic liquid. In the crystalline state the constituent molecules of a substance are arranged in such a way to give rise to a long-range, three-dimensional lattice with both orientational and positional order. In addition, while the molecules are fixed in place, with little to no rotational or translational freedom they do undergo vibrational and oscillatory motion. Conversely in the liquid the molecules have translational and rotational freedom, with little to no order. In the liquid crystal state the molecules retain a degree of the rotational and translational freedom that they possessed in the isotropic liquid, while also exhibiting a degree of orientational/positional order, dependent on the phase type.¹ Liquid crystalline phases can be nominally separated into two broad families; thermotropic and lyotropic mesophases. Lyotropic liquid crystals exhibit liquid crystalline behaviour when mixed with a solvent, with the phase behaviour being dependent on both the concentration of the material, as well as the temperature of the system. Lyotropic materials often rely on a difference in compatibility with the solvent at differing parts of the molecule. For example the standard model of a lyotropic material is based on the structure of an amphiphile, with a hydrophilic "head" group and a hydrophobic "tail".² The second family is thermotropic liquid crystals, where the materials exhibit liquid crystalline phases as a function of temperature when not in a solvent. These materials tend to rely on anisotropy of molecular shape as opposed to solvent affinity in order to form liquid crystal phases.³ Thermotropic liquid crystals specifically will be discussed in further sections.

1.2. Thermotropic liquid crystals

When a crystalline solid is heated, the energy imparted on the molecules allows them more freedom to rotate and vibrate about their lattice sites. At a critical point, the melting point of the solid, this increase in motion becomes such that the crystal lattice breaks down and the molecules become free to move and rotate, resulting in an isotropic liquid (Figure 1).

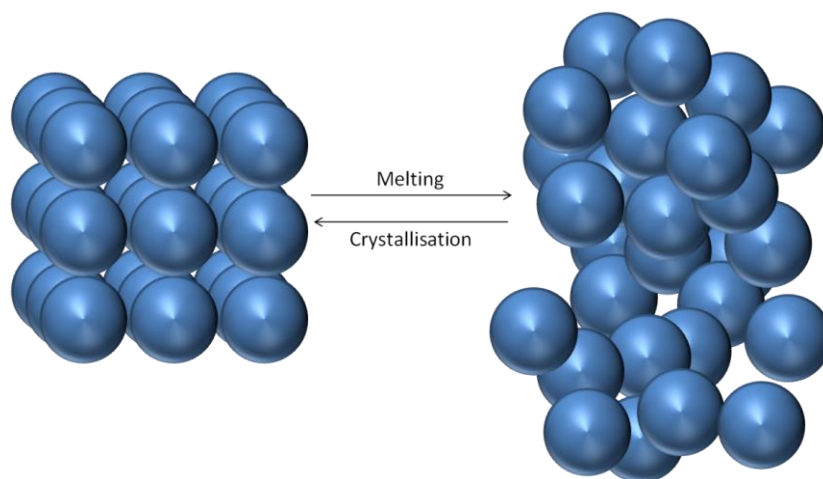


Figure 1: Schematic diagram of the transition between a crystalline solid and an isotropic fluid.

In a thermotropic liquid crystal the molecular anisotropy allows for this process to pass through one or more thermodynamically stable intermediate phases, these are referred to as mesophases.⁴ Thermotropic liquid crystals are often divided into two broad families based on the shape of the molecule. Calamitic systems have molecules that adopt rod-like molecular architectures, with the molecules being much longer in one direction than the other two. Discotic systems on the other hand, adopt disc-like shapes, with one molecular axis being significantly shorter than the other two, a schematic representation of this is shown in Figure 2.⁵

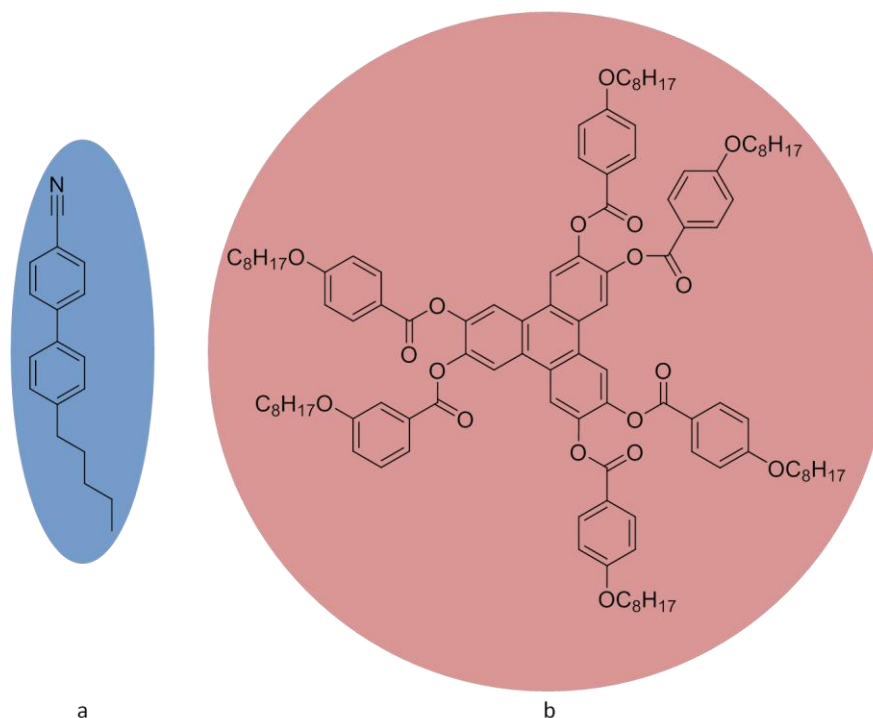


Figure 2: Examples of a) a calamitic molecule and b) a discotic molecule.

The molecules found in calamitic and discotic phases have either rod- or disc-like molecular architectures, and the phases of these molecules are the most widely studied in liquid crystals, but other molecular architectures, such as bent ⁶ or bowl ⁷ shaped molecules have also been known to support mesomorphic behaviour. These materials will be discussed in more depth in Section 1.4 where the work will focus primarily on the phases exhibited by liquid crystals of unusual shape and their comparison with the phases exhibited by calamitic systems.

1.3. Calamitic phases formed by rod-like molecules

For a material formed of rod-like molecules the process of transitioning from the crystalline solid to the isotropic liquid can pass through several, distinct steps relating to the decay of the order of the crystalline lattice. Initially the molecules, when locked into the crystalline state, are positioned on their lattice points with little to no translational or rotational freedom. Upon initial heating this constraint is relaxed somewhat allowing the molecules to rotate about their long axes, this "soft-crystal" or "anisotropic plastic crystal" retains the long-range positional order of the crystal, with the molecules still being fixed onto the lattice. ¹ Upon further heating the long-range positional order is disrupted, thereby forming a material composed of molecules arranged in diffuse layers, retaining

long-range orientational order but being overall liquid-like within the layers themselves. The phases in which the molecules adopt this arrangement are known collectively as "smectic". Upon further heating the ordering of the layers also breaks down, this removes all remaining traces of positional order from the material, leaving only the orientational order. This phase is referred to as the nematic phase. Finally the material undergoes a transition into an isotropic liquid, wherein the remaining orientational order in the nematic phase is broken down. It should be noted that this is an idealised case and it is common for rod-like materials to exhibit one or two of these transitions without the others. Further discussion on the nature of these mesophases will be made in Section 1.5. and onwards. A chart summarising the structures of the common calamitic mesophases is shown in Figure 3.

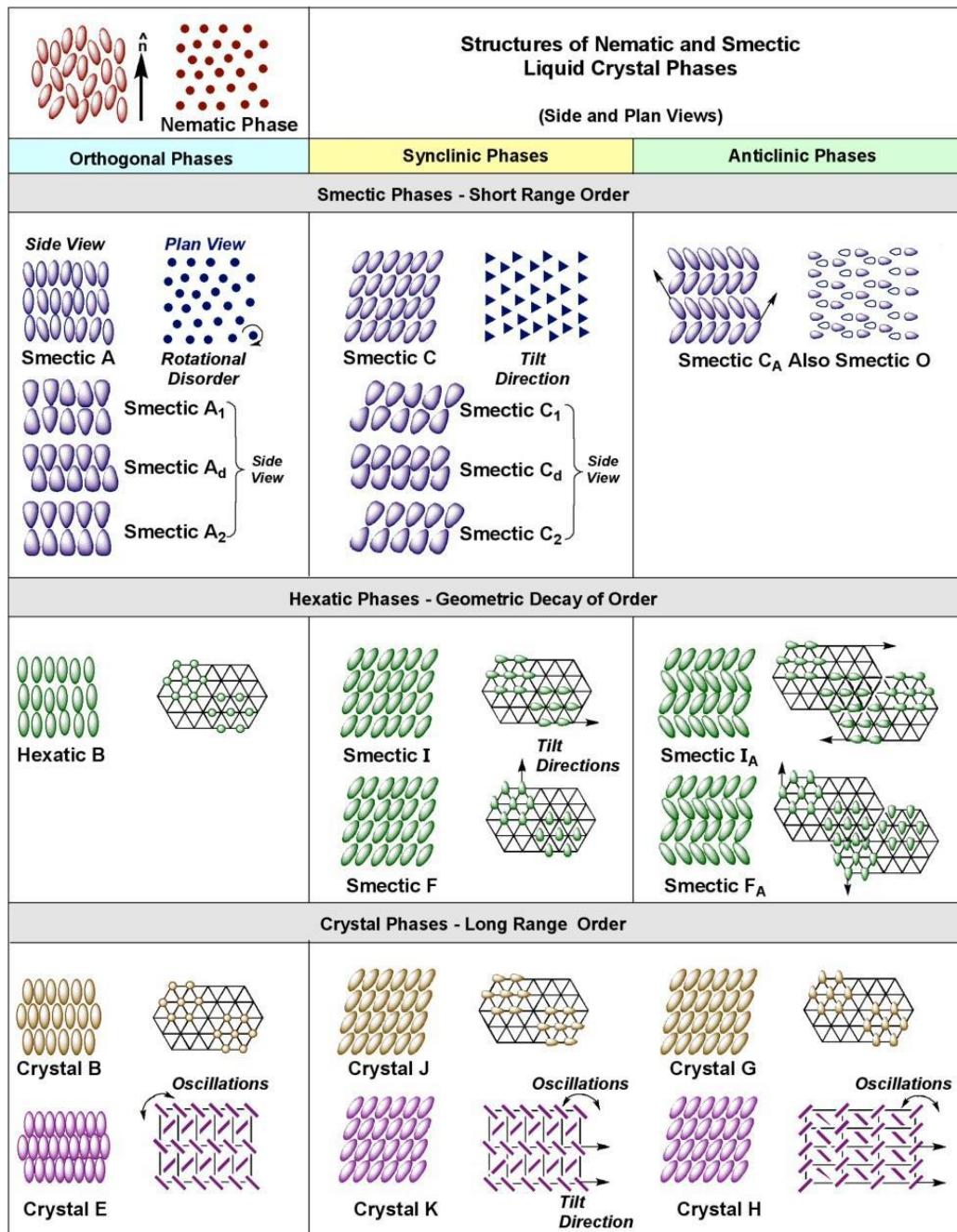


Figure 3: Structural features of some of the common calamitic phases.^{8,9}

1.4. Liquid Crystals of Unusual Shape

1.4.1 Bent Core Liquid crystals

As stated in section 1.2, although thermotropic liquid crystals are primarily formed by rod or disc-like molecules these are far from the only molecular architectures capable of introducing the needed molecular anisotropy for mesophase formation. As early as 1932 a material reported by Vorlander and Apel^{10,11} was shown to exhibit a nematic phase, despite being neither rod nor disc-like in molecular architecture, indeed the molecular structure of the material was based on a rigid, bow-shaped central core with terminal chains attached, the molecular architecture of this material is shown in Figure 4.

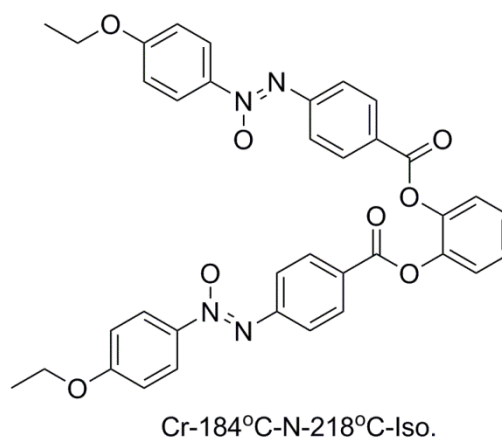


Figure 4: Molecular architecture and transition temperatures of the material presented by Vorlander and Apel.¹⁰

This material shares many structural features in common with another family of liquid crystals with unusually shaped bent cores. “Bent core” materials in general are composed of a rigid core unit, usually formed by cyclic units such as phenyl or oxadiazole rings that are terminated by long, flexible chains. The general shape of a bent core material is presented graphically below, in Figure 5 and exemplified by an oxadiazole based compound.

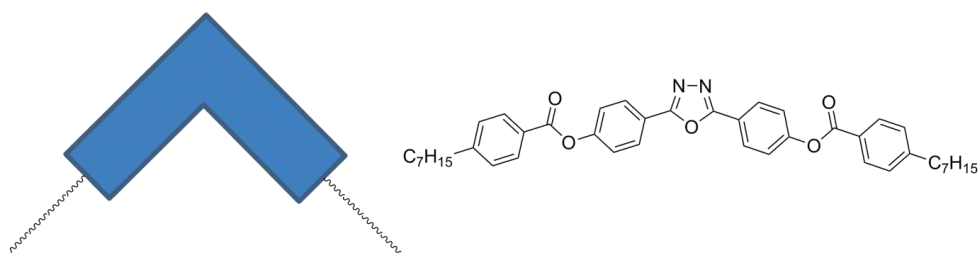


Figure 5: General structure of a bent core material, and an example of one possible molecular architecture.

Bent core liquid crystals have provoked significant interest due to their propensity to form unusual mesophases such as the much discussed biaxial nematic phase^{12–14}, B phases^{11,15–17}, and the dark conglomerate phase^{18–20}. Bent core materials have also been shown to exhibit smectic phases, particularly chiral smectics that do not possess stereogenic centres.^{21–25}

1.4.2. Liquid Crystal Dimers

As an almost inversion of bent core liquid crystals there exists another subset of so called liquid crystals of unusual shape, the dimers. Dimers, or in the case of liquid crystals "bimesogens or dimesogens" consist of two rigid units, usually made up of cyclic groups linked by a flexible spacer, which is commonly composed of methylene or ether units.^{26,27} The general structure of a liquid crystal dimer with a spacer of odd parity is shown in Figure 6.

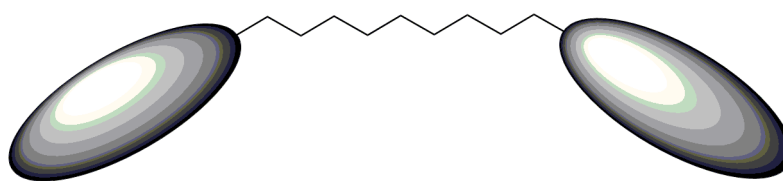


Figure 6: Schematic representation of a bimesogen.

It can be seen from Figure 6 that these materials are structured in the opposite way to bent core molecules, and as such have a unique set of properties all of their own. Dimers tend to have more in common with standard calamitics than with bent core materials, with many exhibiting nematic^{28,29} or smectic³⁰ phases similar to those of standard rod-like molecules. Liquid crystal dimers can show a wide range of mesophases depending on the arrangements of the mesogenic units and the linking chain(s). The most commonly observed structure-property relationship in conventional bimesogens is a highly

pronounced odd-even effect with respect to the parity of the linking chain.^{30,31} The effect sees a pronounced increase in melting point and I-N transition temperature when the central spacer of a cyanobiphenyl dimer consists of an even number of methylene units. This is attributed to the differences in molecular topology imparted by this change in the spacer chain, with the spacer of even parity causing the molecules to adopt a more linear overall geometry (Figure 7), increasing their ability to pack into a crystal lattice inducing a higher melting point, as well as making the molecule overall more rod-like, causing the formation of a more thermodynamically stable nematic phase. Conversely in the dimer with a spacer of odd parity the overall conformation is more bent, this disrupts the packing, destabilising the crystal lattice as well as the nematic phase thereby lowering the transition temperatures.

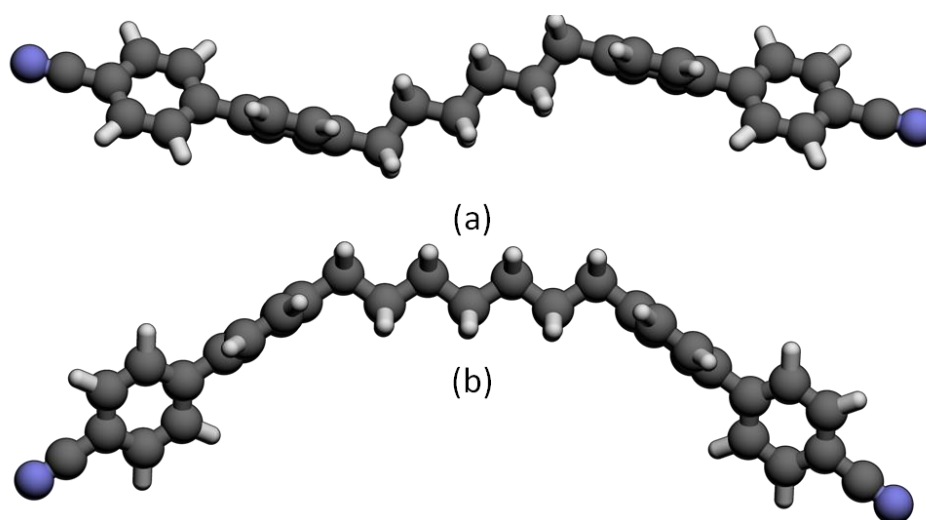


Figure 7: Differences in geometry between a dimer with (a) an even and (b) an odd parity spacer.

This assertion is further supported in that the alternation between the odd and even materials is shown to attenuate as the chain length increases. The increase in chain length causes an increase in the conformational freedom of the molecule, lessening the impact of the spacer parity as the chains are freer to move and fold.

The current interest in bimesogenic materials however stems from the, relatively, recent observation of a novel mesophase, assigned as the twist-bend nematic phase predicted by Dozov, within this family of liquid crystals.^{27,29,32,33} Dozov suggested that an escape from the macroscopic spontaneous polarisation of the nematic phase of bent-shaped dimers

could only be achieved via breaking the symmetry of the uniaxial nematic phase in two ways. The first a biaxial nematic phase with oscillating splay-bend deformations, the other a nematic phase with a two-fold degenerate, chiral helical superstructure i.e. conical twist-bend deformations. This phase has come to be known as the twist-bend nematic (N_{TB}) phase, and has become a hotly debated topic in recent years.

1.5. The nematic phase

As previously mentioned in section 1.3. the nematic phase consists of a liquid-like arrangement of molecules with no positional order, whether short or long range, but in possession of a degree of orientational order in which all of the molecules preferentially align their long axes parallel to a single unit vector referred to as the director, symbolised as \hat{n} . Although the molecules are effectively lath-like in their molecular structures, the rapid rotation and flipping on time scales in the tens of picoseconds (10^{-11} s) means that they can effectively be treated as rods. A graphical representation of the nematic phase is shown in Figure 8.

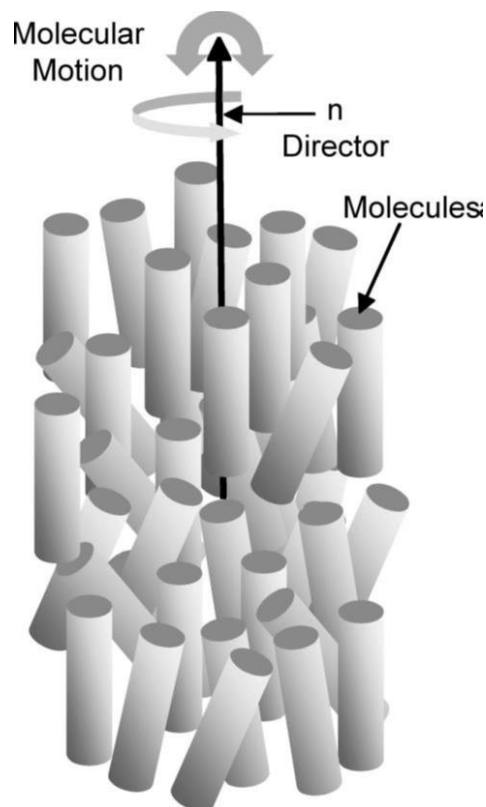


Figure 8: Schematic representation of the nematic phase showing the director (\hat{n}).⁹

Molecules in the nematic phase retain the translational symmetry they possessed in the isotropic liquid, however due to the introduction of orientational order in the form of the bulk director the rotational symmetry available to molecules in the isotropic liquid is lost.¹ The standard uniaxial nematic phase itself exhibits $D_{\infty h}$ symmetry. The level of orientational order within a nematic phase can be quantified using the scalar order parameter (S), calculated *via* Equation 1.³⁴ This value, between 0 and 1 shows how well the molecules in a nematic align with the director, with 0 being isotropic, therefore unaligned and 1 being perfect parallel alignment.

$$S = \frac{1}{2}(3 \cos^2 \theta - 1)$$

Equation 1: Calculation of the nematic order parameter.

The typical values of S for a nematic phase range from 0.4 to 0.7 and the value is dependent on the temperature of the sample, as S sharply decreases to 0 at the clearing point.

1.6. The chiral nematic phase

When a nematic phase is made up of chiral molecules, or chirality is introduced into a nematic material through the addition of a chiral dopant, the properties and structure of the nematic phase change. Due to the chirality in the system the molecules no longer arrange in the same way, they instead adopt a helical arrangement about the director.^{35,36}

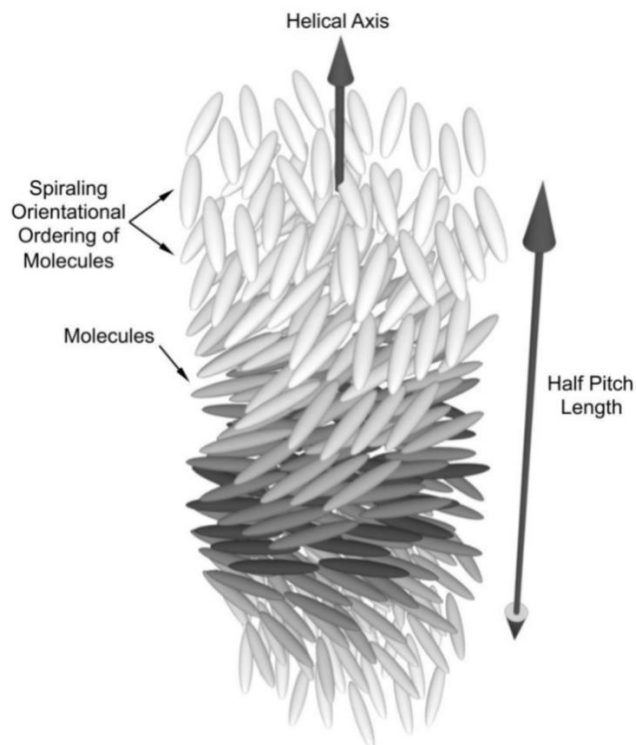


Figure 9: Schematic representation of a chiral nematic phase showing one full pitch.⁹

The helical pitch length of a chiral nematic is intrinsically linked to several of its properties, most notably the wavelength of light selectively reflected by a material.³⁷ The pitch length of a chiral nematic is controlled by several factors; firstly the overall degree of chirality in the system, for example increasing the amount of chiral dopant in a mixture will often cause the pitch to tighten, decreasing the pitch length. Secondly the helical pitch for a chiral nematic phase is also temperature dependent, with the pitch length shortening as the temperature increases. The temperature sensitive reflection of light produced by this effect is known as thermochromism, and is the basis for several liquid crystal technologies including plastic thermometers and thermochromic films.^{38–40}

1.7. The smectic A phase

The smectic phases are more ordered than the nematics, while the nematic phase has only long range orientational order with the molecules aligning roughly parallel to the director the smectic phases adopt a lamellar structure with a clearly defined layer spacing. The arrangement of the molecules within these layers determine which smectic phase the material adopts. The simplest of the smectic phases is the SmA phase, in which the long axes of the molecules lies parallel to the layer normal, as shown in Figure 10.

The molecules in the SmA phases, like those in the nematic phase are undergoing rapid reorientation about their long axis on a timescale of 10^{11} s^{-1} . The molecules are also undergoing relaxations about their long axes on a timescale of 10^6 s^{-1} . Consequently the phase, despite being more ordered than the nematic, is far from static, with the molecules moving diffusely through the bulk material. In the plane of, or between the layers the molecules are arranged in such a way that there is no translational periodic ordering. Therefore within the layers there is only short range ordering extending over a few molecular centres ($\approx 15\text{-}25 \text{ \AA}$), with the ordering decaying in algebraic fashion. Perpendicular to the layers the molecules are essentially arranged in a one-dimensional density wave, therefore the layers themselves must be considered as being weak.

Consequently the concept of a strict, lamellar mesophase is somewhat misleading as the layers are considerably more diffuse than the nomenclature implies. In actuality the molecules are arranged within the layers in a somewhat random fashion, often tilted at slight angles with respect to the layer normal. This results in a layer spacing that is, on average shorter than a single molecular length. Molecules are typically tilted anywhere up to $\approx 15^\circ$ from the layer normal, this tilting however is random across the bulk material, resulting in, on average, an optically uniaxial phase with the optic axis lying perpendicular to the layers. This results in the SmA phase possessing overall D_∞ symmetry.



Figure 10: Schematic representation of the local structure of the SmA phase.⁴¹

1.8. The smectic C phase

Whereas in the smectic A phase the molecular long axes lie on average perpendicular to the layer normal, in the smectic C phase this is not the case. For smectic C materials the molecular long axes tend to lie at an angle (θ) with respect to the layer plane. The tilt angle can take two possible forms, one where the smectic C phase is formed on cooling from the smectic A phase, and one where it is formed on cooling from the nematic phase. For the first possibility, the tilt angle is low, usually between 18 and 30° relative to the angle between the layers and their perpendicular, and varies as a function of temperature. For the second possibility, transition from the nematic to the smectic C the tilt angle is usually in the range of $\approx 45^\circ$ and is invariant with respect to temperature.

Depending on the direction of tilt in each layer relative to those adjacent to it there exist two common variations of the smectic C phase. The synclincic smectic C (SmC_s) has all the molecular tilts in the same direction whereas the anticlincic smectic C (SmC_A) has the tilt directions alternating between layers as shown in Figure 11.

The molecules in the smectic C phase have short range order both in and out of the planes of the layers. Consequently the environmental symmetry of the phase consists of a centre of symmetry, a twofold axis of rotation and a mirror plane perpendicular to the layers i.e. C_{2h} symmetry. Conversely if the molecules in the smectic C phase are optically active the phase becomes helical and chiral, the resulting modification is denoted as SmC^* . The helical structure arises from the rotational progression of the tilt direction from one layer to the next. This change in macrostructure reduces the overall chirality of the SmC^* compared to the SmC ; both the mirror plane and centre of symmetry are eliminated, leaving just the twofold axis of rotation, resulting in an overall symmetry of C_2 . The axis of rotation is polar, as a consequence there is spontaneous coupling of molecular dipoles along this axis, causing the phase to become *ferroelectric*.

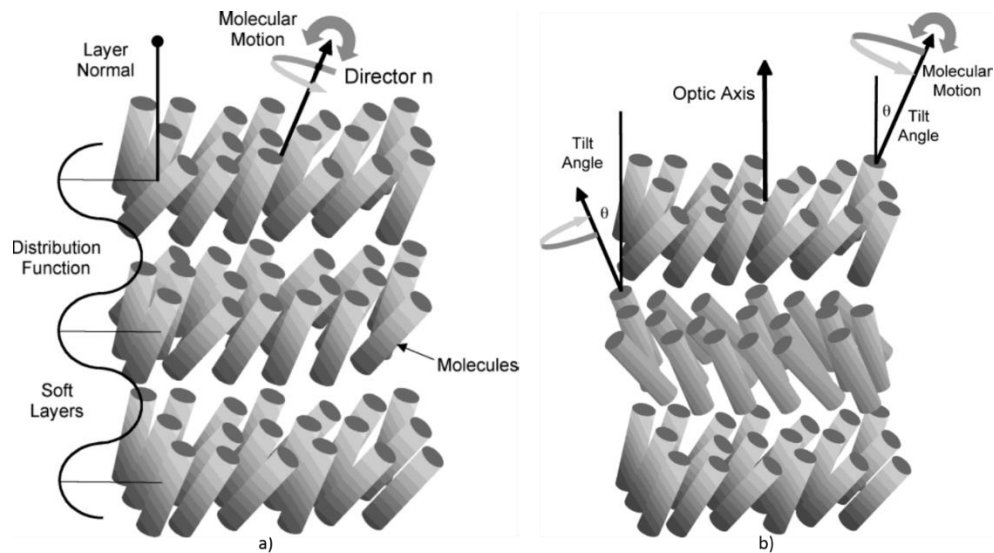


Figure 11: Schematic representation of the local structure of (a) the synclinic and (b) the anticlinic smectic C phases.

1.9. Blue Phases

In highly chiral liquid crystal systems a series of mesophases may occur between the normal chiral nematic phase and the isotropic liquid. These are collectively referred to as "Blue Phases", named for their selective reflection of blue light. Blue phases are formed by a twisted structure as in the chiral nematic phase, however although the molecules in the chiral nematic phase only twist in one direction, in blue phases the molecules twist in different directions with respect to one another, forming a so called "double twist cylinder" (Figure 12).

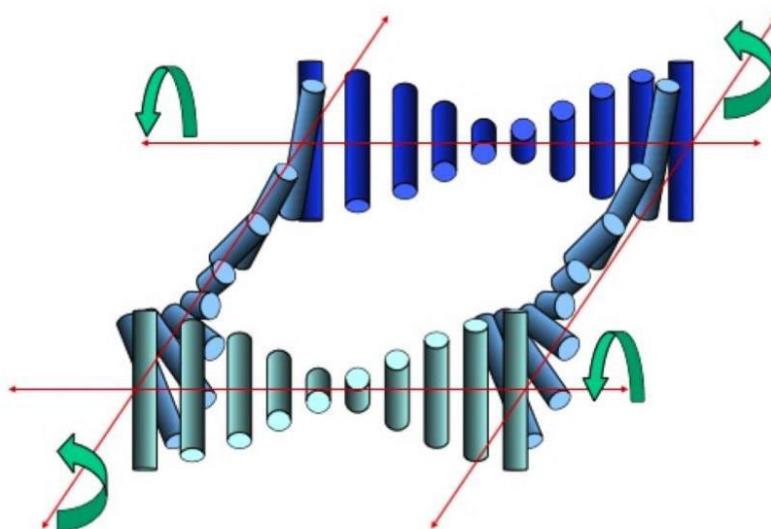


Figure 12: Schematic representation of the double twist arrangement in blue phases. Molecules presented in blue.

The packing of these cylinders determines which of the three blue phases a material will adopt. Blue phases are cubic by nature, with BPI adopting a body centred cubic geometry, BPII a simple cubic geometry (Figure 13), and BPIII, initially also known as the "fog phase" due to its lack of a defect texture, has the same symmetry as the isotropic liquid.

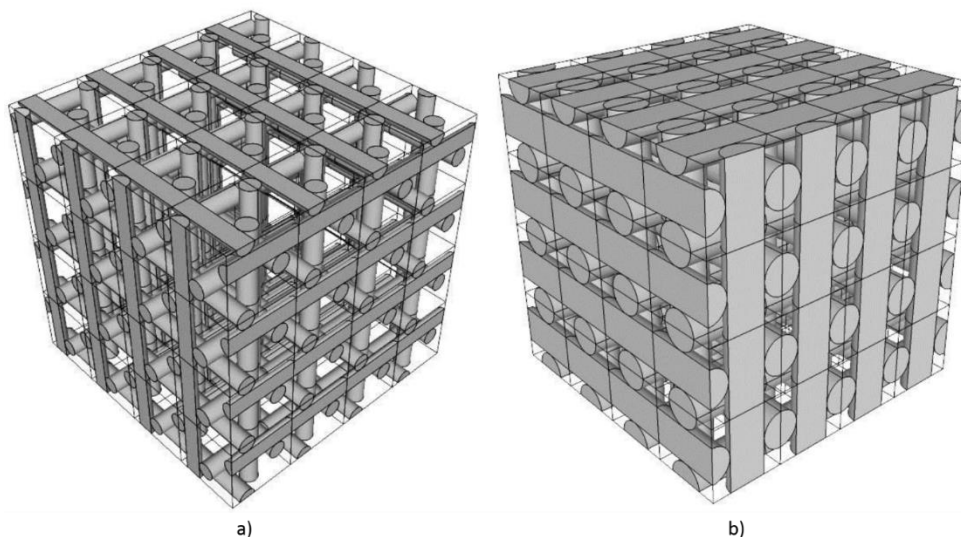


Figure 13: Graphical representation of the structures of (a) BPI and (b) BPII.⁴²

1.10. Liquid Crystal Bimesogens

Liquid crystal bimesogens are commonly comprised of a pair of mesogenic units that are linked by a flexible spacer unit usually an alkyl chain. These materials can be divided into two groups: symmetrical and unsymmetrical. Symmetrical bimesogens (Figure 14a) which are often referred to as dimers, have identical mesogenic units at either end, unsymmetrical bimesogens (Figure 14b), possess different mesogenic units at either end of the molecule.

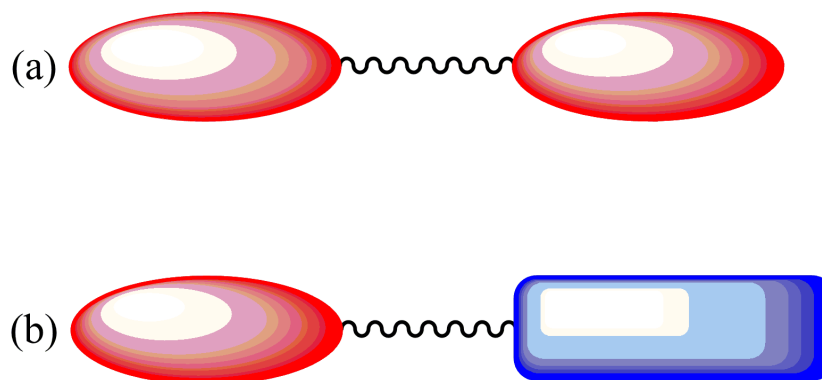


Figure 14: Schematic representations of (a) a symmetrical and (b) an unsymmetrical bimesogen.

Since the first report of a liquid crystal bimesogen there has been a great deal of scientific interest in, and research conducted on this class of liquid crystals. This interest stems largely from the unique properties of these materials, which often differ greatly from the analogous individual mesogenic units. Liquid crystal bimesogens can adopt three different molecular architectures with significantly differing properties, even for materials with the same base monomeric unit. These arrangements are; terminal dimers, as shown in Figure 14, H-shaped bimesogens (Figure 15a) and T-shaped bimesogens (Figure 15b).

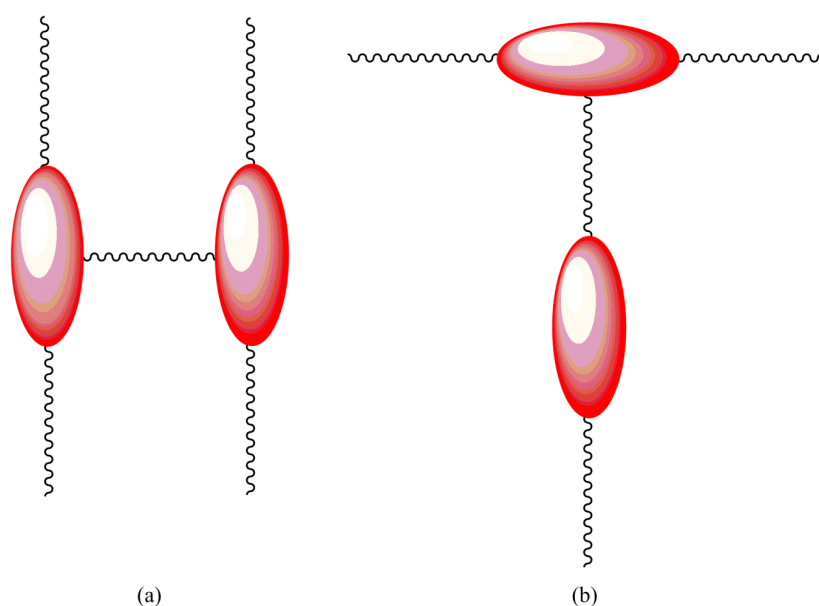


Figure 15: Schematic representations of (a) an H-shaped and (b) a T-shaped bimesogen.

T and H-shaped bimesogens possess interesting properties, both with regards to the effect of changing molecular topology on the transitional behaviour of a bimesogen, and in the ability of chiral T-shaped dimers to stabilise blue phases. However a further discussion of their physical properties is beyond the scope of the work presented in this thesis, which focuses primarily on terminal liquid crystal bimesogens. This focus is due to the molecular architecture of T and H shaped bimesogens not having structural properties that are key to forming the twist-bend nematic phase.

1.11. Terminal Liquid Crystal Bimesogens

Liquid crystal bimesogens have been shown to be very sensitive to changes in their molecular architecture; this sensitivity results in a small change in the chemical or structural makeup of a bimesogen having a pronounced effect on the properties of the bulk material. The structural changes most commonly investigated are: the nature of the terminal mesogen, including, but not limited to the functionality of the end group, and lateral substitution and the nature and parity of the flexible spacer.

1.11.1. The nature of the flexible spacer

In a terminal liquid crystal bimesogen the flexible spacer, often comprised of methylene units but bimesogens with siloxane spacers have also been synthesised. The architecture of this structural component has a pronounced effect on the overall physical properties of the bulk material. The most obvious effect that can be observed is the so called “odd-even effect” identified in 1992 by Date *et al.*³⁰ Date *et al* observed that the nematic-isotropic transition temperatures of a series of α,ω -bis(4-n-alkylanilinebenzylidene-4'-oxy)-alkanes were much lower in bimesogens with flexible spacers containing an odd number of methylene units. The authors attributed these variations to the effect of spacer parity on the shape of the molecule. Specifically in that molecules comprised of spacers with odd parity tend to adopt a more bent molecular architecture, whereas molecules with spacers of even parity adopt a more linear arrangement (Figure 16). In the bimesogens with spacers of odd parity the bent shape makes it more difficult for the molecules to pack together, this destabilises the mesophase and therefore lowers the transition temperature.

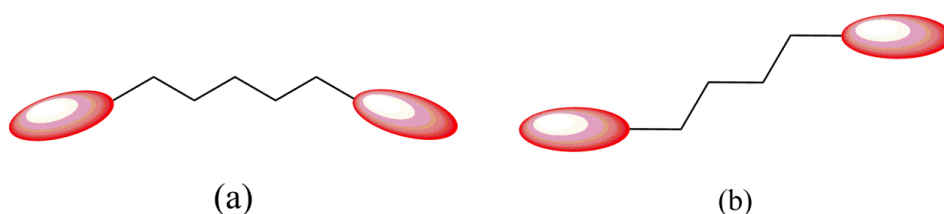


Figure 16: Schematic representation of terminal bimesogens with spacers of (a) odd and (b) even parity.

This effect was further observed by Ferrarini *et al* in a series of symmetrical, methylene linked 4-cyanobiphenyl-4'-yloxy bimesogens.³³ The transitional behaviour of these materials; namely the melting point, I-N transition and the entropy of this transition showed a pattern of alternation, rising when the spacer was of even parity, and falling when the spacer was of odd parity. The transition temperatures, both melting and isotropic to nematic, began to attenuate as the spacer length increased, the entropy of phase transition however does not attenuate. A graphical representation of these results are shown in Figure 17.

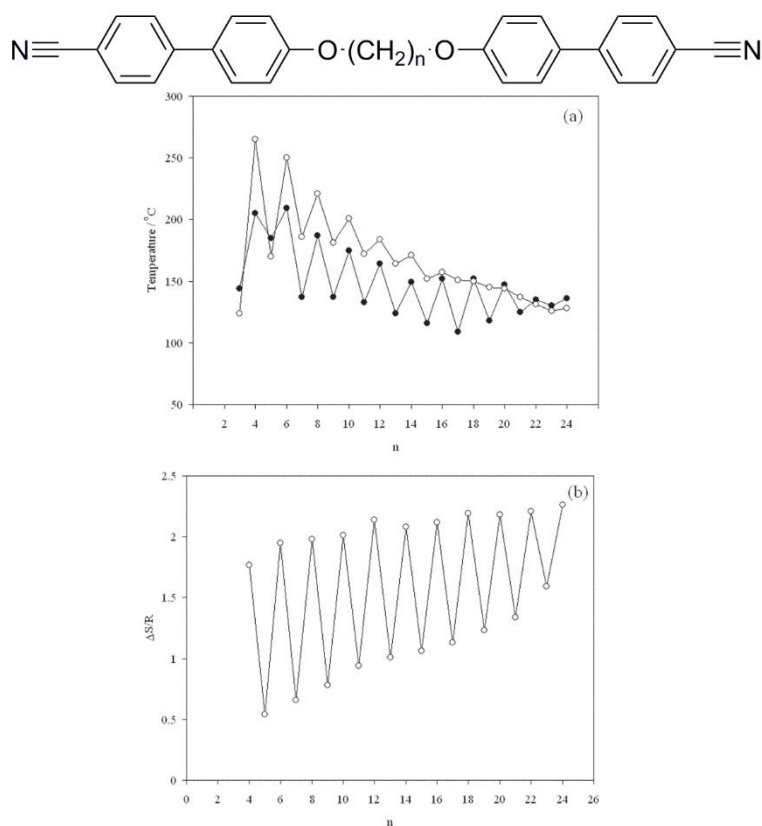


Figure 17: The dependence of (a) the melting point (●) and nematic-isotropic transition temperature (○) and (b) the entropy of the nematic-isotropic transition of α,ω -bis(4'-cyanobiphenyl-4-yloxy)alkanes on the parity of the spacer.³¹

As a result of the bent molecular architecture and low dielectric anisotropy, symmetrical liquid crystal bimesogens with spacers of odd parity have been investigated as components in mixtures for use in flexoelectric devices. Flexoelectric coupling is the polarisation of materials upon elastic deformation. This effect is typically observed in chiral nematic phases, a diagrammatic representation is shown in Figure 18.^{43–50}

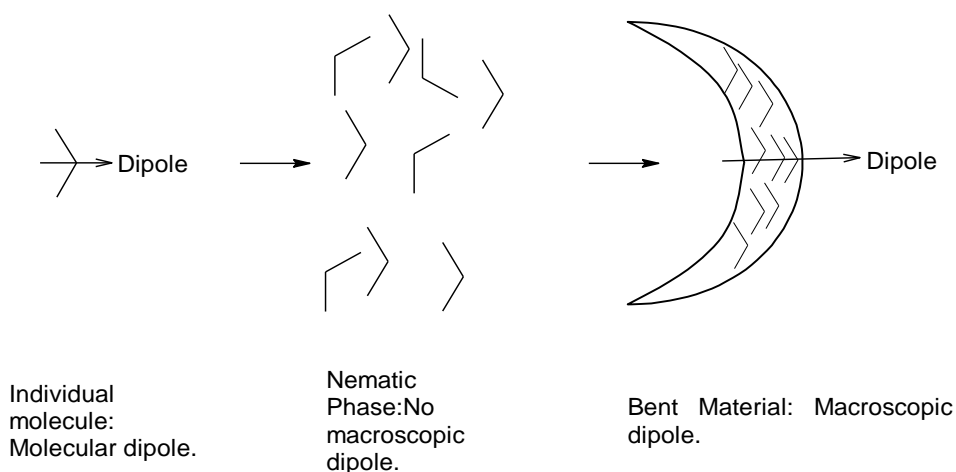


Figure 18: Diagrammatic representation of the flexoelectric effect in the nematic phase of a bent molecule.

Due to the flexoelectric effect being observed typically in chiral systems, when designing mixtures for use in this type of device it is usual to dope a mixture with a chiral dopant of high helical twisting power. Coles *et al* reported mixtures made for flexoelectric devices containing the dimers shown in Figure 19, with a dopant of high helical twisting power, exhibit blue phases over a wide (40-60 °C) temperature range.⁵¹

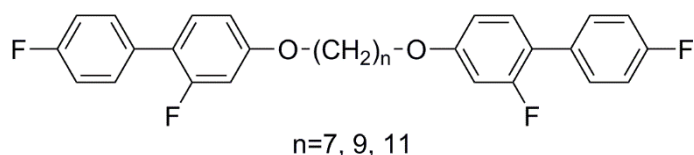


Figure 19: The general structure of the bimesogens used in mixtures that exhibit wide temperature blue phases.

Liquid crystal bimesogens have been shown to be useful as a model to predict the properties of higher order liquid crystal oligomers and polymers, some of the general structures of some types of which are shown below in Figure 20 . Blatch *et al*⁵² theorised that this property stems from the molecular architecture of liquid crystal bimesogens. Specifically that these materials contain the most basic structural unit of a polymeric liquid crystal i.e. mesogenic units linked by a flexible backbone.

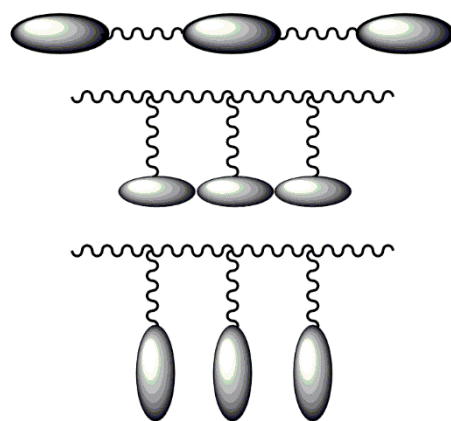


Figure 20: Schematic representation of several possible structures of liquid crystal polymers.⁵³

1.11.2. The nature of the terminal group

In bimesogens consisting of mesogenic units containing ester units the direction in which the mesogens face can have a large effect on the properties of the bulk material. Heggilustoy *et al* carried out work to investigate the effect of changing the facing of mesogenic units on the properties of bimesogens.⁵⁴ In this work a variety of dimeric derivatives of 4'-hydroxybiphenyl-4-carboxylic acid (Figure 21) were synthesised.

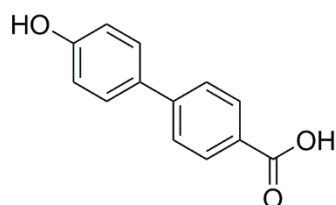


Figure 21: Structure of 4'-hydroxybiphenyl-4-carboxylic acid.

The bimesogens synthesised were the “head to head” (Figure 22a), the “tail to tail” (Figure 22b) and the “head to tail” (Figure 22c) configurations. The phase behaviour of these materials was analysed using POM and DSC, the results showing that the three configurations exhibited very different thermal behaviour. Figure 22a exhibited an anticlinic smectic C phase, Figure 22b displayed only soft crystalline phases, and Figure 22c was entirely non mesogenic.

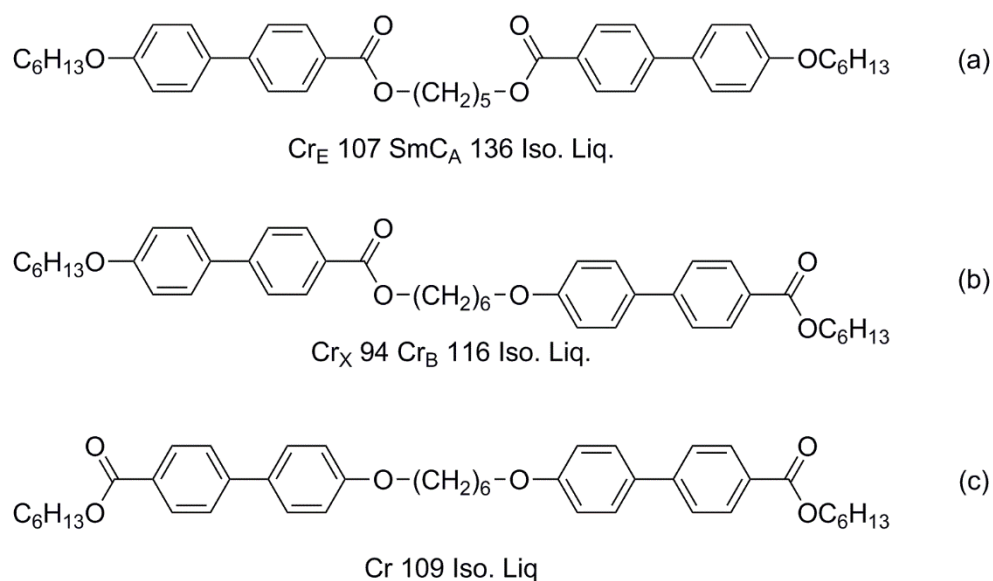


Figure 22: Structures of the dimers reported by Heggilustoy *et al* and the observed transition temperatures (°C).

1.11.3. Unsymmetrical Bimesogens

Bimesogens with two different mesogenic units at either end can possess very different properties from their symmetrical counterparts. Recent research into the properties of unsymmetrical bimesogens has been focussed on their ability to form a series of novel smectic phases referred to as intercalated smectic phases. In these phases the differing mesogenic units associate with one another within the phase, causing the molecules to span across multiple layers, as shown in Figure 23.⁵⁵

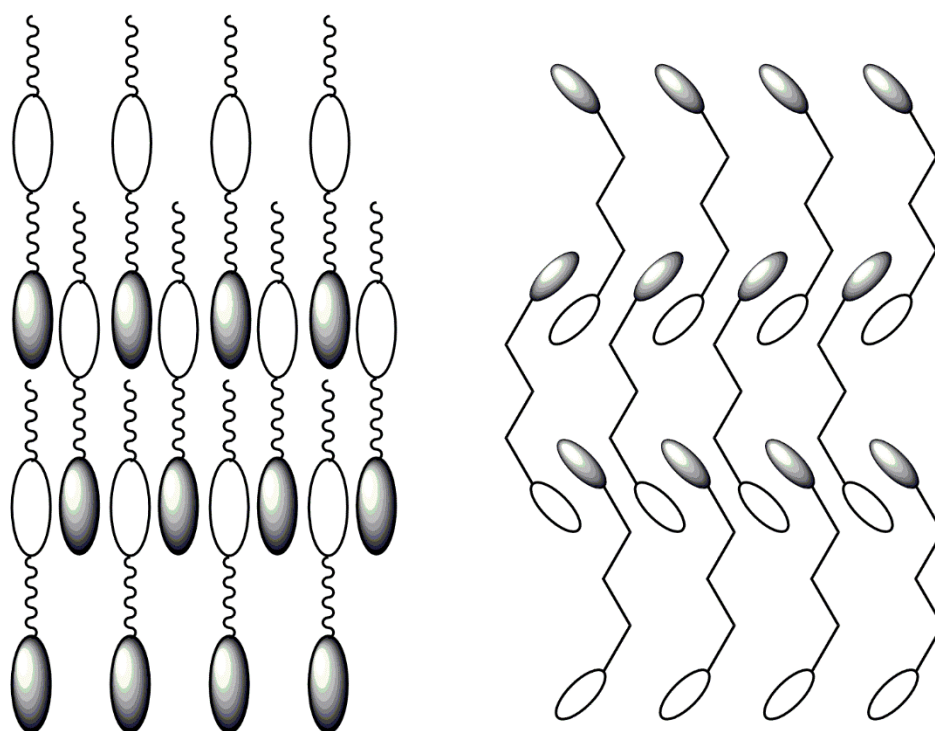


Figure 23: Diagrammatic representations of the intercalated smectic A (left) and smectic C (right) phases.

Unsymmetrical bimesogens can also form frustrated mesophases, such as the twist grain boundary (TGB) phase across wide temperature ranges. The TGB phase is an intermediate phase that lies between the chiral nematic and chiral smectic A phases.^{56,57} A representation of this phase is shown in Figure 24.⁵⁸ The mechanism by which unsymmetrical bimesogens stabilise this phase is through the use of one mesogen prone to forming the chiral nematic phase, and one which forms the smectic A phase. This causes a degree of frustration within the phase, where one side of the molecule is attempting to form a helical chiral nematic structure, and the other side is attempting to form a layered smectic A phase. This frustration results in the formation of the intermediate TGB phase.

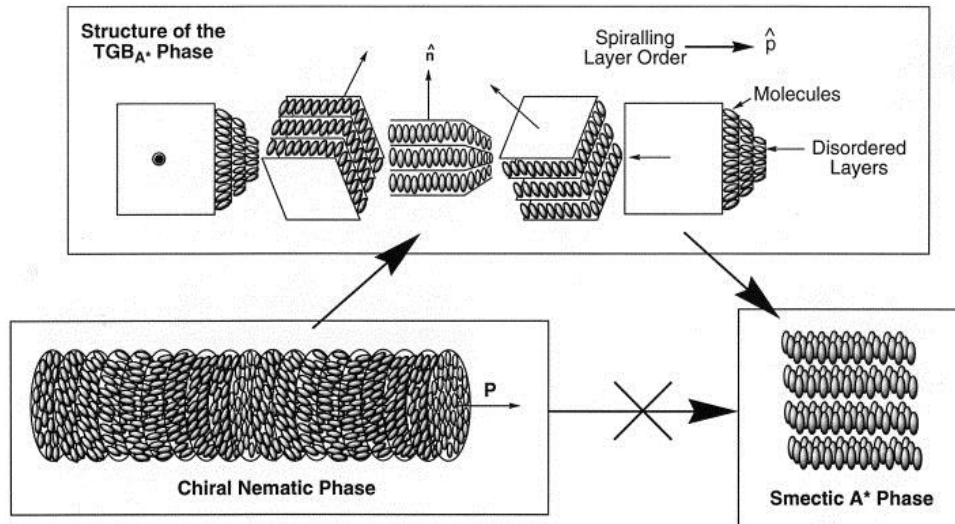


Figure 24: Schematic representation of the TGB phase.

1.12. The twist-bend nematic (N_{TB}) phase

The existence of the twist bend deformation of the nematic phase was first postulated by Meyer in 1973.⁵⁹ In 2001 Dozov put forward a prediction on the properties a material would have to possess in order to adopt this phase.³² Dozov predicted that, most predominantly, a material would need to have a negative bend elastic constant. When adopting the twist bend nematic phase the molecules retain their long range orientational order but curve around an axis (z). This curve is caused by the deviation of the local director away from the average director of the bulk material, with the degree of deviation given by angle θ . This deviation from the director is caused by the introduction of a spontaneous bend, when this deformation is introduced it becomes more difficult, if not impossible to fill space within the phase effectively, therefore the molecules begin to twist around the director in order to compensate for this. This phase is distinct from the chiral nematic phase as the helix curves around the director, rather than being perpendicular to it.⁶⁰ A diagrammatic representation of this phase is shown in Figure 25.

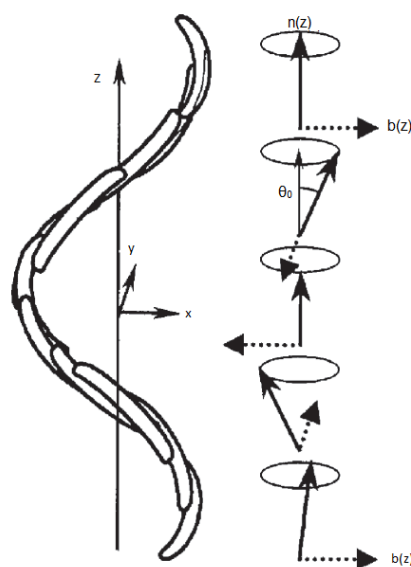


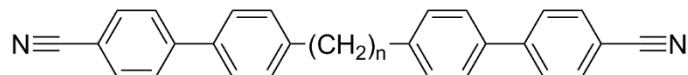
Figure 25: Theorised structure of the twist bend nematic phase.

Since its prediction and discovery, the N_{TB} phase has been studied in depth with a variety of analytical techniques; POM^{26,61–63}, DSC^{26,28,61,62}, XRD^{26,28,62,64,65}, Freeze-fracture transmission electron microscopy (FFTEM)^{66–68}, electron spin resonance (ESR) spectroscopy⁶⁹, dynamic light scattering (DLS)⁶⁵, variable temperature ²HNMR spectroscopy^{26,70} and Raman spectroscopy⁷¹ are all among the techniques that have been used to investigate this phase. While the most widely accepted structure of the N_{TB} phase is the structure presented in Figure 25 a definitive consensus has yet to be reached, with various experiments providing evidence in opposition to the heliconical model.^{72–74}

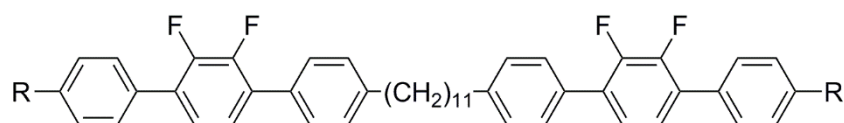
1.12.1. Occurrence of the N_{TB} phase in liquid crystal bimesogens

The N_{TB} phase has been reported in a range of bimesogenic materials, all of which have a common structural factor, a flexible spacer of odd parity. The fact that the bimesogens that adopt this phase have odd numbered spacers implies that the bent molecular shape is a key structural factor in the formation of the N_{TB} phase. Cestari *et al*⁶⁴ reported the occurrence of an enantiotropic nematic to twist-bend nematic phase in the heptamethylene linked cyanobiphenyl dimer CB7CB (Figure 26a) and its nonamethylene linked analogue (Figure 26b) in 2011, Panov *et al*⁶² showed that the undecamethylene linked analogue of this dimer also shows the N_{TB} phase (Figure 26c), as well as demonstrating its occurrence in difluoroterphenyl dimers with terminal alkyl chains (Figure 26d and Figure 26e)³. Also in 2011 Henderson and Imrie²⁶ reported the

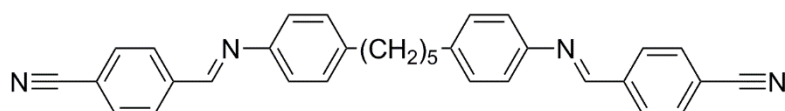
occurrence of the N_{TB} phase in methylene linked dimers with mesogenic units composed of 4-cyanoanilinebenzylidene (Figure 26f), 4-methoxyanilinebenzylidene (Figure 26g) and 4-ethoxyanilinebenzylidene (Figure 26h).



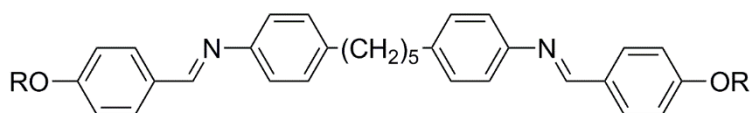
- (a) $n=7$ Cr 102 N_{TB} 103 N 166 Iso. Liq.
 (b) $n=9$ Cr 82 N_{TB} 111 N 129 Iso. Liq.
 (c) $n=11$ Cr 91 N_{TB} 109 N 127 Iso. Liq.



- (d) $R = C_3H_7$ Cr 95 N_{TB} 137 N 193 Iso. Liq.
 (e) $R = C_5H_{11}$ Cr 85 N_{TB} 123 N 170 Iso. Liq.



- (f) Cr 147 (N_{TB} 113 N 125) Iso. Liq.



- (g) $R = CH_3$ Cr 123 (N_{TB} 83 N 86) Iso. Liq.
 (h) $R = C_2H_5$ Cr 130 (N_{TB} 106 N 107) Iso. Liq.

Figure 26: The structures of early materials reported to form the N_{TB} phase and their transition temperatures ($^{\circ}C$).

1.13. The Dark Conglomerate Phase

The dark conglomerate phase is a novel and not well understood optically isotropic, self-assembled state that has been observed in just a few bent-core materials, almost always occurring directly below the isotropic liquid phase. Polarised optical microscopy shows a dark texture, indicating optical isotropy or extremely low birefringence, and uncrossed polarisers usually reveal chiral domains of opposite handedness with dimensions between 10 and 100 μm .¹⁸⁻²⁰

The DC phase is generally thought to consist of highly curved, tilted, polar smectic-like layers (SmCP) with a short interlayer correlation length (\approx a few layers). Four distinct

structures are possible, denoted as: SmC_sP_s ; SmC_sP_A ; SmC_aP_s and SmC_aP_A , where the orientation, tilt and polar direction between layers are syn/anti parallel (Figure 27).

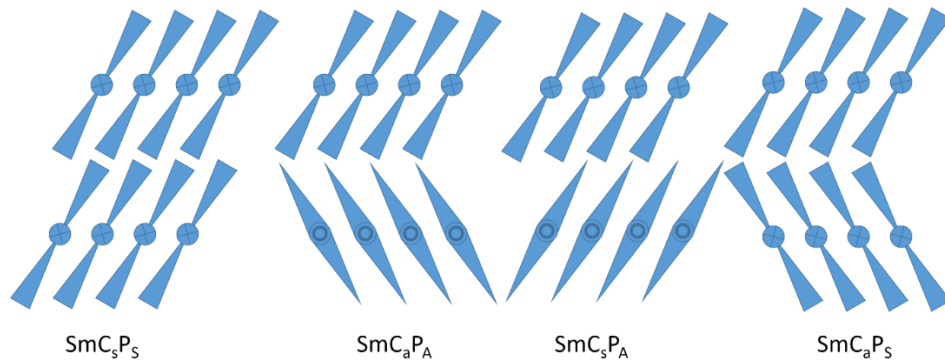


Figure 27: The symmetry in the nanoscale layer structure of the DC phase.

A saddle-splay deformation is associated with the high curvature of the smectic layers into a sponge-like structure, consistent with a very low or negative saddle-splay elastic constant in the nematic phase. The correlation length is such that the structures are of a sub-visible wavelength, making the texture optically isotropic. The origin of the optical activity of this phase is often attributed to layer chirality, of the coupling of layer and molecular chirality.

1.14. Phase Identification techniques

As liquid crystals have only weak molecular ordering, their textures occur over the whole range of a specimen, and the defects present appear on a relatively large scale i.e. from 1 to several hundred micrometres in size. This size range, as well as the nature of the defects makes the polarising transmitted light microscope an ideal instrument for the investigation and classification of liquid crystal phases. The use of a microfurnace with viewing ports through which the light beam can pass has made thermal optical microscopy an essential technique in the investigation of both thermotropic and lyotropic liquid crystals.

The study of defects in liquid crystal systems is based on the understanding of defects in crystalline solids. Crystals are rarely the perfectly arranged lattices of molecules used to exemplify the solid state, they usually contain a variety of defects i.e. point defects, line defects, dislocations, twinning and planar defects such as grain boundaries. In addition to these usual imperfections observed in the solid state, liquid crystals can also exhibit defects known as disclinations. These defects are not usually found in solids and result

from the liquid-like structures of mesophases giving rise to continuous but sharp changes in the orientations of molecules in the director field.

When defects are formed in crystals or liquid crystals the internal energy (H) rises; however the entropy (S) of the system also increases, resulting in a reduction in the overall free energy. The Gibbs free energy (G) is related to the internal energy and entropy in the manner shown in Equation 2.

$$G = H - TS$$

Equation 2: Calculation of internal Gibbs free energy.

As the number of defects rises the entropy of the system increases, resulting in a decrease in the overall free energy and, as a consequence the presence of defects leads to a stabilisation of the system.

1.14.1 Polarised Optical microscopy

Polarised optical microscopy of liquid crystals involves a magnified view of a thin sample of mesogenic material (5-25 μm thick), usually sandwiched between a glass microscope slide and a glass cover slip. The microscope slide is placed in an oven which can control the temperature, to an accuracy of ± 0.1 $^{\circ}\text{C}$, and the sample examined in transmission between two rotatable polarisers that are usually crossed at 90° with respect to one another. A typical microscope set up is shown in Figure 28.

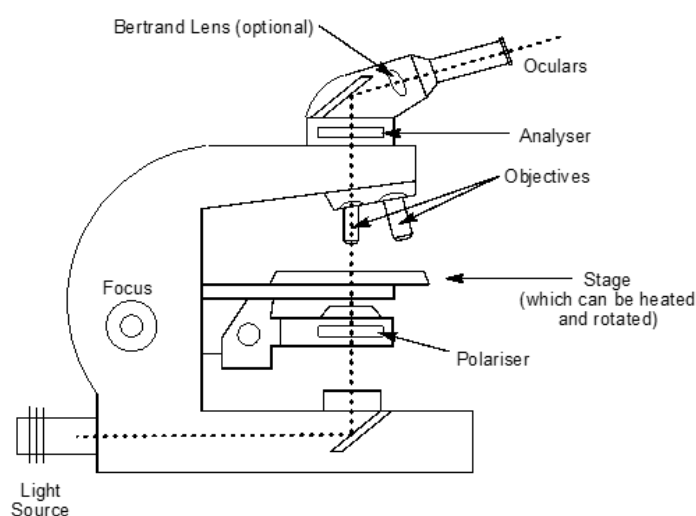


Figure 28: Schematic diagram of a typical microscope set up as used for liquid crystal analysis. The Bertrand lens is optional and allows for conoscopy.

Due to their anisotropic nature, liquid-crystalline materials have at least two refractive indices, a phenomenon known as birefringence, therefore the linearly polarised light (filtered to give vibration in a single plane, Figure 29) is refracted upon passing through the sample. The refracted light gives an interference pattern displaying optical defects. This leads to textures that can be characteristic of particular liquid crystal phases.

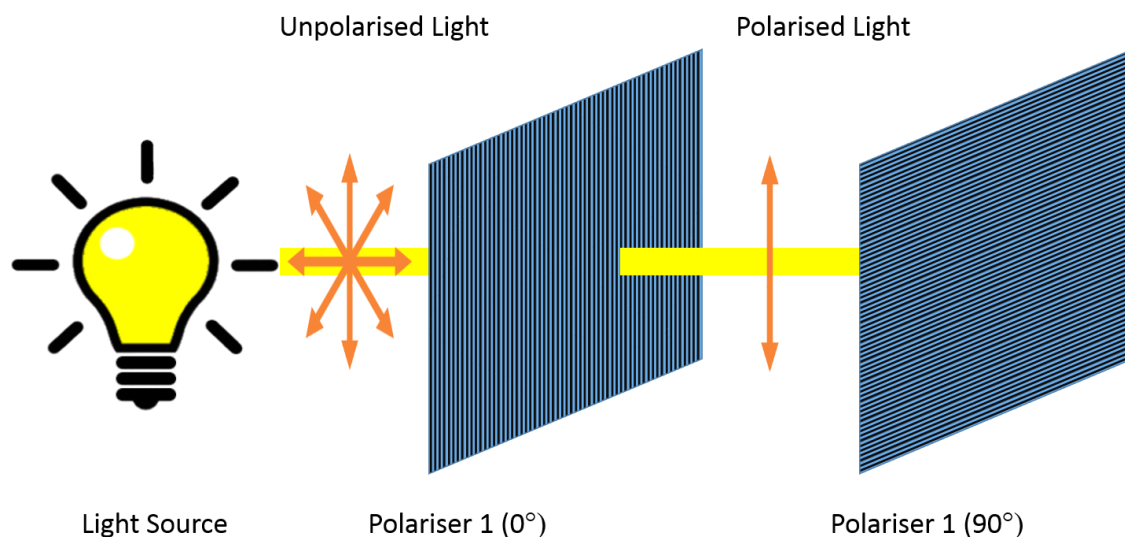


Figure 29: Schematic showing the process of polarisation of light. Samples are placed between polarisers 1 and 2.

The various mesophases can be identified via this method as they all display specific microscopic textures dependent on the ordering of the molecules within the phase. The textures of some of the mesophases described in this thesis are discussed in more detail in the following sections

1.14.1.1 Textures and defects of the nematic phase

As stated previously the nematic phase has the lowest degree of organisational order of the calamitic liquid crystal phases, and as such is most often observed as an optical texture upon cooling a thermotropic material from the isotropic liquid. Upon transition from the isotropic liquid to the nematic phase droplets are observed to form and coalesce, yielding the characteristic *schlieren* (German for streak) texture of the nematic phase, exemplified in Figure 30.

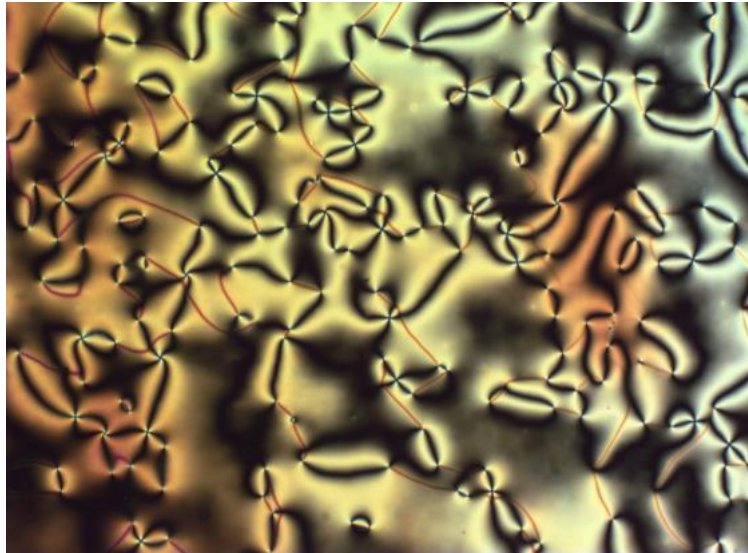


Figure 30: Characteristic *schlieren* texture of the nematic phase under crossed polarisers. (x100)

The nematic phase exhibits a high level of fluidity, therefore upon displacement of the cover slip of a specimen by mechanical force the texture is observed to shimmer intensely due to shear flow and Brownian motion. Singularities (defects) which appear as black crosses due to optical extinction can be clearly seen in these textures. The black lines which emanate from the defect points are known as *schlieren* brushes, and in the nematic phase both two and four brush defects can be clearly observed. The mechanism behind the formation of these defects is shown schematically in Figure 31.

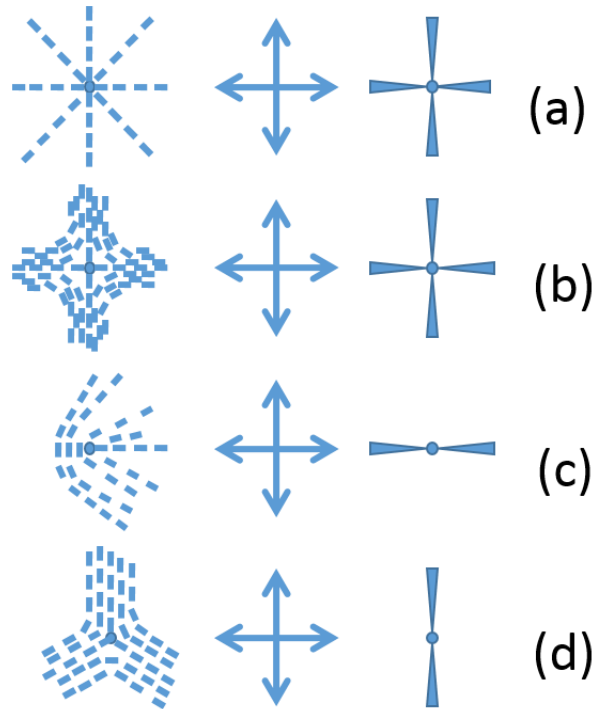


Figure 31: Molecular orientations associated with various *schlieren* defects.

The formation of *schlieren* brushes is associated with the process of creating a point defect, represented by the small circles in Figure 31. In Figure 31a and Figure 31b the formation of four-brush defects is shown, in Figure 31a the molecules are radially aligned and pointing towards the singularity while in Figure 31b the molecules are aligned away from the singularity. In both cases the crossed polarisers cause extinction of light in four regions, hence the four dark brushes. In Figure 31c and Figure 31d the formation of two-brush defects are shown. In these cases there are two regions where the molecules align with the polarisers, hence only two regions of optical extinction. These defects are only visible from above, appearing as a black thread-like disclination line when viewed parallel to the surface.

The nematic phase has also been found to exhibit a homeotropic texture when the molecular director lies perpendicular to the surface of the glass substrate. In this orientation the uniaxial nematic phase appears optically extinct under crossed polarisers, while the biaxial nematic exhibits a weakly birefringent *schlieren* texture.

1.14.1.2 Textures and defects of the Smectic A phase

Focal conic textures are optical textures usually observed in smectic mesophases when the layers are allowed to form curved structures. Focal conic domains (Figure 32) are typically observed in homogeneously oriented samples where the molecular director is in the plane of the glass substrate. The focal conic texture is the natural texture of both the smectic A and smectic C mesophases; consequently smectic phases formed on cooling either of these modifications will exhibit paramorphic textures but based on, but not necessarily true focal conic defects.

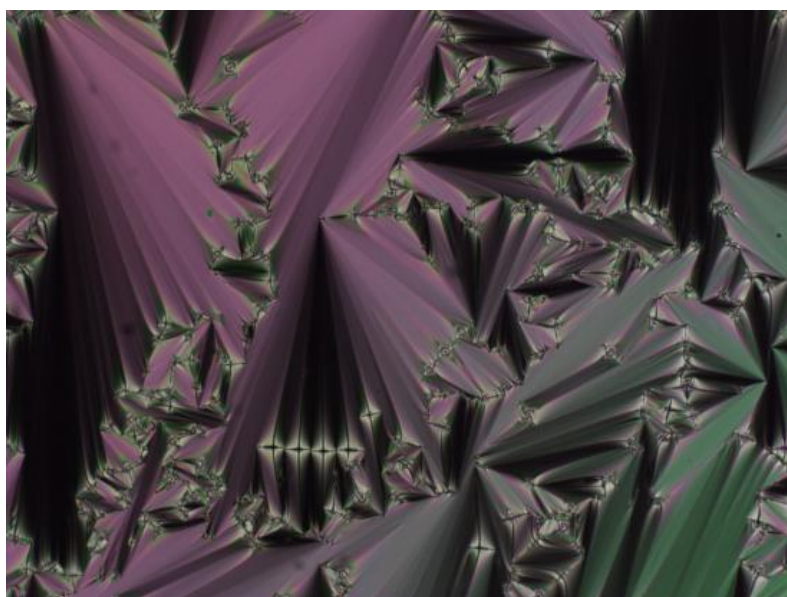


Figure 32: Focal-conic texture of the smectic A phase. (x100)

The curvature of the layers in the smectic phase is supportive of the formation of cylindrical, toric and Dupin cyclide defects, the most common of these defects is the Dupin cyclide. When the smectic A phase nucleates from either the isotropic liquid or the nematic phase it can do so with the formation of curved structures called *bâtonnets* i.e. layers of molecules add to a nucleation in a fashion reminiscent to the layers of an onion. When the phase forms a cylindrical structure this growing superstructure can loop back on itself to form a ring. In this “ring” the cylindrical layers will form a set of concentric tubes, i.e. tori. When the circular tubes grow at disproportionate rates on each side of the cylinder a lop-sided circular tube, or Dupin cyclide is formed. The formation of a focal conic defect is demonstrated pictorially in Figure 33. The growth of layers in the horizontal section of the defect is referred to as the *ellipse*, whereas a *hyperbola* is generated where the two curved layers meet. This structure appears to represent the lowest

energy packing arrangement of molecules in liquid-like layers.⁷⁵

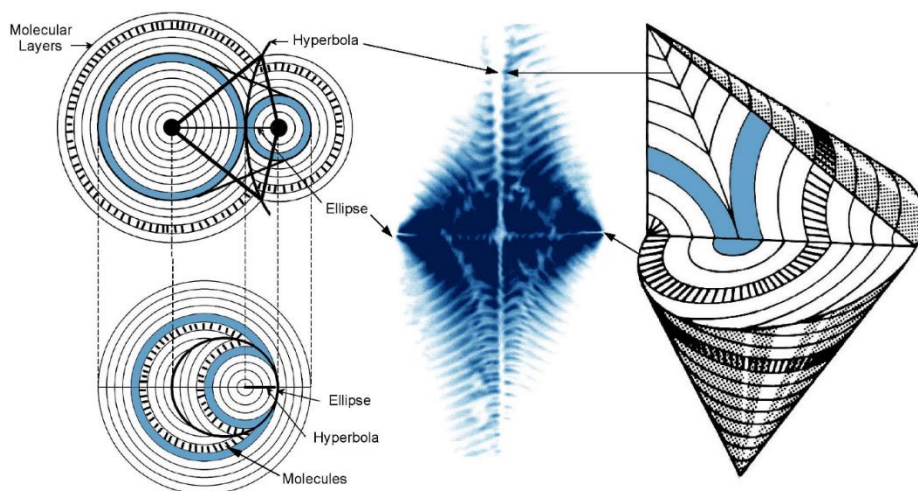


Figure 33: Formation and structure of a focal conic defect.⁹

The existence of the relationship between the ellipses and hyperbolae was confirmed by detailed microscopy studies of the texture of the SmC* phase, where the defect lines are parallel to the molecular layers. Thus in the internal structure of the focal conic domain is exemplified by a cross section of a focal conic domain of the helical SmC* phase. As the phase mirrors the smectic layers the texture at the centre of the figure shows an enhanced version of the molecular layers. In the representation of the focal conic domain to the right, the surface shows that the molecular long axes are radially oriented with respect to the apex of the conical domain but under the surface the layers curve, resulting in a mismatch of the long axes along the hyperbola. At the edge of the ellipse the molecules are also radially distributed, this results in both the ellipse and hyperbola showing up as lines of optical discontinuity i.e. black crosses under crossed polarisers.

Paramorphosis on cooling one focal-conic phase to another can show marked differences in optical texture, and can often be the most accurate measure of transition temperature. An example of this is that, on cooling from the smectic A to the smectic C phase, the molecules in the focal conic domain will tilt, distorting the structure of the domain, causing the observed defect texture to become patchy. This is referred to as the “breaking” of the focal-conic domains and is characteristic of molecular tilting i.e. the patchy domains are due to correlations of the tilt with the different “patches” corresponding to different directions of the tilt director.

As mentioned previously the SmA phase is an orthogonal, uniaxial phase with layer and

orientational ordering. When the molecules align with their long axes perpendicular to the glass substrate (homeotropic alignment) the polarised light is extinguished and the texture appears black as the phase appears isotropic when looking directly down the molecular long axis.

1.14.2 Differential Scanning calorimetry

Transitions between phases of matter are often accompanied by changes in enthalpy and entropy. Differential scanning calorimetry (DSC) is a technique used to measure the change in enthalpy and entropy associated with each phase transition of a material. The enthalpic (ΔH), and entropic (ΔS) change, associated with a phase transition is related to the amount of order that is gained or lost upon moving from one phase to another, however the magnitudes of the enthalpy and entropy changes are not a direct indicator of the mesophase type i.e. the precise phase cannot be determined from DSC alone but the technique can give insights into the degree of molecular ordering within the material. When used in combination with POM DSC is an essential technique in the identification of mesophase behaviour as it can reveal transitions that are difficult to observe optically, for example, the transition from the smectic A to hexatic B phase, both of which have similar defect textures.

Differential scanning calorimetry examines the nature of phase transitions by measuring the heat capacity of a material as a function of temperature against that of a standard reference. The calorimeter measures the relative uptake or output of heat from a sample in reference to the empty sample holder via a reference platinum sensor. The data obtained is output as heat flow in milliwatts as a function of temperature, the plot of which shows peaks at the phase transitions, the areas under which are the latent heats of the transition. Transition temperature is calculated by determining the temperature at which the gradient in the heat flow against temperature is maximum. There are two major varieties of DSC, one of which is shown in Figure 34, that work under similar principles with slight differences in experimental setup with respect to power compensation and heat flux. In

this research a heat-flux set up was used as shown in Figure 34.

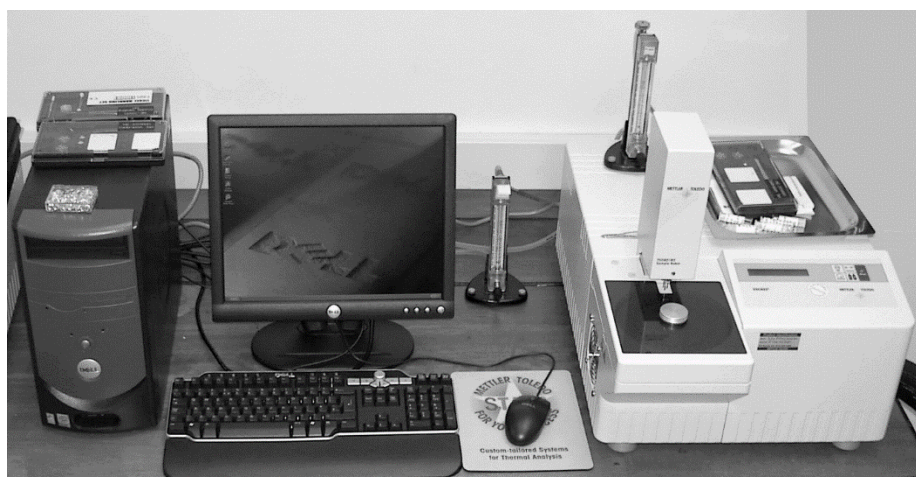


Figure 34: Typical microprocessor controlled differential scanning calorimeter with autosampler.

The internals of the system shown in Figure 34 are shown diagrammatically in Figure 35. The difference in thermal energy required to maintain both the sample and reference pans at the same temperature is measured as a function of temperature. The principle underlying this technique is that, as the material undergoes a physical transformation i.e. a phase transition more/less heat will flow to the sample pan than to the reference in order to maintain the temperature. Whether more or less thermal energy flows to the sample is determined by whether the phase change the material is undergoing is exothermic or endothermic, a typical DSC trace is shown in Figure 36.

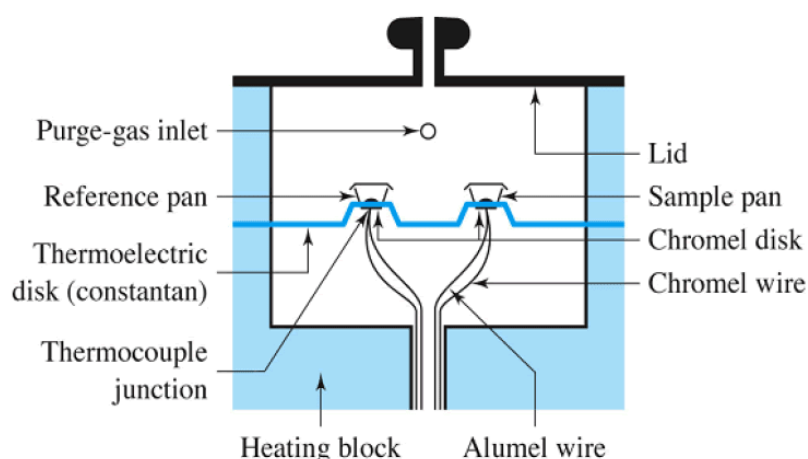


Figure 35: Schematic of the internals of a heat-flux DSC.⁷⁶

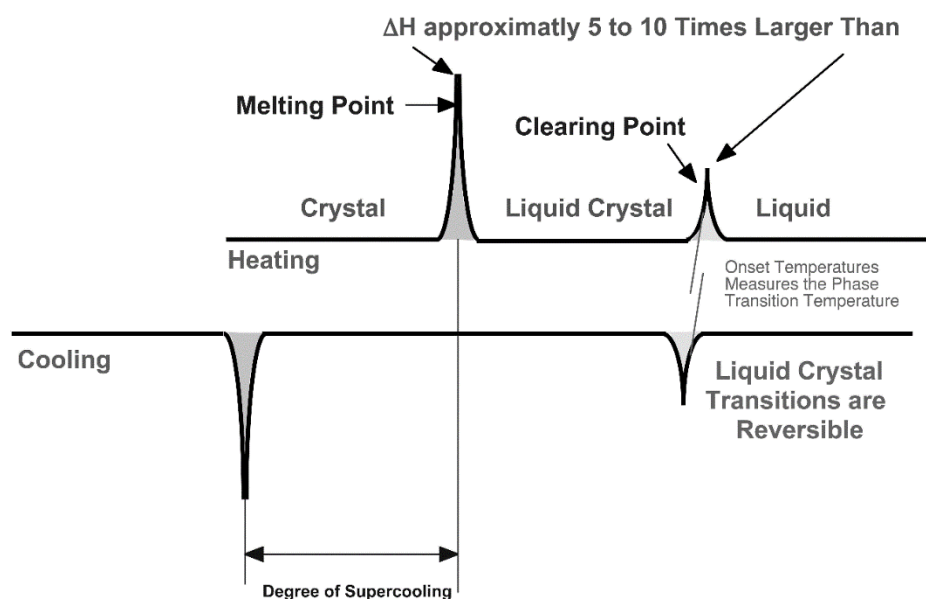


Figure 36: Typical DSC thermogram of a liquid crystal.⁷⁶

In the typical thermogram shown in Figure 36 the phase transition observed for the initial melt from crystal to liquid crystal is an order of magnitude higher than the transition from the liquid crystal to the isotropic liquid. This is due to the enthalpy associated with the melting point being that of the breakdown of the crystal lattice, a highly ordered structure requiring significant energy to break. In DSC onset temperatures of isotropic liquid-liquid crystal and liquid crystal-liquid crystal should be reproducible to within a degree on heating and cooling, while the melting/crystallisation temperatures can vary more widely due to kinetic factors such as the degree of supercooling observed for the sample. The magnitude of the enthalpy change upon transition from one phase to the other varies depending on the difference in the degree of ordering between each successive phase. An example is that, the transition between the nematic and smectic A phases typically has a ΔH in the range of 0.4-3.2 kJ mol⁻¹, showing that the phases possess similar structures. A transition between the more ordered hexatic B phase and the smectic C phase usually has a ΔH in the range of 0.8-4 kJ mol⁻¹ reflecting the change in weak lattice ordering.

1.14.3. X-Ray diffraction

The study of the structures of liquid crystals by X-ray diffraction can be conducted in similar ways to the study of crystalline materials. The main exception is that XRD of liquid crystals provides much less information than similar techniques for crystalline

materials, and the scattering of the X-rays by the liquid crystal is often weak and diffuse. This stems from the fact that, compared to the crystalline solid, liquid crystal phases are inherently disordered, with any ordering being across a relatively short range. Analysis is conducted using the Bragg Law, which concerns the constructive interference of X-rays reflected from different, yet adjacent planes within a structure (Figure 37). In this law the distance between the layers is denoted as d , the angle of the incident X-ray as θ , and the wavelength of the X-ray as λ .

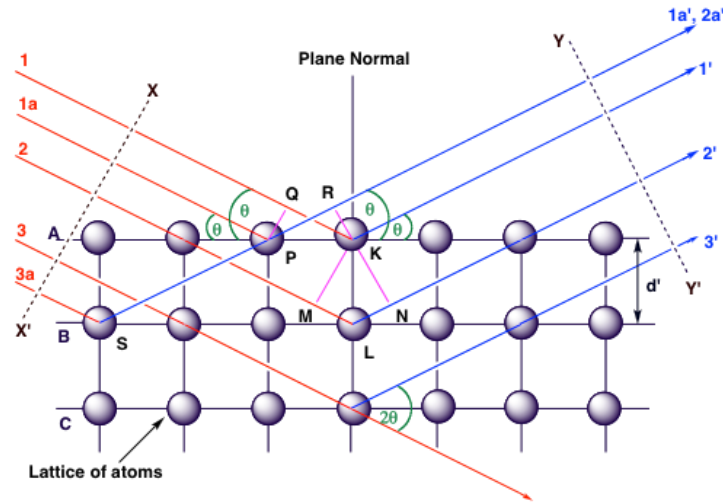


Figure 37: Derivation of the Bragg equation using X-ray scattering from a periodic lattice.

Rays 1 and 1a in the incident beam strike K and P in the first plane of atoms, these X-rays are then scattered in all directions, however in directions 1' and 1a' the resulting scattered X-rays interfere constructively with one another. The difference in the path lengths between wave fronts XX' and YY' is denoted by Equation 3.

$$QK - PR = PK\cos\theta (= 0)$$

Equation 3: Calculation of the distance between XX' and YY' .

This holds true for all atoms in the first plane in a direction parallel to 1', and also for the atoms in adjacent planes. Rays 1 and 2 are scattered by atoms K and L, and the path difference between $1K1'$ and $2L2'$ is denoted by Equation 4.

$$ML + LN = d'\sin\theta + d'\sin\theta$$

Equation 4: Calculation of the path difference between $1K1'$ and $2L2'$.

This is also the path difference for the overlapping rays scattered by S and P in the direction shown, since in this direction there is no path difference between rays scattered by S and L or P and L. Scattered rays 1' and 2' will be completely in phase if this path difference is equal to an integral number of wave lengths, as stated by the Bragg Law (Equation 5).

$$n\lambda = 2d'\sin\theta$$

Equation 5: Bragg Law

Figure 38 shows examples of what the diffraction pattern might look like for solid and soft crystal phases. In both cases the XRD pattern exhibits sharp diffraction peaks caused by the long range order, however due to thermal motion the intensity of the peak decreases as the order of the peak increases.

If the positional order decays with distance from a fixed reference point the diffraction pattern is dependent on how that decay occurs. If the positional order decays algebraically, i.e. it is proportional to L^η where L is the distance from the reference point and η is a temperature-dependent constant, then the diffraction pattern will contain broad peaks instead of narrow ones. This is known as quasi-long range order and is exemplified in Figure 38 by the XRD pattern of the hexatic phase.

Finally if the positional order decays exponentially, meaning it is proportional to $e^{-L/\zeta}$ where ζ is a temperature-dependent constant then the diffraction pattern will contain even broader peaks. This represents short range order and is exemplified in Figure 38 by the XRD pattern of the smectic phase.

The same descriptors used for positional order can also be used to describe the decay of orientational order. However orientational order does not produce the peaks in the diffraction pattern that positional order does. The width of the peaks in the diffraction pattern can also be used to describe the positional order of the material, with a broader peak indicating less positional order.

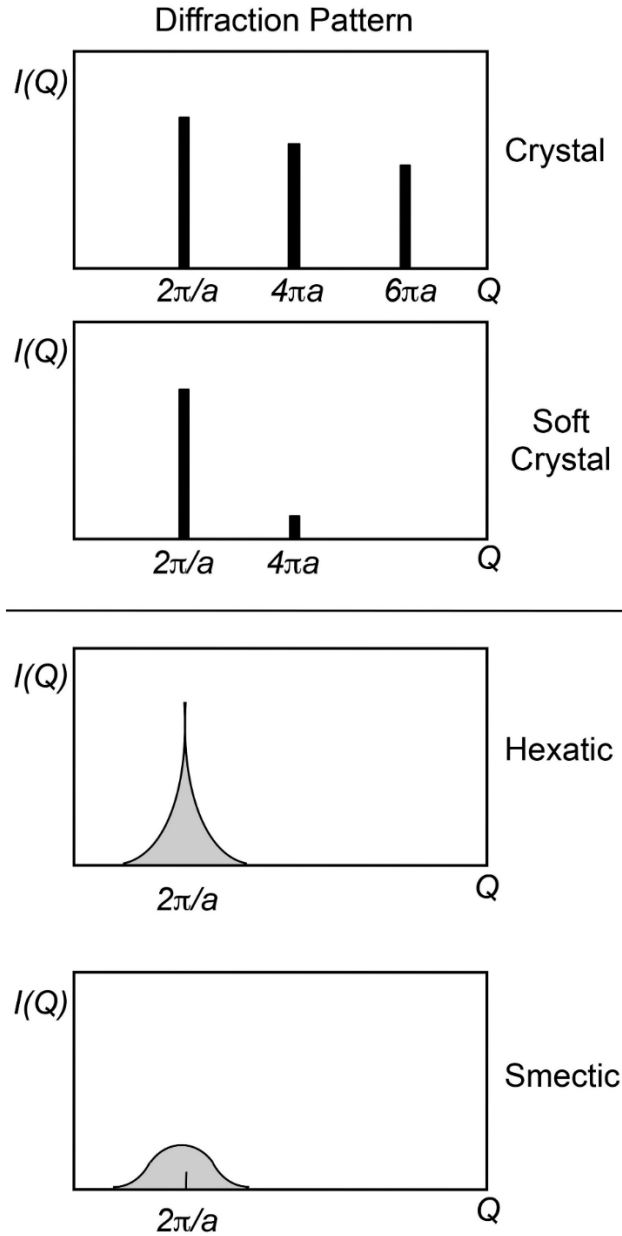


Figure 38: XRD patterns of materials with different degrees of order. Long range for crystal and soft crystal, quasi-long range for hexatic and short range for smectic.

Barring the nematic phase, which has long range orientational order but no short range positional order of the molecules, the other calamitic mesophases are more similar in their local packing arrangement to the crystalline solid, as shown by the related Bravais lattices. The way the molecules in these mesophases arrange with respect to the layer plane can be divided into two groups; either the molecules are, on average, perpendicular to the layer plane (SmA, SmB, Cryst. B, Cryst. E) or they are tilted with respect to the layer plane (SmC, Hexatic I, Hexatic F, and Crystals J, G, H and K) with the layers themselves

repeating over either short or long distances in the direction of the layer normal. As mentioned previously, in the case of some of these materials the explicit definition of “lamellar” is somewhat misleading, as the layers are not so well defined as that nomenclature would imply, indeed in some of the smectic materials the layers are almost non-existent except in the form of a density wave of the masses of molecules as exemplified in Figure 39, with the top example showing a phase in which the molecules are on average upright, while the bottom example shows a phase where the molecules are on average tilted with respect to the layer plane. These schematics show that the layers are not well defined lines of molecules organising into a lamellar structure, but rather a continuous system where the so called layers are best described by the distribution of molecular mass over a number of repeats (>10)

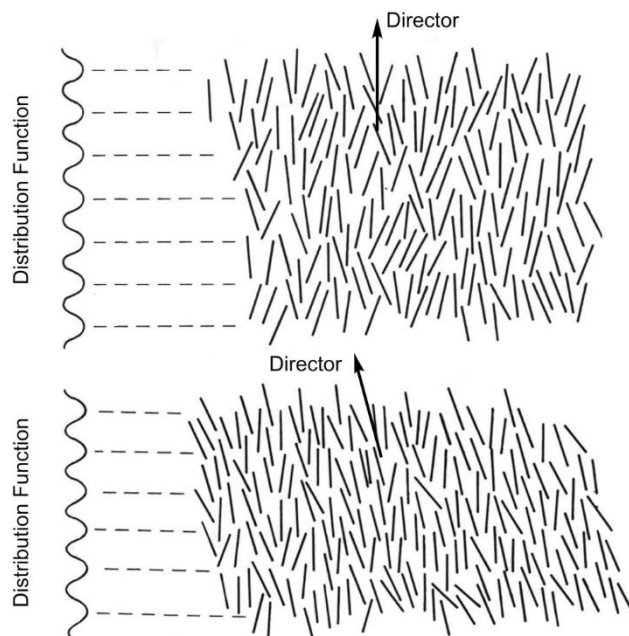


Figure 39: Smectic A (top) and C (bottom) phases represented as density wave patterns.

Chapter 2: Aims

2. Aims

As discussed in the introductory chapter, liquid crystals of unusual shape, particularly those possessing an overall bend within the molecular architecture, are prone to exhibiting novel and unusual mesomorphic behaviour when compared to standard calamitic materials, even those with similar molecular architectures, such as having identical rigid units in the arms of the material.

The phases exhibited by liquid crystals of bent molecular architecture tend to be governed by which family of “bent-core” or “bimesogen”, the material belongs to. Bent core materials tend to be more prone to exhibit phases such as “Banana” phases, also referred to as B phases, while the more flexible bimesogens are more strongly inclined towards nematic phases.

This work aims to outline a set of structure-property relations for materials comprised of bent molecules.

2.1. Synthetic targets

As outlined in the previous chapter, this research is aimed at creating a set of structure-property relationships across all families of materials composed of “bent-shaped” components, with a particular focus on the effect of the difference in molecular bend and conformational freedom between bimesogenic and bent core materials. To this end series of materials belonging to each family were synthesised and the target structures are described schematically below in terms of rigid and flexible moieties.

2.1.1. Pseudo bent-core materials

One study was based on bent-core materials where there is little flexibility at the centre of the molecule as shown in Figure 40. This time, due to the more fixed molecular conformation when compared to the bimesogens the liquid crystal properties of the materials could be related to the “angle of bend” imparted by the rigid spacer unit. There was an alternative motive for this study, and that was the synthesis of materials that exhibited the elusive dark conglomerate phase. As such the target was the design of materials with rigid, bent central cores and flexible aliphatic terminal units, an effective inversion of the first two series of bimesogens. However rather than use a completely rigid core i.e. an oxadiazole or other equivalent it was decided to use a bisphenol central

unit in order to investigate the effects of allowing a slight amount of flexibility on the mesogenic behaviour of these compounds.

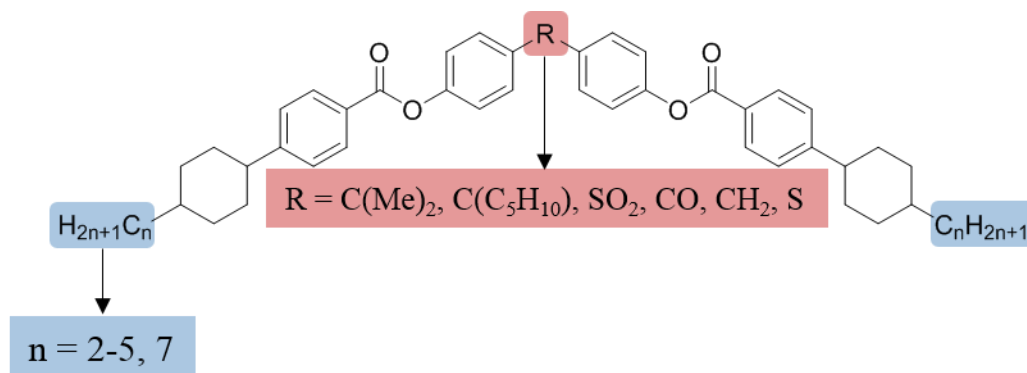


Figure 40: General structure of target pseudo bent-core materials.

The materials were to be prepared by standard synthetic methods and their properties analysed by standard analytical techniques (NMR, IR and MS spectroscopic techniques and POM, DSC and XRD to analyse the mesomorphism). It should be noted that a number of intermediates were supplied by Dr. Richard Mandle and will be indicated as such within the text.

2.1.2. Target Bimesogens

As previously stated, bimesogenic liquid crystals are materials with two rigid groups linked by a flexible spacer unit, which is often a methylene chain, usually of odd parity. These materials have been shown in recent years to have a tendency to exhibit the so called twist bend nematic (N_{TB}) phase. The exact relationship between molecular architecture and the occurrence of the N_{TB} phase is still not fully understood, with early N_{TB} materials tending to be methylene linked biphenyl materials terminated with polar groups such as nitrile and nitro moieties.

The first target is based on the family of bimesogenic phenyl benzoate esters that are terminated with rigid conjugating and non-conjugating polar moieties and flexible non-polar aliphatic chains (Figure 41). The phenyl benzoate esters are linked to one another by methylene or methylene dimethoxy chains of odd parity. This study will allow for a structure property correlation for the N_{TB} phase via both the comparison of polar and non-polar terminal groups, as well as via the investigation of both methylene spacers of different lengths (7 and 9 units) as well as the alteration of the chemical nature of the

spacer chain (heptamethylene vs. pentamethylenedioxy).

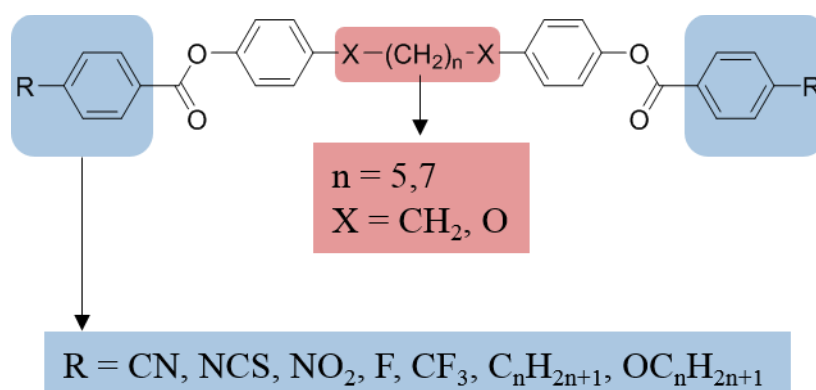


Figure 41: General structure of the target bimesogenic phenyl benzoates.

The second set of materials to be investigated were similar to the first. The bridging chain was again of odd parity and joined to the methylene units by oxygen atoms. In this set of materials however, rather than phenyl benzoate esters the rigid units were based on the biphenyl group, a ubiquitous example of a liquid crystal end group. The selected biphenyl units were primarily polar, in keeping with literature materials. Moreover the synthetic pathway used allowed the synthesis of asymmetric bimesogens as shown in Figure 42.

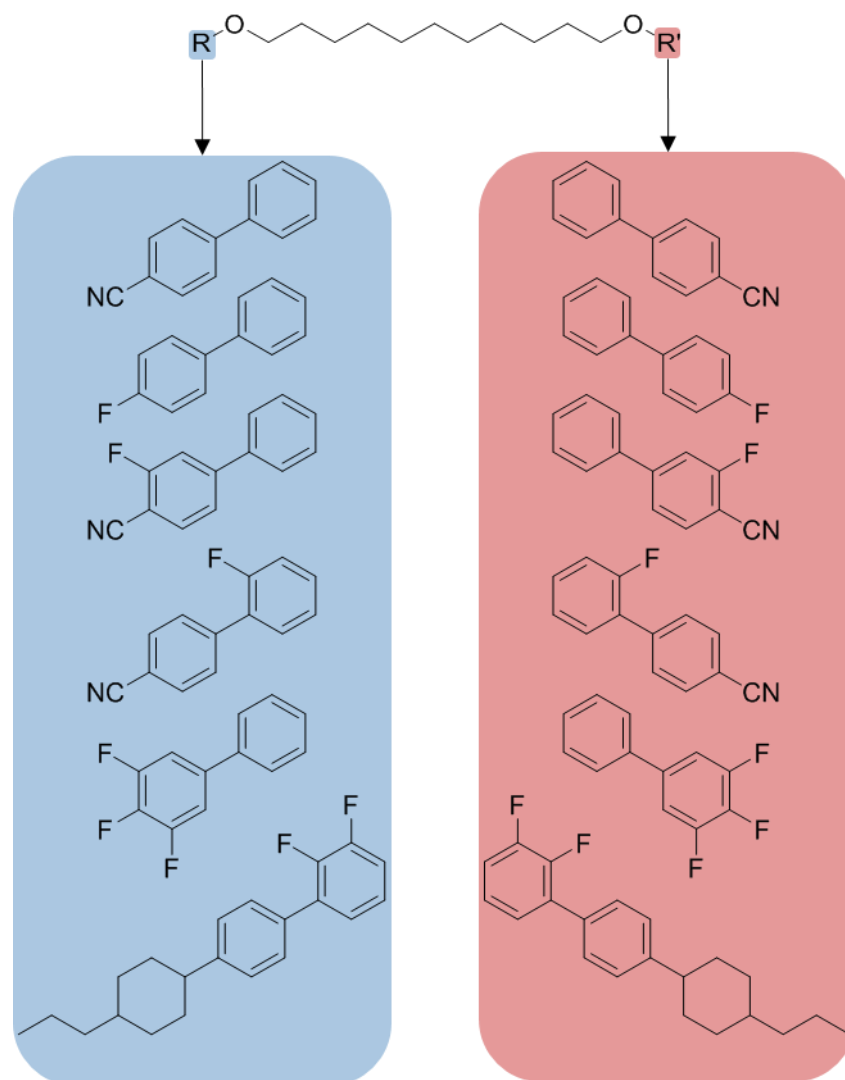


Figure 42: General structure of target unsymmetrical bimesogens.

Chapter 3: Synthetic Methods

3. Synthetic methods

3.1. Reagents

Unless otherwise stated all reagents were procured from Sigma-Aldrich, Fluorochem, Apollo Scientific or Alfa Aesar and used without further purification. Solvents were obtained from Fischer Scientific or VWR. N-(3-Dimethylaminopropyl)-N'-ethylcarbodiimide hydrochloride (EDAC), was purchased from Carbosynth and used as received.

3.2. TLC and column chromatography

Reaction progress was monitored by TLC using appropriate solvent systems with silica coated aluminium plates (Kieselgel 60 F-254) purchased from Merck and visualised using ultraviolet light (254 or 365 nm) or oxidation using potassium permanganate stain. Separation via column chromatography was carried out using flash grade silica gel (Fluka, 70-230 mesh, 63 μm – 200 μm particle size). When appropriate; flash, or dry flash techniques were used to achieve increased flow rate.

3.3. Nuclear Magnetic Resonance spectroscopy

^1H NMR, ^{13}C NMR and ^{19}F NMR were recorded on a JEOL ECX spectrometer operating at a frequency of 400 MHz (^1H), 100.5 MHz (^{13}C) or 376.4 MHz (^{19}F). For all spectra the residual protic solvent was used as an internal standard.

3.4. Mass spectrometry

Electrospray Ionisation Mass Spectra were recorded using a Bruker micrOTOF MS-Agilent series 1200 LC spectrometer.

3.5. Infra-Red Spectroscopy

Infra-red spectra were recorded using an IR Prestige-21 with a Specac Golden Gate diamond ATR IR insert.

3.6. High Performance Liquid Chromatography

HPLC traces were recorded using a Shimadzu Prominence modular HPLC system comprising a LC-20A pump, a DGU-20A5 degasser, a SIL-20A autosampler, a CBM-20A communication bus, a CTO-20A column oven, and a SPO-20A dual wavelength UV-vis detector. The column used was an Alltech C18 bonded reverse-phase silica column with a 5 μm pore size, an internal diameter of 10 mm and a length of 250 mm

3.7. Polarised Optical Microscopy

POM was carried out using a Zeiss Axioskop 40 Pol microscope using a Mettler FP82HT furnace, which was controlled by a Mettler FP90 control unit. Photomicrographs were taken using an InfinityX-21 MP digital camera mounted atop the microscope. Photomicrographs were captured at 100 x magnification unless otherwise stated.

3.8. Electro-optic measurements

Samples were flow filled via capillary action into 5 μm cells purchased from Linkam, maintaining the sample in the isotropic liquid during the filling process. The cells were internally coated with polyimide and buffed in an antiparallel manner to promote planar alignment. The active area of the cell was 0.81 cm^2 . Wires were attached using indium solder. The cells were observed using a Zeiss Universal microscope, equipped with a Mettler FP82HT hotstage, controlled by a Mettler FP90 temperature controller. The external field was generated by a Hewlett Packard 33120A arbitrary waveform generator and amplified by a linear x20 amplifier that was custom built by QinetiQ. The electrical response from the cell was amplified by a nanocurrent amplifier (20 $\text{k}\Omega$ or 100 $\text{k}\Omega$ impedance) and fed into a Hewlett Packard 54600B oscilloscope. Electrical fields used ranged from 1-20 $\text{V } \mu\text{m}^{-1}$ and in all cases a square waveform was used. Electrical fields were not applied during the cooling of samples so as not to influence the formation of mesophases.

3.9. Differential Scanning calorimetry

Differential scanning calorimetry was performed on a Mettler DSC822e fitted with an autosampler operating with Mettler Star-e software and calibrated before use against an indium standard (onset = 156.55 ± 0.2 °C, $\Delta H = 28.45 \pm 0.40$ J g⁻¹) and a zinc standard (onset = 419.53 ± 0.4 °C, $\Delta H = 108.00 \pm 0.8$ J g⁻¹) under an atmosphere of dry nitrogen. Samples were confined in 20 µl aluminium pans and run against an empty reference pan.

3.10. X-Ray Diffraction

Small angle X-ray diffraction was performed using a Bruker D8 Discover diffractometer equipped with a temperature controlled, bored graphite rod furnace, custom built at the University of York. The radiation used was copper K α ($\lambda = 0.154056$ nm) from a 1 µS microfocus source. Diffraction patterns were recorded on a 2048x2048 pixel Bruker VANTEC 500 area detector. Samples were filled into 1mm o/d capillary tubes and aligned with a pair of 1T magnets. Diffraction patterns were collected as a function of temperature and the data processed using Matlab. Typical exposure times ranged from 10-30 seconds and data was collected over a range of $d = 8$ -110 Å.

Resonant Soft X-Ray Scattering experiments were carried out by Chenhui Zhu and Mirosław Salamończyk of the Lawrence Berkeley National Laboratory Advanced Light Source.

3.11. Computational Chemistry

Computational chemistry was performed using the using Gaussian G09 revision d01⁷⁷ on the York Advanced Research Computing Cluster (YARCC). Calculations were carried out to the B3LYP/631G-d level of theory unless stated otherwise.

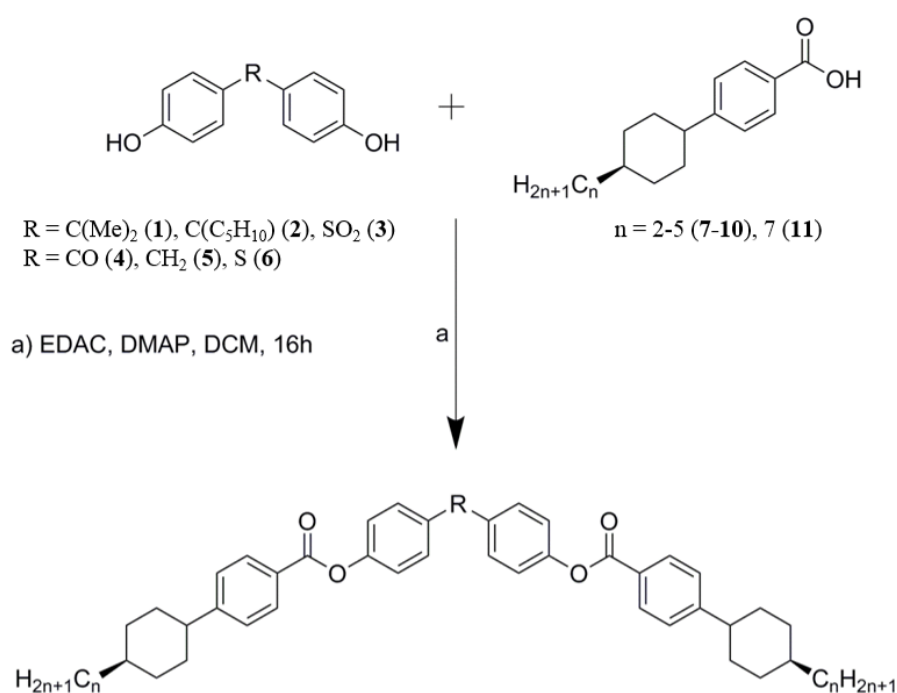
3.12. Preparation of Liquid Crystal mixtures

For 2 component mixtures the materials were accurately weighed into 2 separate 2ml vials using a Mettler XS analytical balance. Dichloromethane was added to the vial containing component A, the resulting solution was then transferred to the vial containing compound B and vial A washed several times to ensure complete transfer. Solvent was removed by heating the open vial to approx. 40 °C for 24 hours. Mixture properties were examined using POM, DSC and, where appropriate, XRD.

3.2. Synthetic procedures

3.2.1. Preparation of pseudo bent-core materials (compounds 12-41)

In order to investigate the effects of slightly increasing molecular flexibility on the properties of bent-shaped liquid crystals series of materials with varying central units were prepared according to the synthetic strategy shown in Scheme 1. Commercially available bisphenols were reacted with a range of benzoic acids with C₂-C₇ terminal chains using EDAC and DMAP in DCM at ambient temperature. The reaction mixture was purified via dry flash column chromatography (DCM over silica) and recrystallisation from an appropriate ethanol/THF mixture.



Scheme 1: General synthesis of pseudo-bent core materials (compounds 12-41).

R	Compound No.
C(Me) ₂	12-16
C(C ₅ H ₁₀)	17-21
SO ₂	22-26
CO	27-31
CH ₂	32-36
S	36-41

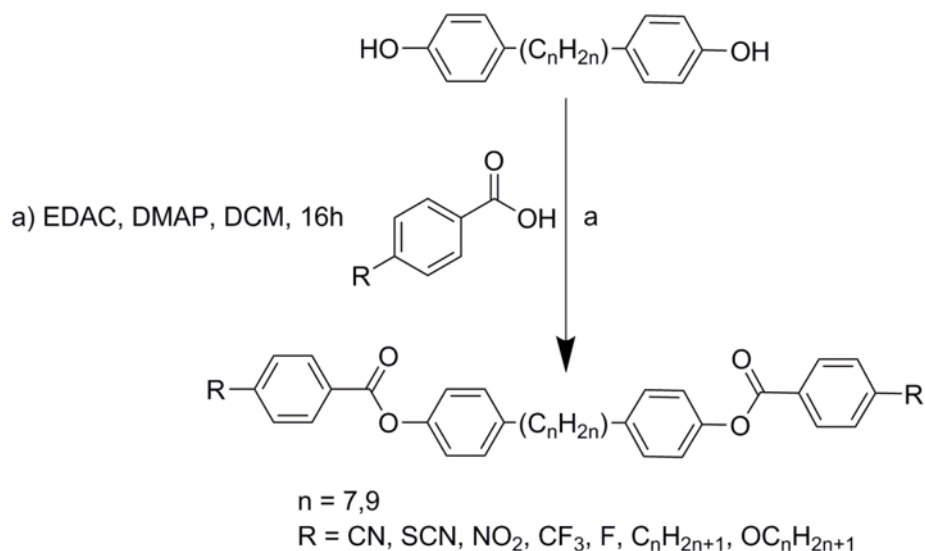
Table 1: Compounds synthesised via Scheme 1.

Preparation of bimesogens with a flexible spacer unit

Two broad families of bimesogens were prepared in this work, symmetrical and unsymmetrical compounds. The symmetrical compounds were either linked by a methylene spacer unit (synthetic pathway outlined in Scheme 2) or with an ether linkage (synthetic pathway outlined in Scheme 3)

3.2.2. Preparation of hepta- and nonamethylene linked bimesogens (compounds 42-52 and 66-76)

4-4'-alkyldiphenols with chain lengths C_7 and C_9 were prepared in house by Dr. Richard Mandle. These diphenols were esterified with a variety of para-substituted benzoic acids via Steglich esterification using EDAC and DMAP in DCM at ambient temperature as shown in Scheme 2. Products were purified via column chromatography (DCM over silica) and recrystallised from an appropriate ethanol/THF mixture.



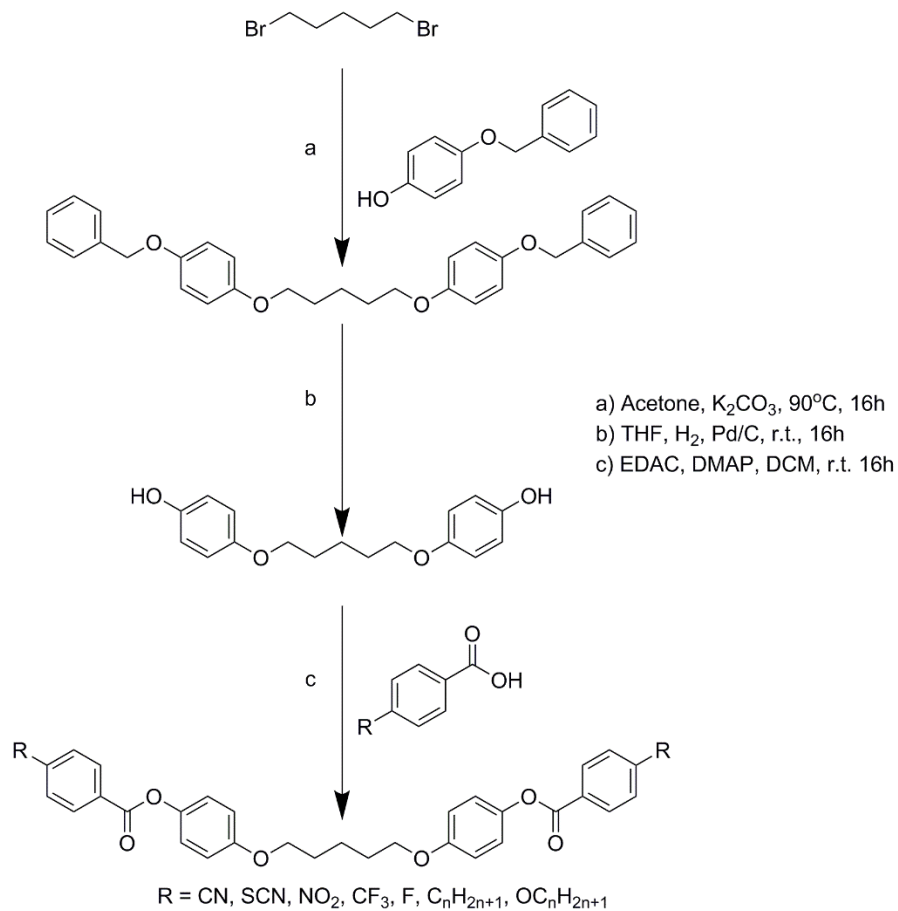
Scheme 2: General synthesis of methylene linked liquid crystal dimers ($n = 7$ compounds 42-52, $n = 9$ compounds 66-76).

R	n	Compound No.
CN	7	42
SCN	7	43
NO ₂	7	44
CF ₃	7	45
F	7	46
C ₂ H ₅ -C ₄ H ₉	7	47-49
OC ₂ H ₅ -OC ₄ H ₉	7	50-52
CN	9	66
SCN	9	67
NO ₂	9	68
CF ₃	9	69
F	9	70
C ₂ H ₅ -C ₄ H ₉	9	71-73
OC ₂ H ₅ -OC ₄ H ₉	9	74-76

Table 2: Compounds synthesised via Scheme 2.

3.2.3. Preparation of ether linked bimesogens (compounds 55-65)

The ether linked compounds were prepared according to the methodology outlined in Scheme 3. Dibromopentane was reacted with 4-benzyloxyphenol via a Williamson ether synthesis using potassium carbonate in acetone to give compound **53** (Scheme 3a). Subsequently the benzyl group was removed via hydrogenation using 10% palladium-on-carbon in THF under an atmosphere of hydrogen, see Scheme 3b). The resulting diphenol (compound **54**) was reacted with a variety of para substituted benzoic acids via Steglich esterification using EDAC and DMAP in DCM at ambient temperature as shown in Scheme 3c).



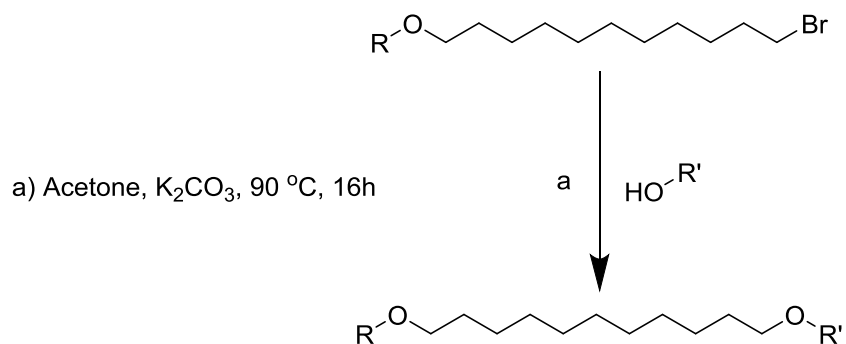
Scheme 3: General synthesis of ether linked liquid crystal dimers (compounds **55-65**).

R	Compound No.
CN	55
SCN	56
NO ₂	57
CF ₃	58
F	59
C ₂ H ₅ -C ₄ H ₉	60-62
OC ₂ H ₅ -OC ₄ H ₉	63-65

Table 3: Compounds synthesised via Scheme 3.

3.2.4 Preparation of unsymmetrical bimesogens (compounds 77-84)

The unsymmetrical compounds were prepared according to the methodology outlined in Scheme 4. Dr. Richard Mandle provided a selection of 4-(ω -bromoalkoxy)biphenyl compounds that had been prepared in house. These compounds were reacted with a variety of substituted 4-hydroxybiphenyls via a Williamson ether synthesis using potassium carbonate in acetone. The products were purified by column chromatography and recrystallised from an appropriate ethanol:THF mixture.



Scheme 4: General synthesis of unsymmetrical materials.

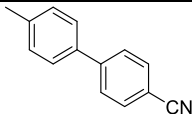
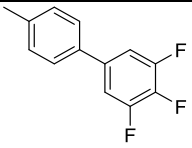
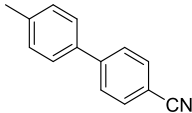
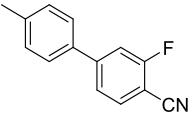
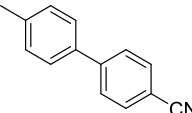
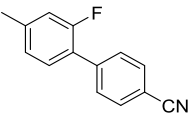
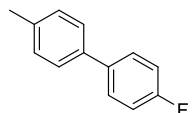
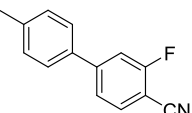
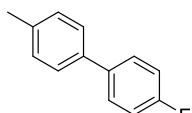
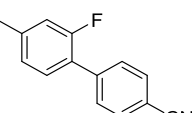
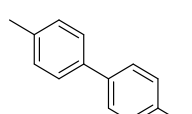
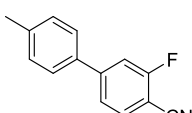
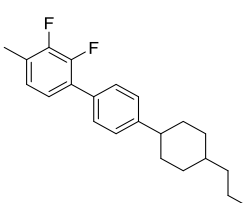
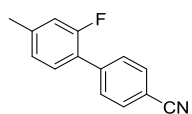
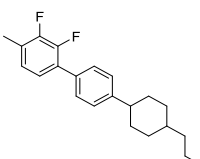
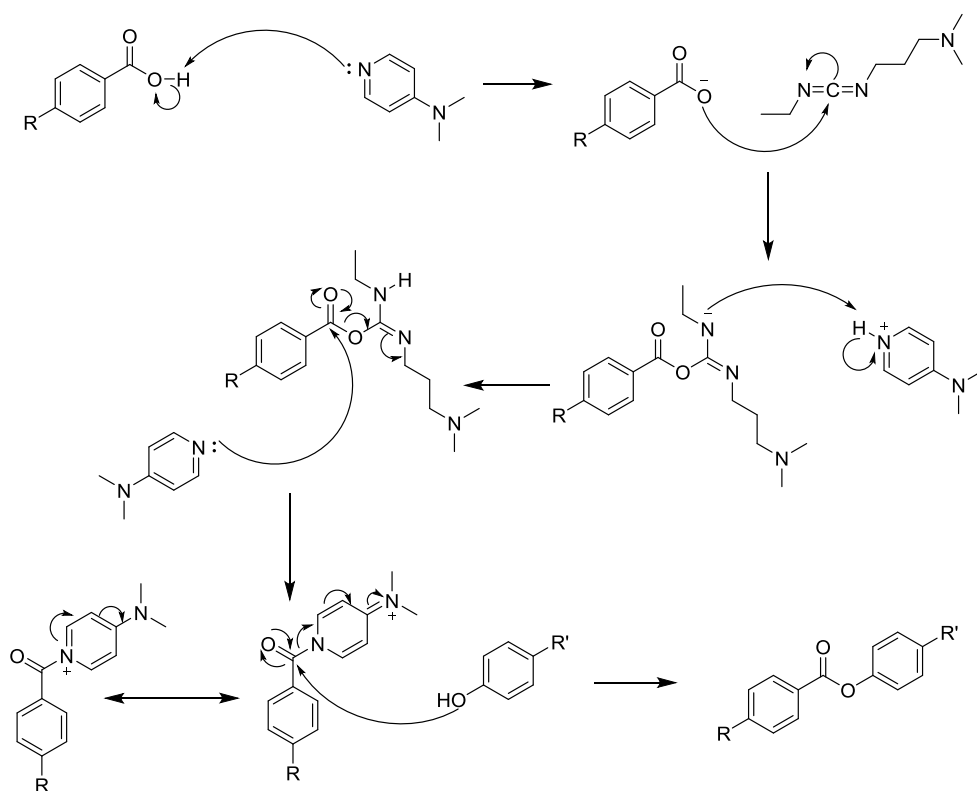
Compound No.	R	R'
77		
78		
79		
80		
81		
82		
83		
84		

Table 4: Compounds synthesised via Scheme 4.

3.2. Synthetic discussion

3.2.1. Steglich Esterification

1 equivalent of the starting biphenol, ≈ 2.2 equivalents of the appropriate benzoic acid, 3 equivalents of EDAC and a catalytic amount of DMAP were dissolved in the minimum amount of DCM. The reaction was stirred at ambient temperature and pressure for 16 hours. The resulting reaction mixture was then purified by flash column chromatography (DCM over silica) and recrystallised from an appropriate ethanol:THF mixture. The resulting pure product was dried via suction prior to characterisation

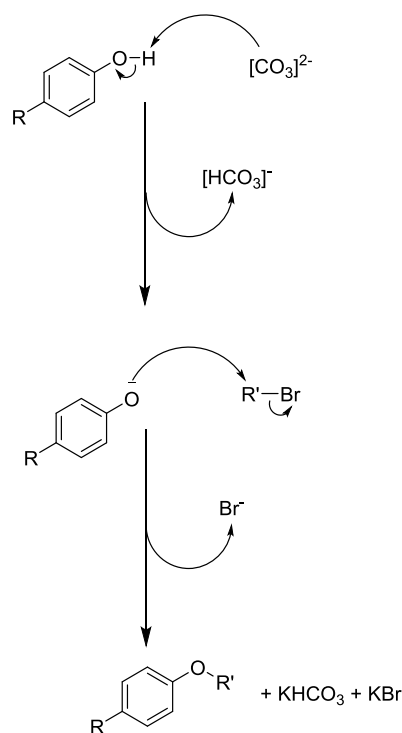


Mechanism 1: Mechanism of the Steglich esterification.

For these reactions it was considered prudent to use a slight excess of the benzoic acid with respect to the biphenol, this served to drive the reaction to completion, and the benzoic acid was trivial to remove during purification as the high polarity of the carboxylic acid group caused it to remain bound to the silica while the product eluted. EDAC was chosen as a coupling agent as opposed to DCC, another commonly used reagent in this reaction, as it can be difficult to remove trace amounts of DCC from the reaction via chromatography and recrystallisation, therefore to pre-emptively address these concerns EDAC, which is easier to remove during purification

3.3.2. Williamson ether synthesis

1 equivalent of the appropriate bromoalkane, 2 (compound **53**) or 1 (compounds **77-84**) equivalents of the corresponding phenol and 3 equivalents of potassium carbonate were suspended in the minimum volume of acetone. The reaction mixture was heated to 90 °C and allowed to reflux. The reaction was monitored via TLC and upon complete consumption of the bromoalkane or after 16 hours the mixture was filtered via vacuum filtration in order to remove any precipitated potassium bromide. The acetone was then removed *in vacuo* and the crude product re-dissolved in DCM. The crude product was then purified via column chromatography (DCM over silica) and then recrystallised from an appropriate ethanol:THF mixture.

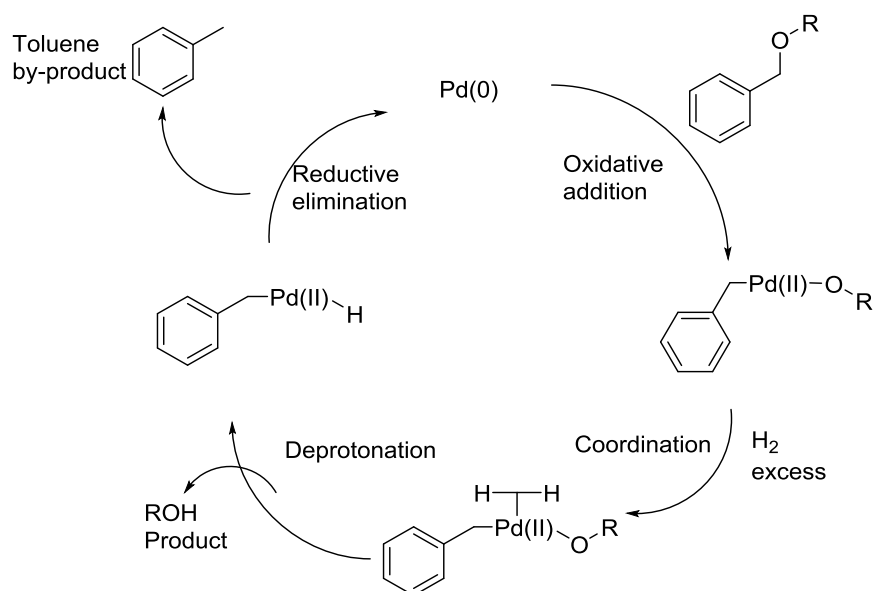


Mechanism 2: Mechanism of the Williamson ether synthesis with K_2CO_3 as a base.

Acetone was chosen as the reaction solvent for two reasons, firstly is the simple reason that both the alkyl halides and the phenols were soluble in acetone, as well as the potassium carbonate dissolving well in acetone once heated. The second reason was the relative insolubility of the potassium bromide in acetone. KBr is one of the by-products of this reaction and, by using a solvent in which it is only sparingly soluble the precipitation of this salt, and thus its effective removal from the system, will drive the equilibrium more towards product formation.

3.3.3. Hydrogenation

Compound **53** and a catalytic amount of 10% Pd/C were added to a flask, followed by dry THF until compound **53** was dissolved. A three way tap was fitted to the flask, with one arm attached to the vacuum line and the other attached to a balloon filled with hydrogen. The reaction mixture was thoroughly degassed by opening the flask to the vacuum until the solvent stopped bubbling, and then letting hydrogen from the balloon backfill the vessel. This process was repeated 3 times then the mixture was stirred under a hydrogen atmosphere. The reaction was monitored via TLC and allowed to continue until the associated spot for the protected material was no longer observed. The mixture was filtered through a celite pad and the solvent removed *in vacuo*. The resulting crude product was recrystallised from ethanol:hexane.



Mechanism 3: Catalytic cycle of Pd(0) catalysed hydrogenation.

It was necessary to add the Pd/C to the flask before the solvent in this reaction as if the catalyst was added to the solvent, the friction of the fine powder could generate enough heat to ignite the flammable THF.

Chapter 4: Results and Discussion

4.1 Pseudo bent-core materials

Bent-core materials are, by definition, rigidly locked into a single conformation with respect to the core. As a result, the overall molecular bend angle is fixed, with next to no conformational freedom within the core unit. In order to investigate the effects of freeing up the core unit slightly, allowing some conformational flexibility, a series of materials herein referred to as "pseudo bent-cores" were synthesised. The only structural difference in this series of materials was the changing of the central unit of the bisphenol moiety. In order to gain some insight into the molecular architecture of these materials, and to understand the influence of the central linking unit, minimum energy models for each central unit were produced using DFT modelling at the B3LYP/631-G* level of theory. The bend angle was then calculated by taking the vectors between 2 atoms on each "arm", extrapolating these vectors then calculating the angle between them (shown graphically in Figure 43). The angles obtained from these calculations are summarised in Table 5.

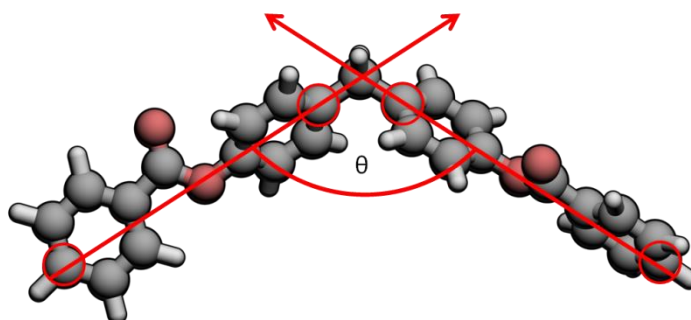
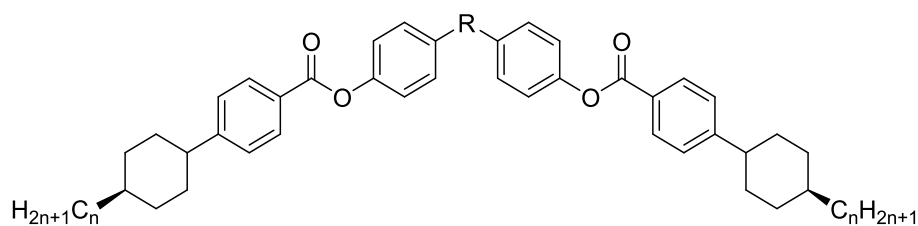


Figure 43: Minimised energy structure of the central unit of compounds **X-Y**. Vectors between the marked atoms were used for the calculation of the angle θ .

Central unit	Bend angle (θ) / °
CH ₂	116.8
CMe ₂	109.6
CO	128.0
C(C ₅ H ₁₀)	98.1
S	105.7
SO ₂	109.5

Table 5: Bend angles calculated for each of the bisphenol units.

The mesogenic properties compounds **12-36** were investigated using POM, DSC and XRD. Although many of the compounds reported in this family were found to be non-mesogenic several trends were apparent with respect to the thermal behaviour. Compounds where the linking group included SO₂, C(C₅H₁₀), and C(CH₃)₂ were all non-mesogenic (see Table 6) but those containing a carbonyl (Table 7), methylene (Table 8) or thioether (Table 10) exhibited liquid crystallinity. Compounds containing a carbonyl linker exhibited a nematic phase whereas compounds containing the methylene linker exhibit smectic-like phases, as well as the so-called "dark conglomerate" phase.

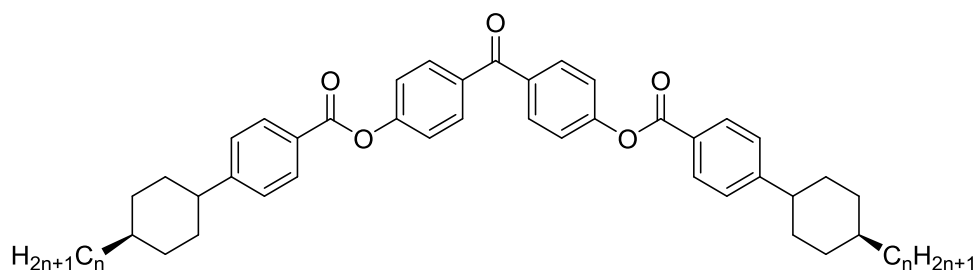


Compound			Transition Temperature / °C		
No.	R	n	Cr		Iso
12	CMe ₂	2	•	206.52 [33.3] {8.36}	•
13	CMe ₂	3	•	190.65 [25.1] {6.52}	•
14	CMe ₂	4	•	204.49 [37.4] {9.41}	•
15	CMe ₂	5	•	158.27 [25.2] {7.03}	•
16	CMe ₂	7	•	207.79 [58.8] {14.72}	•
17	C(C ₅ H ₁₀)	2	•	201.49 [45.9] {11.64}	•
18	C(C ₅ H ₁₀)	3	•	177.78	•

					[30.6]	
					{8.17}	
19	C(C ₅ H ₁₀)	4	•		173.18	•
					[47.2]	
					{12.73}	
20	C(C ₅ H ₁₀)	5	•		200.90	•
					[43.0]	
					{10.91}	
21	C(C ₅ H ₁₀)	7	•		161.21	•
					[48.6]	
					{13.45}	
22	SO ₂	2	•			•
23	SO ₂	3	•		245.48	•
					[31.8]	
					{7.38}	
24	SO ₂	4	•		237.61	•
					[52.2]	
					{12.29}	
25	SO ₂	5	•		223.96	•
					[57.1]	
					{13.81}	
26	SO ₂	7	•		166.28	•
					[29.6]	
					{8.09}	

Table 6: Thermal behaviour and general structure of compounds **12-26**. Enthalpies are presented in [] and quoted in kJ mol⁻¹. Entropies are presented in {} and denoted in ΔS/R.

The materials presented in Table 6 were all found to be non-mesogenic, indeed the melting points of many of these materials were in excess of 200 °C. A common factor for all of the non-mesogenic materials presented here is that the central unit of the bisphenol core consists of a large, sterically bulky group that also, most predominantly in the case of the 1,1-disubstituted cyclohexane core, severely restrict the rotational freedom about the central unit, effectively fixing the bend angle. However, materials with a carbonyl central linking unit were liquid crystalline and the mesogenic behaviour is summarised below in Table 7.



Compound		Transition Temperatures / °C				
No.	n	Cr		N		Iso
27	2	•	207.67	•	226.28	•
			[5.8]		[16.74]	
			{1.46}		{4.03}	
28	3	•	225.37	(*)	-	•
			[40.5]			
			{9.78}			
29	4	•	212.53	•	242.24	•
			[37.6]		[1.08]	
			{9.31}		{0.25}	
30	5	•	211.08	•	236.69	•
			[41.7]		[0.88]	
			{10.37}		{0.21}	
31	7	•	208.46	•	214.88	•
			[42.6]		[0.67]	
			{10.64}		{0.16}	

Table 7: Mesomorphic behaviour of compounds **27-31**. Enthalpies quoted in {} and denoted in kJmol^{-1} . Entropies quoted in {} and denoted in $\Delta S/R$. (*) denotes a transition that occurred simultaneously with crystallisation, enthalpy and transition temperature unobtainable.

Compounds **27-31** all exhibited enantiotropic nematic phases, with the exception of compound **28** where the nematic phase transition and crystallisation of the material occurred simultaneously on cooling. A trend can be clearly observed in the melting points of these materials in that, as the length of the terminal chain is increased the melting point decreases. This is an expected trend as the longer the terminal chain the more it is able to interfere with the packing between the molecules, this serves to disrupt the crystal lattice meaning less energy is needed to break it down.

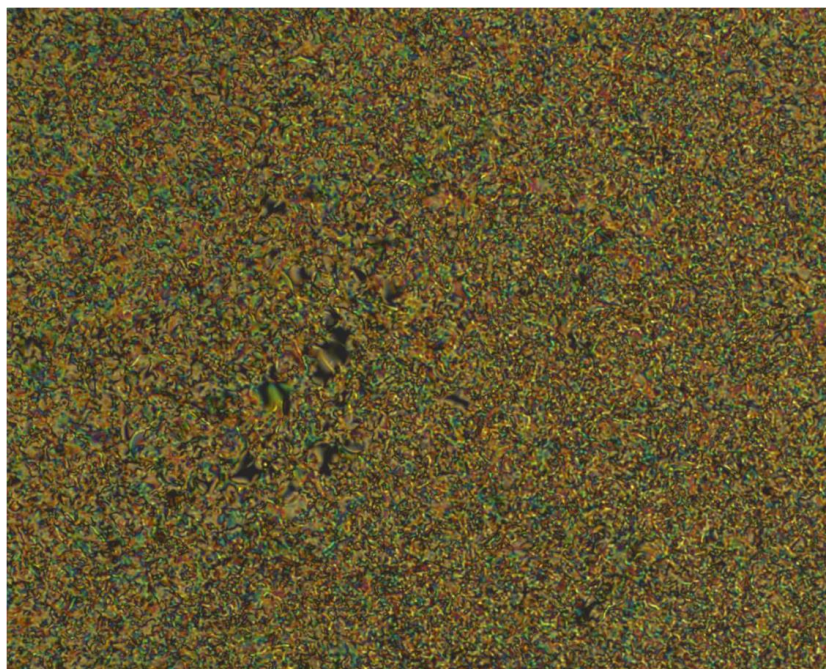


Figure 44: Nematic phase of compound **27** at 223.1 °C. Sample was cooled at 0.1 °C min⁻¹. (x100).

The nematic phases observed in these materials were difficult to characterise due to the high temperatures at which they occurred, over 200 °C, being sufficient to decompose the material. The nematic phase was initially difficult to characterise by polarised optical microscopy, although a grainy texture was observed (Figure 44) that was accompanied by noticeable Brownian motion. XRD analysis was carried out on this series of compounds, and a representative example for compound **27** is reported (Figure 45). At low temperature there is a strong diffraction pattern associated with the crystal lattice (Figure 45b, yellow data). The liquid crystalline phase and the isotropic fluid were both weakly diffracting, but the diffraction pattern obtained within the expected temperature range of the liquid crystal phase is consistent with that of a nematic phase (Figure 45a).

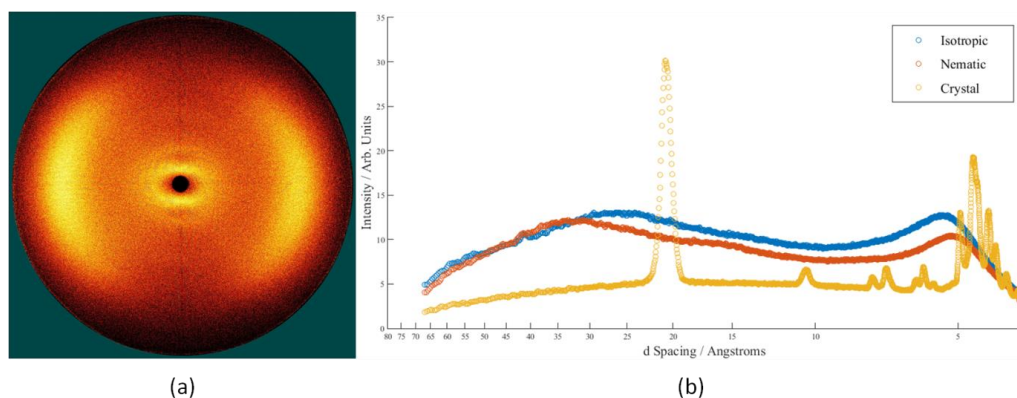
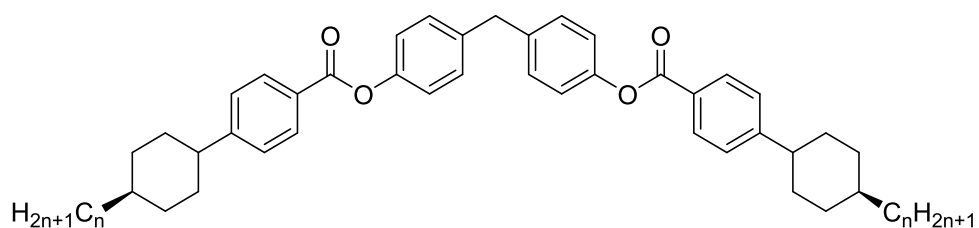


Figure 45: (a) 2d XRD diffraction pattern of compound **27** in the nematic phase at 210 °C (b) 1d plot of d spacing against intensity for compound **27** in the isotropic, nematic and crystal phases.

Molecular modelling has revealed that the carbonyl linker results in a more linear minimum energy geometry, in comparison to the non-mesogenic materials presented in Table 6, with an intermesogen angle of 128°. This more rod like structure lends itself towards standard calamitic phases than the materials with a higher bend angle. An interesting note was that, when viewed under crossed polarisers the nematic phases of these materials were observed to possess red and green domains which alternated with rotation of the polariser, this behaviour is normally observed for materials with molecular chirality.

The observation of this behaviour in compounds **27-31**, despite them being achiral on a molecular scale, indicates that the phases formed exhibit a degree of bulk chirality, this is not uncommon in bent materials due to their shape, making it difficult to pack them into a normal mesophase. Unfortunately the high working temperatures of these compounds made in depth analysis difficult as the materials tended to decompose if held in the isotropic or nematic phases for extended periods of time.

The other group of materials that exhibited mesomorphic properties were those linked by a methylene unit. The mesomorphism displayed by these compounds was significantly more interesting than the behaviour exhibited by compounds **27-31**. The thermal behaviour of these materials is summarised in Table 8.



Compound			Transition Temperatures / °C					
No.	n	Cr	DC	"X"	Iso			
32	2	•	199.02 [58.4] {14.89}	-	-	-	-	•
33	3	•	179.96 [44.3] {11.78}	-	-	(•	165.4) [10.36] {2.84}	•
34	4	•	161.61 [40.0] {11.08}	-	-	•	164.4) [10.40] {2.86}	•
35	5	•	144.9	(•	138.4)	•	159.3	•
36	7	•	-26.65 [0.3] {0.16}	•	153.1 [28.63] {8.0}	-	-	•

Table 8: Mesomorphic behaviour of compounds **32-36**. Enthalpies quoted [] and denoted in in kJmol^{-1} . Entropies quoted in { } and denoted in $\Delta S/R$.

Compound **32** was non-mesogenic but as the terminal chain length was increased the melting point was observed to decrease, consequently compound **33** was shown to exhibit a monotropic mesophase and compounds **34-36** all exhibited enantiotropic phase behaviour. Compounds **33-36** all exhibited a mesophase with a defect texture reminiscent of the smectic A phase (Figure 46). This series of materials displayed significantly lower melting and clearing points than those observed for the materials with a carbonyl linker, with only compound **32**, which was observed to be non-mesogenic, having a clearing point in excess of 170 °C while none of the carbonyl linked materials melted at temperatures below 200 °C. This decrease in the clearing temperature could be attributed to the increased conformational freedom afforded by the methylene central unit as opposed to the carbonyl. In compounds **32-36** the central carbon of the bisphenol unit, the methylene carbon, theoretically has complete freedom of rotation, however in the

carbonyl linked materials this free rotation is limited by the carbon-oxygen double bond. This increase in conformational freedom, combined with the more bent shape adopted by the methylene linked core, could cause the molecules to pack less efficiently into a crystal lattice or a mesophases, thus requiring less energy to break this packing.

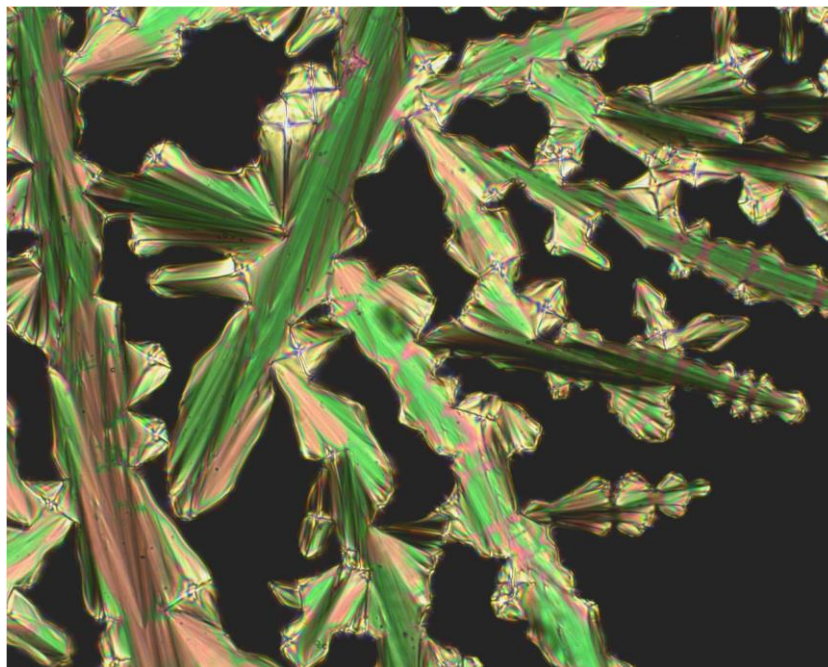


Figure 46: Isotropic-“X” phase transition of compound **35** at 159 °C. Cooled at 0.1 °C min⁻¹. (x100)

While this texture (Figure 46) does resemble the focal conic texture of the smectic A phase there are several structural differences that preclude a definite assignment as this mesophase. Firstly, for a normal smectic A phase it would be expected that the phase would emerge from the isotropic fluid *via* a smooth dendritic pattern, this phase grows in a crawling, finger-like pattern. The defects in Figure 46, while initially appearing similar to focal conic defects are not actually comprised of the ellipse and hyperbola characteristic of this structure. Finally the optical texture of this phase exhibits the same alternating green and pink domains as seen in the carbonyl linked materials, implying a degree of bulk chirality as the constituent molecules remain achiral (Figure 47).

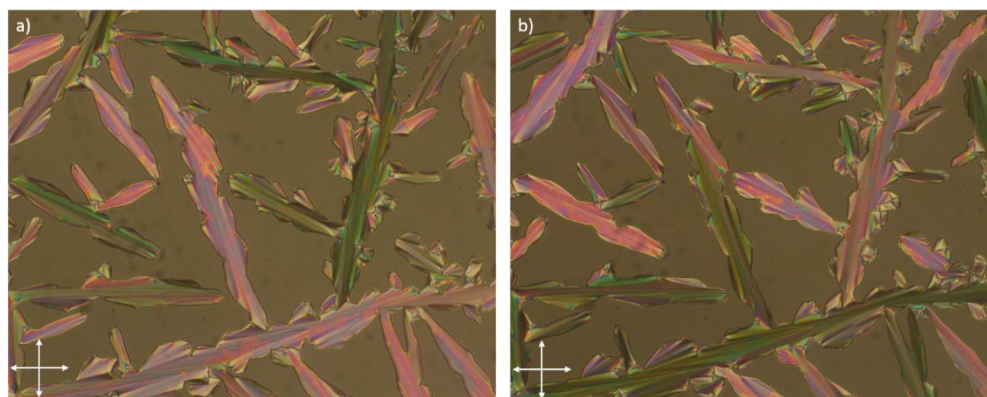


Figure 47: Lamellar "X" phase of compound **34** at 164.4 °C. Polarisers rotated to a) 62° and b) 118°. Sample cooled at 0.1 °C min⁻¹. (x100)

On cooling compound **35** from the "X" phase, a transition was observed wherein the sample became optically extinct when viewed under crossed polars (Figure 48). However when the light levels were increased a weakly birefringent texture could be observed consisting of pale blue-grey blocky domains (Figure 49a). This texture was more easily observed as pink and purple domains with the introduction of a full wave-plate, and were observable under normal light levels (Figure 49b)

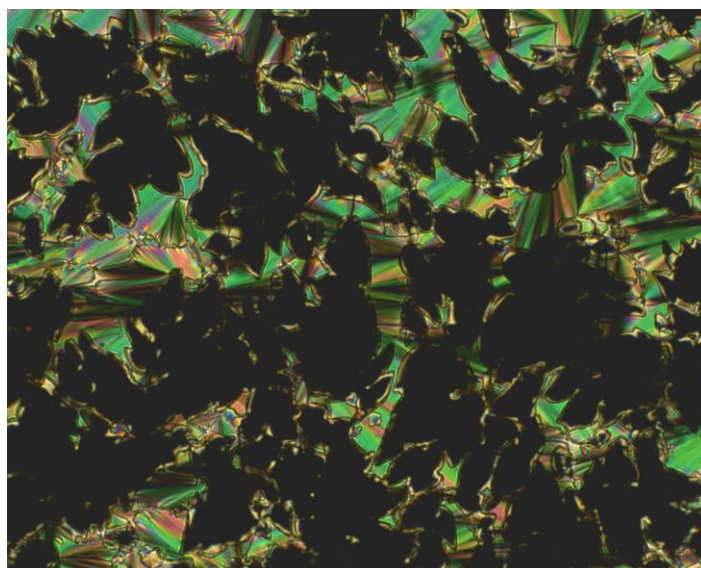


Figure 48: Transition from the lamellar "X" phase to the optically extinct phase of compound **35**. Taken at 142.0 °C, cooled at 0.1 °C min⁻¹. (x100)

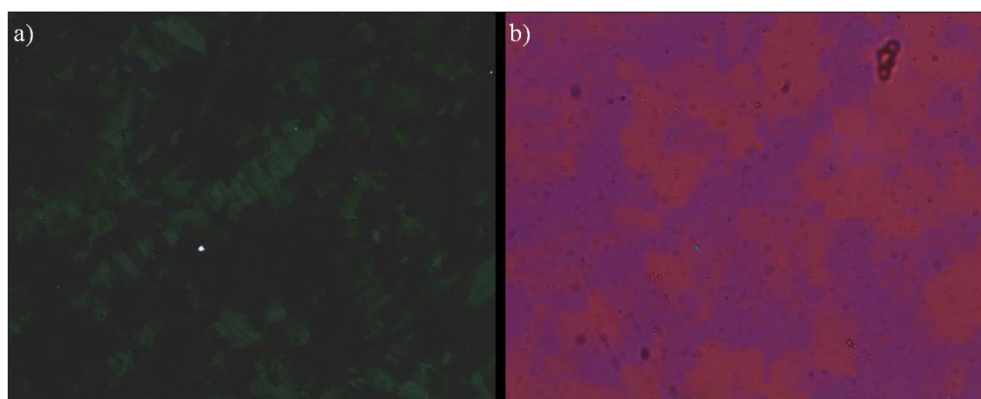


Figure 49: Weakly birefringent phase of compound **35** observed (a) under high light conditions and (b) under normal light conditions with a full waveplate at 138.7 °C. Sample cooled at 0.1 °C min⁻¹. (x100)

This texture is consistent with optical textures reported for the so-called "dark conglomerate" phase exhibited by some bent-core materials^{18–20}. The shape of these domains, blocky and separated by sharp, well defined boundaries (Bequer lines) is indicative of a highly ordered structure; more akin to a soft crystal than a traditional mesophase, which are generally more fluid. The highly ordered nature of this phase was revealed by the diffraction pattern obtained by small angle X-ray scattering (SAXS). Upon cooling from the isotropic liquid both the transition to the lamellar phase, as well as that to the DC phase are observed (Figure 50, Figure 51).

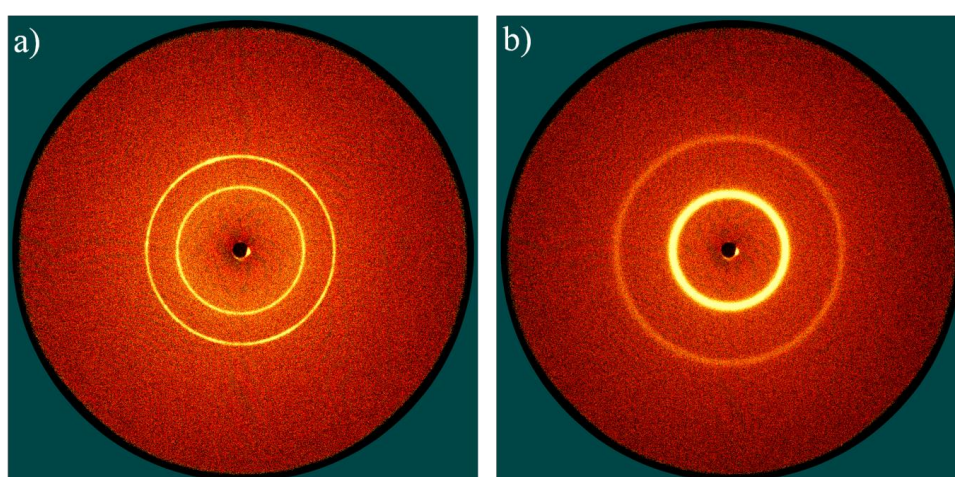


Figure 50: Diffraction patterns obtained for compound **35** (a) in the lamellar phase at 130 °C and (b) in the DC phase at 100 °C

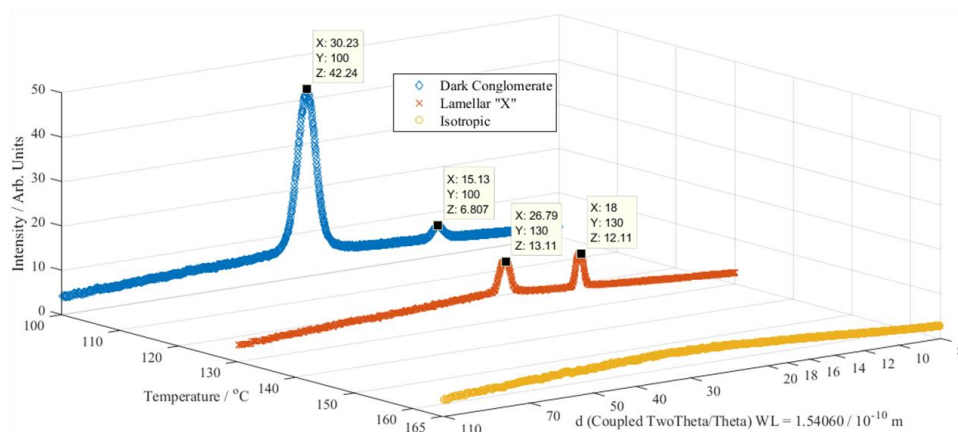


Figure 51: 1d XRD plots of compound **35** in the isotropic fluid at 160 °C, the lamellar “X” phase at 130 °C and the DC phase at 100 °C.

Using XRD analysis, the “X” phase exhibited 2 sharp diffraction peaks of roughly equal intensity, one at $d \approx 27 \text{ \AA}$ and one at $d \approx 18 \text{ \AA}$. DFT calculations found the overall molecular length of compound **35** to be approximately 42 \AA , with each individual "arm" of the molecule being 21 \AA long. This indicates that in the lamellar phase the layers must be intercalated to a degree. Upon cooling into the DC phase of compound **35** a very intense peak at 30 \AA , along with the corresponding first harmonic resonance at 15 \AA ($d/2$) were seen to emerge. The intense signal implies that the DC phase is highly ordered in the direction perpendicular to the layer planes, with a repeat distance of 30 \AA . This, along with the sharp Bequer lines observed *via* POM, suggests that out of the layer plane the DC phase adopts a highly organised structure similar to that of a crystal. Yet the lack of visible reflections in the wide-angle region ($d < 10 \text{ \AA}$) indicates that within the layers the structure is still disorganised.

Although compounds **34** and **35** exhibit the “X” phase upon cooling from the isotropic liquid, compound **36** was unique amongst this series of materials in that, upon cooling from the isotropic liquid no discernible change in the defect texture was observed. Under normal light levels the sample remained optically extinct even after reaching room temperature. Differential scanning calorimetry showed a large, reversible transition at approximately 150 °C (Figure 52).

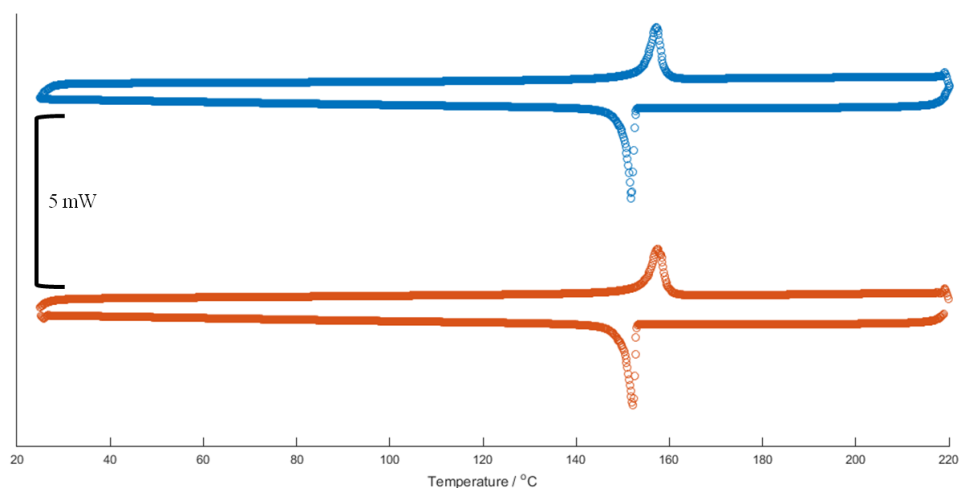


Figure 52: The heating and cooling DSC traces for compound **36**. Taken at a scan rate of $10\text{ }^{\circ}\text{C min}^{-1}$.

These results prompted further studies *via* POM under increasing light intensity, revealing this material to have a transition directly from the isotropic liquid to the dark conglomerate phase, without any preceding “X” phase. The texture observed in the DC phase was too weakly birefringent to obtain photomicrographs, however the phase assignment was supported by XRD studies, which show a transition from the isotropic liquid to a phase with a similar XRD pattern to that observed for compound **35** (Figure 53).

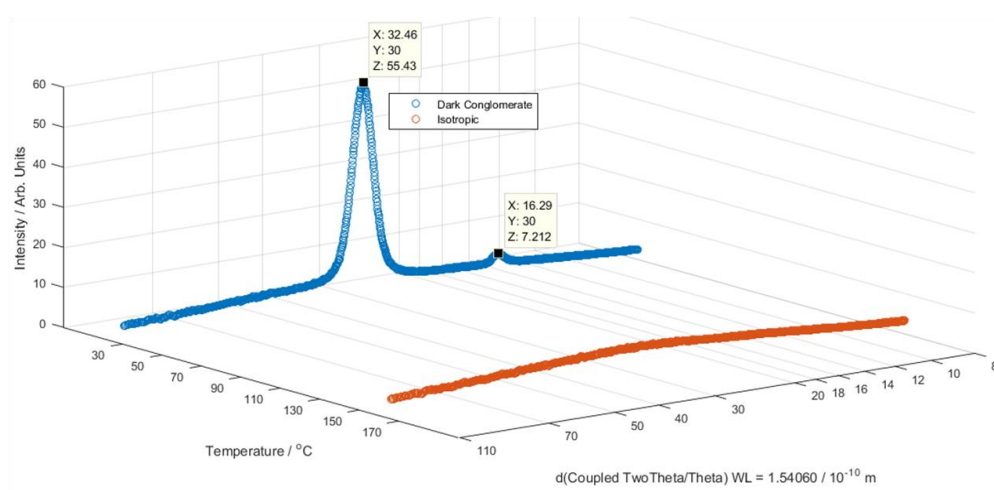


Figure 53: XRD trace for compound **36** in the isotropic liquid at $165\text{ }^{\circ}\text{C}$ and in the dark conglomerate phase at $30\text{ }^{\circ}\text{C}$.

Of particular interest for this material was the lack of any discernible crystallisation peak in the DSC trace, despite the material forming a solid at room temperature when obtained *via* recrystallisation. The material took a significant amount of time, in excess of one month, to fully crystallise when left at room temperature on an untreated glass slide.

In order to determine the point at which crystallisation occurred the material was taken down to a temperature of -50 °C by DSC. The resulting DSC first cycle showed very weak, broad peaks with an onset of 2.22 °C on cooling, and melting again at -26.65 °C (Figure 54). It should be noted that the phase transitions shown in Figure 54 are determined from the tangent at maximum gradient (onset) of the peak for the phase transition. For the very broad peaks found for compound **36**, mirroring of the peaks for the heating and cooling cycles is not usually possible, and there are usually large differences in the values obtained. However the reproducibility of these peaks, along with the small associated enthalpies of transition, suggests that this phase transition could be a change from one form of soft crystal to another, where the low enthalpies imply that there is already significant lattice structure in the preceding DC phase. If this is the case then the transition to the so-called “crystal” phase does not change the structure to a significant degree.

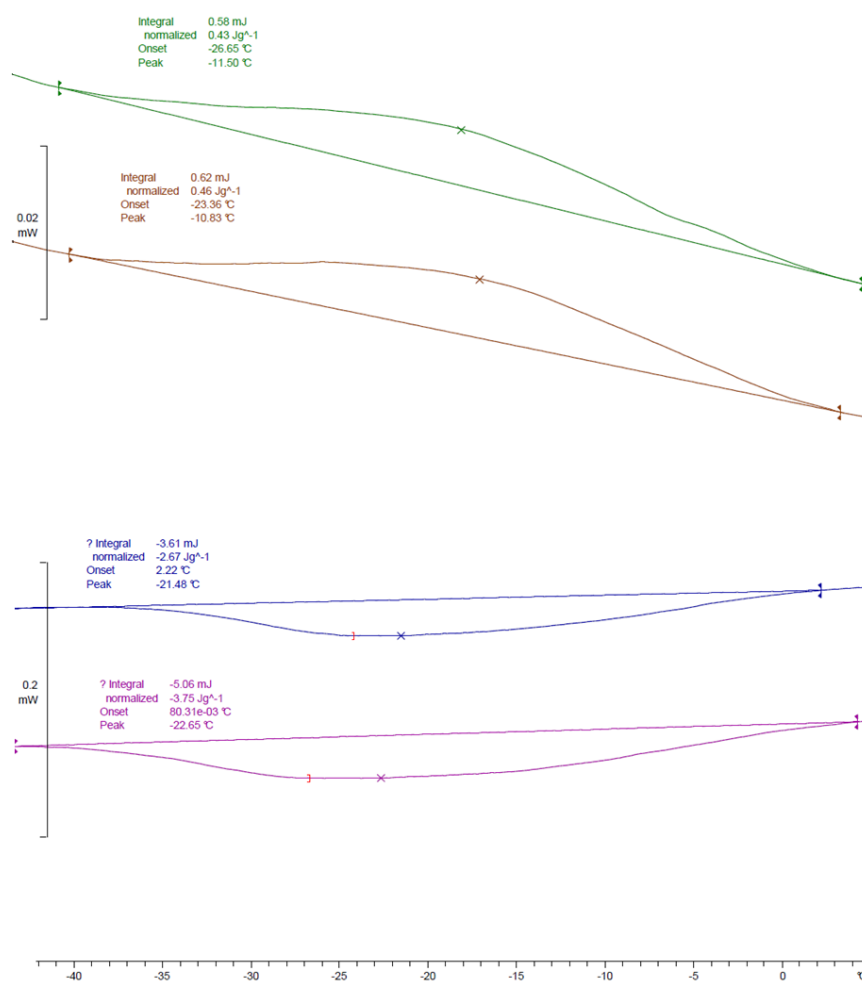
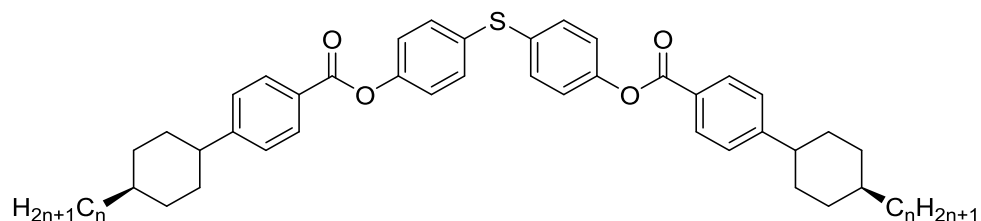


Figure 54: The heating and cooling DSC traces for compound **36**, taken at a scan rate of 10 °C min⁻¹. In order to determine the melting and recrystallization temperatures the material was taken down to a temperature of -50 °C prior to investigation.

The last part of this section describes the mesomorphism of materials linked by a sulfide central unit. The thermal behaviour of these materials is summarised in Table 9.



Compound			Transition Temperatures / °C			
no.	n	Cr	"X"		Iso	
37	2	•	193.16 [53.2] {13.73}	(•	173.73) [37.9] {10.21}	•
38	3	•	193.71 [48.8] {12.59}	-	-	•
39	4	•	180.16 [44.4] {11.78}	(•	152.89) [8.4] {2.36}	•
40	5	•	157.14 [37.6] {10.50}	(•	147.46) [6.1] {1.73}	•
41	7	•	158.30 [39.2] {10.93}	(•	155.91) [2.8] {0.78}	•

Table 9: Mesomorphic behaviour of compounds **37-41**. Enthalpies quoted in [] and denoted in kJmol^{-1} . Entropies quoted in {} and denoted in $\Delta S/R$.

Upon initial examination by POM these materials appeared to be non-mesogenic; recrystallising upon controlled cooling rates. However, studies by DSC showed that two events occurred upon cooling as shown in the thermogram presented in Figure 55. The higher temperature peak observed on cooling was attributed to a monotropic phase transition while the lower temperature peak was attributed to crystallisation.

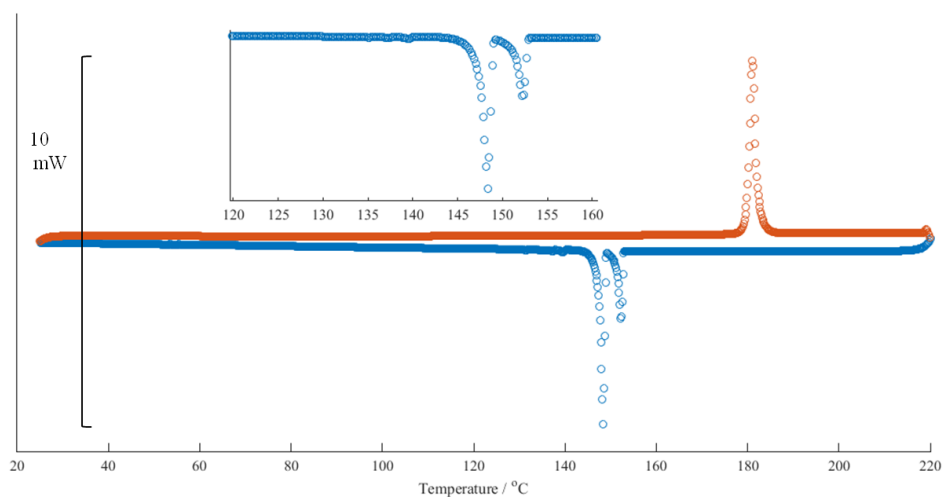


Figure 55: The heating and cooling DSC traces for compound **39**, taken at a scan rate of $10\text{ }^{\circ}\text{C min}^{-1}$.

Subsequent examination *via* POM using rapid, uncontrolled cooling showed compound **39** exhibited a transition from the isotropic liquid to a phase with a texture similar to the lamellar “X” phase observed previously for compounds **32-36** (Figure 56). The green and pink domains were again observed to interconvert upon rotation of the polarisers (Figure 57).

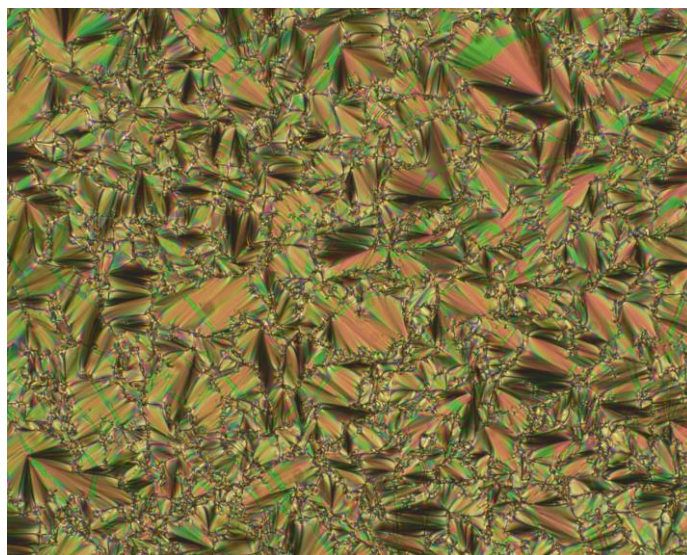


Figure 56: The lamellar “X” phase of compound **39** at $150\text{ }^{\circ}\text{C}$. Observed upon rapid, uncontrolled cooling from the isotropic liquid. ($\times 100$)

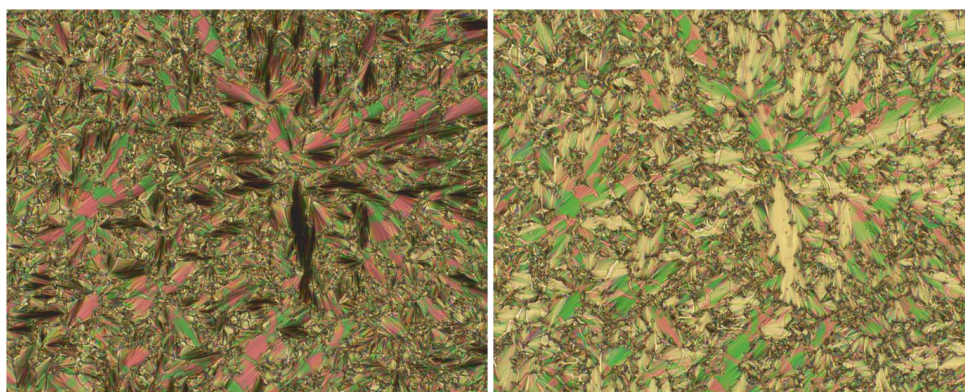


Figure 57: The lamellar "X" phase of compound **39** at 150 °C upon rotation of polarisers. Note the interconverting green and pink domains. Observed upon rapid, uncontrolled cooling from the isotropic liquid. (x100)

Both POM and DSC thus indicate that the mesophase exhibited by the sulphide linked materials is the same as the lamellar phase observed in the methylene linked analogues. Confirmation by XRD however, proved impossible due to the degree of supercooling required for the Iso. Liq.-"X" transition, as well as the ease at which nucleation of crystals occurred.

Conclusions

Altering the chemical architectures and natures of these families of "pseudo bent-core" materials has been shown to have a drastic effect on the thermal properties of the resulting materials. Indeed differing core units, with the rest of the molecular architecture maintained, were shown to display phase behaviour consistent with completely different classes of mesogen; with the carbonyl linked materials behaving similarly to a standard calamitic liquid crystal, whereas those materials with a methylene central unit exhibited phase behaviour more congruent with that of previously reported bent core materials. In the case of the non-mesogenic materials i.e. materials linked by a C(Me₂), SO₂, and cyclohexyl central units, the lack of mesomorphic behaviour can be attributed to the significant steric bulk of the central unit disrupting the packing of the molecules thereby suppressing mesophases formation. In the case of the sulphide linked materials, where the central unit does not possess significant steric bulk it is likely that the low bend angle of these materials, with respect to the methylene and carbonyl linked materials, is the most likely reason this series of compounds exhibits no mesomorphism unless under rapid supercooling. This is due to the bend angle being too low to support the formation of a

nematic phase, unlike the more linear carbonyl materials, as well as being too tight to easily pack into layers like the methylene linked materials.

Thus the predominant factor in determining which mesophases are exhibited by these materials is the bend angle of the core, associated by the central unit, this is best demonstrated by the carbonyl materials, which by DFT have been shown to be the most linear of the pseudo bent-core materials presented here, and also have been shown to have a tendency towards forming nematic phases, a trait most commonly shown by linear, calamitic materials such as 5CB.

The lamellar “X” phase formed by several of the methylene and sulfide linked materials in these series' was initially thought to be a smectic A phase due to the lack of an observable *schlieren* texture *via* POM. XRD studies, however, show this phase to have two distinct layer spacings, with in plane disordering, implying a structure more complicated than a simple SmA phase. Ideally electric field studies would be used to ascertain the properties of this phase in order to aid assignment, however the working temperatures of the materials are higher than the melting point of the indium solder used, rendering this difficult to impossible. Nevertheless, XRD and POM studies do indicate that the “X” phase is a nonstandard form of smectic A, however, there are other possibilities to consider; de Vries, anticlinic, biaxial and bilayer SmA phases. POM of the “X”-phase clearly shows regions of homeotropic texture, the lack of a *schlieren* texture, even close to the focal conic domains however renders this phase unlikely to be anticlinic or biaxial variants of the SmA. The two reflections observed in the XRD also show it is unlikely that this phase is the de Vries SmA, this leaves the bilayer SmA as a possibility, supported by the two reflections at differing d-spacings.

There remains another possibility, it has been shown, both in previous sections and later in this thesis, that dimeric materials are known to exhibit the so-called “twist-bend” nematic (N_{TB}) phase. While the structure of this phase is still often debated, one proposed model involves the bent molecules twisted and positioned about the helical axis with the centres of molecular mass randomly distributed. This gives the material the appearance of nematic ordering when it is, in fact, effectively a 1-D crystal with respect to the heliaxis, with a repeat unit the length of one complete pitch (Figure 58). However, if such a structure were to form with the centres of molecular mass being ordered, rather than randomly distributed throughout the helix it would give rise to a lamellar structure similar

to those produced by chiral smectic phases, in which the molecules twist around the helical axis at defined angles to give a clock-like organisation. These morphologies are often found in ferroelectric smectic phases as shown in Figure 57 and have been shown to exhibit homeotropic and focal conic textures similar to those observed for the “X” phase. The twisted structure would involve overlapping of molecules, consistent with the XRD data in Figure 51 where neither of the observed d-spacings were shown to correspond to the molecular length. Therefore it is possible that the lamellar “X” phase is in fact a twist-bend deformation of the SmA phase, however this bears more thorough investigation in order to see if this is indeed a possibility.

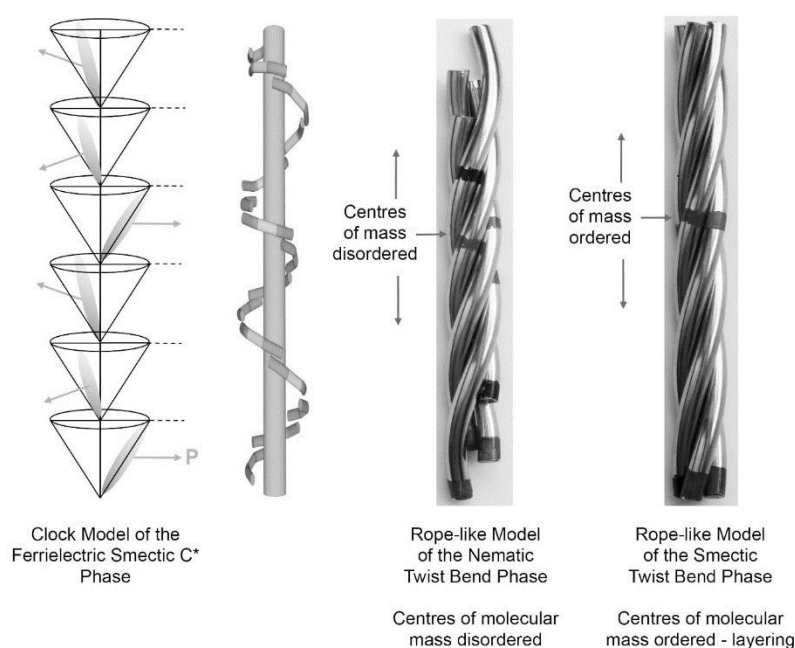


Figure 58: Schematic for the potential formation of a twist-bend deformation of the SmA phase.

The so called "dark conglomerate phase" observed for compounds **35** and **36** seems likely to be a soft crystal phase rather than an actual mesophase, this is supported by the appearance of the peaks both in the XRD and DSC traces. In the XRD trace, upon transition into the DC phase, the signal produced is much more intense than that of the preceding lamellar phase in compound **52**, this indicates a high degree of order in this mesophase. The crystallisation behaviour observed both optically and *via* DSC also lends support to the assignment of this phase as a soft crystal. By eye the material does not transition from the DC phase to a crystal without several weeks of annealing at room temperature, also, the DSC peaks observed for the transitions to this phase have enthalpy

and entropy changes much larger than those typically seen for a liquid crystal phase transition. However it should be noted that the crystallisation peak for compound **36** is unusually weak. These factors imply a high degree of both thermal and kinetic stability of the DC phase, with only a slight difference between it and a normal 3D crystal lattice.

4.1.1. Synthetic Procedures

Compound 12: Propane-2,2-diylbis(4,1-phenylene) bis(4-(4-ethylcyclohexyl)benzoate)

Prepared according to Scheme 1. Compound **1** (1g, 4.4 mmol), Compound **7** (2.05 g, 8.8mmol), EDAC (2.53 g, 13.2 mmol), DMAP (10 mg), DCM (10 cm³). Recrystallisation from ethanol:THF (10:1) yielded **12** as a white powder.

Yield: 2.46 g (3.7 mmol, 85%)

¹H NMR (δ /ppm, 400 MHz, CDCl₃): 8.126 (4H, d, J = 8.24 Hz, ArH), 7.350 (4H, d, J = 8.24 Hz, ArH), 7.305 (4H, d, J = 8.70 Hz, ArH), 7.123 (4H, d, J = 8.70 Hz, ArH), 2.575 (2H, tdd, J = 12.15, 3.21, 2.75, Ar-CH-(CH₂)₂), 1.927 (8H, d, J = 10.07 Hz, Ar-CH-(CH₂)₂), 1.723 (6H, s, C(CH₃)₂), 1.549-1.445 (4H, m, CyHexH), 1.329-1.185 (6H, m, CH-CH₂-CH₃), 1.128-1.011 (4H, m, CyHexH), 0.932 (6H, t, J = 7.3 Hz, CH₂-CH₃)

¹³C NMR (δ /ppm, 100.5 MHz, CDCl₃): 165.25, 154.08, 148.84, 147.84, 130.26, 127.86, 127.12, 127.06, 121.09, 44.79, 42.50, 38.95, 33.97, 32.95, 30.97, 29.90, 11.51

IR (ν max cm⁻¹): 652.0, 669.3, 672.7, 690.5, 699.7, 726.2, 748.9, 760.4, 811.1, 820.7, 858.3, 876.7, 990.0, 1015.5, 1068.6, 1155.4, 1170.3, 1180.0, 1202.1, 1263.4, 1361.3, 1377.7, 1413.8, 1447.1, 1465.9, 1507.4, 1606.8, 1731.1, 2844.1, 2925.6, 2963.7

ESI-MS (m/z): 679.3758 (C₄₅H₅₂NaO₄ [M+Na⁺])

Elemental Analysis (mass %): Calculated: C, 82.28 %; H, 7.98 %; N 0 %; Other, 9.74 %.
Found: C, 82.24 %; H, 7.98 %; N, 0 %; Other, 9.78 %.

Compound 13: Propane-2,2-diylbis(4,1-phenylene) bis(4-(4-propylcyclohexyl)benzoate)

Prepared according to Scheme 1. Compound **1** (1g, 4.4 mmol), Compound **8** (2.17 g, 8.8mmol), EDAC (2.53 g, 13.2 mmol), DMAP (10 mg), DCM (10 cm³). Recrystallisation from ethanol:THF (10:1) yielded **13** as a white powder.

Yield: 2.59 g (3.8 mmol, 86%)

¹H NMR (δ/ppm, 400 MHz, CDCl₃): 8.123 (4H, d, J = 8.24 Hz, ArH), 7.347 (4H, d, J = 8.24 Hz, ArH), 7.303 (4H, d, J = 8.70 Hz, ArH), 7.120 (4H, d, J = 8.70 Hz, ArH), 2.572 (2H, tdd, J = 12.15, 3.21, 2.75, Ar-CH-(CH₂)₂), 1.913 (8H, dd, J = 10.07, 9.62 Hz, Ar-CH-(CH₂)₂), 1.72 (6H, s, Ar-C(CH₃)₂-Ar), 1.549-1.443 (4H, m, CyHexH), 1.413-1.206 (10H, m, CH-CH₂-CH₂-CH₃), 1.130-1.027 (4H, m, CyHexH), 0.921 (6H, t, J = 7.33 Hz, CH₂-CH₃)

¹³C NMR (δ/ppm, 100.5 MHz, CDCl₃): 165.26, 154.09, 148.85, 147.85, 130.27, 127.86, 127.13, 127.06, 121.10, 44.80, 42.51, 39.61, 36.90, 34.00, 33.34, 30.98, 19.98, 14.39

IR (νmax cm⁻¹): 698.7, 726.7, 747.9, 760.4, 808.7, 856.9, 868.5, 877.6, 989.5, 1015.5, 1065.2, 1170.3, 1179.0, 1201.7, 1263.4, 1356.9, 1414.3, 1441.8, 1463.5, 1504.0, 1606.2, 1732.6, 2841.7, 2919.3, 2959.8

ESI-MS (*m/z*): 707.4045 (C₄₇H₅₆NaO₄ [M+Na⁺])

Elemental Analysis (mass %): Calculated: C, 82.42 %; H, 8.24 %; N 0 %; Other, 9.34 %.
Found: C, 82.30 %; H, 8.24 %; N, 0 %; Other, 9.54 %.

Compound 14: Propane-2,2-diylbis(4,1-phenylene) bis(4-(4-butylcyclohexyl)benzoate)

Prepared according to Scheme 1. Compound **1** (1g, 4.4 mmol), Compound **9** (2.30 g, 8.8 mmol), EDAC (2.53 g, 13.2 mmol), DMAP (10 mg), DCM (10 cm³). Recrystallisation from ethanol:THF (10:1) yielded **14** as a white powder.

Yield: 2.45 g (3.4 mmol, 78%)

¹H NMR (δ/ppm, 400 MHz, CDCl₃): 8.125 (4H, d, J = 8.24 Hz, ArH), 7.348 (4H, d, J = 8.24 Hz, ArH), 7.304 (4H, d, J = 8.70 Hz, ArH), 7.122 (4H, d, J = 8.70 Hz, ArH), 2.574 (2H, tdd, J = 12.15, 3.21, 2.75, Ar-CH-(CH₂)₂), 1.927-1.865 (8H, m, Ar-CH-(CH₂)₂), 1.723 (6H, s, C(CH₃)₂), 1.574-1.444 (4H, m, CyHexH), 1.374-1.214 (14H, m, CH-CH₂-CH₂-CH₂-CH₃), 1.124-1.039 (4H, m, CyHexH), 0.923 (6H, t, J = 6.87 Hz, CH₂-CH₃)

¹³C NMR (δ/ppm, 100.5 MHz, CDCl₃): 166.26, 154.09, 148.85, 147.85, 130.27, 127.86, 127.13, 127.06, 121.10, 44.80, 42.51, 37.18, 37.02, 34.01, 33.39, 30.98, 29.18, 22.98, 14.16

IR (νmax cm⁻¹): 652.0, 657.3, 663.0, 667.9, 684.7, 696.3, 749.8, 759.5, 809.1, 851.1, 871.8, 1015.1, 1067.6, 1169.4, 1201.7, 1263.4, 1362.2, 1415.8, 1446.6, 1503.5, 1606.7, 1733.1, 2844.5, 2922.7, 2963.7

ESI-MS (*m/z*): 735.4393 (C₄₉H₆₀NaO₄ [M+Na⁺])

Elemental Analysis (mass %): Calculated: C, 82.54 %; H, 8.48 %; N, 0 %; Other, 8.98 %. Found: C, 82.68 %; H, 8.48 %; N, 0 %; Other, 8.84 %.

Compound 15: Propane-2,2-diylbis(4,1-phenylene) bis(4-(4-pentylcyclohexyl)benzoate)

Prepared according to Scheme 1. Compound **1** (500 mg, 2.2 mmol), Compound **10** (1.20 g, 4.4 mmol), EDAC (1.76 g, 6.6 mmol), DMAP (10 mg), DCM (10 cm³). Recrystallisation from ethanol:THF (10:1) yielded **15** as a white powder.

Yield: 1.45 g (2.0 mmol, 89%)

¹H NMR (δ/ppm, 400 MHz, CDCl₃): 8.127 (4H, d, J = 8.24 Hz, ArH), 7.349 (4H, d, J = 8.24 Hz, ArH), 7.306(4H, d, J = 8.70 Hz, ArH), 7.124(4H, d, J = 8.70 Hz, ArH), 2.570 (2H, tdd, J = 12.15, 3.21, 2.75, Ar-CH-(CH₂)₂) 1.967-1.860 (8H, m, Ar-CH-(CH₂)₂), 1.724 (6H, s, C(CH₃)₂), 1.550-1.445 (4H, m, CyHexH), 1.393-1.207 (18H, m, CH-CH₂-CH₂-CH₂-CH₂-CH₃), 1.141-1.019 (4H, m, CyHexH), 0.916 (6H, t, J = 6.87 Hz, CH₂-CH₃)

¹³C NMR (δ/ppm, 100.5 MHz, CDCl₃): 165.24, 154.08, 148.85, 147.84, 130.26, 127.85, 127.13, 127.05, 121.10, 44.80, 42.50, 37.29, 37.18, 34.00, 33.38, 32.16, 30.97, 26.6, 22.69, 14.11

IR (νmax cm⁻¹): 666.9, 699.7, 730.6, 737.3, 802.9, 837.1, 869.9, 895.0, 909.0, 977.0, 1012.6, 1066.6, 1168.9, 1205.5, 1261.0, 1412.9, 1445.2, 1501.1, 1608.7, 1729.2, 1960.7, 1993.9, 2141.7, 2175.7, 2857.6, 2925.6

ESI-MS (*m/z*): 763.4702 (C₅₁H₆₄NaO₄ [M+Na⁺])

Elemental Analysis (mass %): Calculated: C, 82.66 %; H, 8.70 %; N, 0 %; Other, 8.64 %. Found: C, 82.77 %; H, 8.74 %; N, 0 %; Other, 8.49 %.

Compound 16: Propane-2,2-diylbis(4,1-phenylene) bis(4-(4-heptylcyclohexyl)benzoate)

Prepared according to Scheme 1. Compound **1** (1g, 4.4 mmol), Compound **11** (2.70 g, 8.8 mmol), EDAC (2.53 g, 13.2 mmol), DMAP (10 mg), DCM (10 cm³). Recrystallisation from ethanol:THF (10:1) yielded **16** as a white powder.

Yield: 2.63 g (3.3 mmol, 75%)

¹H NMR (δ/ppm, 400 MHz, CDCl₃): 8.090 (4H, d, J = 8.24 Hz, ArH), 7.317 (4H, d, J = 8.24 Hz, ArH), 7.273 (4H, dd, J = 8.70, 1.83 Hz, ArH), 7.069 (4H, dd, J = 8.70, 1.83 Hz, ArH), (2H, t, J = 12.14 Hz, Ar-CH-(CH₂)₂), 1.928-1.883 (8H, m, Ar-CH-(CH₂)₂), 1.692 (6H, s, C(CH₃)₂), 1.513-1.423 (4H, m, CyHexH), 1.267 (26H, s (broad), CH-CH₂-CH₂-CH₂-CH₂-CH₂-CH₃), 1.090-1.003 (4H, m, CyHexH), 0.875 (6H, t, J = 5.95 Hz, CH₂-CH₃)

¹³C NMR (δ/ppm, 100.5 MHz, CDCl₃): 165.26, 154.10, 148.86, 147.85, 130.27, 127.87, 127.13, 127.07, 121.10, 44.81, 42.51, 37.35, 37.20, 34.02, 33.39, 31.91, 30.98, 29.93, 29.38, 26.95, 22.69, 14.13

IR (νmax cm⁻¹): 652.0, 655.3, 667.9, 678.5, 690.5, 699.2, 714.2, 716.6, 756.1, 803.8, 848.7, 867.5, 968.3, 1014.6, 1065.2, 1169.8, 1180.0, 1201.7, 1263.4, 1362.2, 1416.7, 1446.6, 1463.0, 1502.6, 1609.1, 1725.3, 1733.5, 2839.7, 2921.7, 2951.6

ESI-MS (*m/z*): 819.5294 (C₅₅H₇₂NaO₄ [M+Na⁺]) 835.5019 (C₅₅H₇₂KO₄ [M+K⁺])

Elemental Analysis (mass %): Calculated: C, 82.87 %; H, 9.10 %; N, 0 %; Other, 8.03 %. Found: C, 82.89 %; H, 9.10 %; N, 0 %; Other, 8.01 %.

Compound 17: Cyclohexane-1,1-diylbis(4,1-phenylene) bis(4-(4-ethylcyclohexyl)benzoate)

Prepared according to Scheme 1. Compound **2** (1 g, 3.7 mmol), Compound **7** (1.72 g, 7.4 mmol), EDAC (2.13 g, 11.1 mmol), DMAP (10 mg), DCM (10 cm³). Recrystallisation from ethanol:THF (10:1) yielded **17** as a white powder.

Yield: 2.24 g (3.2 mmol, 87%)

¹H NMR (δ /ppm, 400 MHz, CDCl₃): 8.086 (4H, d, J = 8.24 Hz, ArH), 7.320 (4H, d, J = 8.24 Hz, ArH), 7.309 (4H, d, J = 8.70 Hz, ArH), 7.099 (4H, d, J = 8.70 Hz, ArH), 2.544 (2H, tdd, J = 12.15, 3.21, 2.75, Ar-CH-(CH₂)₂), 2.279 (4H, s, Ar-(C(CH₂)₂)-Ar), 1.896 (8H, d, J = 10.53 Hz, Ar-CH-(CH₂)₂), 1.576-1.416 (12H, m, CyHexH), 1.300-1.157 (6H, m, CH-CH₂-CH₃), 1.100-0.998 (4H, m, CyHexH), 0.904 (6H, t, J = 7.33 Hz, CH-CH₂-CH₃)

¹³C NMR (δ /ppm, 100.5 MHz, CDCl₃): 165.20, 154.06, 148.62, 145.78, 130.25, 128.22, 127.16, 127.6, 121.27, 45.79, 44.80, 38.96, 37.34, 33.98, 32.96, 29.91, 26.27, 22.79, 11.50

IR (ν max cm⁻¹): 663.0, 667.9, 686.2, 699.7, 755.6, 777.8, 801.9, 832.8, 851.6, 867.0, 969.7, 1013.1, 1065.2, 1104.3, 1168.4, 1176.6, 1202.1, 1243.6, 1262.9, 1413.8, 1445.2, 1463.5, 1501.1, 1606.7, 1725.3, 1732.1, 2847.4, 2922.7

ESI-MS (m/z): 719.4052 (C₄₈H₅₆NaO₄ [M+Na⁺])

Elemental Analysis (mass %): Calculated: C, 82.72 %; H, 8.10 %; N, 0 %; Other, 9.18 %. Found: C, 82.73 %; H, 8.10 %; N, 0 %; Other, 9.17 %.

Compound 18: Cyclohexane-1,1-diylbis(4,1-phenylene) bis(4-(4-propylcyclohexyl)benzoate)

Prepared according to Scheme 1. Compound **2** (1 g, 3.7 mmol), Compound **8** (1.82 g, 7.4 mmol), EDAC (2.13 g, 11.1 mmol), DMAP (10 mg), DCM (10 cm³). Recrystallisation from ethanol:THF (10:1) yielded **18** as a white powder.

Yield: 2.07g (2.8 mmol, 77%)

¹H NMR (δ/ppm, 400 MHz, CDCl₃): 8.110 (4H, d, J = 8.24 Hz, ArH), 7.340 (4H, d, J = 8.24 Hz, ArH), 7.333 (4H, d, J = 8.70 Hz, ArH), 7.123 (4H, d, J = 8.70 Hz, ArH), 2.566 (2H, tdd, J = 12.15, 3.21, 2.75, Ar-CH-(CH₂)₂), 2.303 (4H, s, Ar-(C(CH₂)₂)-Ar), 1.908 (8H, tt, J = 9.62, 3.66 Hz, Ar-CH-(CH₂)₂), 1.636-1.439 (10H, m, CyHexH), 1.411-1.204 (10H, m, CH-CH₂-CH₂-CH₃), 1.127-1.024 (4H, m, CyHexH), 0.919 (6H, t, J = 7.33 Hz, CH₂-CH₃)

¹³C NMR (δ/ppm, 100.5 MHz, CDCl₃): 165.20, 154.06, 148.61, 145.78, 130.25, 128.21, 127.16, 127.05, 121.27, 45.78, 44.79, 39.61, 37.33, 36.90, 34.00, 33.34, 26.27, 22.78, 19.98, 14.38

IR (νmax cm⁻¹): 652.0, 666.4, 668.3, 678.5, 699.7, 759.5, 800.5, 865.1, 969.7, 1013.1, 1065.2, 1105.2, 1168.4, 1204.6, 1264.8, 1311.1, 1411.9, 1443.7, 1500.2, 1608.7, 1724.4, 2847.0, 2915.4

ESI-MS (*m/z*): 747.4370 (C₅₀H₆₀NaO₄ [M+Na⁺]), 763.4128 (C₅₀H₆₀KO₄ [M+K⁺])

Elemental Analysis (mass %): Calculated: C, 82.83 %; H, 8.34 %; N, 0 %; Other, 8.83 %. Found: C, 82.86 %; H, 8.37 %; N, 0 %; Other, 8.77 %.

Compound 19: Cyclohexane-1,1-diylbis(4,1-phenylene) bis(4-(4-butylcyclohexyl)benzoate).

Prepared according to Scheme 1. Compound **2** (1 g, 3.7 mmol), Compound **9** (1.93 g, 7.4 mmol), EDAC (2.13 g, 11.1 mmol), DMAP (10 mg), DCM (10 cm³). Recrystallisation from ethanol:THF (10:1) yielded **19** as a white powder.

Yield: 2.12g (2.8 mmol, 76%)

¹H NMR (δ/ppm, 400 MHz, CDCl₃): 8.104 (4H, d, J = 8.24 Hz, ArH), 7.334 (4H, d, J = 8.24 Hz, ArH), 7.328 (4H, d, J = 9.16 Hz, ArH), 7.118 (4H, d, J = 9.16 Hz, ArH), 2.561 (2H, tdd, J = 12.15, 3.21, 2.75, Ar-CH-(CH₂)₂), 2.299 (4H, s, Ar-(C(CH₂)₂)-Ar), 1.944-1.893 (8H, m, Ar-CH-(CH₂)₂), 1.634-1.432 (10H, m, CyHexH), 1.360-1.213 (14H, m, CH-CH₂-CH₂-CH₂-CH₃), 1.132-1.016 (4H, m, CyHexH), 0.913 (6H, t, J = 7.33 Hz, CH₂-CH₃)

¹³C NMR (δ/ppm, 100.5 MHz, CDCl₃): 165.20, 154.07, 148.62, 130.25, 128.22, 127.16, 127.05, 121.27, 45.78, 44.80, 37.34, 37.18, 37.02, 34.01, 33.39, 30.92, 29.18, 22.98, 22.78, 14.15

IR (νmax cm⁻¹): 652.0, 655.8, 665.9, 669.8, 678.5, 687.2, 698.2, 704.0, 716.1, 730.1, 733.9, 755.6, 782.1, 801.0, 838.1, 848.2, 868.5, 898.4, 956.7, 968.8, 983.7, 1013.1, 1068.2, 1105.2, 1168.4, 1177.6, 1204.6, 1261.0, 1411.4, 1445.2, 1501.1, 1608.7, 1724.9, 2848.9, 2921.7

ESI-MS (*m/z*): 775.4673 (C₅₂H₆₄NaO₄ [M+Na⁺]), 791.4398 (C₅₂H₆₄KO₄ [M+K⁺])

Elemental Analysis (mass %): Calculated: C, 82.94 %; H, 8.57 %; N, 0 %; Other, 8.49 %. Found: C, 83.02 %; H, 8.55 %; N, 0 %; Other, 8.43 %.

Compound 20: Cyclohexane-1,1-diylbis(4,1-phenylene) bis(4-(4-pentylcyclohexyl)benzoate)

Prepared according to Scheme 1. Compound **2** (1 g, 3.7 mmol), Compound **10** (2.02 g, 7.4 mmol), EDAC (2.13 g, 11.1 mmol), DMAP (10 mg), DCM (10 cm³). Recrystallisation from ethanol:THF (10:1) yielded **20** as a white powder.

Yield: 2.37g (3.0 mmol, 82%)

¹H NMR (δ/ppm, 400 MHz, CDCl₃): 8.083 (4H, d, J = 8.24 Hz, ArH), 7.311 (4H, d, J = 8.24 Hz, ArH), 7.305 (4H, d, J = 8.70 Hz, ArH), 7.097 (4H, d, J = 8.70 Hz, ArH), 2.538 (2H, tdd, J = 12.15, 3.21, 2.75, Ar-CH-(CH₂)₂), 2.277 (4H, s, Ar-(C(CH₂)₂)-Ar), 1.926-1.839 (8H, m, Ar-CH-(CH₂)₂), 1.616-1.402 (10H, m, CyHexH), 1.360-1.178 (18H, m, CH-CH₂-CH₂-CH₂-CH₂-CH₃), 1.111-0.987 (4H, m, CyHexH), 0.884 (6H, t, J = 7.33 Hz, CH₂-CH₃)

¹³C NMR (δ/ppm, 100.5 MHz, CDCl₃): 162.78, 151.65, 146.22, 143.37, 127.85, 125.81, 124.76, 124.64, 118.86, 43.38, 42.40, 34.93, 34.89, 34.79, 31.61, 30.98, 29.76, 24.2, 23.87, 20.38, 20.29, 11.71

IR (νmax cm⁻¹): 652.0, 660.6, 663.0, 667.9, 67805, 722.8, 756.1, 801.4, 826.5, 847.7, 868.5, 955.7, 982.7, 1012.2, 1065.2, 1105.2, 1168.4, 1261.0, 1411.9, 1451.9, 1500.6, 1608.7, 1724.9, 2010.9, 2847.4, 2918.8

ESI-MS (*m/z*): 803.5010 (C₅₄H₆₈NaO₄ [M+Na⁺]), 819.4698 (C₅₄H₆₈KO₄ [M+K⁺])

Elemental Analysis (mass %): Calculated: C, 83.03 %; H, 8.77 %; N, 0 %; Other, 8.20 %. Found: C, 83.13 %; H, 8.79 %; N, 0 %; Other, 8.08 %.

Compound 21: Cyclohexane-1,1-diylbis(4,1-phenylene) bis(4-(4-heptylcyclohexyl)benzoate)

Prepared according to Scheme 1. Compound **2** (1 g, 3.7 mmol), Compound **11** (2.24 g, 7.4 mmol), EDAC (2.13 g, 11.1 mmol), DMAP (10 mg), DCM (10 cm³). Recrystallisation from ethanol:THF (10:1) yielded **21** as a white powder.

Yield: 2.60 g (3.1 mmol, 84%)

¹H NMR (δ /ppm, 400 MHz, CDCl₃): 8.123 (4H, d, J = 8.24 Hz, ArH), 7.347 (4H, d, J = 8.24 Hz, ArH), 7.343 (4H, d, J = 8.70 Hz, ArH), 7.136 (4H, d, J = 8.70 Hz, ArH), 2.575 (2H, tt, J = 12.15, 2.75, Ar-CH-(CH₂)₂), 2.313 (4H, s, Ar-(C(CH₂)₂)-Ar), 1.967-1.861 (8H, m, Ar-CH-(CH₂)₂), 1.667-1.440 (10H, m, CyHexH), 1.391-1.213 (26H, m, CH-CH₂-CH₂-CH₂-CH₂-CH₂-CH₂-CH₃), 1.144-1.025 (4H, m, CyHexH), 0.916 (6H, t, J = 6.87 Hz, CH₂-CH₃)

¹³C NMR (δ /ppm, 100.5 MHz, CDCl₃): 165.16, 154.03, 148.62, 145.75, 130.24, 128.20, 127.16, 127.03, 121.26, 45.77, 44.79, 37.34, 37.19, 34.00, 33.38, 31.90, 29.93, 29.37, 26.94, 26.27, 22.78, 22.68, 14.12

IR (ν max cm⁻¹): 656.8, 666.9, 668.8, 672.2, 677.0, 701.6, 736.8, 744.1, 746.9, 759.0, 803.8, 867.0, 972.6, 1012.6, 1066.6, 1169.4, 1205.0, 1261.9, 1416.7, 1445.7, 1501.1, 1608.7, 1731.1, 2161.7, 2850.8, 2922.2

ESI-MS (m/z): 859.5636 (C₅₈H₇₆NaO₄ [M+Na⁺]), 875.5375 (C₅₈H₇₆KO₄ [M+K⁺])

Elemental Analysis (mass %): Calculated: C, 83.21 %; H, 9.15 %; N, 0 %; Other, 7.64 %. Found: C, 83.26 %; H, 9.17 %; N, 0 %; Other, 7.57 %.

Compound 22: Sulfonylbis(4,1-phenylene) bis(4-(4-ethylcyclohexyl)benzoate)

Prepared according to Scheme 1. Compound **3** (500 mg, 2.0 mmol), Compound **7** (0.93 g, 4.0 mmol), EDAC (1.15 g, 6.0 mmol), DMAP (10 mg), DCM (10 cm³). Recrystallisation from ethanol:THF (10:1) yielded **22** as a white powder.

Yield: 1.17 g (1.7 mmol, 86%)

¹H NMR (δ /ppm, 400 MHz, CDCl₃): 8.072 (4H, d, J = 8.24 Hz, ArH), 8.005 (4H, ddd, J = 8.70, 2.75, 1.83 Hz, ArH), 7.383-7.310 (8H, m, ArH), 2.549 (2H, tdd, J = 12.15, 3.21, 2.75, Ar-CH-(CH₂)₂), 1.893 (8H, d, J = 11.45 Hz, Ar-CH-(CH₂)₂), 1.512-1.407 (4H, m, CyHexH), 1.306-1.153 (6H, m, CH-CH₂-CH₃), 1.104-0.985 (4H, m, CyHexH), 0.897 (6H, t, J = 7.33 Hz, CH₂-CH₃)

¹³C NMR (δ /ppm, 100.5 MHz, CDCl₃): 164.34, 154.82, 154.79, 135.56, 130.44, 123.43, 127.26, 126.17, 122.81, 44.85, 38.95, 33.95, 32.92, 29.89, 11.50

IR (ν_{\max} cm⁻¹): 665.4, 700.2, 719.5, 758.0, 810.1, 832.2, 881.5, 987.6, 1012.6, 1058.9, 1109.1, 1151.5, 1178.5, 1201.7, 1263.4, 1298.1, 1327.0, 1367.5, 1410.0, 1446.6, 1458.2, 1489.1, 1585.5, 1608.6, 1735.9, 2333.9, 2362.8, 2846.9, 2920.2, 2960.7

ESI-MS (m/z): 679.3094 (C₄₂H₄₇O₆S [M+H⁺]), 701.2882 (C₄₂H₄₆NaO₆S [M+Na⁺])

Elemental Analysis (mass %): Calculated: C, 74.31 %; H, 6.83 %; N, 0 %; Other, 18.86 %. Found: C, 74.17 %; H, 6.83 %; N, 0 %; Other, 19.01 %.

Compound 23: Sulfonylbis(4,1-phenylene) bis(4-(4-propylcyclohexyl)benzoate)

Prepared according to Scheme 1. Compound **3** (500 mg, 2.0 mmol), Compound **8** (0.99 g, 4.0 mmol), EDAC (1.15 g, 6.0 mmol), DMAP (10 mg), DCM (10 cm³). Recrystallisation from ethanol:THF (10:1) yielded **23** as a white powder.

Yield: 1.23 g (1.7 mmol, 87%)

¹H NMR (δ/ppm, 400 MHz, CDCl₃): 8.103 (4H, d, J = 8.24 Hz, ArH), 7.408 (4H, ddd, J = 8.70, 2.75, 1.83 Hz, ArH), 7.339 (4H, d, J = 8.24 Hz, ArH), 7.162 (4H, ddd, J = 8.70, 2.75, 1.83 Hz, ArH), 2.561 (2H, dddd, J = 12.36, 11.91, 3.21, 2.75, Ar-CH-(CH₂)₂), (8H, t, J = 9.35 Hz, Ar-CH-(CH₂)₂), 1.535-1.431 (4H, m, CyHexH), 1.385-1.193 (10H, m, CH-CH₂-CH₂-CH₃), 1.118-1.015 (4H, m, CyHexH), 0.906 (6H, t, J = 7.33 Hz, CH₂-CH₂-CH₃)

¹³C NMR (δ/ppm, 100.5 MHz, CDCl₃): 164.31, 154.77, 138.53, 130.41, 129.40, 127.23, 126.14, 122.80, 44.81, 39.56, 36.86, 33.94, 33.28, 30.89, 19.96, 14.34

IR (νmax cm⁻¹): 665.4, 700.2, 719.5, 731.0, 756.1, 785.0, 810.1, 839.0, 879.5, 956.7, 1012.6, 1057.0, 1109.1, 1149.6, 1166.9, 1178.5, 1197.8, 1263.4, 1300.0, 1325.0, 1408.0, 1446.6, 1489.1, 1506.4, 1585.5, 1608.6, 1735.9, 2843.1, 2918.3, 2951.1

ESI-MS (*m/z*): 707.3401 (C₄₄H₅₁O₆S [M+H⁺]), 729.3213 (C₄₄H₅₀NaO₆S [M+Na⁺])

Elemental Analysis (mass %): Calculated: C, 74.76 %; H, 7.13 %; N, 0 %; Other, 18.11 %. Found: C, 74.54 %; H, 7.11 %; N, 0 %; Other, 18.35 %.

Compound 24: Sulfonylbis(4,1-phenylene) bis(4-(4-butylcyclohexyl)benzoate)

Prepared according to Scheme 1. Compound **3** (500 mg, 2.0 mmol), Compound **9** (1.04 g, 4.0 mmol), EDAC (1.15 g, 6.0 mmol), DMAP (10 mg), DCM (10 cm³)
Recrystallisation from ethanol:THF (10:1) yielded **24** as a white powder.

Yield: 1.31 g (1.8 mmol, 89%)

¹H NMR (δ /ppm, 400 MHz, CDCl₃): 8.090 (4H, d, J = 8.47 Hz, ArH), 8.025 (4H, d, J = 8.70 Hz, ArH), 7.404- 7.326 (8H, m, ArH), 2.566 (2H, tdd, J = 12.15, 3.21, 2.75, Ar-CH-(CH₂)₂), 1.901 (8H, d, J = 10.07 Hz, Ar-CH-(CH₂)₂), 1.545-1.423 (4H, m, CyHexH), 1.360-1.190 (14H, m, CH-CH₂-CH₂-CH₂-CH₃), 1.124-1.007 (4H, m, CyHexH), 0.905 (6H, t, J = 6.87 Hz, CH₂-CH₃)

¹³C NMR (δ /ppm, 100.5 MHz, CDCl₃): 164.34, 154.83, 154.79, 135.55, 130.43, 129.42, 127.25, 126.16, 122.81, 44.84, 37.17, 36.99, 33.97, 33.35, 30.93, 29.18, 22.97, 14.14

IR (ν max cm⁻¹): 665.4, 698.2, 717.5, 731.0, 754.2, 812.0, 837.1, 850.6, 881.5, 968.3, 1012.6, 1055.1, 1109.1, 1151.5, 1178.5, 1195.9, 1261.5, 1298.1, 1327.0, 1406.1, 1446.6, 1489.1, 1506.4, 1558.5, 1583.6, 1608.6, 1739.8, 2846.9, 2916.4

ESI-MS (m/z): 735.3714 (C₄₆H₅₅O₆S [M+H⁺]), 757.3520 (C₄₆H₅₄NaO₆S [M+Na⁺])

Elemental Analysis (mass %): Calculated: C, 75.17 %; H, 7.41 %; N, 0 %; Other, 17.42 %.
Found: C, 75.24 %; H, 7.43 %; N, 0 %; Other, 17.33 %.

Compound 25: Sulfonylbis(4,1-phenylene) bis(4-(4-pentylcyclohexyl)benzoate)

Prepared according to Scheme 1. Compound **3** (500 mg, 2.0 mmol), Compound **10** (1.10 g, 4.0 mmol), EDAC (1.15 g, 6.0 mmol), DMAP (10 mg), DCM (10 cm³). Recrystallisation from ethanol:THF (10:1) yielded **25** as a white powder.

Yield: 1.25 g (1.6 mmol, 82%)

¹H NMR (δ /ppm, 400 MHz, CDCl₃): 8.090 (4H, d, J = 8.24 Hz, ArH), 8.023 (4H, d, J = 8.70 Hz, ArH), 7.408- 7.325 (8H, m, ArH), 2.566 (2H, tdd, J = 12.15, 3.21, 2.75, Ar-CH-(CH₂)₂), 1.901 (8H, d, J = 9.62 Hz, Ar-CH-(CH₂)₂), 1.541-1.428 (4H, m, CyHexH), 1.376-1.190 (14H, m, CH-CH₂-CH₂-CH₂-CH₂-CH₃), 1.127-1.001 (4H, m, CyHexH), 0.897 (6H, t, J = 6.87 Hz, CH₂-CH₃)

¹³C NMR (δ /ppm, 100.5 MHz, CDCl₃): 164.30, 154.79, 154.76, 138.53, 130.40, 129.39, 127.22, 126.13, 122.79, 44.81, 37.24, 37.15, 33.94, 33.31, 32.13, 30.89, 26.57, 22.66, 14.08

IR (ν max cm⁻¹): 665.4, 698.2, 717.5, 731.0, 754.2, 812.0, 839.0, 881.5, 970.2, 1012.6, 1057.0, 1107.1, 1149.6, 1165.0, 1178.5, 1195.9, 1261.5, 1298.1, 1327.0, 1406.1, 1446.6, 1489.1, 1506.4, 1539.2, 1558.5, 1583.6, 1608.6, 1653.0, 1699.3, 1739.8, 2848.9, 2920.2

ESI-MS (m/z): 785.3834 (C₄₈H₅₈NaO₆S [M+Na⁺])

Elemental Analysis (mass %): Calculated: C, 75.56 %; H, 7.66 %; N, 0 %; Other, 16.78 %. Found: C, 75.50 %; H, 7.62 %; N, 0 %; Other, 16.88 %.

Compound 26: Sulfonylbis(4,1-phenylene) bis(4-(4-heptylcyclohexyl)benzoate)

Prepared according to Scheme 1. Compound **3** (500 mg, 2.0 mmol), Compound **11** (1.21 g, 4.0 mmol), EDAC (1.15 g, 6.0 mmol), DMAP (10 mg), DCM (10 cm³). Recrystallisation from ethanol:THF (10:1) yielded **26** as a white powder.

Yield: 1.23g (1.5 mmol, 75%)

¹H NMR (δ /ppm, 400 MHz, CDCl₃): 8.092 (4H, d, J = 8.24 Hz, ArH), 8.025 (4H, d, J = 8.70 Hz, ArH), 7.379 (4H, d, J = 8.70 Hz, ArH), 7.348 (4H, d, J = 8.24 Hz, ArH), 2.566 (2H, ddt, J = 12.36, 11.91, 2.75, Ar-CH-(CH₂)₂), 1.901 (8H, d, J = 9.62 Hz, Ar-CH-(CH₂)₂), 1.530-1.429 (4H, m, CyHexH), 1.376-1.196 (24H, m, CH-CH₂-CH₂-CH₂-CH₂-CH₂-CH₂-CH₂-CH₃), 1.130-1.008 (4H, m, CyHexH), 0.891 (6H, t, J = 6.87 Hz, CH₂-CH₃).

¹³C NMR (δ /ppm, 100.5 MHz, CDCl₃): 164.28, 154.78, 154.76, 138.53, 130.40, 129.38, 127.21, 126.13, 122.78, 44.80, 37.29, 37.16, 33.94, 33.31, 31.87, 30.88, 29.89, 29.34, 26.92, 22.65. 14.10

IR (ν max cm⁻¹): 667.4, 698.2, 715.6, 729.1, 754.2, 810.1, 837.1, 879.5, 968.3, 1012.6, 1055.1, 1107.1, 1151.5, 1165.00, 1178.5, 1199.7, 1261.5, 1296.2, 1327.0, 1408.0, 1456.3, 1489.1, 1585.5, 1608.6, 1735.9, 2848.9, 2918.3

ESI-MS (m/z): 841.4472 (C₅₂H₆₆NaO₆S [M+Na⁺])

Elemental Analysis (mass %): Calculated: C, 76.25 %; H, 8.12 %; N, 0 %; Other, 15.63 %. Found: C, 76.25 %; H, 8.15 %; N, 0 %; Other, 15.6 %.

Compound 27: Carbonylbis(4,1-phenylene) bis(4-(4-ethylcyclohexyl)benzoate)

Prepared according to Scheme 1. Compound **4** (500 mg, 2.3 mmol), Compound **7** (1.07 g, 4.6 mmol), EDAC (1.30 g, 6.9 mmol), DMAP (10 mg), DCM (10 cm³). Recrystallisation from ethanol:THF (10:1) yielded **27** as a white powder.

Yield: 1.30g (2.0 mmol, 88%)

¹H NMR (δ /ppm, 400 MHz, CDCl₃): 8.142 (4H, d, J = 8.24 Hz, ArH), 7.925 (4H, ddd, J = 8.7, 2.29, 1.83 Hz, ArH), 7.360 (8H, dd, J = 8.70, 8.24 Hz, ArH), 2.583 (2H, dddd, J = 12.36, 11.91, 3.21, 2.75 Hz, Ar-CH-(CH₂)₂), 1.950-1.889 (8H, m, Ar-CH-(CH₂)₂), 1.551-1.447 (4H, m, CyHexH), 1.329-1.184 (6H, m, CH-CH₂-CH₃), 1.128-1.026 (4H, m, CyHexH), 0.928 (6H, t, J = 7.33 Hz CH-CH₂-CH₃)

¹³C NMR (δ /ppm, 100.5 MHz, CDCl₃): 194.46, 164.71, 154.58, 154.35, 134.91, 131.63, 130.40, 127.21, 126.55, 121.73, 44.84, 38.96, 33.96, 32.94, 29.89, 11.50

IR (ν max cm⁻¹): 667.4, 700.2, 756.1, 798.5, 848.7, 1012.6, 1064.7, 1163.1, 1178.5, 1203.6, 1263.4, 1400.3, 1415.8, 1450.5, 1487.1, 1591.3, 1610.6, 1726.3, 1739.8, 2850.8, 2926.0, 2964.6

ESI-MS (m/z): 643.3148 (C₄₃H₄₇O₅ [M+H⁺]), 665.3227 (C₄₃H₄₆NaO₅ [M+Na⁺])

Elemental Analysis (mass %): Calculated: C, %; 80.34 H, 7.21 %; N, 0 %; Other, 12.45 %. Found: C, 80.326 %; H, 7.163 %; N, 0 %; Other, 12.505 %.

Compound 28: Carbonylbis(4,1-phenylene) bis(4-(4-propylcyclohexyl)benzoate)

Prepared according to Scheme 1. Compound **4** (500 mg, 2.3 mmol), Compound **8** (1.13 g, 4.6 mmol), EDAC (1.30 g, 6.9 mmol), DMAP (10 mg), DCM (10 cm³). Recrystallisation from ethanol:THF (10:1) yielded **28** as a white powder.

Yield: 1.22 g (1.8 mmol, 79%)

¹H NMR (δ /ppm, 400 MHz, CDCl₃): 8.100 (4H, d, J = 8.24 Hz, ArH), 7.887 (4H, ddd, J = 8.70, 2.29, 1.83 Hz, ArH), 7.333 (4H, d, J = 8.24 Hz, ArH), 7.320 (4H, d, J = 8.70 Hz, ArH), 2.545 (2H, dddd, J = 12.36, 11.91, 3.21, 2.75 Hz, Ar-CH-(CH₂)₂), 1.887 (8H, t, J = 10.53 Hz, Ar-CH-(CH₂)₂), 1.515-1.411 (4H, m, CyHexH), 1.372-1.166 (10H, m, CH-CH₂-CH₂-CH₃), 1.095-0.999 (4H, m, CyHexH), 0.876 (6H, t, J = 7.33 Hz, CH-CH₂-CH₂-CH₃)

¹³C NMR (δ /ppm, 100.5 MHz, CDCl₃): 206.94, 194.56, 164.68, 154.57, 154.32, 134.88, 131.60, 130.37, 127.18, 126.50, 121.77, 44.80, 39.57, 36.86, 33.95, 33.29, 30.87, 19.95, 14.33

IR (ν max cm⁻¹): 665.4, 756.1, 765.7, 783.1, 806.3, 848.7, 864.1, 891.1, 929.7, 954.8, 976.0, 1012.6, 1060.9, 1097.5, 1153.4, 1176.6, 1195.9, 1244.1, 1265.3, 1292.3, 1375.3, 1410.0, 1421.5, 1440.8, 1456.3, 1496.8, 1539.2, 1558.5, 1595.1, 1608.6, 1645.3, 1728.2, 2843.1, 2918.3, 2955.0

ESI-MS (m/z): 671.3745 (C₄₅H₅₁O₅ [M+H⁺]), 693.3552 (C₄₅H₅₀NaO₅ [M+Na⁺])

Elemental Analysis (mass %): Calculated: C, 80.56 %; H, 7.51 %; N, 0 %; Other, 11.93 %. Found: C, 80.40 %; H, 7.52 %; N, 0 %; Other, 12.09 %.

Compound 29: Carbonylbis(4,1-phenylene) bis(4-(4-butylcyclohexyl)benzoate)

Prepared according to Scheme 1. Compound **4** (500 mg, 2.3 mmol), Compound **9** (1.20 g, 4.6 mmol), EDAC (1.30 g, 6.9 mmol), DMAP (10 mg), DCM (10 cm³). Recrystallisation from ethanol:THF (10:1) yielded **29** as a white powder.

Yield: 1.32g (1.9 mmol, 82%)

¹H NMR (δ /ppm, 400 MHz, CDCl₃): 8.133 (4H, d, J = 8.24 Hz, ArH), 7.918 (4H, ddd, J = 8.70, 2.29, 1.83 Hz, ArH), 7.352 (8H, dd, J = 8.70, 8.24 Hz, ArH), 2.575 (2H, dddd, J = 12.36, 11.91, 3.21, 2.75 Hz, Ar-CH-(CH₂)₂), 1.912 (8H, t, J = 9.39 Hz, Ar-CH-(CH₂)₂), 1.543-1.439 (4H, m, CyHexH), 1.334-1.235 (14H, m, CH-CH₂-CH₂-CH₂-CH₃), 1.126-1.024 (4H, m, CyHexH), 0.908 (6H, t, J = 7.10 Hz, CH-CH₂-CH₂-CH₂-CH₃)

¹³C NMR (δ /ppm, 100.5 MHz, CDCl₃): 194.48, 164.73, 154.60, 154.35, 134.92, 131.64, 130.41, 127.22, 126.55, 121.80, 44.85, 37.18, 37.01, 34.00, 33.38, 29.18, 22.98, 14.15

IR (ν max cm⁻¹): 665.4, 696.3, 731.0, 754.2, 765.7, 787.0, 806.3, 848.7, 891.1, 927.8, 1012.6, 1058.9, 1153.4, 1176.6, 1195.9, 1263.4, 1419.6, 1438.9, 1456.3, 1489.1, 1506.4, 1539.2, 1558.5, 1595.1, 1645.3, 1683.9, 1726.3, 2341.6, 2360.9, 2845.0, 2922.2

ESI-MS (m/z): 699.4043 (C₄₇H₅₅O₅ [M+H⁺]), 721.3880 (C₄₇H₅₄NaO₅ [M+Na⁺])

Elemental Analysis (mass %): Calculated: C, 80.77 %; H, 7.79 %; N, 0 %; Other, 11.44 %. Found: C, 80.859 %; H, 7.821 %; N, 0 %; Other, 11.32 %.

Compound 30: Carbonylbis(4,1-phenylene) bis(4-(4-pentylcyclohexyl)benzoate)

Prepared according to Scheme 1. Compound **4** (500 mg, 2.3 mmol), Compound **10** (1.26 g, 4.6 mmol), EDAC (1.30 g, 6.9 mmol), DMAP (10 mg), DCM (10 cm³). Recrystallisation from ethanol: THF (10:1) yielded **30** as a white powder.

Yield: 1.47 g (2.0 mmol, 88%)

¹H NMR (δ /ppm, 400 MHz, CDCl₃): 8.142 (4H, d, J = 8.24 Hz, ArH), 7.926 (4H, d, J = 8.70 Hz, ArH), 7.364 (8H dd, 8.7, 8.24 Hz, ArH), 2.582 (2H, dddd, J = 12.36, 11.91, 3.21, 2.75 Hz, Ar-CH-(CH₂)₂), 1.920 (8H, t, 9.39 Hz, Ar-CH-(CH₂)₂), 1.551-1.448 (4H, m, CyHexH), 1.354-1.219 (18H, m, CH-CH₂-CH₂-CH₂-CH₂-CH₃), 1.133-1.031 (4H, m, CyHexH), 0.908 (6H, t, J = 6.87 Hz, CH-CH₂-CH₂-CH₂-CH₂-CH₃)

¹³C NMR (δ /ppm, 100.5 MHz, CDCl₃): 194.43, 164.69, 154.57, 154.34, 134.90, 131.62, 130.39, 127.20, 126.54, 121.78, 44.83, 37.27, 37.18, 33.99, 33.36, 32.16, 26.60, 22.69, 14.11

IR (ν_{\max} cm⁻¹): 667.4, 698.2, 756.1, 846.8, 889.2, 929.7, 1012.6, 1060.9, 1155.4, 1176.6, 1195.9, 1263.4, 1489.1, 1506.4, 1539.2, 1558.5, 1595.1, 1608.6, 1645.3, 1683.9, 1730.2, 2848.9, 2920.23

ESI-MS (m/z): 727.4392 (C₄₉H₅₉O₅ [M+H⁺]), 749.4174 (C₄₉H₅₈NaO₅ [M+Na⁺])

Elemental Analysis (mass %): Calculated: C, 80.95 %; H, 8.04 %; N, 0 %; Other, 11.01 %. Found: C, 81.03 %; H, 8.10 %; N, 0 %; Other, 10.9 %.

Compound 31: Carbonylbis(4,1-phenylene) bis(4-(4-heptylcyclohexyl)benzoate)

Prepared according to Scheme 1. Compound **4** (500 mg, 2.3 mmol), Compound **11** (1.40 g, 4.6 mmol), EDAC (1.30 g, 6.9 mmol), DMAP (10 mg), DCM (10 cm³). Recrystallisation from ethanol:THF (10:1) yielded **31** as a white powder.

Yield: 1.62 g (2.1 mmol, 90%)

¹H NMR (δ /ppm, 400 MHz, CDCl₃): 8.129 (4H, d, J 8.24 Hz, ArH), 7.903 (4H, d, J = 8.70 Hz, ArH), 7.340 (8H dd, 8.7, 8.24 Hz, ArH), (2H, dddd, J = 12.36, 11.91, 3.21, 2.75 Hz, Ar-CH-(CH₂)₂), 1.897 (8H, t, J = 9.85 Hz, Ar-CH-(CH₂)₂), 1.528-1.424 (4H, m, CyHexH), 1.299-1.196 (24H, m, CH-CH₂-CH₂-CH₂-CH₂-CH₂-CH₂-CH₃), 1.100-1.039 (4H, m, CyHexH), 0.877 (6H, dd, J = 7.33, 6.41 Hz, CH-CH₂-CH₂-CH₂-CH₂-CH₂-CH₂-CH₃)

¹³C NMR (δ /ppm, 100.5 MHz, CDCl₃): 194.46, 164.71, 154.59, 154.35, 134.90, 131.63, 130.40, 127.21, 126.54, 121.79, 44.85, 37.33, 37.20, 34.00, 33.37, 31.90, 29.92, 29.37, 26.95, 22.69, 14.12

IR (ν max cm⁻¹): 671.2, 700.2, 723.3, 761.9, 808.2, 848.7, 889.2, 929.7, 970.2, 1012.6, 1058.9, 1107.1, 1159.2, 1174.7, 1192.0, 1261.5, 1302.0, 1446.6, 1496.8, 1539.2, 1558.5, 1595.1, 1647.2, 1735.9, 2848.9, 2918.3, 2953.0

APCI-MS (m/z): 783.498 (C₅₃H₆₇O₅ [M+H⁺])

Elemental Analysis (mass %): Calculated: C, 81.29 %; H, 8.49 %; N, 0 %; Other, 10.22 %. Found: C, 81.40 %; H, 8.59 %; N, 0 %; Other, 10.01 %.

Compound 32: Methylenebis(4,1-phenylene) bis(4-(4-ethylcyclohexyl)benzoate)

Prepared according to Scheme 1. Compound **5** (200 mg, 1 mmol), Compound **7** (465 mg, 2 mmol), EDAC (570 mg, 3 mmol), DMAP (10 mg), DCM (10 cm³). Recrystallisation from ethanol:THF (10:1) yielded **32** as a white powder.

Yield: 530 mg (0.8 mmol, 84%)

¹H NMR (δ/ppm, 400 MHz, CDCl₃): 8.09 (4H, d, J = 8.24 Hz, ArH), 7.32 (4H, d, J = 8.24 Hz, ArH), 7.22 (4H, d, J = 8.7 Hz, ArH), 7.11 (4H, d, J = 8.7 Hz, ArH), 4.03 (2H, s, Ar-CH₂-Ar), 2.54 (2H, tt, J = 11.91, 2.75 Hz, Ar-CH-(CH₂)₂), 1.89 (8H, d, J = 10.53 Hz, Ar-CH-(CH₂)₂), 1.47 (4H, m, CyHexH), 1.3-1.16 (6H, m, (CH₂)₂-CH-CH₂-CH₃), 1.095-0.994 (4H, m, CyHexH), 0.90 (6H, t, J = 7.33 Hz, CH₂-CH₃)

¹³C NMR (δ/ppm, 100.5 MHz, CDCl₃): 165.29, 154.11, 149.34, 138.29, 130.28, 129.90, 127.07, 121.71, 44.81, 40.65, 38.96, 33.98, 32.96, 29.91, 11.52

IR (νmax cm⁻¹): 654.8, 662.6, 667.4, 676.6, 681.4, 684.7, 700.2, 710.8, 733.9, 758.0, 793.7, 802.9, 816.9, 986.1, 1012.6, 1068.6, 1206.0, 1262.4, 1365.6, 1413.4, 1447.1, 1500.6, 1608.65, 1698.8, 1728.7, 2034.4, 2040.2, 3042.2, 2160.8, 2849.4, 2916.9

ESI-MS (*m/z*): 651.3470 (C₄₃H₄₈NaO₄ [M+Na⁺])

Elemental Analysis (mass %): Calculated: C, 82.13 %; H, 7.69 %; N, 0 %; Other, 10.18 %. Found: C, 82.13 %; H, 7.73 %; N, 0 %; Other, 10.14 %.

Compound 33: Methylenebis(4,1-phenylene) bis(4-(4-propylcyclohexyl)benzoate)

Prepared according to Scheme 1. Compound **5** (200 mg, 1 mmol), Compound **8** (493 mg, 2 mmol), EDAC (570 mg, 3 mmol), DMAP (10 mg), DCM (10 cm³). Recrystallisation from ethanol:THF (10:1) yielded **33** as a white powder.

Yield: 590 mg (0.9 mmol, 90%)

¹H NMR (δ /ppm, 400 MHz, CDCl₃): 8.125 (4H, d, J = 8.24 Hz, ArH), 7.346 (4H, d, J = 8.24 Hz, ArH), 7.250 (4H, d, J = 8.24 Hz, ArH), 7.137 (4H, d, J = 8.24 Hz, ArH), 4.031 (2H, s, Ar-CH₂-Ar), 2.566 (2H, tt, J = 11.91, 3.21 Hz, Ar-CH-(CH₂)₂), 1.912 (8H, t, J = 10.07 Hz, Ar-CH-(CH₂)₂), 1.484 (4H, m, CyHexH), 1.416-1.210 (10H, m, (CH₂)₂-CH-CH₂-CH₂-CH₃), 1.077 (4H, m, CyHexH), 0.921 (6H, t, J = 7.33 Hz, CH₂-CH₃)

¹³C NMR (δ /ppm, 100.5 MHz, CDCl₃): 165.27, 154.10, 149.34, 138.28, 130.27, 129.89, 127.06, 121.70, 44.79, 40.64, 39.61, 36.89, 33.99, 33.34, 19.98, 14.39

IR (ν max cm⁻¹): 654.4, 656.3, 658.2, 665.0, 667.9, 671.2, 674.6, 679.4, 691.5, 693.4, 698.2, 702.1, 741.2, 746.9, 754.2, 783.6, 803.4, 813.5, 838.6, 869.5, 1012.6, 1070.0, 1171.3, 1207.5, 1261.9, 1365.6, 1412.9, 1449.0, 1500.2, 1510.3, 1608.2, 1698.3, 2844.6, 2921.7

ESI-MS (m/z): 679.3758 (C₄₅H₅₂NaO₄ [M+Na⁺])

Elemental Analysis (mass %): Calculated: C, 82.28 %; H, 7.98 %; N, 0 %; Other, 9.74 %. Found: C, 82.19 %; H, 7.94 %; N, 0 %; Other, 9.87 %.

Compound 34: Methylenebis(4,1-phenylene) bis(4-(4-butylcyclohexyl)benzoate)

Prepared according to Scheme 1. Compound **5** (200 mg, 1 mmol), Compound **9** (520 mg, 2 mmol), EDAC (570 mg, 3 mmol), DMAP (10 mg), DCM (10 cm³). Recrystallisation from ethanol:THF (10:1) yielded **34** as a white powder.

Yield: 600 mg (0.9 mmol, 88%)

¹H NMR (δ /ppm, 400 MHz, CDCl₃): 8.124 (4H, d, J = 8.24 Hz, ArH), 7.346 (4H, d, J = 8.24 Hz, ArH), 7.249 (4H, d, J = 8.24 Hz, ArH), 7.137 (4H, d, J = 8.24 Hz, ArH), 4.032 (2H, s, Ar-CH₂-Ar), 2.570 (2H, tdd, J = 12.15, 3.21, 2.75 Hz, Ar-CH-(CH₂)₂), 1.937-1.893 (8H, m, Ar-CH-(CH₂)₂), 1.545-1.441 (4H, m, CyHexH), 1.337-1.244 (14H, m, (CH₂)₂-CH-CH₂-CH₂-CH₂-CH₃), 1.130-1.029 (4H, m, CyHexH), 0.921 (6H, t, J = 7.33 Hz, CH₂-CH₃)

¹³C NMR (δ /ppm, 100.5 MHz, CDCl₃): 165.28, 154.11, 149.34, 138.28, 130.27, 129.90, 127.07, 121.70, 44.80, 40.64, 37.17, 37.02, 34.01, 33.39, 29.18, 22.99, 14.16

IR (ν max cm⁻¹): 662.6, 667.9, 669.3, 674.6, 676.5, 704.0, 717.5, 736.8, 744.5, 867.0, 1012.6, 1071.0, 1173.2, 1207.5, 1262.4, 1365.6, 1412.9, 1449.0, 1502.1, 1608.7, 1698.8, 1728.2, 2849.4, 2916.9

ESI-MS (m/z): 707.4071 (C₄₇H₅₆NaO₄ [M+Na⁺])

Elemental Analysis (mass %): Calculated: C, 82.42 %; H, 8.24 %; N, 0 %; Other, 9.34 %. Found: C, 81.98 %; H, 8.20 %; N, 0 %; Other, 9.82 %.

Compound 36: Methylenebis(4,1-phenylene) bis(4-(4-heptylcyclohexyl)benzoate)

Prepared according to Scheme 1. Compound **5** (200 mg, 1 mmol), Compound **11** (600 mg, 2 mmol), EDAC (570 mg, 3 mmol), DMAP (10 mg), DCM (10 cm³). Recrystallisation from ethanol:THF (10:1) yielded **35** as a white powder.

Yield: 670 mg (0.9 mmol, 87%)

¹H NMR (δ /ppm, 400 MHz, CDCl₃): 8.127 (4H, d, J = 8.24 Hz, ArH), 7.345 (4H, d, J = 8.24 Hz, ArH), 7.249 (4H, d, J = 8.24 Hz, ArH), 7.140 (4H, d, J = 8.24 Hz, ArH), 4.030 (2H, s, Ar-CH₂-Ar), 2.570 (2H, tdd, J = 12.15, 3.21, 2.75, Ar-CH-(CH₂)₂), 1.958-1.872 (8H, m, Ar-CH-(CH₂)₂), 1.574-1.444 (4H, m, CyHexH), 1.388-1.214 (26H, m, (CH₂)₂-CH-CH₂-CH₂-CH₂-CH₂-CH₂-CH₂-CH₃), 1.132-1.030 (4H, m, CyHexH), 0.911 (6H, t, J = 7.33 Hz, CH₂-CH₃)

¹³C NMR (δ /ppm, 100.5 MHz, CDCl₃): 165.24, 154.08, 149.35, 138.26, 130.27, 129.88, 127.10, 127.05, 121.69, 44.80, 40.63, 37.34, 37.20, 34.00, 33.39, 31.90, 29.93, 29.38, 26.95, 22.68, 14.13

IR (ν max cm⁻¹): 667.4, 679.4, 686.2, 697.8, 704.0, 723.3, 764.3, 798.1, 828.0, 842.9, 873.3, 883.4, 914.8, 939.3, 967.8, 1015.1, 1075.3, 1098.0, 1106.2, 1165.5, 1176.1, 1190.6, 1211.3, 1261.9, 1275.9, 1367.5, 1418.7, 1449.6, 1466.9, 1503.5, 1611.1, 1698.3, 1726.3, 2847.9, 2916.9

APCI-MS (m/z): 769.519 (C₅₃H₆₉O₄ [M+H⁺])

Elemental Analysis (mass %): Calculated: C, 82.77 %; H, 8.91 %; N, 0 %; Other, 8.32 %. Found: C, 82.28 %; H, 8.93 %; N, 0 %; Other, 8.80 %.

Compound 37: Thiobis(4,1-phenylene) bis(4-(4-ethylcyclohexyl)benzoate)

Prepared according to Scheme 1. Compound **6** (500 mg, 2.3 mmol), Compound **7** (1.07 g, 4.6 mmol), EDAC (1.30 g, 6.9 mmol), DMAP (10 mg), DCM (10 cm³). Recrystallisation from ethanol:THF (10:1) yielded **37** as a white powder.

Yield: 1.32 g (2.0 mmol, 89%)

¹H NMR (δ/ppm, 400 MHz, CDCl₃): 8.109 (4H, d, J = 8.24 Hz, ArH), 7.415 (4H, d, J = 8.24 Hz, ArH), 7.347 (4H, d, J = 8.24 Hz, ArH), 7.168 (4H, d, J = 8.24 Hz, ArH), 2.569 (2H, tt, J = 12.15, 2.75, Ar-CH-(CH₂)₂), 1.919 (8H, d, J = 10.53 Hz, Ar-CH-(CH₂)₂), 1.557-1.431 (4H, m, CyHexH), 1.322-1.177 (6H, m, CH-CH₂-CH₃), 1.129-1.009 (4H, m, CyHexH), 0.922 (6H, t, J = 7.33 Hz, CH₂-CH₃)

¹³C NMR (δ/ppm, 100.5 MHz, CDCl₃): 165.03, 154.41, 150.12, 132.82, 132.20, 130.33, 127.14, 126.81, 122.68, 44.84, 37.98, 33.98, 32.96, 29.91, 11.51

IR (ν_{max} cm⁻¹): 698.2, 760.0, 781.2, 839.0, 871.8, 939.3, 985.6, 1012.6, 1058.9, 1095.6, 1161.2, 1178.5, 1197.8, 1259.5, 1381.0, 1398.4, 1417.7, 1446.6, 1483.3, 1575.8, 1589.3, 1608.6, 1732.1, 2848.9, 2918.3, 2960.7

APCI-MS (*m/z*): 647.319 (C₄₂H₄₇O₄S [M+H⁺])

Elemental Analysis (mass %): Calculated: C, 77.98 %; H, 7.17 %; N, 0 %; Other, 14.85 %. Found: C, 77.99 %; H, 7.22 %; N, 0 %; Other, 14.79 %.

Compound 38: Thiobis(4,1-phenylene) bis(4-(4-propylcyclohexyl)benzoate)

Prepared according to Scheme 1. Compound **6** (500 mg, 2.3 mmol), Compound **8** (1.13 g, 4.6 mmol), EDAC (1.30 g, 6.9 mmol), DMAP (10 mg), DCM (10 cm³). Recrystallisation from ethanol:THF (10:1) yielded **38** as a white powder.

Yield: 1.18 g (1.7 mmol, 76%)

¹H NMR (δ/ppm, 400 MHz, CDCl₃): 8.103 (4H, d, J = 8.24 Hz, ArH), 7.408 (4H, ddd, J = 8.70, 2.75, 1.83 Hz, ArH), 7.339 (4H, d, J = 8.24 Hz, ArH), 7.162 (4H, ddd, J = 8.70, 2.75, 1.83 Hz, ArH), 2.561 (2H, tdd, J = 12.15, 3.21, 2.75, Ar-CH-(CH₂)₂), 1.900 (8H, dddd, J = 11.45, 11.22, 3.21, 2.75 Hz, Ar-CH-(CH₂)₂), 1.535-1.431 (4H, m, CyHexH), 1.403-1.193 (10H, m, CH-CH₂-CH₂-CH₃), 1.118-1.015 (4H, m, CyHexH), 0.906 (6H, t, J = 7.33 Hz, CH₂-CH₃)

¹³C NMR (δ/ppm, 100.5 MHz, CDCl₃): 65.02, 154.35, 150.25, 132.85, 132.19, 130.33, 127.13, 126.81, 122.68, 44.83,

39.62, 36.91, 34.00, 33.34, 19.99, 14.39

IR (νmax cm⁻¹): 655.8, 698.2, 721.4, 756.1, 777.3, 802.4, 839.0, 848.7, 866.0, 939.3, 986.3, 1012.6, 1060.9, 1093.6, 1161.2, 1193.9, 1261.5, 1396.5, 1417.7, 1446.6, 1487.1, 1506.4, 1558.5, 1608.6, 1734.0, 2335.8, 2358.9, 2841.2, 2912.5, 2951.1

APCI-MS (*m/z*): 675.350 (C₄₄H₅₁O₄S [M+H⁺])

Elemental Analysis (mass %): Calculated: C, 78.30 %; H, 7.47 %; N, 0 %; Other, 14.23 %. Found: C, 78.19 %; H, 7.39 %; N, 0 %; Other, 14.43 %.

Compound 39: Thiobis(4,1-phenylene) bis(4-(4-butylcyclohexyl)benzoate)

Prepared according to Scheme 1. Compound **6** (500 mg, 2.3 mmol), Compound **9** (1.20 g, 4.6 mmol), EDAC (1.30 g, 6.9 mmol), DMAP (10 mg), DCM (10 cm³). Recrystallisation from ethanol:THF (10:1) yielded **39** as a white powder.

Yield: 1.46 g (2.1 mmol, 90%)

¹H NMR (400 MHz, CDCl₃): 8.094 (4H, d, J = 8.24 Hz, ArH), 7.394 (4H, ddd, J = 8.70, 2.75, 1.83 Hz, ArH), 7.330 (4H, d, J = 8.24 Hz, ArH), 7.154 (4H, ddd, J = 8.70, 2.75, 1.83 Hz, ArH), 2.552 (2H, tdd, J = 12.15, 3.21, 2.75, Ar-CH-(CH₂)₂), 1.943-1.837 (8H, m, Ar-CH-(CH₂)₂), 1.523-1.419 (4H, m, CyHexH), 1.348-1.189 (14H, m, CH-CH₂-CH₂-CH₂-CH₃), 1.110-1.008 (4H, m, CyHexH), 0.898 (6H, t, J = 7.33 Hz, CH₂-CH₃)

¹³C NMR (100.5 MHz, CDCl₃): 165.01, 154.35, 150.25, 132.85, 132.19, 130.33, 123.13, 126.81, 122.68, 44.83, 37.19, 37.02, 34.01, 33.39, 29.19, 22.99, 14.16

IR (ν_{max} cm⁻¹): 698.2, 711.7, 727.2, 754.2, 761.9, 785.0, 806.3, 848.7, 873.8, 949.0, 1012.6, 1062.8, 1163.1, 1178.5, 1193.9, 1261.5, 1375.3, 1417.7, 1446.6, 1487.1, 1506.4, 1608.6, 1732.1, 2850.8, 2920.2, 2955.0

APCI-MS (*m/z*): 703.382 (C₄₆H₅₅O₄S [M+H⁺])

Elemental Analysis (mass %): Calculated: C, 78.59 %; H, 7.74 %; N, 0 %; Other, 13.67 %. Found: C, 78.64 %; H, 7.76 %; N, 0 %; Other, 13.61 %.

Compound 40: Thiobis(4,1-phenylene) bis(4-(4-pentylcyclohexyl)benzoate)

Prepared according to Scheme 1. Compound **6** (500 mg, 2.3 mmol), Compound **10** (1.26 g, 4.6 mmol), EDAC (1.30 g, 6.9 mmol), DMAP (10 mg), DCM (10 cm³). Recrystallisation from ethanol:THF (10:1) yielded **40** as a white powder.

Yield: 1.43 g (2.0 mmol, 85%)

¹H NMR (δ/ppm, 400 MHz, CDCl₃): 8.115 (4H, d, J = 8.24 Hz, ArH), 7.420 (4H, ddd, J = 8.70, 2.75, 1.83 Hz, ArH), 7.349 (4H, d, J = 8.24 Hz, ArH), 7.175 (4H, ddd, J = 8.70, 2.75, 1.83 Hz, ArH), 2.576 (2H, tdd, J = 12.15, 3.21, 2.75, Ar-CH-(CH₂)₂), 1.977-1.851 (8H, m, Ar-CH-(CH₂)₂), 1.544-1.440 (4H, m, CyHexH), 1.393-1.200 (18H, m, CH-CH₂-CH₂-CH₂-CH₃), 1.129-1.026 (4H, m, CyHexH), 0.911 (6H, t, J = 7.33 Hz, CH₂-CH₃)

¹³C NMR (δ/ppm, 100.5 MHz, CDCl₃): 165.00, 154.34, 150.25, 132.84, 132.18, 130.32, 127.12, 126.80, 122.67, 44.83, 37.29, 37.19, 34.00, 33.38, 32.17, 26.61, 22.70, 14.11

IR (νmax cm⁻¹): 653.9, 698.2, 732.3, 760.0, 802.4, 842.9, 875.7, 939.3, 968.3, 1012.6, 1058.9, 1163.1, 1176.6, 1192.0, 1261.5, 1417.7, 1446.6, 1487.1, 1608.6, 1732.1, 2848.9, 2918.3, 2951.1

APCI-MS (*m/z*): 731.413 (C₄₈H₅₉O₄S [M⁺])

Elemental Analysis (mass %): Calculated: C, 78.86 %; H, 8.00 %; N, 0 %; Other, 13.14 %. Found: C, 78.94 %; H, 8.05 %; N, 0 %; Other, 13.02 %.

Compound 41: Thiobis(4,1-phenylene) bis(4-(4-heptylcyclohexyl)benzoate)

Prepared according to Scheme 1. Compound **6** (500 mg, 2.3 mmol), Compound **11** (1.40 g, 4.6 mmol), EDAC (1.30 g, 6.9 mmol), DMAP (10 mg), DCM (10 cm³). Recrystallisation from ethanol:THF (10:1) yielded **41** as a white powder.

Yield: 1.36 g (1.7 mmol, 75%)

¹H NMR (δ /ppm, 400 MHz, CDCl₃): 8.088 (4H, d, J = 8.24 Hz, ArH), 7.393 (4H, ddd, J = 8.70, 2.75, 1.83 Hz, ArH), 7.324 (4H, d, J = 8.24 Hz, ArH), 7.148 (4H, ddd, J = 8.70, 2.75, 1.83 Hz, ArH), (2H, tdd, J = 12.85, 3.21, 2.75, Ar-CH-(CH₂)₂), 1.930-1.840 (8H, m, Ar-CH-(CH₂)₂), 1.518-1.413 (4H, m, CyHexH), 1.350-1.183 (26H, m, CH-CH₂-CH₂-CH₂-CH₂-CH₂-CH₃), 1.102-1.000 (4H, m, CyHexH), 0.876 (6H, t, J = 7.33 Hz, CH₂-CH₃)

¹³C NMR (δ /ppm, 100.5 MHz, CDCl₃): 165.01, 154.35, 150.25, 132.85, 132.19, 130.32, 127.13, 126.81, 122.68, 44.83, 37.34, 37.21, 34.01, 33.39, 31.91, 29.93, 29.38, 26.95, 22.69, 14.13

IR (ν_{\max} cm⁻¹): 653.9, 698.2, 732.3, 761.9, 802.4, 842.9, 875.7, 939.3, 968.3, 1012.6, 1058.9, 1163.1, 1176.6, 1193.4, 1261.5, 1417.7, 1446.6, 1487.1, 1587.4, 1608.6, 1732.1, 2848.9, 2918.3, 2953.0

APCI-MS (m/z): 787.475 (C₅₂H₆₇O₄S [M+H⁺])

Elemental Analysis (mass %): Calculated: C, 79.34 %; H, 8.45 %; N, 0 %; Other, 12.21 %. Found: C, 79.36 %; H, 8.47 %; N, 0 %; Other, 12.18 %.

4.2 Bimesogens with a 7-unit spacer

4.2.1. Bimesogens with a heptamethylene spacer

Following on from the pseudo bent-core materials, a series of symmetrical bimesogens, consisting of terminally substituted phenyl benzoates linked by a heptamethylene (C_7) spacer unit were investigated (Figure 59). The primary focus was to investigate the effects of the terminal substituent on phase behaviour, and on the occurrence of the so-called "twist-bend nematic" (N_{TB}) phase. Work prior to this study has found the N_{TB} phase to occur most commonly in polar materials such as the CB_nCB series of bimesogens, so both polar and non-polar terminal groups were examined, as shown in Figure 59.

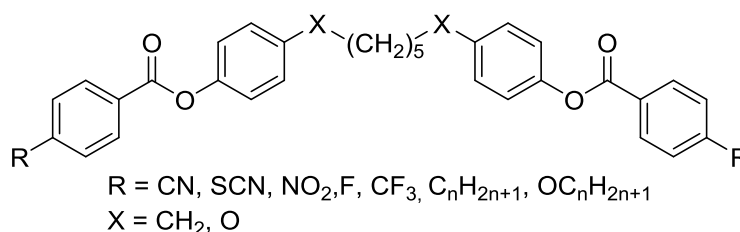


Figure 59: General structure of the compounds used in these studies.

The heptamethylene spacer was initially selected to allow direct comparison to CB_7CB which is a well-documented N_{TB} material in the surrounding literature. The mesogenic properties of the synthesised materials were analysed *via* POM, DSC and XRD. The mesomorphic behaviour of the compounds with polar terminal groups is summarised below in Table 10 and the compounds with the non-polar alkyl or alkyloxy is given in Table 11.

Compound			Transition Temperature / °C					
No.	R	Cr		N _{TB}		N		Iso
42	CN	•	149.0	(•	120.0	•	139.0)	•
			[43.18]		[0.62]		[1.43]	
			{12.30}		{0.19}		{0.42}	
43	NCS	•	105.0	(•	103.3)	•	120.5	•
			[36.51]		[0.4]		[0.18]	
			{11.61}		{0.08}		{0.05}	
44	NO ₂	•	113.3	-	-	-	-	•
			[24.22]					
			{7.54}					
45	F	•	91.5	-	-	-	-	•
			[48.31]					
			{15.94}					
46	CF ₃	•	114.9	-	-	-	-	•
			[39.15]					
			{12.14}					

Table 10: Thermal properties of compounds **42-46**. Enthalpies reported in [] and denoted in kJ mol⁻¹. Entropies quoted in {} and denoted in ΔS/R.

As shown in Table 10, of the materials in which the terminal group has a relatively large dipole moment, only compounds **42** and **43** exhibited any mesomorphic properties, whereas the others were found to be non-mesogenic. The liquid crystal phases of compound **42** were found to be entirely monotropic, exhibiting an isotropic to nematic transition, as well as a transition from the nematic phase to a lower temperature mesophase with a blocky, broken-fan texture (Figure 60). The mesomorphic behaviour of compound **43** was much the same, with the exception that the nematic phase occurred above the melting point.

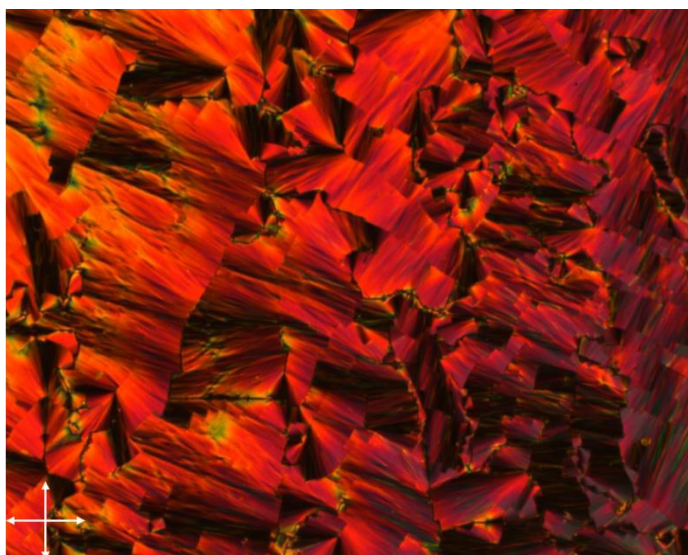


Figure 60: Compound **42** in the N_{TB} phase at 118.5 C. Sample cooled at $0.1\text{ }^{\circ}\text{C min}^{-1}$. (x100)

The lower temperature mesophases of compounds **42** and **43** exhibited an optical texture that was consistent with those reported for the twist bend nematic phase, however this texture is also reminiscent of phases with lamellar ordering, such as smectic phases, therefore, in order to categorically assign the lower temperature phase as the N_{TB} phase, a binary Gibbs phase diagram was constructed using compound **42** and CB11CB, a known N_{TB} material. The lower temperature phase of compound **42** was found to be exhibited across all concentrations of compound **42** in CB11CB, thus confirming it as the N_{TB} phase.

When looking at the relationship between the terminal groups and the phase behaviour for the materials in Table 10 the end groups can be separated into two broad groups, conjugated groups i.e. CN, SCN and NO_2 and non-conjugating i.e. F and CF_3 . In terms of phase behaviour only dimers with a conjugating terminal group, in this case CN and SCN were shown to exhibit the N_{TB} phase, or indeed any mesomorphic properties at all, this is consistent with previous assertions that quadrupolar interactions between polarisable end groups plays a part in the stabilisation of the N_{TB} phase in liquid crystal dimers.⁷⁸ While the NO_2 material, despite possessing a conjugating terminal group does not display any mesomorphic behaviour this could be attributed to the exceedingly high dipole moment of the nitro group causing intermolecular repulsive forces to outweigh any stabilisation gained from possible quadrupolar interactions. This could also be a factor in why the F and CF_3 terminated materials do not exhibit mesomorphic behaviour, as since they lack

any stabilising element from quadrupolar forces the intermolecular repulsion caused by the polar end groups dominates when determining structure, preventing the molecules packing into a mesophase.

As a point of comparison a series of materials with terminal groups exhibiting little to no observable dipole moment were synthesised. These consisted of materials with alkyl and alkyloxy terminal groups of varying lengths. The mesomorphic behaviour of these compounds was analysed in the same way as the previous series, and the results obtained are summarised in Table 11.

Compound			Transition Temperature / °C					
No.	R	Cr	N _{TB}		N		Iso	
47	C ₂ H ₅	•	71.5 [30.8] {10.75}	-	-	-	-	•
48	C ₃ H ₇	•	108.0 [33.0] {10.41}	(•	47.6 [*]	•	49.5) [1.40] {0.52}	•
49	C ₄ H ₉	•	56.3 [32.0] {11.68}	-	-	-	-	•
50	OC ₂ H ₅	•	108.3 [58.83] {18.55}	(•	95.3) [0.65] {0.21}	•	108.8 [0.54] {0.17}	•
51	OC ₃ H ₇	•	89.6 [52.80] {17.51}	(•	69.1 [1.0] {0.35}	•	75.5) [0.2] {0.07}	•
52	OC ₄ H ₉	•	87.0 [36.60] {12.22}	(•	79.2 [1.2] {0.41}	•	85.9) [0.4] {0.13}	•

Table 11: Thermal properties of compounds **47-52**. Enthalpies displayed in square brackets and quoted in kJ mol⁻¹. Entropies quoted { } and denoted in ΔS/R.

Of these materials, the vast majority were found to exhibit the same phase sequence as compounds **42** and **43**, with a nematic phase followed by a phase with a blocky optical texture. The exceptions to this trend are compounds **47** and **49** which were found to be

entirely non-mesogenic. The optical texture of the lower temperature phase was found to be consistent with previously reported observations for the twist-bend nematic (N_{TB}) phase. A photomicrograph demonstrating this texture is shown in Figure 61. This phase assignment was confirmed *via* miscibility studies with the compound **42**.

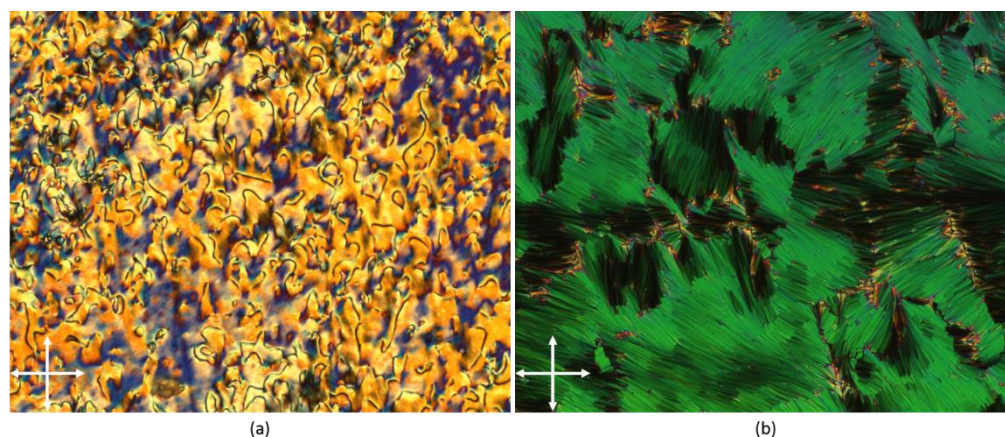


Figure 61: Compound **51** in the nematic phase (a) and N_{TB} phase (b) at 74.8 °C and 68.9 °C respectively. The sample was cooled at 0.1 °C min⁻¹ (x100).

DSC was used to further investigate the phase behaviour of these materials. In a slight deviation from previous reports both observed transitions were found to be first order, despite the N- N_{TB} transition having been shown to be weakly first order. An example of these DSC traces, in this case that of compound **52**, is shown in Figure 62.

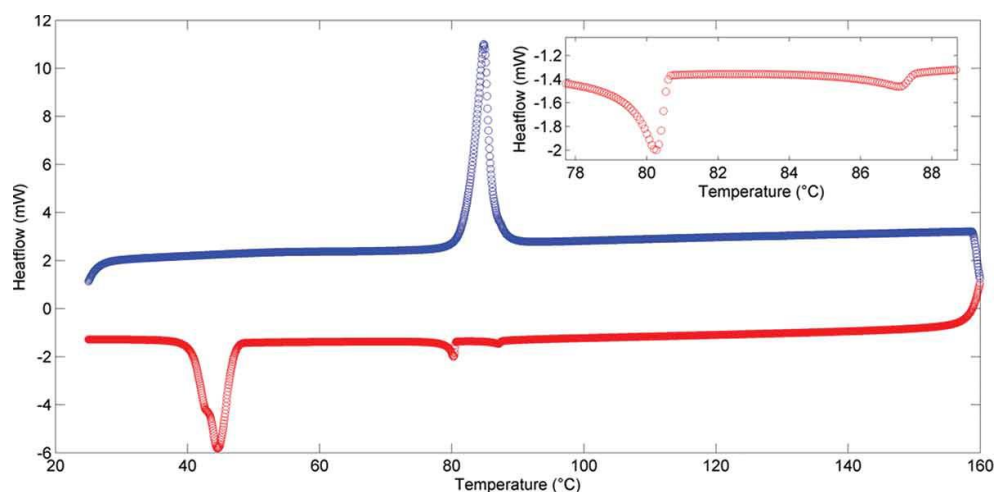


Figure 62: DSC thermogram of compound **52**. Heating/Cooling rate 10 °C min⁻¹

The nematic and N_{TB} phases were also analysed *via* variable temperature XRD. Upon cooling from the isotropic liquid into the nematic phase the scattering intensity in the

small angle region was observed to increase significantly, the peak exhibited becoming slightly more defined when the material was further cooled into the N_{TB} phase. In the wide angle region the broad, diffuse peak observed in the isotropic liquid narrows and becomes less intense when the material undergoes the I-N transition, broadening again when the material enters the N_{TB} phase. An example XRD plot, for compound **43**, is shown in Figure 63, demonstrating the increased intensity in the wide angle region as a function of temperature, as well as the slight broadening and intensifying of the signal at $d \approx 4.5 \text{ \AA}$ upon transition to the N_{TB} phase.

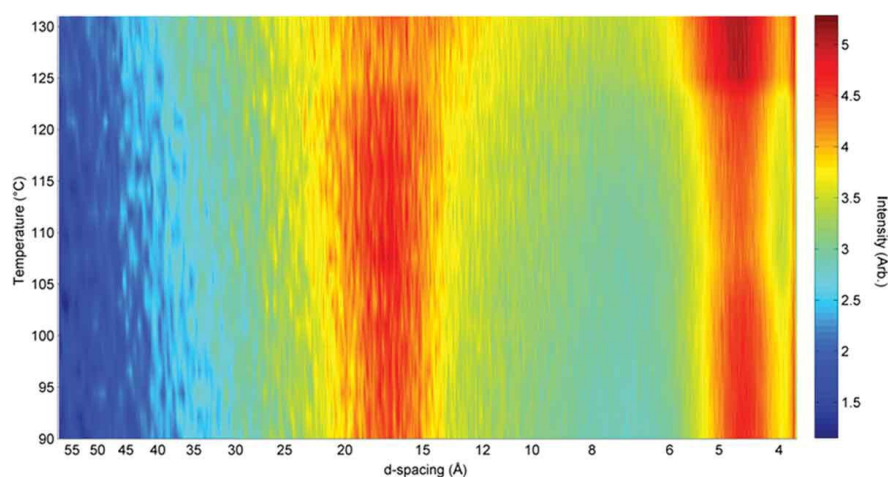
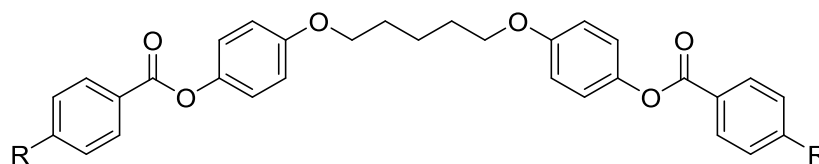


Figure 63: SAXS data for compound **43**, showing scattered intensity (arb. units, z axis), d-spacing (\AA , x-axis) and temperature ($^{\circ}\text{C}$, y-axis).

These results show that, in the case of apolar terminal chains, the N_{TB} phase occurs more readily in materials with alkyloxy chains rather than those with purely alkyl chains. Furthermore, a slight odd-even effect can be discerned with respect to the parity of the terminal chains of the materials presented in this series, primarily evidenced by the propyl terminated material being the only one of the alkyl terminated materials to exhibit the N_{TB} phase. This is also evidenced in the alkyloxy terminated materials, for which the ethyloxy and butyloxy terminated materials, 3 and 5 parity respectively, showed a more stable N_{TB} phase than the propyloxy terminated material, parity 4. Odd-even effects are a common sight in the study of bimesogens however the effect is usually exhibited with respect to the spacer unit rather than the terminal chain.

4.2.2. Bimesogens with an ether linked pentamethylene spacer

In order to investigate the effects of altering the spacer unit on the formation of the N_{TB} phase a series of compounds analogous to **42-52**, but where the first and last methylene units of the spacer have been replaced with ether linking groups, were synthesised. The mesomorphic behaviour of these materials is summarised in Table 12.



Compound		Transition Temperatures / °C				
No.	R	Cr		N		Iso. Liq.
55	CN	•	166.6	•	189.2	•
			[53.52]		[3.67]	
			{14.64}		{0.96}	
56	SCN	•	142.8	•	178.8	•
			[35.59]		[2.27]	
			{10.30}		{0.60}	
57	NO ₂	•	150.5	(•	141.2)	•
			[77.26]		[0.13]	
			{21.94}		{0.04}	
58	F	•	125.1	-	-	•
			[51.83]			
			{14.69}			
59	CF ₃	•	151.4	-	-	•
			[51.83]			
			{14.69}			
60	C ₂ H ₅	•	116.1	-	-	•
			[39.38]			
			{12.17}			
61	C ₃ H ₇	•	127.0	-	-	•
			[44.63]			
			{13.42}			
62	C ₄ H ₉	•	125.4	-	-	•

			[63.92]		
			{19.30}		
63	OC ₂ H ₅	•	139.9	•	171.4
			[57.14]		[2.9]
			{16.65}		{0.78}
64	OC ₃ H ₇	•	108.3	•	143.1
			[24.82]		[1.83]
			{7.83}		{0.53}
65	OC ₄ H ₉	•	109.0	•	142.2
			[27.17]		[1.79]
			{8.55}		{0.52}

Table 12: General structure and mesomorphic behaviour of compounds **55-65**. Enthalpies are quoted in [] denoted in in kJ mol⁻¹. Transition entropies are quoted in {} and denoted in ΔS/R.

As shown in Table 12, replacing the methylene units with ether linking groups has the effect of drastically increasing the melting and clearing points of all of the materials when compared to the purely methylene linked analogues, an effect that has been observed in previously reported cyanobiphenyl bimesogens.⁷⁹ In addition, unlike the methylene linked materials none of the ether linked bimesogens exhibited the twist-bend nematic phase in their neat state.

The lack of an exhibited N_{TB} phase in the neat state of these materials can be attributed to the change in the average angle of the bend within the molecule caused by the change in the nature of the spacer chain. While it is true that the conformational freedom imparted by the long, flexible spacer chain results in many different feasible conformations that these molecules can adopt, for the purposes of this study we assume that the predominant conformer is that in which the spacer adopts an all-trans arrangement. While this assumption is not ideal it is a common simplification used in studies of flexible bimesogens^{67,80,81}, and has been supported by previous studies, which have used 1D-NOESY NMR⁸² and XRD⁶¹ to show that, while the all-trans conformer is not the sole conformation, it is highly favoured.

Upon the introduction of an ether moiety into the spacer chain the topology of the molecule changes as the bond angle of a C-O-C bond (≈118°) is generally larger than that of a C-C-C bond (109.5°), this leads to a more linear average molecular geometry in the

ether linked materials. As a bent molecular geometry is one of the known requirements for the formation of the N_{TB} phase it stands to reason that a more linear molecule would be less likely to form the N_{TB} phase.^{83–85} This increase in linearity can also be said to cause the increase in both the melting and clearing points of these materials, as a more linear molecule will be able to pack more effectively into both crystal and nematic phases when compared to more bent molecules.

That the ether linked molecules are more linear can be supported by the use of molecular modelling to calculate the angle between the mesogenic units for each family of compounds. This is demonstrated in Figure 64 using compounds **42** and **55** as examples.

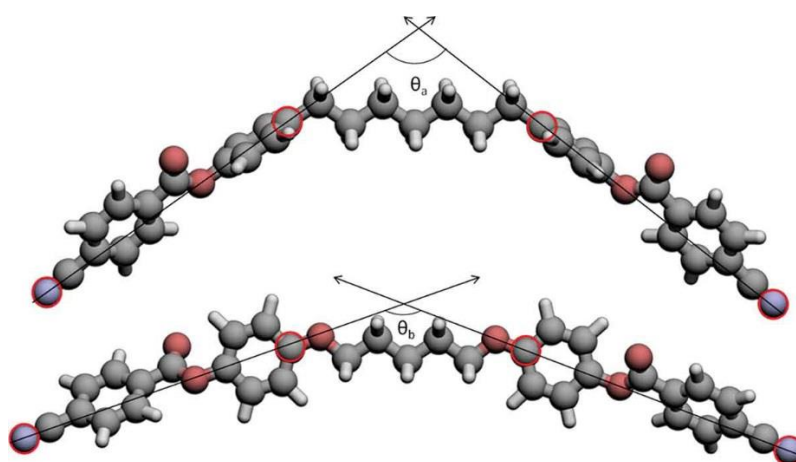


Figure 64: Energy minimised geometries of compounds **42** and **55** showing the differences in the intermesogen angle (θ). Optimised at the B3LYP/6-31G(d) level of theory.

By calculating the vectors between the highlighted atoms and extrapolating them, the intermesogen angles of the all-trans conformers can be calculated to be 106.8° for compound **42**, and 140.8° for compound **55**.

Conclusions

The increase in flexibility between the pseudo bent-core materials presented in the previous chapter and the bimesogens presented in this chapter has been shown to have a significant effect on the mesomorphic behaviour, moving from the smectic-like properties of those materials to the more nematic-like behaviour of the series' of materials presented in this section. In addition, unlike the pseudo bent-core materials, several of the bimesogens presented here were shown to exhibit a phase shown by miscibility to be the

much-debated N_{TB} phase. It was shown that, in the more linear ether linked materials, the materials had significantly higher clearing points, and where relevant I-N transitions. This was attributed to the more linear molecules being able to pack more easily into both the crystal and nematic phases.

The formation of the N_{TB} phase in the compounds **42** and **43** was attributed to the gross bent molecular shape of these molecules, as one of the known structural prerequisites for the N_{TB} phase is bent molecular architecture. The key difference between these materials and the pseudo-bent core materials is the flexibility imparted by the spacer chain, as opposed to the more rigid bisphenol units. This allows for the molecules to twist when packing in order to minimise the free volume, this is attained by the molecules twisting about the director, thus forming the N_{TB} phase.

A slight decrease in transition temperature was observed between the materials with inflexible, polar terminal chains and those with flexible, polar terminating groups. This was also attributed to the ability of the molecules to pack into phases, with the bulkier, flexible alkyl and alkyloxy chains interfering with the packing into any ordered phase. The phase behaviour of the alkyl and alkyloxy terminated materials was also notably less stable than for compounds **42** and **43**, this was attributed to the antiparallel arrangement of the polar end groups, caused by dipoles induced thanks to the conjugation of electron density through the group, promoting mesophase formation. This is supported by the fact that, as seen in Table 10 only the compounds with conjugating polar groups (CN and NCS) exhibited any mesomorphic behaviour, while the non-conjugating end groups (F and CF_3) resulted in compounds with no liquid crystallinity. The nitro terminated compound was an interesting exception to this trend, as it is a conjugating group but the corresponding dimer displayed no mesomorphism, however nitro groups are known to have very high dipole moments compared to other polar groups, it is therefore likely that intermolecular repulsion caused by this high dipole moment outweighs any attraction caused by quadrupolar interactions.

4.2.3. Synthetic Procedures

Compound 42: 4,4'-(heptane-1,7-diyl)bis(4,1-phenylene) bis(4-cyanobenzoate)

Prepared according to Scheme 2. 4,4'-(heptane-1,7-diyl)diphenol (400 mg, 1.41 mmol), 4-cyanobenzoic acid (630 mg, 4.23 mmol), EDAC (810 mg, 4.23 mmol), DMAP (10 mg), DCM (25 ml). Recrystallisation from ethanol/THF (20:1) yielded **42** as a white powder.

Yield: 550 mg (1.0 mmol, 71%)

¹H NMR (δ /ppm, 400 MHz, CDCl₃): 8.22 (4H, ddd, J=1.8, J=2.1, J=8.5, ArH), 7.74 (4H, ddd, J=1.8, 2.1, 8.5, ArH), 7.17 (4H, ddd, J=2.1, J=2.4, J=8.5, ArH), 7.03 (4H, ddd, J=2.1, J=2.4, J=8.5, ArH), 2.56 (4H, t Ar-CH₂-CH₂-(CH₂)₃), 1.51 – 1.62 (4H, m Ar-CH₂-CH₂-(CH₂)₃), 1.23 – 1.34 (6H, m, Ar-CH₂-CH₂-(CH₂)₃)

¹³C NMR (δ /ppm, 100.5 MHz, CDCl₃): 29.15, 29.31, 31.39, 35.33, 116.80, 117.86, 121.03, 129.47, 130.60, 132.35, 133.53, 141.00, 148.37, 163.73

ESI-MS (*m/z*): 285.1850 (C₁₉H₂₅O₂, [M+H]⁺), 307.1664 (C₁₉H₂₄NaO₂, [M+Na]⁺)

IR (ν_{\max} cm⁻¹): 501, 771, 817, 894, 1018, 1111, 1172, 1226, 1365, 1450, 1512, 1604, 1743, 2846, 2916, 3024, 3340

Assay (HPLC, MeCN, 225/255 nm): 98.06%

Compound 43: Heptane-1,7-diylbis(4,1-phenylene) bis(4-isothiocyanobenzoate)

Prepared according to Scheme 2. 4,4'-(heptane-1,7-diyl)diphenol (250 mg, 0.669 mmol), 4-isothiocyanobenzoic acid (347 mg, 2.01 mmol), EDAC (382 mg, 2.01 mmol), DMAP (10 mg), DCM (5 ml). Recrystallisation from ethanol/THF (3:1) yielded **43** as white plates

Yield: 380 mg (0.55 mmol, 82%)

¹H NMR (δ /ppm, 400 MHz, CDCl₃): 8.12 (ddd, J = 1.8 Hz, J = 2.1, J = 8.9 Hz, ArH), 7.26 (4H, ddd, J = 1.8, J = 2.1 Hz, J = 8.9, ArH), 7.15 (4H, ddd, J = 2.1, J = 2.4, J = 8.5 Hz, ArH), 7.03 (4H, ddd, J = 2.1, J = 2.8, J = 8.5 Hz, ArH), 2.55 (4H, t, J = 7.0 Hz, Ar-CH₂-CH₂-(CH₂)₃), 1.55 (4H, quintet, J = 7.0 Hz, Ar-CH₂-CH₂-(CH₂)₃), 1.24 - 1.32 (6H, m, Ar-CH₂-CH₂-(CH₂)₃).

¹³C NMR (δ /ppm, 100.5 MHz, CDCl₃): 29.12, 29.30, 31.38, 35.33, 121.17, 125.81, 128.16, 129.39, 131.61, 136.22, 138.19, 140.70, 148.59, 161.17

ESI-MS (m/z): 607.1722 ($C_{35}H_{31}N_2O_4S_2$, $[M+H^+]$), 629.1558 ($C_{35}H_{30}N_2NaO_4S_2$, $[M+Na^+]$), 645.1300 ($C_{35}H_{30}N_2KO_4S_2$, $[M+K^+]$)

IR (ν_{max} cm^{-1}): 678, 756, 802, 848, 933, 1010, 1064, 1165, 1195, 1257, 1411, 1465, 1504, 1597, 1728, 2044, 2846, 2024

Assay (HPLC, C18, H₃CCN, 254/270 nm): 99.52%

Compound 44: Heptane-1,7-diylbis(4,1-phenylene) bis(4-nitrobenzoate)

Prepared according to Scheme 2. 4-4'-(heptane-1,7-diyl)diphenol (250 mg, 0.669 mmol), 4-nitrobenzoic acid (334 mg, 2.01 mmol), EDAC (382 mg, 2.01 mmol), DMAP (10 mg), DCM (5 ml). Recrystallisation from ethanol yielded **44** as yellow plates

Yield: 370 mg (0.64 mmol, 95%)

1H NMR (δ /ppm, 400 MHz, $CDCl_3$): 8.26 - 8.36 (8H, m, ArH), 7.17 (4H, ddd, J = 2.1, J = 2.4, J = 7.9, ArH), 7.06 (4H, ddd, J = 2.1, J = 2.8, J = 8.5 Hz, ArH), 2.57 (4H, t, J = 7.0 Hz, Ar- CH_2 - CH_2 -(CH_2)₃), 1.56 (4H, quintet, J = 7.3 Hz, Ar- CH_2 - CH_2 - (CH_2)₃), 1.26 - 1.32 (6H, m, Ar- CH_2 - CH_2 -(CH_2)₃).

^{13}C NMR (δ /ppm, 100.5 MHz, $CDCl_3$): 29.13, 29.29, 31.37, 35.33, 121.01, 123.68, 129.48, 131.24, 135.07, 141.05, 148.39, 150.83, 163.48

ESI-MS (m/z): 583.2104 ($C_{33}H_{31}N_2O_8$ $[M+H^+]$), 605.1920 ($C_{33}H_{30}N_2NaO_8$ $[M+Na^+]$).

IR (ν_{max} cm^{-1}): 570, 632, 709, 810, 848, 871, 1010, 1072, 1165, 1188, 1257, 1342, 1465, 1519, 1604, 1735, 2854, 2924

Assay (HPLC, C18, H₃CCN, 254/270 nm): 99.80%

Compound 45: Heptane-1,7-diylbis(4,1-phenylene) bis(4-fluorobenzoate)

Prepared according to Scheme 2. 4-4'-(heptane-1,7-diyl)diphenol (250 mg, 0.669 mmol), 4-fluorobenzoic acid (281 mg, 2.01 mmol), EDAC (382 mg, 2.01 mmol), DMAP (10 mg), DCM (5 ml). Recrystallisation from ethanol/THF (10:1) yielded **45** as white plates.

Yield: 340 mg (0.64 mmol, 96%)

1H NMR (δ /ppm, 400 MHz, $CDCl_3$): 8.19 (4H, dddd, J = 2.1, J = 2.8, J = 5.5, J = 8.9 Hz, ArH), 7.08 - 7.18 (8H, m, ArH), 7.02 (4H, ddd J = 1.8, J = 2.8, J = 8.5 Hz, ArH), 2.55

(4H, t, J = 7.6 Hz, Ar-CH₂-CH₂-(CH₂)₃), 1.55 (4H, quintet, J = 7.6 Hz, Ar-CH₂-CH₂-(CH₂)₃), 1.24 - 1.32 (6H, m, Ar-CH₂-CH₂-(CH₂)₃).

¹³C NMR (δ/ppm, 100.5 MHz, CDCl₃): 29.14, 29.30, 31.40, 35.33, 115.73 (d, J = 22.3 Hz), 124.24, 125.91 (d, J = 3.1), 129.35, 132.74 (d, J = 9.2 Hz), 140.58, 148.68, 164.35, 164.82

¹⁹F NMR (δ/ppm, 376.4 MHz, CDCl₃): -104.51 (1F, m, ArF).

ESI-MS (*m/z*): 551.1987 (C₃₃H₃₀F₂NaO₄, [M+Na⁺]), 529.2170 (100%, C₃₃H₃₁F₂O₄ [M+H⁺])

IR (ν_{max} cm⁻¹): 524, 570, 609, 678, 756, 848, 941, 1010, 1072, 1157, 1195, 1265, 1411, 1504, 1597, 1728, 2846, 2916.

Assay (HPLC, C18, H₃CCN, 254/270 nm): 99.61%

Compound 46: Heptane-1,7-diylbis(4,1-phenylene) bis(4-(trifluoromethyl)benzoate)

Prepared according to Scheme 2. 4-4'-(heptane-1,7-diyl)diphenol (100 mg, 0.35mmol), 4-trifluoromethylbenzoic acid (190 mg, 1 mmol), EDAC (191 mg, 1 mmol), DMAP (10 mg), DCM (5 ml). Recrystallisation from ethanol/THF (12:1) yielded **46** as white plates.

Yield: 140 mg (0.22 mmol, 64%)

¹H NMR (δ/ppm, 400 MHz, CDCl₃): 8.24 (4H, d, J = 8.2 Hz, 4H, ArH), 7.70 (4H, d, J = 8.2 Hz, ArH), 7.17 (4H, ddd J = 2.1, J = 2.8, J = 8.5 Hz, ArH), 7.05 (4H, ddd J = 2.1, J = 2.8, J = 8.5 Hz, ArH), 2.56 (4H, t, J = 7.6 Hz, Ar-CH₂-CH₂-(CH₂)₃), 1.56 (4H, quintet, J = 7.6 Hz, Ar-CH₂-CH₂-(CH₂)₃), 1.24 - 1.32 (6H, m, Ar-CH₂-CH₂-(CH₂)₃).

¹³C NMR (δ/ppm, 100.5 MHz, CDCl₃): 29.22, 29.39, 31.49, 35.43, 121.24, 123.66 (d, J = 273.2 Hz), 125.67 (Quartet, J = 3.8 Hz), 129.53, 130.62, 133.02, 135.03 (Quartet, J = 32.6 Hz), 140.95, 148.63, 164.25

¹⁹F NMR (δ/ppm, 376.4 MHz, CDCl₃): -63.00 (3F, s, CF₃)

ESI-MS (*m/z*): 651.1937 (C₃₅H₃₀F₆NaO₄ [M+Na⁺]), 667.1676 (C₃₅H₃₀F₆KO₄ [M+K⁺]),

IR (ν_{max} cm⁻¹): 516, 563, 632, 694, 725, 763, 825, 871, 1010, 1072, 1172, 1203, 1265, 1365, 1388, 1458, 1504, 1604, 1728, 2229, 2846, 2924, 3032.

Assay (HPLC, C18, H₃CCN, 254/270 nm): 99.3%

Compound 47: 4,4'-(heptane-1,7-diyl)bis(4,1-phenylene) bis(4-ethylbenzoate)

Prepared according to Scheme 2. 4-4'-(heptane-1,7-diyl)diphenol (200mg, 0.704 mmol) 4-ethylbenzoic acid (316 mg, 2.11 mmol), EDAC (403 mg, 2.11 mmol) DMAP (10 mg) ,DCM (5 ml). Recrystallisation from ethanol/THF (20:1) yielded **47** as a white powder.

Yield: 230 mg (0.46 mmol, 65%)

¹H NMR (δ/ppm, 400 MHz, CDCl₃): 8.12 (d, J = 6 Hz, 4H, ArH), 7.32 (d, J = 6 Hz, 4H, ArH), 7.22 (d, J = 6.6 Hz, 4H, ArH), 7.11 (dt, J = 6.6, 3.3 Hz, 4H, ArH), 2.74, (q, J = 6 Hz, 4H, Ar-CH₂-CH₃), 2.62 (t, J = 6 Hz, 4H, Ar-CH₂-CH₂), 1.63 (quint, J = 5.4 Hz, 4H, Ar-CH₂-CH₂-CH₂), 1.37-1.33 (m, 6H, Ar-CH₂-CH₂-(CH₂)₃), 1.28 (t, J = 6 Hz, 6H, Ar-CH₂-CH₃)

¹³C NMR (δ/ppm, 100.5 MHz, CDCl₃): 166.36, 150.42, 148.84, 140.30, 130.25, 129.26, 128.02, 127.09, 121.34, 35.31, 31.41, 29.29, 29.12, 28.98, 15.23

ESI-MS (*m/z*): 571.2838 (C₃₇H₄₀O₄Na, [M+Na⁺])

IR (ν_{max} cm⁻¹): 517, 617, 694, 756, 1011, 1072, 1173, 1265, 1366, 1458, 1505, 1605, 1728, 2322, 2847, 2916, 3024

Assay (HPLC, MeCN, 225/255 nm): >99%

Compound 48: 4,4'-(heptane-1,7-diyl)bis(4,1-phenylene) bis(4-propylbenzoate)

Prepared according to Scheme 2. 4-4'-(heptane-1,7-diyl)diphenol (400 mg, 1.41 mmol) 4-propylbenzoic acid (696 mg, 4.23 mmol), EDAC (810 mg, 4.23 mmol) DMAP (10 mg), DCM (25 ml). Recrystallisation from ethanol/THF (20:1) yielded **48** as a white powder.

Yield: 380 mg (0.66 mmol, 47 %)

¹H NMR (δ/ppm, 400 MHz, CDCl₃): 8.10 (d, J = 8.8 Hz, 4H, ArH), 7.30 (d, J = 8.4 Hz, 4H, ArH), 7.21 (d, J = 8.4 Hz, 4H, ArH), 7.10 (d, J = 8.8 Hz, 4H, ArH), 2.64 (dt, J = 24.0, 7.6 Hz, 8H, Ar-CH₂-CH₂-CH₃, Ar-CH₂-CH₂-(CH₂)₃), 1.76 – 1.56 (m, 8H, Ar-CH₂-CH₂-

CH₃, Ar-CH₂-CH₂-(CH₂)₃), 1.34 (s, 6H, Ar-CH₂-CH₂-(CH₂)₃), 0.96 (t, *J* = 7.6 Hz, 6H, Ar-CH₂-CH₂-CH₃).

¹³C NMR (δ/ppm, 100.5 MHz, CDCl₃): 165.41, 148.94, 148.86, 140.34, 130.18, 129.23, 128.65, 127.13, 121.36, 38.10, 35.33, 31.43, 29.31, 29.15, 24.26, 13.74

ESI-MS (*m/z*): 599.3107 (C₃₉H₄₄O₄Na, [M+Na⁺])

IR (ν_{max} cm⁻¹): 756, 934, 1065, 1072, 1165, 1265, 1412, 1505, 1728, 2237, 2847, 2916, 3055

Assay (HPLC, MeCN, 225/255 nm): >99%

Compound 49: 4,4'-(heptane-1,7-diyl)bis(4,1-phenylene) bis(4-butylbenzoate)

Prepared according to Scheme 2. 4-4'-(heptane-1,7-diyl)diphenol (200 mg, 0.705 mmol) 4-butylbenzoic acid (375 mg, 2.12 mmol), EDAC (405 mg, 2.12 mmol) DMAP (10 mg), DCM (25 ml). Crystallisation from ethanol/THF (20:1) yielding **49** as a white powder.

Yield: 0.21 mg (0.34 mmol, 48 %)

¹H NMR (δ/ppm, 400 MHz, CDCl₃): 8.09 (d, *J* = 8.4 Hz, 4H, Ar*H*), 7.30 (d, *J* = 8.8 Hz, 4H, Ar*H*), 7.21 (d, *J* = 8.8 Hz, 4H, Ar*H*), 7.09 (d, *J* = 8.4 Hz, 4H, Ar*H*), 2.65 (dt, *J* = 32.4, 8.0 Hz, 8H, Ar-CH₂-CH₂-CH₂-CH₃, Ar-CH₂-CH₂-(CH₂)₃), 1.70 – 1.56 (m, 8H, Ar-CH₂-CH₂-CH₂-CH₃, Ar-CH₂-CH₂-(CH₂)₃), 1.44 – 1.26 (m, 10H, Ar-CH₂-CH₂-CH₂-CH₃, Ar-CH₂-CH₂-(CH₂)₃), 0.94 (t, *J* = 7.2 Hz, 6H, Ar-CH₂-CH₂-CH₂-CH₃).

¹³C NMR (δ/ppm, 100.5 MHz, CDCl₃): 165.41, 149.18, 148.86, 140.33, 130.19, 129.23, 128.59, 127.08, 121.36, 35.75, 35.33, 33.27, 31.43, 29.31, 29.15, 22.29, 13.90

ESI-MS (*m/z*): 627.3425 (C₄₁H₄₈O₄Na, [M+Na⁺])

IR (ν_{max} cm⁻¹): 509, 748, 1072, 1165, 1196, 1273, 1412, 1505, 1613, 1728, 2847, 2916, 2924

Assay (HPLC, MeCN, 225/255 nm): >98%

Compound 50: 4,4'-(heptane-1,7-diyl)bis(4,1-phenylene) bis(4-ethoxybenzoate)

Prepared according to Scheme 2. 4-4'-(heptane-1,7-diyl)diphenol (200 mg, 0.705 mmol) 4-ethoxybenzoic acid (360 mg, 2.12 mmol), EDAC (405 mg, 2.12 mmol) DMAP (10 mg), DCM (25 ml). Recrystallisation from ethanol/THF (20:1) yielded **50** as a white powder.

Yield: 0.19 g (0.32 mmol, 46%)

^1H NMR (δ /ppm, 400 MHz, CDCl_3): 8.13 (d, $J = 8.8$ Hz, 4H, ArH), 7.20 (d, $J = 8.4$ Hz, 4H, ArH), 7.09 (d, $J = 8.4$ Hz, 4H, ArH), 6.95 (d, $J = 8.8$ Hz, 4H, ArH), 4.11 (q, $J = 6.8$ Hz, 4H, $\text{CH}_3\text{-CH}_2\text{-O}$), 2.61 (t, $J = 7.6$ Hz, 4H, Ar- $\text{CH}_2\text{-CH}_2\text{-(CH}_2\text{)}_3$), 1.61 (quint, $J = 7.6$ Hz, 4H, Ar- $\text{CH}_2\text{-CH}_2\text{-(CH}_2\text{)}_3$), 1.45 (t, $J = 6.8$ Hz, 6H, $\text{CH}_3\text{-CH}_2\text{-O}$), 1.34 (s, 6H, Ar- $\text{CH}_2\text{-CH}_2\text{-(CH}_2\text{)}_3$).

^{13}C NMR (δ /ppm, 100.5 MHz, CDCl_3): 164.99, 163.14, 148.86, 140.15, 132.13, 129.18, 121.68, 121.32, 114.12, 63.68, 35.26, 31.35, 30.81, 29.23, 29.07, 14.57

ESI-MS (m/z): 603.2717 ($\text{C}_{37}\text{H}_{40}\text{O}_6\text{Na}$, $[\text{M}+\text{Na}^+]$)

IR (ν_{max} cm^{-1}): 764, 845, 1072, 1165, 1196, 1258, 1412, 1466, 1505, 1605, 1613, 1728, 2855, 2924

Assay (HPLC, MeCN, 225/255 nm): 98%

Compound 51: 4,4'-(heptane-1,7-diyl)bis(4,1-phenylene) bis(4-propoxybenzoate)

Prepared according to Scheme 2. 4-4'-(heptane-1,7-diyl)diphenol (400 mg, 1.41 mmol) 4-propoxybenzoic acid (762 mg, 4.23 mmol), EDAC (810 mg, 4.23 mmol) DMAP (10 mg), DCM (25 ml). Crystallisation from ethanol/THF (20:1) afforded **51** as white powder.

Yield: 0.47 mg (0.78 mmol, 55 %)

^1H NMR (δ /ppm, 400 MHz, CDCl_3): 8.12 (d, $J = 8.8$ Hz, 4H, ArH), 7.20 (d, $J = 8.4$ Hz, 4H, ArH), 7.09 (d, $J = 8.4$ Hz, 4H, ArH), 6.95 (d, $J = 8.8$ Hz, 4H, ArH), 4.00 (t, $J = 6.4$ Hz, 4H, $\text{CH}_3\text{-CH}_2\text{-CH}_2\text{-O}$), 2.60 (t, $J = 7.6$ Hz, 4H, Ar- $\text{CH}_2\text{-CH}_2\text{-(CH}_2\text{)}_3$), 1.84 (qt, $J = 7.6, 6.4$ Hz, 4H, $\text{CH}_3\text{-CH}_2\text{-CH}_2\text{-O}$), 1.61 (quint, $J = 7.6$ Hz, 4H, Ar- $\text{CH}_2\text{-CH}_2\text{-(CH}_2\text{)}_3$), 1.34 (s, 6H, Ar- $\text{CH}_2\text{-CH}_2\text{-(CH}_2\text{)}_3$), 1.05 (t, $J = 7.6$ Hz, 6H, $\text{CH}_3\text{-CH}_2\text{-CH}_2\text{-O}$).

^{13}C NMR (δ /ppm, 100.5 MHz, CDCl_3): 165.09, 163.39, 148.91, 140.21, 132.19, 129.24, 121.69, 121.38, 114.19, 69.71, 35.32, 31.41, 29.29, 29.14, 22.42, 10.44

ESI-MS (m/z): 631.3030 ($\text{C}_{39}\text{H}_{44}\text{O}_6\text{Na}$, $[\text{M}+\text{Na}^+]$)

IR (ν_{max} cm^{-1}): 764, 1072, 1165, 1196, 1258, 1512, 1605, 1728, 2855, 2924, 2970

Assay (HPLC, MeCN, 225/255 nm): >99%

Compound 52: 4,4'-(heptane-1,7-diyl)bis(4,1-phenylene) bis(4-butoxybenzoate)

Prepared according to Scheme 2. 4-4'-(heptane-1,7-diyl)diphenol (200 mg, 0.705 mmol) 4-butoxybenzoic acid (411 mg, 2.12 mmol), EDAC (405 mg, 2.12 mmol) DMAP (10 mg), DCM (25 ml). Crystallisation from ethanol/THF (20:1) afforded **52** as a white powder.

Yield: 235 mg (0.37 mmol, 52%)

¹H NMR (δ/ppm, 400 MHz, CDCl₃): 8.13 (d, *J* = 8.8 Hz, 4H, ArH), 7.20 (d, *J* = 8.4 Hz, 4H, ArH), 7.09 (d, *J* = 8.4 Hz, 4H, ArH), 6.96 (d, *J* = 8.8 Hz, 4H, ArH), 4.04 (t, *J* = 6.8 Hz, 4H, CH₃-CH₂-CH₂-CH₂-O), 2.61 (t, *J* = 7.6 Hz, 4H, Ar-CH₂-CH₂-(CH₂)₃), 1.80 (tt, *J* = 7.6, 6.8 Hz, 4H, CH₃-CH₂-CH₂-CH₂-O), 1.62 (quint, *J* = 7.6 Hz, 4H, Ar-CH₂-CH₂-(CH₂)₃), 1.51 (sext, *J* = 7.6 Hz, 4H, CH₃-CH₂-CH₂-CH₂-O), 1.34 (s, 6H, Ar-CH₂-CH₂-(CH₂)₃), 0.99 (t, *J* = 7.6 Hz, 6H, CH₃-CH₂-CH₂-CH₂-O).

¹³C NMR (δ/ppm, 100.5 MHz, CDCl₃): 165.12, 163.42, 140.23, 132.21, 129.28, 121.70, 121.40, 114.22, 67.91, 35.38, 31.44, 31.08, 29.36, 29.16, 13.82

ESI-MS (*m/z*): 659.3376 (C₄₁H₄₈O₆Na, [M+Na⁺])

IR (ν_{max} cm⁻¹): 517, 648, 764, 849, 964, 1011, 1065, 1157, 1196, 1258, 1412, 1466, 1505, 1512, 1605, 1613, 1728, 2855, 2924

Assay (HPLC, MeCN, 225/255 nm): 97%

Compound 53: 1,5-bis(4-(Benzyloxy)phenoxy) pentane

Prepared according to Scheme 3. 4-(benzyloxy) phenol (39.7 g, 0.20 mol), 1,5-dibromopentane (11.9 mL, 0.09 mol) and potassium hydroxide (20.2 g, 0.36 mol). Recrystallisation from ethanol/THF (10:2), yielding **53** as a white powder

Yield: 34.0 g (0.073 mol, 81%)

¹H NMR (δ/ppm, 400 MHz, CDCl₃): 7.36- 7.16 (m, 10H, ArH), 6.84- 6.73 (m, 8H, ArH), 4.94 (s, 4H, O-CH₂-Ar), 3.85 (t, 4H, *J*= 6.4 Hz, O-CH₂-CH₂-CH₂-CH₂-CH₂-O), 1.75 (quint, 4H, *J*= 6.4 Hz, O-CH₂-CH₂-CH₂-CH₂-CH₂-O), 1.59- 1.53 (m, 2H, O-CH₂-CH₂-CH₂-CH₂-CH₂-O).

ESI-MS (*m/z*): 491.2192 (C₃₁H₃₂NaO₄ [M+Na⁺])

IR (ν_{\max} cm^{-1}): 2927, 2861, 1508, 1466, 1453, 1394, 1380, 1286, 1234, 1115, 1066, 1016, 946, 912, 843, 826, 777, 757, 733, 691, 534, 510.

Compound 54: 4,4'-(Pentane-1,5-diylbis(oxy)) diphenol

Prepared according to Scheme 3. **53** (34.0 g, 0.15 mol), palladium on carbon (0.2 g), THF (250 mL). Recrystallisation from ethanol/hexane (1:1) yielded **54** as a white powder.

Yield: 37.5 g (0.13 mol, 87%)

^1H NMR (δ/ppm , 400 MHz, CDCl_3): 6.71-6.65 (m, 8H, *ArH*), 3.83 (t, 4H, $J = 6.8$ Hz, $\text{O-CH}_2\text{-CH}_2\text{-CH}_2\text{-CH}_2\text{-CH}_2\text{-O}$), 1.73 (quint, 4H, $J = 6.8$ Hz, $\text{O-CH}_2\text{-CH}_2\text{-CH}_2\text{-CH}_2\text{-CH}_2\text{-O}$), 1.57 – 1.50 (m, 2H, $\text{O-CH}_2\text{-CH}_2\text{-CH}_2\text{-CH}_2\text{-CH}_2\text{-O}$).

ESI-MS (m/z): 311.1255 ($\text{C}_{17}\text{H}_{20}\text{NaO}_4$, $[\text{M}+\text{Na}]^+$)

IR (ν_{\max} cm^{-1}): 3039, 2947, 2926, 2874, 1850, 1606, 1509, 1471, 1461, 1392, 1373, 1290, 1270, 1233, 1167, 1105, 1068, 1040, 990, 950, 821, 811, 801, 778, 739, 642, 563, 523, 513, 464.

Compound 55: (Pentane-1,5-diylbis(oxy))bis(4,1-phenylene)bis(4-cyanobenzoate)

Prepared according to Scheme 3. **54** (200 mg, 0.69 mmol), 4-cyanobenzoic acid (300g, 2.07 mmol), EDAC (400g, 2.07 mmol), DMAP (10 mg) and DCM (5ml). Recrystallisation from ethanol/THF (10:2), yielded **55** as a white powder.

Yield: 190 mg (0.35 mmol, 50%)

^1H NMR (δ/ppm , 400 MHz, CDCl_3): 8.28 (ddd, 4H, $J = 8.4, 2.0, 1.6$ Hz, *ArH*), 7.80 (ddd, 4H, $J = 8.4, 2.4, 1.6$ Hz, *ArH*), 7.10 (ddd, 4H, $J = 9.2, 3.6, 2.4$ Hz, *ArH*), 6.93 (ddd, 4H, $J = 9.2, 3.6, 2.0$ Hz, *ArH*), 3.99 (t, 4H, $J = 6.4$ Hz, $\text{O-CH}_2\text{-CH}_2\text{-CH}_2\text{-CH}_2\text{-CH}_2\text{-O}$), 1.90-1.82 (m, 6H, $\text{O-CH}_2\text{-CH}_2\text{-CH}_2\text{-CH}_2\text{-CH}_2\text{-O}$).

^{13}C NMR (δ/ppm , 100.5 MHz, CDCl_3): 163.93, 157.08, 143.87, 133.49, 132.35, 130.58, 122.16, 117.86, 116.89, 115.19, 68.15, 28.97, 22.72.

ESI-MS (m/z): 569.1658 ($\text{C}_{33}\text{H}_{26}\text{N}_2\text{NaO}_6$, $[\text{M}+\text{Na}]^+$)

IR (ν_{\max} cm^{-1}): 2925, 2850, 1726, 1649, 1606, 1583, 1509, 1469, 1456, 1426, 1410, 1384, 1362, 1314, 1270, 1249, 1193, 1167, 1115, 1076, 1016, 989, 983, 932, 920, 877, 844, 805, 789, 779, 762, 729, 690, 670, 633, 588, 572, 548, 526, 514.

Assay (HPLC, MeCN, 225/255 nm.): >99%

Compound 56: (Pentane-1,5-diylbis(oxy))bis(4,1-phenylene)bis(4-isothiocyanatobenzoate)

Prepared according to Scheme 3. **54** (200 mg, 0.69 mmol), 4-isothiocyanobenzoic acid (370g, 2.07 mmol), EDAC (400g, 2.07 mmol), DMAP (10 mg) and DCM (5ml). Recrystallisation from ethanol/THF (10:2), yielded **56** as a white powder.

Yield = 180 mg (0.30 mmol, 43%)

^1H NMR (δ /ppm, 400 MHz, CDCl_3): 8.11 (dt, 4H, $J = 8.8, 2.0$ Hz, ArH), 7.25 (dt, 4H, $J = 8.8, 2.0$ Hz, ArH), 7.04 (ddd, 4H, $J = 9.6, 3.6, 2.4$ Hz, ArH), 6.86 (ddd, 4H, $J = 9.2, 3.6, 2.4$ Hz, ArH), 3.93 (t, 4H, $J = 6.8$ Hz, OCH₂-CH₂-CH₂-CH₂-CH₂-O), 1.81 (quint, 4H, $J = 6.8$ Hz, O-CH₂-CH₂-CH₂-CH₂-CH₂-O), 1.63-1.56 (m, 2H, O-CH₂-CH₂-CH₂-CH₂-CH₂-O).

^{13}C NMR (δ /ppm, 100.5 MHz, CDCl_3): 164.47, 157.02, 144.18, 138.28, 136.32, 131.69, 128.24, 125.91, 122.39, 115.25, 68.25, 29.09, 22.82.

ESI-MS (m/z): 633.1139 ($\text{C}_{33}\text{H}_{26}\text{N}_2\text{NaO}_6\text{S}_2$, $[\text{M}+\text{Na}]^+$)

IR (ν_{\max} cm^{-1}): 2926, 2850, 2022, 1727, 1604, 1506, 1456, 1411, 1386, 1314, 1303, 1267, 1244, 1194, 1166, 1113, 1077, 1016, 1008, 998, 986, 932, 877, 844, 823, 805, 789, 760, 730, 711, 690, 671, 633, 588, 573, 527, 514.

Assay (HPLC, MeCN, 225/255 nm.): >98%

Compound 57: (Pentane-1,5-diylbis(oxy))bis(4,1-phenylene)bis(4-nitrobenzoate)

Prepared according to Scheme 3. **54** (200 mg, 0.69 mmol), 4-nitrobenzoic acid (850g, 2.07 mmol), EDAC (400g, 2.07 mmol), DMAP (10 mg) and DCM (5ml). Recrystallisation from ethanol/THF (10:2), yielded **57** as a yellow powder.

Yield = 270 mg (0.47 mmol, 68%)

^1H NMR (δ /ppm, 400 MHz, CDCl_3): 8.37-8.32 (m, 8H, ArH), 7.12 (ddd, 4H, $J = 9.2, 3.6, 2.4$ Hz, ArH), 7.94 (ddd, 4H, $J = 9.2, 3.6, 2.4$ Hz, ArH), 4.00 (t, 4H, $J = 6.8$ Hz, O-CH₂-CH₂-CH₂-CH₂-O), 1.88 (quint, 4H, $J = 6.8$ Hz, O-CH₂-CH₂-CH₂-CH₂-O), 1.71 – 1.63 (m, 2H, O-CH₂-CH₂-CH₂-CH₂-O).

^{13}C NMR (δ /ppm, 100 MHz, CDCl_3): 163.68, 157.09, 150.82, 143.88, 135.04, 131.25, 123.69, 122.11, 115.21, 68.18, 28.92, 22.70.

ESI-MS (m/z): 609.1474 ($\text{C}_{31}\text{H}_{26}\text{N}_2\text{NaO}_{10}$, $[\text{M}+\text{Na}]^+$)

IR (ν_{max} cm^{-1}): 2925, 2850, 1726, 1607, 1583, 1538, 1507, 1456, 1426, 1410, 1384, 1348, 1315, 1269, 1246, 1194, 1167, 1116, 1077, 1010, 998, 933, 877, 845, 829, 806, 779, 762, 729, 714, 690, 671, 633, 588, 573, 514.

Assay (HPLC, MeCN, 225/255 nm): >99%

Compound 58: (Pentane-1,5-diylbis(oxy))bis(4,1-phenylene)bis(4-fluorobenzoate)

Prepared according to Scheme 3. **54** (200 mg, 0.69 mmol), 4-fluorobenzoic acid (290g, 2.07 mmol), EDAC (400g, 2.07 mmol), DMAP (10 mg) and DCM (5ml). Recrystallisation from ethanol/THF (10:2), yielded **58** as white needles.

Yield = 270 mg (0.52 mmol, 74%)

^1H NMR (δ /ppm, 400 MHz, CDCl_3): 8.16-8.11 (m, 4H, ArH), 7.13-7.07 (m, 4H, ArH), 7.04 (ddd, 4H, $J = 9.2, 3.6, 2.4$ Hz, ArH), 6.86 (ddd, 4H, $J = 9.2, 3.6, 2.4$ Hz, ArH), 3.93 (t, 4H, $J = 6.4$ Hz, O-CH₂-CH₂-CH₂-CH₂-O), 1.81 (quint, 4H, $J = 6.4$, O-CH₂-CH₂-CH₂-CH₂-O), 1.64-1.56 (m, 2H, O-CH₂-CH₂-CH₂-CH₂-O).

^{13}C NMR (δ /ppm, 100.5 MHz, CDCl_3): 166.18 (d, $J = 252.7$ Hz), 164.67, 156.95, 144.28, 132.82 (d, $J = 8.6$ Hz), 125.99 (d, $J = 2.9$ Hz), 122.45, 115.82 (d, $J = 21.9$ Hz), 115.23, 68.25, 29.10, 22.82.

^{19}F NMR (δ /ppm, 376 MHz, CDCl_3): -104.54 (quint, 2F, $J = 7.2$ Hz, ArF).

ESI-MS (m/z): 555.1581 ($\text{C}_{31}\text{H}_{26}\text{F}_2\text{NaO}_6$, $[\text{M}+\text{Na}]^+$)

IR (ν_{max} cm^{-1}): 2926, 2850, 1727, 1605, 1583, 1508, 1468, 1456, 1411, 1362, 1314, 1269, 1248, 1193, 1167, 1154, 1115, 1105, 1074, 1009, 998, 933, 876, 845, 823, 805, 761, 689, 671, 633, 619, 588, 565, 522, 514.

Assay (HPLC, MeCN, 225/255 nm): >99%

Compound 59: (Pentane-1,5-diylbis(oxy))bis(4,1-phenylene)bis(4-(trifluoromethyl)benzoate)

Prepared according to Scheme 3. **54** (200 mg, 0.69 mmol), 4-trifluoromethylbenzoic acid (510g, 2.07 mmol), EDAC (400g, 2.07 mmol), DMAP (10 mg) and DCM (5ml). Recrystallisation from ethanol/THF (10:2), yielded **59** as a white powder.

Yield = 320 mg (0.50 mmol, 73%)

¹H NMR (δ/ppm, 400 MHz, CDCl₃): 8.23 (d, 4H, J = 8.0 Hz, ArH), 7.69 (d, 4H, J = 8.0 Hz, ArH), 7.05 (ddd, 4H, J = 9.2, 3.6, 2.4 Hz, ArH), 7.87 (ddd, 4H, J = 9.2, 3.6, 2.4 Hz, ArH), 3.94 (t, 4H, J = 6.8 Hz, O-CH₂-CH₂-CH₂-CH₂-O), 1.81 (quint, 4H, J = 6.8 Hz, O-CH₂-CH₂-CH₂-CH₂-O), 1.64 – 1.57 (m, 2H, O-CH₂-CH₂-CH₂-CH₂-O).

¹³C NMR (δ/ppm, 100.5 MHz, CDCl₃): 193.28, 164.44, 157.11, 144.12, 135.01 (q, J = 32.4 Hz), 133.07, 130.61, 125.67 (q, J = 3.8 Hz), 122.35, 155.27, 68.26, 29.08, 22.82.

¹⁹F NMR (δ/ppm, 376 MHz, CDCl₃): -63.21 (s, 6F, CF₃).

ESI-MS (*m/z*): 655.1547 (C₃₃H₂₆F₆NaO₆, [M+Na]⁺)

IR (ν_{max} cm⁻¹): 2926, 2850, 1728, 1606, 1583, 1508, 1470, 1456, 1426, 1410, 1385, 1362, 1314, 1272, 1248, 1195, 1165, 1131, 1115, 1077, 1017, 998, 933, 920, 877, 865, 844, 830, 806, 789, 779, 762, 729, 690, 671, 633, 588, 572, 522.

Assay (HPLC, MeCN, 225/255 nm): >99%

Compound 60: (Pentane-1,5-diylbis(oxy))bis(4,1-phenylene)bis(4-ethylbenzoate)

Prepared according to Scheme 3. **54** (200 mg, 0.69 mmol), 4-ethylbenzoic acid (310g, 2.07 mmol), EDAC (400g, 2.07 mmol), DMAP (10 mg) and DCM (5ml). Recrystallisation from ethanol/THF (1:1), yielded **60** as a white powder.

Yield = 340 mg (0.62 mmol, 90%)

¹H NMR (δ/ppm, 400 MHz, CDCl₃): 8.04 (d, 4H, J = 8.0 Hz, ArH), 7.26 (d, 4H, J = 8.0 Hz, ArH), 7.04 (ddd, 4H, J = 9.2, 3.6, 2.4 Hz, ArH), 6.86 (ddd, 4H, J = 9.2, 3.6, 2.4 Hz,

ArH), 3.94 (t, 4H, J = 6.8 Hz, O-CH₂-CH₂-CH₂-CH₂-CH₂-O), 2.67 (q, 4H, J = 7.6 Hz, Ar-CH₂-CH₃), 1.81 (quint, 4H, J = 6.8 Hz, O-CH₂-CH₂-CH₂-CH₂-CH₂-O), 1.64 – 1.57 (m, 2H, O-CH₂-CH₂-CH₂-CH₂-CH₂-O), 1.21 (t, 6H, J = 7.6 Hz, Ar-CH₂-CH₃).

¹³C NMR (δ/ppm, 100.5 MHz, CDCl₃): 165.61, 156.7, 150.45, 144.36, 130.27, 128.06, 127.08, 122.45, 115.07, 68.13, 38.09, 29.01, 22.71, 15.25.

ESI-MS (*m/z*): 575.2389 (C₃₅H₃₆NaO₆, [M+Na]⁺)

IR (ν_{max} cm⁻¹): 2928, 2850, 1727, 1607, 1506, 1468, 1457, 1417, 1385, 1362, 1313, 1269, 1249, 1192, 1167, 1104, 1076, 1016, 1009, 933, 875, 843, 821, 805, 789, 761, 735, 690, 671, 634, 588, 567, 526, 516.

Assay (HPLC, MeCN, 225/255 nm): 99%

Compound 61: (Pentane-1,5-diylbis(oxy))bis(4,1-phenylene)bis(4-propylbenzoate)

Prepared according to Scheme 3. **54** (200 mg, 0.69 mmol), 4-propylbenzoic acid (340g, 2.07 mmol), EDAC (400g, 2.07 mmol), DMAP (10 mg) and DCM (5ml). Recrystallisation from ethanol/THF (1:1), yielded **61** as a white powder.

Yield = 320 mg (80%)

¹H NMR (δ/ppm, 400 MHz, CDCl₃): 8.03 (dt, 4H, J = 8.4, 2.0 Hz, ArH), 7.24 (d, 4H, J = 8.4 Hz, ArH), 7.04 (ddd, 4H, J = 9.2, 3.6, 2.4 Hz, ArH), 6.86 (ddd, 4H, J = 9.2, 3.6, 2.4 Hz, ArH), 3.94 (t, 4H, J = 6.8 Hz, O-CH₂-CH₂-CH₂-CH₂-CH₂-O), 2.61 (t, 4H, J = 7.6 Hz, Ar-CH₂-CH₂-CH₃), 1.81 (quint, 4H, J = 6.8 Hz, O-CH₂-CH₂-CH₂-CH₂-CH₂-O), 1.67-1.57 (m, 6H, O-CH₂-CH₂-CH₂-CH₂-CH₂-O, Ar-CH₂-CH₂-CH₃), 0.89 (t, 6H, J = 7.6 Hz, Ar-CH₂-CH₂-CH₃).

¹³C NMR (δ/ppm, 100.5 MHz, CDCl₃): 165.62, 156.70, 148.94, 144.36, 130.17, 128.65, 127.10, 122.44, 115.07, 68.13, 38.09, 29.01, 24.26, 22.71, 13.75.

ESI-MS (*m/z*): 603.2701 (C₃₇H₄₀NaO₆, [M+Na]⁺)

IR (ν_{max} cm⁻¹): 2931, 2852, 1728, 1608, 1504, 1468, 1416, 1391, 1300, 1269, 1248, 1190, 1169, 1103, 1075, 1009, 933, 873, 845, 823, 804, 759, 735, 699, 634, 569, 518.

Assay (HPLC, MeCN, 225/255 nm): >99%

Compound 62: (Pentane-1,5-diylbis(oxy))bis(4,1-phenylene)bis(4-butylbenzoate)

Prepared according to Scheme 3. **54** (200 mg, 0.69 mmol), 4-butylbenzoic acid (370g, 2.07 mmol), EDAC (400g, 2.07 mmol), DMAP (10 mg) and DCM (5ml). Recrystallisation from ethanol/THF (1:1), yielded **62** as a white powder.

Yield = 390 mg (0.64 mmol, 93%)

¹H NMR (δ/ppm, 400 MHz, CDCl₃): 8.03 (ddd, 4H, J= 8.8, 2.0, 1.6 Hz, ArH), 7.23 (d, 4H, J= 8.0 Hz, ArH), 7.04 (ddd, 4H, J= 8.8, 4.0, 2.0 Hz, ArH), 6.86 (ddd, 4H, J= 8.8, 4.0, 2.0 Hz, ArH), 3.93 (t, 4H, J= 6.8 Hz, O-CH₂-CH₂-CH₂-CH₂-O), 2.63 (t, 4H, J= 7.6 Hz, Ar-CH₂-CH₂-CH₂-CH₃), 1.81 (quint, 4H, J= 6.8 Hz, O-CH₂-CH₂-CH₂-CH₂-O), 1.64- 1.53 (m, 6H, O-CH₂-CH₂-CH₂-CH₂-O, Ar-CH₂-CH₂-CH₂-CH₃), 1.30 (sex, 4H, J= 7.6 Hz, Ar-CH₂-CH₂-CH₂-CH₃), 0.87 (t, 6H, J= 7.6 Hz, Ar-CH₂-CH₂-CH₂-CH₃).

¹³C NMR (δ/ppm, 100.5 MHz, CDCl₃): 165.61, 156.69, 149.19, 144.36, 130.17, 128.59, 127.04, 122.44, 115.06, 35.75, 33.27, 29.70, 29.00, 22.70, 22.29, 13.90.

IR (ν_{max} cm⁻¹): 2931, 2858, 1732, 1607, 1593, 1500, 1468, 1415, 1391, 1299, 1268, 1246, 1186, 1167, 1104, 1081, 1067, 1009, 932, 872, 846, 826, 800, 777, 757, 699, 635, 570, 521, 467.

ESI-MS (*m/z*): 631.3043 (C₃₉H₄₄NaO₆, [M+Na]⁺)

Assay (HPLC, MeCN, 225/255 nm): >99%

Compound 63: (Pentane-1,5-diylbis(oxy))bis(4,1-phenylene)bis(4-ethoxybenzoate)

Prepared according to Scheme 3. **54** (200 mg, 0.69 mmol), 4-ethoxybenzoic acid (340g, 2.07 mmol), EDAC (400g, 2.07 mmol), DMAP (10 mg) and DCM (5ml). Recrystallisation from ethanol/THF (1:1), yielded **63** as a white powder.

Yield = 320 mg (0.55 mmol, 80%)

¹H NMR (δ/ppm, 400 MHz, CDCl₃): 8.06 (dt, 4H, J= 9.2, 2.4 Hz, ArH), 7.03 (ddd, 4H, J= 8.8, 3.6, 2.0 Hz, ArH), 6.91-6.84 (m, 8H, ArH), 4.06 (q, 4H, J= 6.8 Hz, O-CH₂-CH₃), 3.93 (t, 4H, J= 6.6 Hz, O-CH₂-CH₂-CH₂-CH₂-O), 1.81 (quint, 4H, J= 6.6 Hz, O-CH₂-CH₂-CH₂-CH₂-O), 1.64- 1.56 (m, 2H, O-CH₂-CH₂-CH₂-CH₂-O), 1.39 (t, 6H, J= 6.8 Hz, O-CH₂-CH₃).

^{13}C NMR (δ /ppm, 100.5 MHz, CDCl_3): 165.30, 163.19, 156.63, 144.40, 132.21, 122.48, 121.70, 115.04, 114.18, 68.11, 63.76, 29.00, 22.70, 14.66.

ESI-MS (m/z): 607.2275 ($\text{C}_{35}\text{H}_{36}\text{NaO}_8$ $[\text{M}+\text{Na}]^+$)

IR (ν_{max} cm^{-1}): 2979, 2935, 1724, 1609, 1508, 1475, 1443, 1393, 1317, 1271, 1252, 1193, 1167, 1109, 1078, 1042, 1023, 1009, 984, 922, 873, 851, 821, 794, 763, 739, 694, 647, 629, 570, 525, 510, 484.

Assay (HPLC, MeCN, 225/255 nm): >99%

Compound 64: (Pentane-1,5-diylbis(oxy))bis(4,1-phenylene)bis(4-propoxybenzoate)

Prepared according to Scheme 3. **54** (200 mg, 0.69 mmol), 4-propoxybenzoic acid (370g, 2.07 mmol), EDAC (400g, 2.07 mmol), DMAP (10 mg) and DCM (5ml). Recrystallisation from ethanol/THF (1:1), yielded **64** as a white powder.

Yield= 280 mg (0.46 mmol, 67%)

^1H NMR (δ /ppm, 400 MHz, CDCl_3): 8.06 (ddd, 4H, $J= 8.4, 2.8, 2.0$ Hz, ArH), 7.03 (ddd, 4H, $J= 8.4, 3.6, 2.4$ Hz, ArH), 6.91- 6.84 (m, 8H, ArH), 3.95- 3.92 (m, 8H, $\text{O-CH}_2\text{-CH}_2\text{-CH}_3$ and $\text{O-CH}_2\text{-CH}_2\text{-CH}_2\text{-CH}_2\text{-O}$), 1.84- 1.74 (m, 8H, $\text{O-CH}_2\text{-CH}_2\text{-CH}_3$, $\text{O-CH}_2\text{-CH}_2\text{-CH}_2\text{-CH}_2\text{-O}$), 1.64- 1.58 (m, 2H, $\text{O-CH}_2\text{-CH}_2\text{-CH}_2\text{-CH}_2\text{-O}$), 1.00 (t, 6H, $J= 7.2$ Hz, $\text{O-CH}_2\text{-CH}_2\text{-CH}_3$).

^{13}C NMR (δ /ppm, 100.5 MHz, CDCl_3): 165.32, 163.39, 156.63, 144.40, 132.19, 122.49, 121.64, 115.04, 114.20, 69.72, 68.11, 29.012, 22.70, 22.43, 10.46.

ESI-MS (m/z): 635.2614 ($\text{C}_{37}\text{H}_{40}\text{NaO}_8$, $[\text{M}+\text{Na}]^+$)

IR (ν_{max} cm^{-1}): 2969, 2943, 2908, 2878, 1723, 1608, 1512, 1475, 1421, 1393, 1316, 1253, 1190, 1166, 1108, 1080, 1043, 1009, 973, 905, 872, 847, 828, 814, 798, 776, 762, 739, 692, 647, 630, 570, 524.

Assay (HPLC, MeCN, 225/255 nm): >99%

Compound 65: (Pentane-1,5-diylbis(oxy))bis(4,1-phenylene)bis(4-butoxybenzoate)

Prepared according to Scheme 3. **54** (200 mg, 0.69 mmol), 4-butoxybenzoic acid (400g, 2.07 mmol), EDAC (400g, 2.07 mmol), DMAP (10 mg) and DCM (5ml). Recrystallisation from ethanol/THF (1:1), yielded **65** as a white powder.

Yield = 380 mg (0.59 mmol, 86%)

¹H NMR (δ/ppm, 400 MHz, CDCl₃): 8.06 (ddd, 4H, J= 8.8, 2.8, 2.0 Hz, ArH), 7.03 (ddd, 4H, J= 8.8, 3.6, 2.4 Hz, ArH), 6.91 – 6.84 (m, 8H, ArH), 3.98 (t, 4H, J= 6.4 Hz, O-CH₂-CH₂-CH₂-CH₂-O), 3.93 (t, 4H, J= 6.4 Hz, O-CH₂-CH₂-CH₂-CH₃), 1.84- 1.70 (m, 8H, O-CH₂-CH₂-CH₂-CH₂-O, O-CH₂-CH₂-CH₂-CH₃), 1.65- 1.56 (m, 2H, O-CH₂-CH₂-CH₂-CH₂-O), 1.48- 1.40 (m, 4H, O-CH₂-CH₂-CH₂-CH₃), 0.93 (t, 6H, J= 7.6 Hz, O-CH₂-CH₂-CH₂-CH₃).

¹³C NMR (δ/ppm, 100.5 MHz, CDCl₃): 165.32, 163.40, 156.62, 144.39, 132.18, 122.48, 121.61, 115.03, 114.19, 68.11, 67.94, 31.10, 29.00, 22.69, 19.16, 13.81.

ESI-MS (*m/z*): 663.2903 (C₃₉H₄₄NaO₈, [M+Na]⁺)

IR (ν_{max} cm⁻¹): 2936, 2870, 1720, 1603, 1577, 1508, 1468, 1421, 1390, 1311, 1274, 1250, 1185, 1162, 1105, 1074, 1037, 1023, 1006, 969, 932, 873, 852, 843, 817, 799, 763, 692, 650, 631, 572, 530, 473.

Assay (HPLC, MeCN, 225/255 nm): >98%

4.3 Nonamethylene Spaced Bimesogens

Analogous mesophase behaviour to CB7CB has already been demonstrated in mesogens connected via a heptamethylene spacer in chapter 4.2 compounds **42**, **43**, **47** and **50-52** exhibited monotropic N_{TB} phases. Previous published results have shown that increasing the spacer length of CB7CB by two methylene units, to CB9CB results in a rise in the Iso. Liq.-N and N- N_{TB} transition temperatures, as well as a decrease in the melting point (Figure 65). The decrease in melting point can be attributed to the increased conformational freedom of the material imparted by the additional spacer units.

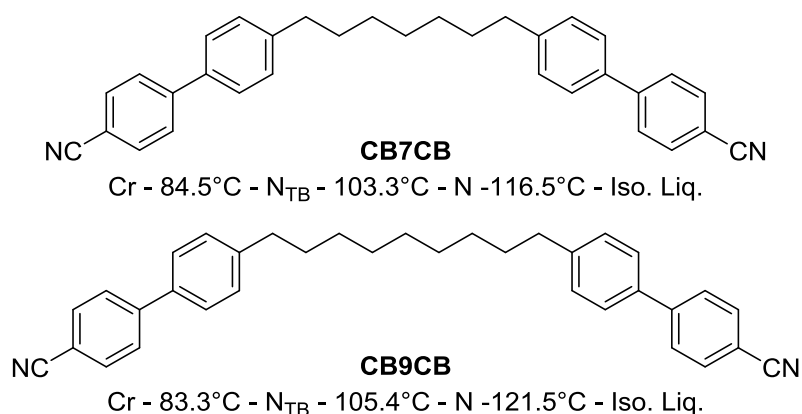
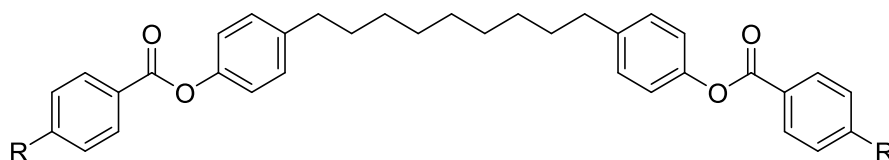


Figure 65: Structure and transition temperatures of CB7CB and CB9CB.

Using these values as a reference it was decided that the transition temperatures of the materials in chapter 4.2 could also be raised by replacing the heptamethylene spacer with a nonamethylene spacer. This would increase the likelihood of the occurrence of an enantiotropic N_{TB} phase. The main focus was to maintain an odd number of methylene units in the spacer in order to retain the gross bent molecular conformation. To this end a series of materials analogous to compounds **53-63**, with spacer lengths increased from 7-9 methylene units were synthesised and analysed using POM and DSC. The mesomorphic behaviour of the materials with inflexible, polar terminal groups is summarised in Table 13 and the mesomorphic behaviour of the compounds with alkyl or alkyloxy chains is summarised in Table 14.



Compound		Transition Temperature / °C					
No.	R	Cr	N _{TB}		N	Iso.	
66	CN	•	157.6 [79.7] {22.26}	(• [1.41] {0.44}	114.5 [1.41] {0.44}	• [2.6] {0.75}	•
67	NCS	•	97.7 [34.2] {11.11}	• [0.09] {0.03}	103.7 [0.09] {0.03}	• [0.27] {0.08}	•
68	NO ₂	•	105.4 [29.4] {9.35}	-	-	(• [0.17] {0.06}	•
69	F	•	97.6 [47.3] {15.35}	-	-	-	•
70	CF ₃	•	102.4 [55.6] {17.81}	-	-	-	•

Table 13: General structure and thermal properties of compounds **66-70**. Enthalpies displayed in square brackets and quoted in kJ mol^{-1} . Entropies quoted in {} and denoted in $\Delta S/R$.

Compounds **66** and **67** exhibited both nematic and N_{TB} phases on cooling from the isotropic liquid. The nematic phase was identified from the characteristic *schlieren* texture containing both two and four brush defects. The N_{TB} phase exhibited a broken fan texture, which is consistent with textures reported in the literature. These results are consistent with those observed for the C7 analogues (compounds **42** and **43**) reported in chapter 4.2. Representative photomicrographs of these phases are shown in Figure 66. Unlike the C7 spaced counterpart, which is non mesogenic, (compound **44**) the nitro terminated C9 material (compound **68**) exhibits a monotropic nematic phase. As in the C7 spaced materials both the fluoro and trifluoromethyl terminated materials exhibited no mesogenic behaviour.

The increase in spacer length lowered the melting points of the majority of the materials in Table 13 by a small margin (5-10 °C on average) with the exception of the cyano compound, in which the melting point increased. For the compounds that exhibited mesomorphic behaviour (compounds **66-68**) the clearing points increased by approximately 7 °C, These results are consistent with the trends observed in the CBnCB materials as shown in Figure 65. The cyano terminated material (**66**) saw a decrease in the N-N_{TB} transition temperature, however the N-N_{TB} transition temperature of the isothiocyanate material remained unchanged. This resulted in the cyano terminated material retaining a monotropic N_{TB} phase while the N_{TB} phase of the isothiocyanate compound became enantiotropic.

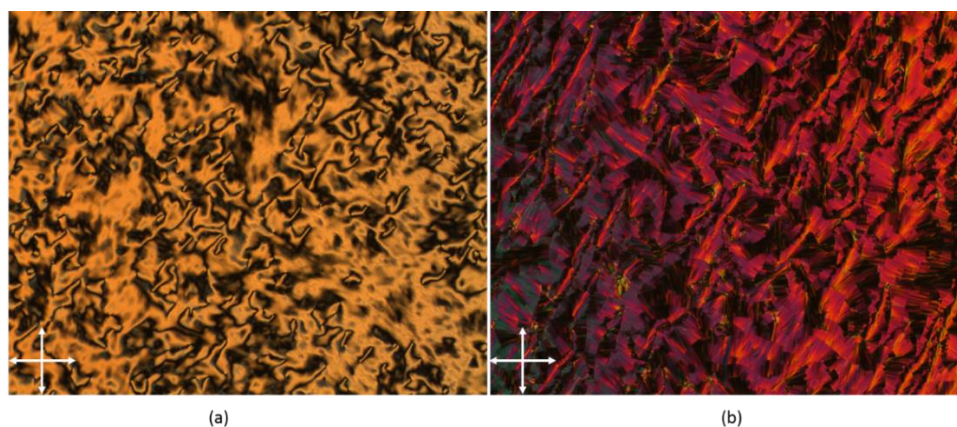
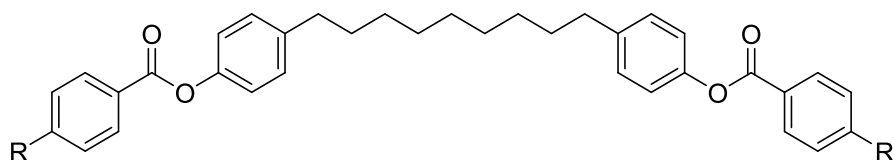


Figure 66: Photomicrographs showing compound **76** in the nematic phase (a) and N_{TB} phase (b) at 97.4 °C and 83.0 °C respectively. Sample was cooled at 0.1 °C min⁻¹ (x100).



Compound			Transition Temperature / °C				
No.	R	Cr	N _{TB}		N	Iso.	
71	C ₂ H ₅	•	66.8	(• 48.4	• 57.2)	•	
			[62.61]	[0.64]	[0.47]		
			{22.16}	{0.24}	{0.17}		
72	C ₃ H ₇	•	77.6	(• 59.5	• 67.1)	•	
			[42.05]	[0.28]	[0.62]		
			{14.43}	{0.10}	{0.22}		
73	C ₄ H ₉	•	67.3	(• 42.6	• 51.0)	•	
			[47.08]	[0.54]	[0.53]		
			{16.64}	{0.21}	{0.197}		
74	OC ₂ H ₅	•	119.6	(• 100.4	• 119.2)	•	
			[43.8]	[1.0]	[0.6]		
			{13.42}	{0.32}	{0.18}		
75	OC ₃ H ₇	•	110.4	(• 75.5	• 91.8)	•	
			[56.90]	[0.5]	[0.6]		
			{17.85}	{0.17}	{0.198}		
76	OC ₄ H ₉	•	83.3	• 84.7	• 99.5	•	
			[37.31]	[0.92]	[0.62]		
			{12.59}	{0.31}	{0.20}		

Table 14: Thermal properties of compounds **71-76**. Enthalpies quoted in [] and denoted in kJ mol⁻¹. Entropies quoted in {} and denoted in ΔS/R.

The lower temperature phases of these materials were confirmed to be the N_{TB} phase *via* miscibility studies with compound **42**, which has been confirmed to exhibit the N_{TB} phase by miscibility with CB9CB, and with cross miscibility studies to other materials found to be miscible with compound **42**. Representative examples of these phase diagrams are given for compounds **66** and **76** in Figure 70.

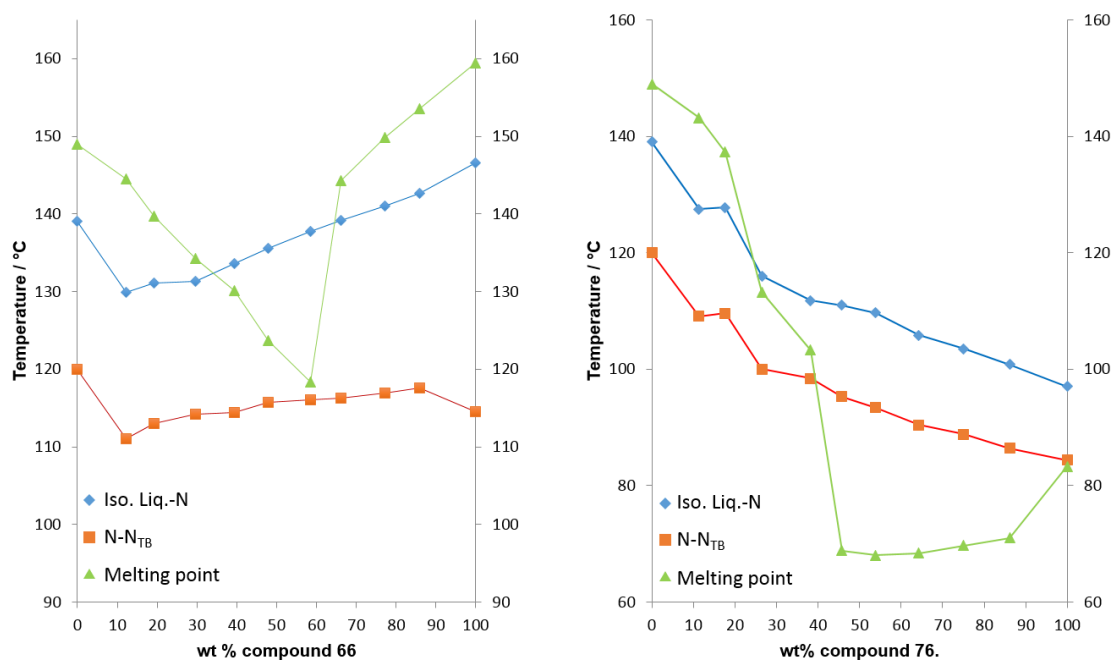


Figure 67: Representative binary phase diagrams for compounds **66** and **76** with compound **42**.

The results presented in Table 14 for compounds **71-76** show all of the dimers with a nonamethylene spacer exhibit both nematic and N_{TB} phases irrespective of whether the terminal unit is an alkyl or an alkyloxy chain. This result is in stark contrast to the results obtained for the shorter, heptamethylene spacer discussed in chapter 4.2, in which the only alkyl terminated compound shown to display liquid crystallinity was the propyl analogue. In the case of the alkyloxy compounds the phase behaviour was consistent with the behaviour of the compounds with a heptamethylene spacer. Without exception the clearing points were increased when the spacer length increased, this increase was accompanied by an increase in the N-N_{TB} transition temperature. The alkyloxy compounds (**74-76**) exhibited increases in the clearing points of approximately 15 °C compared to the heptamethylene analogues (**50-52**), although the effect on the N-N_{TB} transition is less pronounced, showing an increase of approximately 5 °C. In the case of the alkyl terminated materials it becomes difficult to comment in detail on the effect of the increased spacer as the mesomorphic behaviour was limited in the heptamethylene spaced materials to only the propyl terminated compound (**47**). This result however does support the assertion that the increased spacer length does promote mesophase formation in these materials, as all of the nonamethylene spaced dimers (**71-73**) showed liquid crystallinity

There was also, on average, a decrease in the melting points observed for compounds **66-76** as opposed to their heptamethylene spaced analogues (**42-52**). This decrease can be attributed to the increase in the conformational freedom of the spacer chain afforded by the inclusion of two extra methylene units. As these groups both possess, in theory, complete rotational freedom then there would be a drastic increase in the number of possible conformations the spacer chain could adopt with each methylene unit added. This increase in flexibility makes the material less prone to pack into a highly ordered phases such as crystals. This same effect can also be attributed to the decrease in melting point between the polar and apolar terminated materials, as the apolar chains are long, flexible groups, whereas the polar terminal groups are invariably short, inflexible groups. This causes the apolar groups to interfere with the packing of the molecules into a crystalline lattice, thus lowering the melting point.

The phase behaviour of the compounds with inflexible, polar chains (**66-70**) follows the same trends as those observed for the heptamethylene spaced materials, in that the occurrence of any liquid crystallinity can be split into the conjugating terminal groups (**66-68**) exhibit mesophase behaviour while the non-conjugating groups (**69, 70**) do not. As discussed in chapter 4.2 this effect can be attributed to the degree of effect the intermolecular forces between the terminal units have on the overall packing behaviour of the molecules. Cyano, isothiocyanate and nitro groups all have a degree of dispersal of charge within the group, this leads to the induction of relatively strong dipoles in the group and causes them to favourably align with one another, often in an antiparallel manner. In the case of the non-conjugative groups however the effects of induced dipoles are less prevalent, in these cases the dominating force is the repulsion between the terminal groups, which serves as a disruptive force when it comes to packing into a mesophase.

In the same vein as the heptamethylene spaced materials this series of compounds displays a slight odd-even effect in the I-N and N-N_{TB} transition temperatures with respect to the parity of the terminal chain likely caused by the propensity of even chains to adopt linear conformations, whereas odd numbered chains will favour bent conformations, leading to a very slight effect on the overall topology of the molecule. While this effect is not marked enough to affect the phase behaviour in compounds with short terminal chains, it has been shown that when the terminal chain is lengthened significantly the

entire phase behaviour of the material can change, shifting towards more smectic-like behaviour at extreme lengths²⁹.

Also the stability of the nematic phases in these materials showed a more marked increase when compared to the heptamethylene spaced analogues, this can be attributed to the slightly more linear average molecular topology that the longer spacer unit imparts. While an increase in the intermesogen angle would be expected to destabilise the N_{TB} phase these materials show the inverse effect, this indicates that it not necessarily as simple a situation as a more bent molecule leading to a more stable N_{TB} phase, rather that there is an apparent bell curve relationship between the molecular bend and the N_{TB} phase stability.

Conclusions

These results, combined with those presented in chapter 4.2, show that the spacer units have a marked effect on the mesophase behaviour of the compounds presented. For the nonamethylene spaced materials presented in this chapter the general trends observed with respect to the terminal chains are the same as those of the heptamethylene spaced materials, with the conjugating polar chains promoting phase behaviour whereas the non-conjugating polar chains disrupt it. Of interest in the polar terminated materials is compound **68**, the nitro terminated dimer. While the heptamethylene spaced analogue of this material (compound **44**) is non mesogenic compound **68** exhibits a monotropic nematic phase. This indicated that the lengthened spacer is working to stabilise the phase behaviour of the material.

This is supported by the results presented for the materials with apolar terminal chains (**71-76**), particularly those with alkyl terminal chains. While the heptamethylene spaced analogues of these materials (compounds **50-52**) mostly showed no mesogenic behaviour, with only the propyl terminated analogue exhibiting liquid crystallinity, for the nonamethylene spaced compounds (**74-76**) all of the alkyl terminated materials showed liquid crystalline behaviour, specifically an Iso.Liq.-N-N_{TB} phase series. This demonstrates that, despite the slightly more linear average molecular conformation imparted by the longer chain the N_{TB} phase is actually stabilised when moving from a 7 to a 9 unit spacer.

Due to the stabilisation of the N_{TB} phase caused by the lengthening of the spacer unit an odd-even effect was observed with respect to the parity of the terminal chains in the alkyl and alkyloxy terminated materials. Terminal units of odd parity (propyl, ethyloxy, and butyloxy) stabilised the mesophases more than those of even parity (ethyl, butyl, propyloxy). This is analogous to the effects observed in the nCB and nOCB series of calamitic liquid crystals. Indeed it has been shown that, also like the nCB and nOCB materials as the terminal chain is made significantly longer i.e. 8-12 units the materials move from tending towards nematic behaviour to tending towards smectic behaviour.²⁹

4.3.1. Synthetic Procedures

Compound 66: 4,4'-(nonane-1,9-diyl)bis(4,1-phenylene) bis(4-cyanobenzoate)

Prepared *via* Scheme 2. 4-4'-(nonane-,1,9-diyl)diphenol (400 mg, 1.27 mmol) 4-cyanobenzoic acid (561 mg, 3.81 mmol), EDAC (732 mg, 3.81 mmol) DMAP (10 mg), DCM (25 ml). Crystallisation from ethanol/THF (20:1) afforded compound as a white powder.

Yield: 375 mg (0.66 mmol, 52%)

¹H NMR (δ /ppm, 400 MHz, CDCl₃): 8.28 (4H, ddd, J=1.5, J=1.8, J=8.5, ArH), 7.79 (4H, ddd, J=1.5, J=1.8, J=8.5, ArH), 7.23 (4H, ddd, J=2.1, J=2.4, J=8.5, ArH), 7.11 (4H, ddd, J=2.1, J=2.4, J=8.5, ArH), 2.62 (4H, t, J=6.7, Ar-CH₂-CH₂-(CH₂)₅), 1.61 (4H, Quintet, J=6.7, Ar-CH₂-CH₂-(CH₂)₅), 1.24 – 1.40 (10H, M, Ar-CH₂-CH₂-(CH₂)₅).

¹³C NMR (δ /ppm, 100.5 MHz, CDCl₃): 29.16, 29.38, 29.41, 31.37, 35.30, 116.82, 117.82, 120.97, 129.41, 130.53, 132.30, 133.45, 140.99, 148.33, 164.67

ESI-MS (*m/z*): 571.2602 (C₃₇H₃₅N₂O₄, [M+H]⁺), 593.2316 (C₃₇H₃₄N₂O₄Na, [M+Na]⁺), 610.1853 (C₃₇H₃₄N₂O₄K, [M+K]⁺)

IR (ν_{\max} cm⁻¹): 540, 686, 756, 864, 1018, 1072, 1188, 1265, 1411, 1504, 1604, 1735, 2237, 2846, 2916

Assay (HPLC, MeCN, 225/255 nm): 99.12%

Compound 67: Nonane-1,9-diylbis(4,1-phenylene) bis(4-fluorobenzoate)

Prepared *via* Scheme 2. 4-4'-(nonane-,1,9-diyl)diphenol (400 mg, 1.27 mmol) 4-fluorobenzoic acid (534 mg, 3.18 mmol), EDAC (732 mg, 3.81 mmol) DMAP (10 mg), DCM (25 ml). Crystallisation from ethanol/THF (10:1) afforded compound as a white powder.

Yield: 412 mg (0.74 mmol, 58%)

¹H NMR (δ /ppm, 400 MHz, CDCl₃): 8.21 (4H, dddd, J= 2.1, J = 2.8, J = 5.5, J = 8.9 Hz, ArH), 7.22 (4H, ddd, J= 1.8, J = 2.8, J = 8.5 Hz, ArH), 7.17 (4H, ddd, J= 2.1, J = 2.8, J

= 8.5, $J = 8.9$ Hz, ArH), 7.09 (4H, ddd, $J = 2.1$, $J = 2.8$, $J = 8.5$ Hz, ArH), 2.62 (4H, t, $J = 7.6$ Hz, Ar-CH₂-CH₂-(CH₂)₅), 1.62 (4H, quintet, $J = 7.6$ Hz, Ar-CH₂-CH₂-(CH₂)₅), 1.26 - 1.39 (10H, m, Ar-CH₂-CH₂-(CH₂)₅)

¹³C NMR (δ /ppm, 100.5 MHz, CDCl₃): 29.34, 29.55, 29.58, 31.56, 35.47, 115.83 (d, $J = 22.0$ Hz), 121.34, 126.02 (d $J = 2.9$ Hz), 129.47, 132.84 (d, $J = 9.6$ Hz), 140.76, 148.76, 164.49, 166.18 (d, $J = 255.0$ Hz)

¹⁹F NMR (δ /ppm, 376.4 MHz, CDCl₃): -104.52 (1F, m, ArF)

ESI-MS (m/z): 557.2532 (C₃₅H₃₄F₂O₄, [M]⁺), 579.2317 (C₃₅H₃₄F₂O₄Na, [M+Na]⁺), 595.2043 (C₃₅H₃₄F₂O₄K, [M+K]⁺)

IR (ν_{\max} cm⁻¹): 756, 802, 1072, 1165, 1265, 1427, 1504, 1604, 1720, 2985

Assay (HPLC, MeCN, 250/275 nm): 99.45%

Compound 68: Nonane-1,9-diylbis(4,1-phenylene) bis(4-(trifluoromethyl)benzoate)

Prepared *via* Scheme 2. 4-4'-(nonane-1,9-diyl)diphenol (200 mg, 0.641 mmol) 4-trifluoromethylbenzoic acid (364 mg, 1.92 mmol), EDAC (367 mg, 1.92 mmol) DMAP (10 mg), DCM (5 ml). Crystallisation from ethanol/THF (8:1) afforded compound as a white powder.

Yield: 330 mg (0.50 mmol, 78%)

¹H NMR (δ /ppm, 400 MHz, CDCl₃): 8.23 (4H, d, $J = 8.2$ Hz, ArH), 7.69 (4H, d, $J = 8.2$ Hz, ArH), 7.16 (4H, ddd, $J = 2.1$, $J = 2.4$, $J = 8.5$ Hz, ArH), 7.04 (4H, ddd, $J = 2.1$, $J = 2.4$, $J = 8.5$ Hz, ArH), 2.55 (4H, t, $J = 7.0$ Hz, Ar-CH₂-CH₂-(CH₂)₅), 1.56 (4H, quintet, $J = 7.0$ Hz, 4H, Ar-CH₂-CH₂-(CH₂)₅), 1.18 - 1.32 (10H, m, Ar-CH₂-CH₂-(CH₂)₅).

¹³C NMR (δ /ppm, 100.5 MHz, CDCl₃): 29.33, 29.55, 29.57, 31.55, 35.47, 121.32, 123.67 (d, $J = 273.2$ Hz), 125.61 (Quartet, $J = 3.8$ Hz), 129.54, 130.63, 133.03, 135.02 (Quartet, $J = 32.6$ Hz), 141.02, 148.63, 164.25

¹⁹F NMR (δ /ppm, 376.4 MHz, CDCl₃): -63.00 (s, 3F, CF₃)

ESI-MS (m/z): 679.2260 (C₃₇H₃₄F₆NaO₄, [M+Na]⁺), 695.1995 (C₃₇H₃₄F₆KO₄, [M+K]⁺)

IR (ν_{\max} cm^{-1}): 516, 563, 632, 694, 725, 763, 825, 871, 1010, 1072, 1172, 1195, 1265, 1365, 1396, 1465, 1504, 1604, 1728, 2229, 2846, 2924, 3032.

Assay (HPLC, MeCN, 254/270 nm): 99.21%

Compound 69: Nonane-1,9-diylbis(4,1-phenylene) bis(4-isothiocyanobenzoate)

Prepared *via* Scheme 2. 4-4'-(nonane-1,9-diyl)diphenol (200 mg, 0.641 mmol) 4-isothiocyanobenzoic acid (343 mg, 1.92 mmol), EDAC (367 mg, 1.92 mmol) DMAP (10 mg), DCM (5 ml). Crystallisation from ethanol/THF (7:3) afforded compound as white plates.

Yield: 275 mg (0.44 mmol, 68%)

^1H NMR (δ /ppm, 400 MHz, CDCl_3): 8.10 (4H, ddd, $J = 1.8, J = 2.1, J = 8.5$ Hz, 4H, ArH), 7.25 (4H, ddd, $J = 1.8, J = 2.1, J = 8.5$ Hz, ArH), 7.15 (4H, ddd, $J = 1.8, J = 2.8, J = 8.5$ Hz, ArH), 7.02 (4H, ddd, $J = 1.8, J = 2.8, J = 8.5$ Hz, ArH), 2.54 (4H, t, $J = 7.0$ Hz, Ar- $\text{CH}_2\text{-CH}_2\text{-(CH}_2\text{)}_5$), 1.54 (4H, quintet, $J = 7.6$ Hz, Ar- $\text{CH}_2\text{-CH}_2\text{-(CH}_2\text{)}_5$), 1.18 -1.31 (10H, m, Ar- $\text{CH}_2\text{-CH}_2\text{-(CH}_2\text{)}_5$).

^{13}C NMR (δ /ppm, 100.5 MHz, CDCl_3): 29.33, 29.54, 29.57, 31.55, 35.47, 121.28, 125.92, 128.27, 129.50, 131.71, 136.30, 183.24, 140.87, 148.69, 164.28

ESI-MS (m/z): 657.1845 (100%, $\text{C}_{37}\text{H}_{34}\text{N}_2\text{NaO}_4\text{S}_2$, $[\text{M}+\text{Na}]^+$)

IR (ν_{\max} cm^{-1}): 516, 563, 632, 694, 717, 763, 825, 871, 1010, 1072, 1118, 1157, 1203, 1265, 1365, 1458, 1504, 1604, 1728, 2229, 2846, 2924, 3032.

Assay (HPLC, MeCN, 254/270 nm): 99.46%

Compound 70: Nonane-1,9-diylbis(4,1-phenylene) bis(4-nitrobenzoate)

Prepared *via* Scheme 2. 4-4'-(nonane-1,9-diyl)diphenol (200 mg, 0.641 mmol) 4-nitrobenzoic acid (322 mg, 1.92 mmol), EDAC (367 mg, 1.92 mmol) DMAP (10 mg), DCM (5 ml). Crystallisation from ethanol/THF (5:1) afforded compound as pale yellow plates.

Yield: 290 mg (0.47 mmol, 74%)

^1H NMR (δ /ppm, 400 MHz, CDCl_3): 8.23 -8.30 (8H, m, ArH), 7.16 (4H, ddd, $J = 1.8$, $J = 2.4$, $J = 8.5$ Hz, ArH), 7.04 (4H, ddd, $J = 1.8$, $J = 2.4$, $J = 8.5$ Hz, ArH), 2.54 (4H, t, $J = 7.0$ Hz, Ar- CH_2 - CH_2 -(CH_2)₅), 1.54 (4H, quintet, $J = 7.0$ Hz, Ar- CH_2 - CH_2 -(CH_2)₅), 1.17 -1.31 (10H, m, Ar- CH_2 - CH_2 -(CH_2)₅).

^{13}C NMR (δ /ppm, 100.5 MHz, CDCl_3): 29.33, 29.54, 29.57, 31.54, 35.47, 121.12, 123.78, 129.60, 131.35, 135.18, 141.23, 148.50, 150.92, 163.57

ESI-MS (m/z): 633.2186 ($\text{C}_{35}\text{H}_{34}\text{NaN}_2\text{O}_8$, $[\text{M}+\text{Na}]^+$), 649.1962 ($\text{C}_{35}\text{H}_{34}\text{KN}_2\text{O}_8$, $[\text{M}+\text{K}]^+$),

IR (ν_{max} cm^{-1}): 516, 563, 632, 709, 763, 825, 871, 1010, 1072, 1118, 1165, 1195, 1265, 1365, 1465, 1504, 1604, 1735, 2229, 2846, 2924, 3032.

Assay (HPLC, MeCN, 254/270 nm): 99.35%

Compound 71: Nonane-1,9-diyl bis(4,1-phenylene) bis(4-ethylbenzoate)

Prepared *via* Scheme 2. 4-4'-(nonane-,1,9-diyl)diphenol (400 mg, 1.27 mmol) 4-ethylbenzoic acid (576 mg, 3.84 mmol), EDAC (732 mg, 3.81 mmol) DMAP (10 mg), DCM (25 ml). Crystallisation from ethanol/THF (20:1) afforded compound as a white powder.

Yield: 580 mg (1.18 mmol, 93%)

^1H NMR (δ /ppm, 400 MHz, CDCl_3): 8.15 (4H, d, $J = 8.5$ Hz, ArH), 7.35 (4H, d, $J = 8.5$ Hz, ArH), 7.25 (4H, d, $J = 8.5$ Hz, ArH), 7.13 (4H, d, $J = 8.5$ Hz, ArH), 2.76 (4H, Quartet, $J = 7.6$ Hz, Ar- CH_2 - CH_3), 2.65 (4H, t, $J = 7.6$ Hz, Ar- CH_2 -(CH_2)₇- CH_2 -Ar), 1.60 - 1.67 (4H, m, - CH_2 - CH_2 -(CH_2)₅- CH_2 - CH_2 -), 1.33 - 1.43 (10H, m, - CH_2 -(CH_2)₅- CH_2 -), 1.31 (6H, t, $J = 7.6$ Hz, CH_3 - CH_2 -Ar)

^{13}C NMR (δ /ppm, 100.5 MHz, CDCl_3): 15.19, 28.95, 29.18, 29.41, 29.44, 31.40, 35.30, 121.29, 127.07, 127.99, 129.23, 130.23, 140.31, 148.82, 150.36, 165.30

IR (ν_{max} cm^{-1}): 509, 617, 694, 756, 1010, 1072, 1172, 1265, 1365, 1458, 1504, 1604, 1728, 2322, 2731, 2846, 2916, 3024

Assay (HPLC, MeCN, 230/255 nm): 99.6%

Compound 72: 4,4'-(nonane-1,9-diyl)bis(4,1-phenylene) bis(4-propylbenzoate)

Prepared *via* Scheme 2. 4-4'-(nonane-,1,9-diyl)diphenol (200 mg, 0.635 mmol) 4-propylbenzoic acid (313.5 mg, 1.905 mmol), EDAC (366 mg, 1.905 mmol) DMAP (10 mg), DCM (25 ml). Crystallisation from ethanol/THF (20:1) afforded compound as white a powder.

Yield: 196 mg (0.32 mmol, 51%)

¹H NMR (δ /ppm, 400 MHz, CDCl₃): 8.10 (d, J = 8.4 Hz, 4H, *ArH*), 7.30 (d, J = 8.8 Hz, 4H, *ArH*), 7.21 (d, J = 8.8 Hz, 4H, *ArH*), 7.10 (d, J = 8.4 Hz, 4H, *ArH*), 2.64 (dt, J = 24.0, 7.6 Hz, 8H, *Ar-CH₂-CH₂-(CH₂)₅, Ar-CH₂-CH₂-CH₃), 1.79 – 1.47 (m, 8H, *Ar-CH₂-CH₂-(CH₂)₅, Ar-CH₂-CH₂-CH₃), 1.31 (s, 10H, *-CH₂-CH₂-(CH₂)₅), 0.96 (t, J = 7.6 Hz, 6H, *Ar-CH₂-CH₂-CH₃).****

¹³C NMR (δ /ppm, 100.5 MHz, CDCl₃): 165.53, 149.05, 148.97, 140.52, 130.29, 129.40, 128.76, 127.26, 121.45, 77.43, 77.11, 76.79, 38.20, 35.48, 31.58, 29.57, 29.36, 24.37, 13.85.

ESI-MS (m/z): 605.3634 (C₄₁H₄₉O₄, [M+H]⁺), 627.3430 (C₄₁H₄₈O₄Na, [M+Na]⁺)

IR (ν_{\max} cm⁻¹): 687, 756, 880, 1011, 1072, 1234, 1273, 1358, 1412, 1497, 1605, 1728, 3009

Assay (HPLC, MeCN, 225/255 nm): 98.45%

Compound 73: 4,4'-(nonane-1,9-diyl)bis(4,1-phenylene) bis(4-butylbenzoate)

Prepared *via* the same methodology as compound 7. 4-4'-(nonane-,1,9-diyl)diphenol (400 mg, 1.27 mmol) 4-butylbenzoic acid (678 mg, 3.81 mmol), EDAC (732 mg, 3.81 mmol) DMAP (10 mg),DCM (25 ml). Crystallisation from ethanol/THF (20:1) afforded compound as a white powder.

Yield: 410 mg (0.65 mmol, 51 %)

¹H NMR (δ /ppm, 400 MHz, CDCl₃): 8.09 (d, J = 8.0 Hz, 4H, *ArH*), 7.30 (d, J = 8.0 Hz, 4H, *ArH*), 7.21 (d, J = 8.4 Hz, 4H, *ArH*), 7.09 (d, J = 8.4 Hz, 4H, *ArH*), 2.65 (dt, J = 32.8,

8.0 Hz, 8H, Ar-CH₂-CH₂), 1.77 – 1.58 (m, 8H, Ar-CH₂-CH₂-CH₂), 1.49 – 1.17 (m, 14H, Ar-CH₂-CH₂-(CH₂)₅, Ar-CH₂-CH₂-CH₂-CH₃), 0.95 (t, *J* = 7.2 Hz, 6H, Ar-CH₂-CH₂-CH₂-CH₃).

¹³C NMR (δ/ppm, 100.5 MHz, CDCl₃): 130.30, 129.40, 128.71, 121.45, 113.50, 77.42, 77.10, 76.79, 31.10, 31.04.

ESI-MS (*m/z*): 655.3758 (C₄₃H₅₂O₄Na, [M+Na]⁺)

IR (ν_{max} cm⁻¹): 748, 1072, 1165, 1258, 1412, 1505, 1613, 1728, 2847, 2924

Assay (HPLC, MeCN, 225/255 nm): 99.11%

Compound 74: 4,4'-(nonane-1,9-diyl)bis(4,1-phenylene) bis(4-ethoxybenzoate)

Prepared *via* Scheme 2. 4-4'-(nonane-1,9-diyl)diphenol (400 mg, 1.27 mmol) 4-ethoxybenzoic acid (633 mg, 3.81 mmol), EDAC (732 mg, 3.81 mmol) DMAP (10 mg), DCM (25 ml). Crystallisation from ethanol/THF (20:1) afforded compound as white powder.

Yield: 367 mg (0.61 mmol, 48 %)

¹H NMR (δ/ppm, 400 MHz, CDCl₃): 8.13 (d, *J* = 8.8 Hz, 4H, ArH), 7.21 (d, *J* = 8.8 Hz, 4H, ArH), 7.09 (d, *J* = 8.8 Hz, 4H, ArH), 6.96 (d, *J* = 8.8 Hz, 4H, ArH), 4.11 (q, *J* = 6.8 Hz, 4H, CH₃-CH₂-O), 2.61 (t, *J* = 7.6 Hz, 4H, Ar-CH₂-CH₂-(CH₂)₅), 1.59 (quint, *J* = 7.6 Hz, 4H, Ar-CH₂-CH₂-(CH₂)₅), 1.45 (t, *J* = 6.8 Hz, 6H, CH₃-CH₂-O), 1.31 (s, 10H, Ar-CH₂-CH₂-(CH₂)₅).

¹³C NMR (δ/ppm, 100.5 MHz, CDCl₃): 132.33, 129.37, 121.49, 114.29, 77.41, 77.10, 76.78, 63.87, 35.47, 31.58, 29.56, 29.35.

ESI-MS (*m/z*): 631.3005 (C₃₉H₄₄O₆Na, [M+Na]⁺)

IR (ν_{max} cm⁻¹): 764, 849, 1065, 1165, 1196, 1258, 1412, 1466, 1505, 1605, 1613, 1728, 2855, 2924

Assay (HPLC, MeCN, 225/255 nm): 98.87%

Compound 75: 4,4'-(nonane-1,9-diyl)bis(4,1-phenylene) bis(4-propoxybenzoate)

Prepared *via* Scheme 2. 4-4'-(nonane-1,9-diyl)diphenol (400 mg, 1.27 mmol) 4-propoxybenzoic acid (687 mg, 3.81 mmol), EDAC (732 mg, 3.81 mmol) DMAP (10 mg), DCM (25 ml). Crystallisation from ethanol/THF (20:1) afforded compound as a white powder.

Yield: 650 mg (1.02 mmol, 80 %)

^1H NMR (δ /ppm, 400 MHz, CDCl_3): 8.18 – 8.05 (m, 4H, ArH), 7.23 – 7.04 (m, 8H, ArH), 7.00 – 6.89 (m, 4H, ArH), 4.00 (t, $J = 6.8$ Hz, 4H, $\text{CH}_3\text{-CH}_2\text{-CH}_2\text{-O}$), 2.61 (t, $J = 7.6$ Hz, 4H, Ar- $\text{CH}_2\text{-CH}_2$), 1.84 (sext, $J = 7.2, 6.8$ Hz, 4H, $\text{CH}_3\text{-CH}_2\text{-CH}_2\text{-O}$), 1.61 (quint, $J = 7.2$ Hz, 4H, Ar- $\text{CH}_2\text{-CH}_2\text{-CH}_3$), 1.31 (s, 10H, Ar- $\text{CH}_2\text{-CH}_2\text{-(CH}_2\text{)}_5\text{-CH}_2\text{-CH}_2\text{-Ar}$), 1.06 (t, $J = 7.2$ Hz, 6H, $\text{CH}_3\text{-CH}_2\text{-CH}_2\text{-O}$).

^{13}C NMR (δ /ppm, 100.5 MHz, CDCl_3): 163.51, 149.01, 132.32, 129.37, 121.81, 121.49, 114.32, 77.42, 77.10, 76.79, 69.84, 35.48, 31.58, 29.57, 29.36, 22.54, 10.56.

ESI-MS (m/z): 637.3524 ($\text{C}_{41}\text{H}_{49}\text{O}_6$, $[\text{M}+\text{H}]^+$), 659.3343 ($\text{C}_{41}\text{H}_{48}\text{O}_6\text{Na}$, $[\text{M}+\text{Na}]^+$)

IR (ν_{max} cm^{-1}): 756, 1072, 1165, 1196, 1258, 1512, 1605, 1728, 2454, 2847, 2924

Assay (HPLC, MeCN, 225/255 nm): 98.29%

Compound 76: 4,4'-(nonane-1,9-diyl)bis(4,1-phenylene) bis(4-butoxybenzoate)

Prepared *via* Scheme 2. 4-4'-(nonane-1,9-diyl)diphenol (400 mg, 1.27 mmol) 4-butoxybenzoic acid (750 mg, 3.81 mmol), EDAC (732 mg, 3.81 mmol) DMAP (10 mg), DCM (25 ml). Crystallisation from ethanol/THF (20:1) afforded compound as a white powder.

Yield: 438 mg (0.66 mmol, 52 %)

^1H NMR (δ /ppm, 400 MHz, CDCl_3): 8.12 (d, $J = 8.8$ Hz, 4H, ArH), 7.20 (d, $J = 8.4$ Hz, 4H, ArH), 7.08 (d, $J = 8.4$ Hz, 4H, ArH), 6.95 (d, $J = 8.8$ Hz, 4H, ArH), 4.04 (t, $J = 6.4$ Hz, 4H, O- $\text{CH}_2\text{-CH}_2\text{-CH}_2\text{-CH}_3$), 2.61 (t, $J = 7.6$ Hz, 4H, Ar- $\text{CH}_2\text{-CH}_2\text{-(CH}_2\text{)}_5$), 1.86 – 1.73 (m, 8H, , Ar- $\text{CH}_2\text{-CH}_2\text{-(CH}_2\text{)}_5$, O- $\text{CH}_2\text{-CH}_2\text{-CH}_2\text{-CH}_3$), 1.69 – 1.57 (m, 4H, O- $\text{CH}_2\text{-}$

CH₂-CH₂-CH₃), 1.30 (s, 10H, Ar-CH₂-CH₂-(CH₂)₅), 0.99 (t, *J* = 7.2 Hz, 6H, O-CH₂-CH₂-CH₂-CH₃).

¹³C NMR (δ/ppm, 100.5 MHz, CDCl₃): 132.31, 129.37, 121.49, 114.32, 77.55, 77.42, 77.24, 77.10, 76.92, 76.79.

ESI-MS (*m/z*): 687.3656 (C₄₃H₅₂O₆Na, [M+Na]⁺)

IR (ν_{max} cm⁻¹): 764, 965, 1072, 1165, 1196, 1250, 1412, 1505, 1613, 1728, 2662, 2847, 2924

Assay (HPLC, MeCN, 225/255 nm): 99.21%

4.4 Unsymmetrical bimesogens

In all of the previous sections of this work the focus has been on the synthesis and characterisation of symmetrical liquid crystal dimers such as the CBnCB materials. In this brief study an investigation was made into the effects of breaking that symmetry on the phase behaviour of flexible bimesogens. To that end a short series of unsymmetrical, ether linked materials were synthesised based on the molecular architecture of CBO11OCB³³ shown in Figure 68. CBO11OCB itself exhibits only a nematic phase, however it has been shown in previously published work that breaking the symmetry of liquid crystal dimers can promote the formation of the N_{TB} phase in systems where it does not occur in symmetrical materials^{86,87}. The structures of these compounds (**77-84**) are shown in Table 15. The phase behaviour of these materials were analysed via POM and DSC, and the data is presented in Table 16.

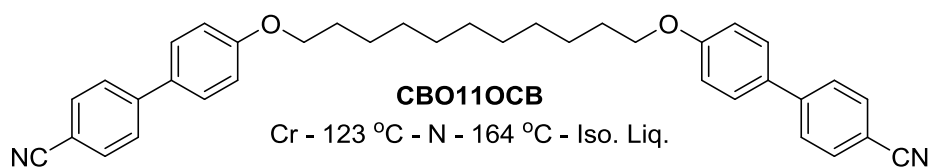
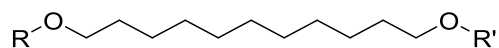


Figure 68: Structure of CBO11OCB.⁸⁸



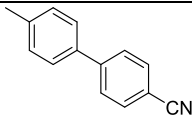
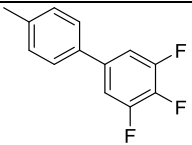
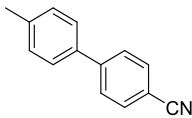
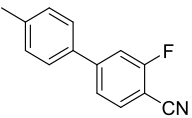
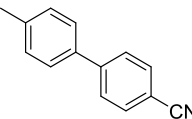
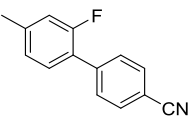
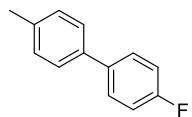
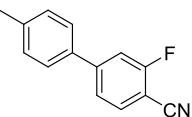
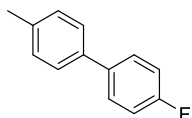
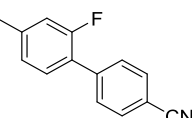
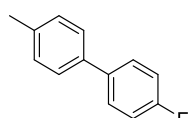
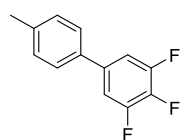
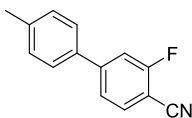
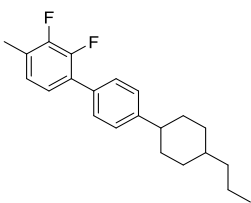
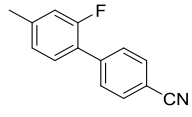
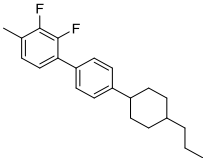
Compound	R	R'
77		
78		
79		
80		
81		
82		
83		
84		

Table 15: General structures of unsymmetrical bimesogens (77-84).

Compound	Transition Temperatures / °C						
	Cr		N _{TB}		N		Iso. Liq.
77	•	80.3	-	-	•	97.7	•
		[39.9]				[1.19]	
		{13.57}				{0.39}	
78	•	121.4	-	-	•	140.3	•
		[52.49]				[3.19]	
		{16.01}				{0.93}	
79	•	100.4	-	-	•	146.3	•
		[42.18]				[4.18]	
		{13.45}				{1.20}	
80	•	83.1	(•	37.5)	•	107.5	•
		[34.46]		[*]		[1.56]	
		{11.64}		{*}		{0.49}	
81	•	83.2	-	-	•	109.1	•
		[42.91]				[2.74]	
		{14.49}				{0.86}	
82	•	68.4	-	-	(•	63.3)	•
		[40.66]				[0.87]	
		{14.33}				{0.31}	
83	•	78.1	(•	67.7)	•	174.4	•
		[22.12]		[*]		[2.72]	
		{7.57}		{*}		{0.73}	
84	•	81.1	-	-	•	169.2	•
		[6.03]				[2.91]	
		{2.05}				{0.79}	

Table 16: Mesomorphic behaviour of compounds **77-84**. Enthalpies are quoted in [] and denoted in kJ mol⁻¹. Entropies are quoted in {} and denoted in ΔS/R. Values denoted by a * were unobtainable via DSC.

As can be seen from Table 16 compounds **77-84** generally favour the formation of nematic phases, with all of the compounds listed exhibiting a nematic phase on cooling from the isotropic liquid and, with the exception of compound **82**, all of these nematic phases were enantiotropic with the clearing point occurring well (17-96 °C) above the melting point. These high clearing points were unsurprising, as stated in section 4.2, ether

linkages in the spacer chain of a liquid crystal dimer tend to promote a more linear average molecular shape, this, combined with the lengthened spacer (13 units overall) which will also serve to decrease the overall molecular bend, will cause these molecules to pack much more efficiently into the nematic phase as opposed to previously presented dimers.

Of particular interest are compounds **80** and **83**, which both exhibited a transition to a phase below the nematic. While the lower temperature phase of compound **80** was impossible to analyse, as due to the transition occurring well into the supercooling region of the crystal, 45.6 °C below the melting point, the phase was only observed under rapid cooling, and the material crystallised soon after, brief observation showed it to have a blocky texture consistent with that of previously published N_{TB} materials. The lower temperature phase of compound **83** however was more easily analysed, as the transition occurred only 10.4 °C below the melting point, allowing the phase to be observed more easily than in compound **80**. The phase was, as in compound **80** observed to behave in accordance with previous N_{TB} materials, however the same problem arose in that, due to the degree of supercooling required for the phase to form the material quickly nucleated crystals. A representative photomicrograph of compound **83** is shown in Figure 69.

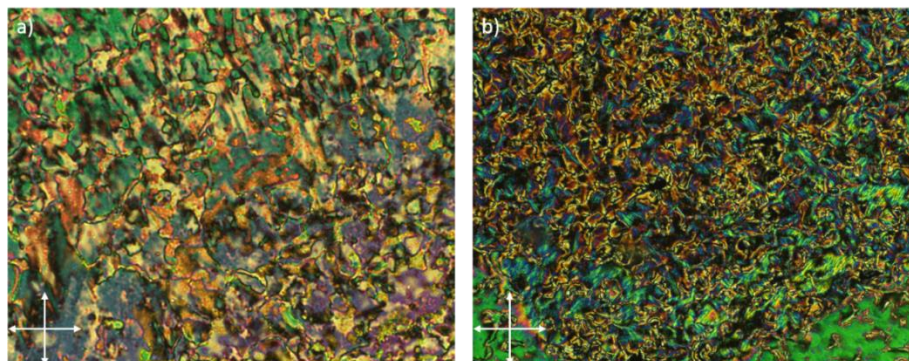


Figure 69: Photomicrographs of compound **83** in a) the nematic phase at 157.8 °C and b) the N_{TB} phase at 66.2 °C. Sample cooled at 1 °C min⁻¹. (x100)

Of interest in these materials is that, while the shorter spaced ether linked dimers presented in section 4.2 universally did not display the N_{TB} phase, compounds **80** and **83** possibly exhibit it. This, along with previous work into the occurrence of the N_{TB} phase in ether linked materials serves to demonstrate that ether linked materials do possess the potential to support this phase. It is possible that the introduction of more conformational freedom through the lengthening of the spacer unit is a key factor in the formation of the N_{TB} phase by these two materials when compared to compounds **55-75**, as this increased

freedom could offset the more linear average molecular shape imparted by the ether linkage.

Conclusions

When compared to ether linked materials with shorter spacer units the compounds presented in this chapter display broadly lower melting points. This could be attributed to the increased flexibility of the spacer unit disrupting the packing of the molecules into a crystal lattice, lowering the melting points. Conversely the clearing points of these materials remained relatively high, the nematic phase being stabilised by the more linear molecular architecture. This resulted in materials with very wide nematic phase ranges, approaching 100 °C for some compounds.

While compounds **77-84** were all nematogens, an expected result given the compound they were based on, CBO11OCB exhibits a nematic phase, compounds **80** and **83** were found to, under rapid cooling exhibit a transition to a mesophase with an optical texture reminiscent of the N_{TB} phase. In the case of both of these materials the N_{TB} phase occurred significantly into the supercooling range of the crystal, making it difficult to analyse in depth.

This result does however show that ether linked materials, while more linear than their methylene linked counterparts do have the potential to support the N_{TB} phase and that the breaking of the molecular symmetry appears to enhance this potential. Of particular note is that both of the materials found to exhibit the N_{TB} phase both had a 2-fluoro cyanobiphenyl mesogenic unit. While it is logical to assume that the insertion of the fluoro substituent would disrupt the intermolecular interactions previously stated to be key to stabilising the N_{TB} phase in cyano terminated materials these results imply that the effect of the substituent on the packing of the crystal phase outweighs this effect very slightly, allowing for the formation of the N_{TB} phase.

4.4.1 Synthetic procedures

Compound 77: 4'-((11-((3',4',5'-trifluoro-[1,1'-biphenyl]-4-yl)oxy)undecyl)oxy)-[1,1'-biphenyl]-4-carbonitrile.

Prepared according to Scheme 4. 4'-((11-bromoundecyl)oxy)-[1,1'-biphenyl]-4-carbonitrile (300 mg, 0.7 mmol), 3,4,5-trifluoro-4'-methoxy-1,1'-biphenyl (160 mg, 0.7 mmol), potassium carbonate (200 mg, 1.4 mmol) and acetone (50 ml). Recrystallisation from ethanol yielded the target compound as white plates.

Yield: 320 mg (0.56 mmol, 80 %)

^1H NMR (δ /ppm, 400 MHz, CDCl_3): 7.61 (2H, dd, 2.1, 6.7 Hz, ArH), 7.56 (2H, dd, 2.1, 6.6 Hz, ArH), 7.45 (2H, ddd, 2.1, 3.1, 9.1 Hz, ArH), 7.33 (2H, ddd, 1.8, 3.1, 9.1 Hz, ArH), 7.05 (2H, m, ArH), 6.91 (2H, ddd, 2.1, 3, 8.9 Hz, ArH), 6.88 (2H, ddd, 2.1, 3, 8.9 Hz, ArH), 3.9 (4H, t, 6.4 Hz, O-CH₂-CH₂-CH₂-(CH₂)₅-CH₂-CH₂-CH₂-O), 1.73 (4H, dddq, 3.4, 6.4, 7, 7.9 Hz, O-CH₂-CH₂-CH₂-(CH₂)₅-CH₂-CH₂-CH₂-O), 1.40 (4H, ddt, 6.1, 7, 7.3 Hz, O-CH₂-CH₂-CH₂-(CH₂)₅-CH₂-CH₂-CH₂-O), 1.26 (10H, s, O-CH₂-CH₂-CH₂-(CH₂)₅-CH₂-CH₂-CH₂-O)

^{13}C NMR (δ /ppm, 100.5 MHz, CDCl_3): 25.99, 29.18, 29.33, 29.46, 29.50, 68.10, 109.97, 110.23, 110.29, 110.39, 110.44, 114.94, 115.02, 119.08, 127, 127.83, 128.26, 130.31, 131.18, 132.51, 145.21, 151.33 (ddd, 3.84, 4.60, 248.94 Hz), 159.44, 159.76.

^{19}F NMR (δ /ppm, 376.4 MHz, CDCl_3): -134.4 (2F, dd, 20.7, 9.2 Hz), -163.8 (1F, ddd, 20.7, 6.9, 5.8 Hz)

IR (ν_{max} cm⁻¹): 819.75, 1082.07, 1178.51, 1217.08, 1228.66, 1292.31, 1435.04, 1456.26, 1471.69, 1506.41, 1521.84, 1539.20, 1558.48, 1575.84, 1602.85, 1616.35, 1635.64, 1647.21, 1653.00, 1683.86, 1699.29, 1716.65, 1791.89, 1843.95, 1869.02, 2222.00, 2358.94, 2852.72, 2924.09.

ESI-MS (m/z): 594.2594 (C₃₆H₃₆F₃NO₂Na, [M+Na]⁺)

Elemental Analysis (mass %): Calculated: C, 75.64 %; H, 6.35 %; N, 2.45 %; Other, 15.56, %. Found: C, 75.40 %; H, 6.36 %; N, 2.45 %; Other, 15.79 %.

Compound 78: 4'-((11-((4'-cyano-[1,1'-biphenyl]-4-yl)oxy)undecyl)oxy)-3-fluoro-[1,1'-biphenyl]-4-carbonitrile)

Prepared according to Scheme 4. 4'-((11-bromoundecyl)oxy)-[1,1'-biphenyl]-4-carbonitrile (300 mg, 0.7 mmol), 3-fluoro-4'-hydroxy-[1,1'-biphenyl]-4-carbonitrile (150 mg, 0.7 mmol), potassium carbonate (200mg, 1.4 mmol), acetone (50 ml). Recrystallisation from ethanol yielded the target compound as white plates

Yield: 180 mg (0.32 mmol, 46%)

¹H NMR (δ/ppm, 400 MHz, CDCl₃): 7.62 (2H, dd, 2.14, 6.41 Hz, ArH), 7.54-7.58 (3H, m, ArH), 7.42-7.47 (4H, m, ArH), 7.36 (1H, dd, 1.53, 8.24, ArH), 7.3 (1H, dd, 1.53, 10.68 Hz, ArH), 6.92 (4H, dd, 1.83, 3.05, 8.54 Hz, ArH), 3.93 (4H, dd, 6.4, 6.7 Hz, O-CH₂-CH₂-CH₂-(CH₂)₅-CH₂-CH₂-CH₂-O), 1.74 (4H, dddd, 6.4, 6.7, 7, 7.9 Hz, O-CH₂-CH₂-CH₂-(CH₂)₅-CH₂-CH₂-CH₂-O), 1.40 (4H, ddt, 6.7, 7, 7.6 Hz, O-CH₂-CH₂-CH₂-(CH₂)₅-CH₂-CH₂-CH₂-O), 1.26 (10H, s, O-CH₂-CH₂-CH₂-(CH₂)₅-CH₂-CH₂-CH₂-O).

¹³C NMR (δ/ppm, 100.5 MHz, CDCl₃): 25.97, 29.12, 29.31, 29.45, 68.09, 68.14, 98.65, 98.80, 109.94, 113.77, 113.97, 114.23, 115.01, 115.10, 119.06, 122.58 (d, 3.07 Hz), 126.97, 128.25 (d, 3.07 Hz), 129.90, 129.92, 131.15, 132.49, 133.53, 145.17, 148.06, 148.14, 159.73, 160.22, 163.44 (d, 258.53 Hz)

¹⁹F NMR (δ/ppm, 376.4 MHz, CDCl₃): -106.3 (1F, dd, 10.3, 6.9 Hz)

IR (ν_{max} cm⁻¹): 661.58, 723.31, 736.81, 781.17, 815.83, 848.68, 877.61, 900.76, 958.62, 1002.98, 1041.56, 1120.64, 1217.08, 1244.09, 1311.59, 1325.10, 1338.60, 1436.97, 1458.18, 1473.62, 1490.97, 1506.41, 1521.84, 1541.12, 1558.48, 1600.92, 1635.64, 1647.21, 1653.00, 1683.86, 1699.29, 1716.65, 1734.01, 1749.44, 1772.58, 1791.87, 1843.95, 1869.02, 2218.14, 2358.94, 2852.72, 2926.01

ESI-MS (*m/z*): 583.2736 (C₃₇H₃₇FN₂O₂Na, [M+Na]⁺)

Elemental Analysis (mass %): Calculated: C, 79.26 %; H, 6.65 %; N, 5.00 %; Other, 9.09 %. Found: C, 78.81 %; H, 6.64 %; N, 4.86 %; Other, 9.54 %.

Compound 79: 4'-((11-((4'-cyano-[1,1'-biphenyl]-4-yl)oxy)undecyl)oxy)-2'-fluoro-[1,1'-biphenyl]-4-carbonitrile

Prepared according to Scheme 4. 4'-((11-bromoundecyl)oxy)-[1,1'-biphenyl]-4-carbonitrile (300 mg, 0.7 mmol), 2'-fluoro-4'-hydroxy-[1,1'-biphenyl]-4-carbonitrile (150 mg, 0.7 mmol), potassium carbonate (200 mg, 1.4 mmol), acetone (50 ml). Recrystallisation from ethanol yielded the target compound as white plates

Yield: 280 mg (0.5 mmol, 71%)

¹H NMR (δ /ppm, 400 MHz, CDCl₃): 7.61-7.64 (4H, m, ArH), 7.53-7.57 (4H, m, ArH), 7.45 (2H, ddd, 2.14, 3.05, 8.85 Hz, ArH), 7.26 (1H, t, 8.85 Hz, ArH), 6.92 (2H, ddd, 2.14, 3.05, 8.85 Hz, ArH), 6.72 (1H, dd, 2.44, 8.54 Hz, ArH), 6.65 (1H, dd, 2.44, 12.81 Hz, ArH), 1.74 (4H, dqu, 2.14, 6.71 Hz, O-CH₂-CH₂-CH₂-(CH₂)₅-CH₂-CH₂-CH₂-O), 3.94 (4H, dd, 5.4, 7.32 Hz, O-CH₂-CH₂-CH₂-(CH₂)₅-CH₂-CH₂-CH₂-O), 1.40 (4H, ddt, 3.97, 4.27, 5.80, 7.32 Hz, O-CH₂-CH₂-CH₂-(CH₂)₅-CH₂-CH₂-CH₂-O), 1.26 (10H, s, O-CH₂-CH₂-CH₂-(CH₂)₅-CH₂-CH₂-CH₂-O).

¹³C NMR (δ /ppm, 100.5 MHz, CDCl₃): 25.90, 25.96, 28.98, 29.14, 29.56, 29.30, 29.43, 29.45, 29.46, 68.07, 68.47, 102.47, 102.73, 109.92, 110.47, 111.19 (d, 3.07 Hz), 114.99, 118.90 (d, 3.07 Hz), 119.04, 126.96, 128.22, 129.15, 129.19, 130.67, 130.72, 131.12, 132.11, 132.47, 140.43, 140.45, 145.15, 159.72, 160.28 (d, 249.33 Hz) 160.76, 160.87.

¹⁹F NMR (δ /ppm, 376.4 MHz, CDCl₃): 115.0 (1F, dd, 11.5, 10.3 Hz)

IR (ν max cm⁻¹): 721.38, 738.74, 796.60, 823.60, 840.96, 894.97, 1012.63, 1037.70, 1080.14, 1105.21, 1176.58, 1217.08, 1228.66, 1253.73, 1298.09, 1435.04, 1456.26, 1471.69, 1506.41, 1521.84, 1541.12, 1558.48, 1575.84, 1602.85, 1635.64, 1647.21, 1653.00, 1683.86, 1739.79, 1869.02, 2227.78, 2358.94, 2850.79, 2924.09, 2970.38.

ESI-MS (m/z): 583.2753, (C₃₇H₃₇FN₂O₂Na, [M+Na]⁺)

Elemental Analysis (mass %): Calculated: C, 79.26 %; H, 6.65 %; N, 5.00 %; Other, 9.09 %. Found: C, 78.96 %; H, 6.66 %; N, 5.00 %; Other, 9.38 %.

Compound 80: 3-fluoro-4'-((11-((4'-fluoro-[1,1'-biphenyl]-4-yl)oxy)undecyl)oxy)-[1,1'-biphenyl]-4-carbonitrile

Prepared according to Scheme 4. 4-((11-bromoundecyl)oxy)-4'-fluoro-1,1'-biphenyl (150 mg, 0.3 mmol), 3-fluoro-4'-hydroxy-[1,1'-biphenyl]-4-carbonitrile (70 mg, 0.33 mmol), potassium carbonate (130 mg, 0.94 mmol), acetone (50 ml). Recrystallisation from ethanol yielded the target compound as white plates

Yield: 30 mg (0.05 mmol, 17%)

¹H NMR (δ/ppm, 400 MHz, CDCl₃): 7.56 (1H, ddd, 6.71, 7.93 Hz, *ArH*), 7.29-7.46 (8H, m, *ArH*), 7.02 (2H, tdd, 2.14, 3.05, 8.85 Hz, *ArH*), 6.92 (2H, ddd, 2.14, 3.05, 8.85 Hz, *ArH*), 6.88 (2H, ddd, 2.14, 3.05, 8.85 Hz, *ArH*), 3.93 (4H, dt, 6.4, 6.7 Hz, O-CH₂-CH₂-CH₂-(CH₂)₅-CH₂-CH₂-O), 1.73 (4H, dtqq, 3.05, 3.36, 3.66, 4.88 Hz, O-CH₂-CH₂-CH₂-(CH₂)₅-CH₂-CH₂-O), 1.4 (4H, dddd, 6.7, 7, 7.3, 7.6 Hz, O-CH₂-CH₂-CH₂-(CH₂)₅-CH₂-CH₂-O), 1.26 (10H, s, O-CH₂-CH₂-CH₂-(CH₂)₅-CH₂-CH₂-O).

¹³C NMR (δ/ppm, 100.5 MHz, CDCl₃): 25.99, 26.03, 29.16, 29.26, 29.34, 29.36, 29.47, 29.51, 53.41, 68.07, 68.19, 98.73, 98.88, 113.95 (d, 19.95 Hz), 114.27, 114.97 (d, 37.59 Hz), 115.49 (d, 21.48 Hz), 122.64 (d, 3.07 Hz), 127.96, 128.10, 128.18, 128.32, 130.00 (d, 1.53 Hz), 132.58, 133.59, 136.97 (d, 3.84 Hz), 148.18 (d, 8.44 Hz), 158.65, 160.27, 162.03 (d, 245.49 Hz), 163.50 (d, 257.77 Hz)

¹⁹F NMR (δ/ppm, 376.4 MHz, CDCl₃): -106.35 (dd, 6.89, 10.34 Hz), -116.67 (ttt, 3.45, 4.60, 5.75 Hz)

ESI-MS (*m/z*): 576.2683, (C₃₆H₃₇F₂NO₂Na, [M+Na]⁺)

Compound 81: 2'-fluoro-4'-((11-((4'-fluoro-[1,1'-biphenyl]-4-yl)oxy)undecyl)oxy)-[1,1'-biphenyl]-4-carbonitrile

Prepared according to Scheme 4. 4-((11-bromoundecyl)oxy)-4'-fluoro-1,1'-biphenyl (150 mg, 0.3 mmol), 2'-fluoro-4'-hydroxy-[1,1'-biphenyl]-4-carbonitrile (70 mg, 0.33 mmol), potassium carbonate (130 mg, 0.94 mmol), acetone (50 ml). Recrystallisation from ethanol yielded the target compound as white plates

Yield: 120 mg (0.2 mmol, 66%)

^1H NMR (δ /ppm, 400 MHz, CDCl_3): 7.62 (2H, dddd, 1.53, 2.14, 2.29, 8.85 Hz, ArH), 7.54 (2H, ddd, 1.53, 1.83, 8.54 Hz, ArH), 7.36-7.44 (4H, m, ArH), 7.26 (1H, t, 8.85 Hz, ArH), 7.02 (2H, ddd, 2.44, 3.05, 8.85 Hz, ArH), 6.88 (2H, ddd, 2.14, 3.05, 8.85 Hz, ArH), 6.72 (1H, dd, 2.44, 8.54 Hz, ArH), 6.65 (1H, dd, 2.44, 12.81 Hz, ArH), 3.92 (4H, ddd, 2.75, 6.41, 6.71 Hz, O-CH₂-CH₂-CH₂-(CH₂)₅-CH₂-CH₂-CH₂-O), 1.73 (4H, dddd, 6.41, 6.71, 7.02, 7.63 Hz, O-CH₂-CH₂-CH₂-(CH₂)₅-CH₂-CH₂-CH₂-O), 1.40 (4H, dddd, 5.19, 7.02, 9.15, 9.76 Hz, O-CH₂-CH₂-CH₂-(CH₂)₅-CH₂-CH₂-CH₂-O), 1.26 (10H, s, O-CH₂-CH₂-CH₂-(CH₂)₅-CH₂-CH₂-CH₂-O).

^{13}C NMR (δ /ppm, 100.5 MHz, CDCl_3): 25.92, 26.0, 29.01, 29.23, 29.28, 29.33, 29.44, 29.47, 29.49, 68.02, 68.49, 102.63 (d, 26.1 Hz), 110.50, 111.21 (d, 3.1 Hz), 114.75, 115.45 (d, 21.5 Hz), 118.91, 118.94, 119.07, 127.9, 128.05, 128.12, 129.2 (d, 3.1 Hz), 130.68, 130.73, 132.12, 132.50, 136.92 (d, 3.1 Hz), 140.46, 158.62, 160.30 (d, 249.33 Hz), 160.76, 160.79, 161.54, 162.0 (d, 243.19 Hz)

^{19}F NMR (δ /ppm, 376.4 MHz, CDCl_3): -115.05 (1F, dd, 10.34, 11.49 Hz), -116.69 (1F, dtq, 3.45, 3.45, 4.60, 5.75, 5.75, 5.75)

IR (ν_{max} cm⁻¹): 659.66, 680.87, 707.88, 723.31, 742.59, 763.81, 779.24, 810.10, 821.68, 848.68, 958.62, 1002.98, 1028.06, 1045.42, 1109.07, 1122.57, 1219.01, 1230.58, 1263.37, 1290.38, 1309.67, 1325.10, 1361.74, 1429.25, 1456.26, 1473.62, 1496.76, 1506.41, 1521.84, 1541.12, 1558.48, 1575.84, 1622.13, 1635.64, 1647.21, 1653.00, 1683.86, 1699.29, 1716.65, 1734.01, 1749.44, 1772.58, 1791.87, 1843.95, 1869.02, 2223.92, 2360.87, 2852.72, 2922.16

ESI-MS (m/z): 576.2703 (C₃₆H₃₇F₂NO₂Na, [M+Na]⁺)

Elemental Analysis (mass %): Calculated: C, 78.09 %; H, 6.74 %; N, 2.53 %; Other, 12.64 %. Found: C, 77.66 %; H, 6.72 %; N, 2.53 %; Other, 13.09 %.

Compound 82: 3,4,5-trifluoro-4'-((11-((4'-fluoro-[1,1'-biphenyl]-4-yl)oxy)undecyl)oxy)-1,1'-biphenyl

Prepared according to Scheme 4. 4-((11-bromoundecyl)oxy)-4'-fluoro-1,1'-biphenyl (150 mg, 0.3 mmol), 3',4',5'-trifluoro-[1,1'-biphenyl]-4-ol (70 mg, 0.3 mmol), potassium carbonate (130 mg, 0.94 mmol), acetone (50 ml). Recrystallisation from ethanol yielded the target compound as white plates

Yield: 90 mg (0.16 mmol, 53%)

¹H NMR (δ/ppm, 400 MHz, CDCl₃): 7.32-7.45 (6H, m, ArH), 6.99-7.09 (4H, m, ArH), 6.88 (4H, ddd, 2.14, 3.05, 9.3 Hz, ArH), 3.92 (4H, t, 6.4 Hz, O-CH₂-CH₂-CH₂-(CH₂)₅-CH₂-CH₂-CH₂-O), 1.73 (4H, ddt, 6.4, 6.7, 8.24 Hz, O-CH₂-CH₂-CH₂-(CH₂)₅-CH₂-CH₂-CH₂-O), 1.40 (4H dddd, 6.4, 6.7, 7.02, 8.24 Hz, O-CH₂-CH₂-CH₂-(CH₂)₅-CH₂-CH₂-CH₂-O), 1.26 (10H, s, O-CH₂-CH₂-CH₂-(CH₂)₅-CH₂-CH₂-CH₂-O)

¹³C NMR (δ/ppm, 100.5 MHz, CDCl₃): 26.01, 26.04, 29.20, 29.27, 29.36, 29.49, 29.52, 68.06, 68.13, 110.37 (ddd, 5.4, 6.1, 15.7 Hz), 114.78, 114.97, 115.48 (d, 20.7 Hz), 127.86, 127.95, 128.09, 128.18, 131.42 (d, 221.7 Hz), 136.98 (d, 3.1 Hz), 151.36 (dddd, 3.8, 4.6, 10.0, 248.9 Hz), 158.66, 159.47, 162.03 (d, 245.5 Hz)

¹⁹F NMR (δ/ppm, 376.4 MHz, CDCl₃): -116.69 (1F, dtq, 3.45, 4.60, 5.75), -134.42 (2F, dd, 8.04, 20.68 Hz), 163.79 (1F, ddt, 5.75, 6.89, 19.53, 20.68 Hz).

IR (ν_{max} cm⁻¹): 655.08, 704.02, 723.31, 738.74, 775.38, 785.03, 798.53, 848.68, 854.47, 893.04, 1002.98, 1039.63, 1078.21, 1103.28, 1126.43, 1161.15, 1197.79, 1232.51, 1290.38, 1309.67, 1338.60, 1361.74, 1394.53, 1417.68, 1446.61, 1458.18, 1473.62, 1494.83, 1506.41, 1541.12, 1558.48, 1575.84, 1608.63, 1622.13, 1635.64, 1647.21, 1653.00, 1683.86, 1699.29, 1716.65, 1734.01, 1749.44, 1772.58, 17+1.87, 1843.95, 1869.02, 2225.85, 2358.94, 2852.72, 2922.16

ESI-MS (*m/z*): N/A (ESI, APCI and EI attempted, all delivered negative results)

Elemental Analysis (mass %): Calculated: C, 74.45 %; H, 6.43 %; N, 0 %; Other, 19.12 %. Found: C, 73.49 %; H, 6.26 %; N, 0 %; Other, 19.8 %.

Compound 83: 4'-((11-((2,3-difluoro-4'-(4-propylcyclohexyl)-[1,1'-biphenyl]-4-yl)oxy)undecyl)oxy)-3-fluoro-[1,1'-biphenyl]-4-carbonitrile

Prepared according to Scheme 4. 4'-((11-bromoundecyl)oxy)-3-fluoro-[1,1'-biphenyl]-4-carbonitrile (500 mg, 1.2 mmol), 2,3-difluoro-4'-(4-propylcyclohexyl)-[1,1'-biphenyl]-4-ol (386 mg, 1.2 mmol), potassium carbonate (415 mg, 3 mmol), acetone (50 ml). Recrystallisation from ethanol yielded the target compound as white plates

Yield: 510 mg (0.7 mmol, 58%)

^1H NMR (δ /ppm, 400 MHz, CDCl_3): 7.53 (1H, dd, 6.71, 7.78 Hz, *ArH*), 7.42 (2H, ddd, 2.14, 3.05, 8.85 Hz, *ArH*), 7.33 (3H, dd, 1.53, 8.24 Hz, *ArH*), 7.28 (1H, dd, 1.53, 10.37 Hz, *ArH*), 7.18 (2H, dd, 1.83, 6.41 Hz, *ArH*), 6.99 (1H, ddd, 2.44, 8.24, 8.54 Hz, *ArH*), 6.90 (2H, ddd, 2.14, 3.05, 8.85 Hz, *ArH*), 6.69 (1H, td, 1.83, 8.24 Hz, *ArH*), 3.97 (2H, dd, 6.3, 6.7 Hz, O- $\text{CH}_2\text{-CH}_2\text{-CH}_2\text{-(CH}_2)_5$), 3.91 (2H, dd, 6.4, 6.7 Hz, O- $\text{CH}_2\text{-CH}_2\text{-CH}_2\text{-(CH}_2)_5$), 2.41 (1H, dt, 3.05, 12.2 Hz, Ar- $\text{CH-C}_2\text{H}_4\sim$), 1.69-1.85 (8H, m, CyHex*H*), 1.10-1.44 (21H, m, CyHex*H*, O- $\text{CH}_2\text{-CH}_2\text{-CH}_2\text{-(CH}_2)_5\text{-CH}_2\text{-CH}_2\text{-CH}_2\text{-O}$, Cy- $\text{CH}_2\text{-CH}_2\text{-CH}_3$), 0.925-1.022 (2H, m, Cy- $\text{CH}_2\text{-CH}_2\text{-CH}_3$), 0.82 (3H, t, 7.32 Hz, Cy- $\text{CH}_2\text{-CH}_2\text{-CH}_3$).

^{13}C NMR (δ /ppm, 100.5 MHz, CDCl_3): 14.39, 18.30, 19.95, 25.79, 25.92, 29.07, 29.10, 29.22, 29.27, 29.39, 29.40, 29.43, 33.43, 34.18, 36.91, 39.63, 44.20, 58.27, 68.08, 69.69, 98.53, 98.69, 109.34, 109.37, 113.63, 113.84, 114.17, 115.04, 122.50 (d, 3.1 Hz), 122.75, 122.86, 123.37 (dd, 3.8, 4.6 Hz), 126.92, 128.19, 128.45 (d, 3.1 Hz), 129.76 (d, 1.5 Hz), 132.2, 133.44, 141.65 (ddd, 14.6, 15.3, 246.6 Hz), 147.26, 147.48 (ddd, 2.3, 3.1, 8.1 Hz), 148.01, 148.10, 149.90, 150.01, 160.21, 163.38 (d, 257.8 Hz).

^{19}F NMR (δ /ppm, 376.4 MHz, CDCl_3): -158.76 (1F, dd, 6.89, 19.53 Hz), -141.77 (1F, dd, 8.04, 20.68 Hz), -106.36 (1F, dd, 6.89, 10.34 Hz)

IR (ν_{max} cm^{-1}): 673.14, 690.52, 725.23, 738.74, 794.67, 808.17, 823.60, 840.96, 894.97, 1014.56, 1035.77, 1080.14, 1105.21, 1176.58, 1199.72, 1253.73, 1274.95, 1298.09, 1435.04, 1471.69, 1490.97, 1504.48, 1523.76, 1541.12, 1558.48, 1602.85, 1683.86, 2233.57, 2850.79, 2922.16.

ESI-MS (m/z): 718.3843 ($\text{C}_{45}\text{H}_{52}\text{F}_3\text{NO}_2\text{Na}$, $[\text{M}+\text{Na}]^+$)

Elemental Analysis (mass %): Calculated: C, 77.67 %; H, 7.53 %; N, 2.01 %; Other, 12.79 %. Found: C, 77.38 %; H, 7.42 %; N, 1.94 %; Other, 13.26 %. *Awaiting Data*

Compound 84: 4'-((11-((2,3-difluoro-4'-(4-propylcyclohexyl)-[1,1'-biphenyl]-4-yl)oxy)undecyl)oxy)-2'-fluoro-[1,1'-biphenyl]-4-carbonitrile

Prepared according to Scheme 4. 4'-((11-bromoundecyl)oxy)-2'-fluoro-[1,1'-biphenyl]-4-carbonitrile (500 mg, 1.2 mmol), 2,3-difluoro-4'-(4-propylcyclohexyl)-[1,1'-biphenyl]-4-ol (386 mg, 1.2 mmol), potassium carbonate (415 mg, 3 mmol), acetone (50 ml). Recrystallisation from ethanol yielded the target compound as white plates

Yield: 470 mg (0.68 mmol, 57%)

¹H NMR (δ/ppm, 400 MHz, CDCl₃): 7.61 (2H, dt, 1.83, 8.54 Hz, ArH), 7.23 (2H, dd, 1.22, 8.54 Hz, ArH), 7.34 (2H, dd, 1.53, 8.24 Hz, ArH), 7.25 (1H, t, 8.85 Hz, ArH), 7.19 (2H, d, 8.24 Hz, ArH), 6.99 (1H, ddd, 2.44, 8.24, 8.54 Hz, ArH), 6.70 (2H, dd, 2.14, 8.85 Hz, ArH), 6.64 (1H, dd, 2.44, 12.81 Hz, ArH), 3.98 (2H, dd, 6.4 Hz, O-CH₂-CH₂-CH₂-(CH₂)₅), 3.90 (2H, dd, 6.4, 6.7 Hz, O-CH₂-CH₂-CH₂-(CH₂)₅), 2.42 (1H, ddt, 3.05, 11.9, 12.2 Hz, Ar-CH-C₂H₄~), 1.69-1.86 (8H, m, CyHexH), 1.11-1.50 (21H, m, CyHexH, O-CH₂-CH₂-CH₂-(CH₂)₅-CH₂-CH₂-CH₂-O, Cy-CH₂-CH₂-CH₃), 0.93-1.03 (2H, m, Cy-CH₂-CH₂-CH₃), 0.83 (3H, t, 7.32 Hz, Cy-CH₂-CH₂-CH₃).

¹³C NMR (δ/ppm, 100.5 MHz, CDCl₃): 14.31, 19.91, 25.75, 25.83, 28.94, 29.03, 29.20, 29.36, 29.38, 33.39, 34.13, 36.87, 39.59, 44.15, 68.37, 69.61, 102.52 (d, 26.08 Hz), 109.27, 110.36, 111.08 (d, 3.07 Hz), 118.75 (d, 2.30 Hz), 118.87, 122.73 (d, 10.74), 123.32 (dd, 3.84, 4.60 Hz), 126.86, 128.40 (d, 3.07 Hz), 129.05 (d, 3.84 Hz), 130.59 (d, 4.60 Hz), 131.96, 140.34 (d, 1.53 Hz), 141.59 (ddd, 14.58, 15.34, 246.64 Hz), 147.17, 147.44 (d, 5.37 Hz), 148.68 (ddd, 10.74, 11.51, 248.18 Hz)

¹⁹F NMR (δ/ppm, 376.4 MHz, CDCl₃): -114.83 (1F, dd, 10.34, 11.49 Hz), -141.72 (1F, dd, 8.04, 19.53 Hz), -158.68 (1F, dd, 5.75, 19.53 Hz)

IR (ν_{max} cm⁻¹): 655.80, 688.59, 709.80, 723.31, 738.74, 775.38, 785.03, 798.53, 848.68, 854.47, 893.04, 1002.98, 1039.63, 1078.21, 1103.28, 1126.43, 1161.15, 1197.79, 1290.38, 1309.67, 1394.53, 1406.11, 1417.68, 1458.18, 1473.62, 1494.83, 1506.41, 1521.84, 1533.41, 1541.12, 1558.48, 1575.84, 1608.63, 1622.13, 1635.64, 1647.21,

1653.00, 1683.86, 1699.29, 1717.65, 1734.01, 1749.44, 1772.58, 1791.87, 1843.95, 1869.02, 2225.85, 2358.94, 2852.72, 2922.16.

ESI-MS (m/z): 718.3852 ($C_{45}H_{52}F_3NO_2Na$, $[M+Na]^+$)

Elemental Analysis (mass %): Calculated: C, 77.67 %; H, 7.53 %; N, 2.01 %; Other, 12.79 %. Found: C, 76.71 %; H, 7.48 %; N, 2.07 %; Other, 13.74 %.

4.5 Mixture Studies

In order to conclusively confirm that the lower temperature mesophase observed for compounds **53** and **54** is indeed the N_{TB} phase, as well as to investigate the potential of virtual $N-N_{TB}$ phase transitions for the other compounds in section 4.3 that did not display an N_{TB} phase, miscibility studies were carried out using CB9CB. This study allows the full effect of the ether linkage and the terminal functional groups on the N_{TB} phase to be probed.

In addition, it was prudent to study the effects of introducing a chiral dopant to an enantiotropic N_{TB} phase to determine what role, if any, chirality played in the formation of the phase. For this purpose compound **76** was selected owing to its convenient working temperatures (sub 100 °C) and its wide temperature enantiotropic N_{TB} phase.

4.5.1 Mixtures of compounds 44-52 and 55-65 with CB9CB

In section 4.2. it was shown that, the formation of the N_{TB} phase was extremely sensitive to the nature of the end group of the aromatic unit for the heptamethylene linked dimers (**44-52**) but was completely absent when an ether linkage was incorporated into the spacer (**55-65**). The absence of the N_{TB} phase in the ether linked dimers was attributed to the near linearity of the molecules in the all-trans conformer as shown through DFT modelling, this linearity favoured the formation of the nematic phase. The melting points of the compounds were also elevated compared to the alkyl analogues (**42-52**) owing to the linearity facilitating packing into a crystal lattice.

This presented a difficulty in quantifying the effects of the addition of the ether linkage on the stability of the N_{TB} phase. In order to evaluate the potential of the ether linked dimers (**55-65**) to form the N_{TB} phase, and also to confirm the phase assignment of the N_{TB} phase in the alkyl linked dimers (**42-52**) binary phase diagrams were produced through miscibility studies with CB9CB (Figure 70).

All of the materials tested showed good miscibility with CB9CB across a wide range of concentrations. A strong linear relationship was observed between the concentration of CB9CB (wt%) and both the I-N and $N-N_{TB}$ transitions, a representative example of these phase diagrams is shown in Figure 70, with the remaining data available in the appendices to this thesis. This linear relationship was used to predict the virtual $N-N_{TB}$ and, where required, I-N transitions through extrapolating the line through to 0 wt% CB9CB (the neat

dimer). The extrapolated virtual transition temperatures are presented in Table 17 for compounds **42-52** and Table 18 for compounds **55-65**.

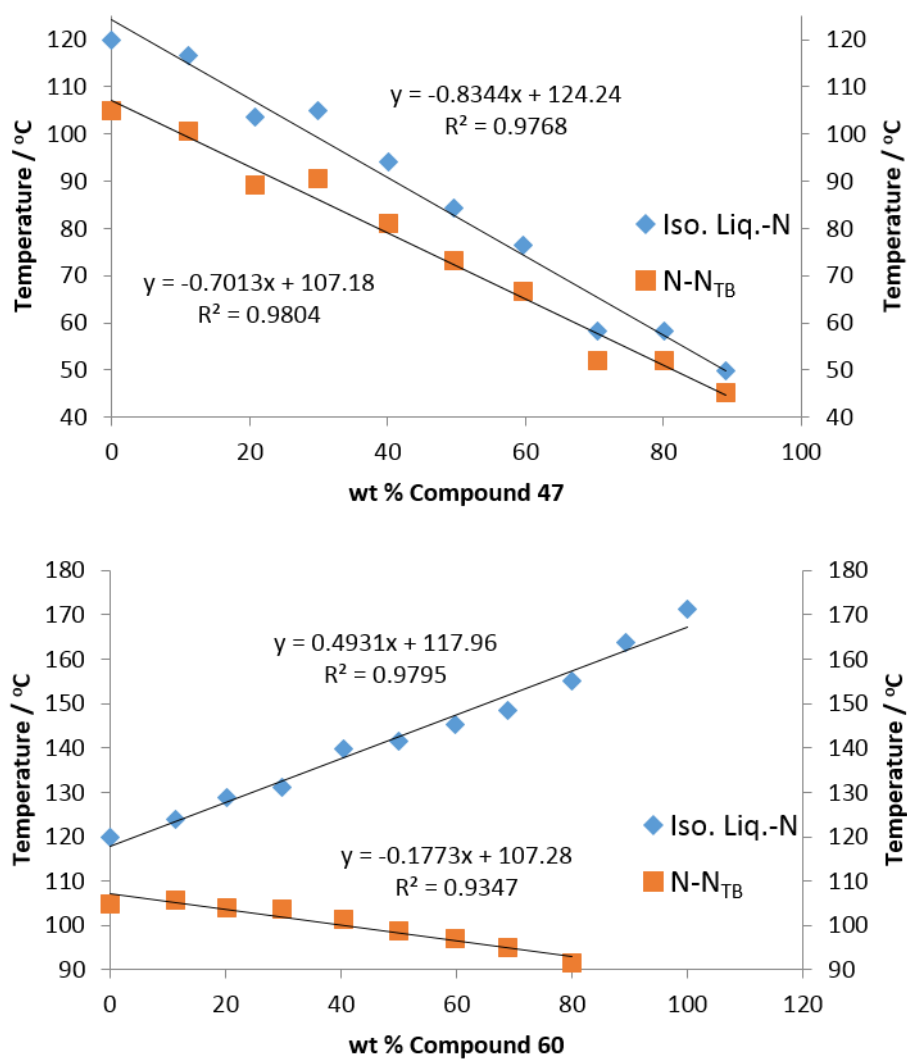
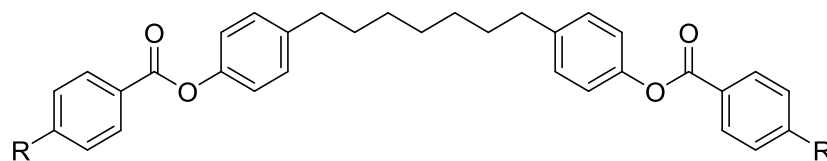
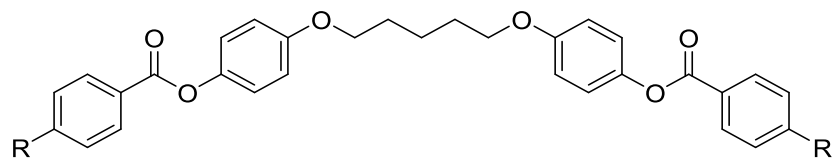


Figure 70: Binary phase diagrams of compounds **47** and **60** mixed with CB9CB.



Compound		Transition Temperatures / °C					
No.	R	Cr	N _{TB}		N		Iso. Liq.
42	CN	•	149.0	(• 120.0	•	139.0)	•
43	NCS	•	105.0	(• 103.3)	•	120.5	•
44	NO ₂	•	113.3	(* 66.1	*	83.1)	•
45	F	•	91.5	(* 34.7	*	56.6)	•
46	CF ₃	•	114.9	(* 49.6	*	56.4)	•
47	C ₂ H ₅	•	71.5	(* 37.1	*	40.1)	•
48	C ₃ H ₇	•	108.0	(• 47.6	•	49.5)	•
49	C ₄ H ₉	•	56.3	(* 34.7	*	37.9)	•
50	OC ₂ H ₅	•	108.3	(• 95.3)	•	108.8	•
51	OC ₃ H ₇	•	89.6	(• 69.1	•	75.5)	•
52	OC ₄ H ₉	•	87.0	(• 79.2	•	85.9)	•

Table 17: Transition Temperatures of compounds **42-52**. Virtual transitions calculated from phase diagrams are presented in italics and denoted with a "*". Monotropic phase transitions are quoted in parenthesis.



Compound		Transition Temperatures / °C					
No.	R	Cr	N _{TB}		N	Iso. Liq.	
55	CN	•	166.6	(* 96.8)	•	189.2	•
56	NCS	•	142.8	(* 87.8)	•	178.8	•
57	NO ₂	•	150.5	(* 88.3)	•	141.2	•
58	F	•	125.1	(* 48.7)	*	85.4	•
59	CF ₃	•	151.4	(* 25.7)	*	49.2	•
60	C ₂ H ₅	•	116.1	(* 49.6)	*	101.8	•
61	C ₃ H ₇	•	127.0	(* 58.6)	*	107.8	•
62	C ₄ H ₉	•	125.4	(* 43.2)	*	89.2	•
63	OC ₂ H ₅	•	139.9	(* 89.6)	•	171.4	•
64	OC ₃ H ₇	•	108.3	(* 72.9)	•	143.1	•
65	OC ₄ H ₉	•	109.0	(* 78.7)	•	142.2	•

Table 18: Transition Temperatures of compounds **55-65**. Virtual transitions calculated from phase diagrams are presented in italics and denoted with a "*". Monotropic phase transitions are quoted in parenthesis.

Using the data presented in Table 17 and Table 18 it is now possible to compare the transitional behaviour of the methylene and ether linked materials in much more detail. In general the addition of the ether moiety to the spacer chain leads to an increase in the clearing point which, once again, supports the argument that the ether linkage reduces the overall bent conformation of the dimer, allowing more efficient packing and interaction of the mesogenic units. However the N-N_{TB} transition temperature was much less sensitive to the spacer and relatively little variation was observed, indicating that despite the need for a bent conformation the relatively more linear ether linked materials still exhibit the potential for supporting the N_{TB} phase.

In both sets of materials the importance of the nature of the terminal group is further emphasised by the calculated virtual transition temperatures. When looking at the extrapolated values for the materials with polar terminal groups the conjugating groups (CN, NCS and NO₂) display much higher N-N_{TB} transition temperatures than the non-conjugating groups (F, CF₃), indicating that interactions between the end groups is a key factor in the formation of the phase, with the NO₂ terminated materials having the lowest N-N_{TB} transitions of the conjugative materials due to the high dipole moment causing repulsion between the mesogenic units to dominate over attractive forces.

The virtual transition temperatures of non-polar terminated materials also follow the same trends as those observed for the neat materials presented in sections 4.2 (47-52) and 4.3 (71-77) with a clearly observable odd-even effect with respect to the N-N_{TB} transition temperature. This corroboration of the virtual transition temperatures with the trends observed in neat materials, along with the high concentrations of the host materials at which the mixtures display the N_{TB} phase shows that the ether linked materials do have the potential to support this mesophase.

However the melting point increase in the ether linked materials prevented sufficient supercooling to be allowed to observe the phase in the neat material. In summary the results show that it was not that the ether linked dimers lacked the necessary molecular bend to form the N_{TB} phase, but that the melting points were so high, due to the linear molecules being able to more effectively pack into a crystal lattice. This is supported by the fact that the majority of the materials that showed an increased N-N_{TB} transition were terminated by flexible, alkyl chains, which serve to help break up the packing into the crystal lattice more so than the inflexible, polar end groups.

Conclusions

This study shows that, despite the relatively lower average molecular bend caused by the introduction of ether moieties into the spacer of these dimers, there was little variation in the N-N_{TB} transition compared to the dimers with an alkyl spacer, and in some cases this transition was found to slightly increase in temperature. This runs counter to the assumption that increased molecular bend would cause the materials to more readily adopt the N_{TB} phase. The most significant barrier to this observation was shown to be the drastic increase in the melting and clearing points caused by the introduction of the ether linkage rather than any suppression of the N-N_{TB} transition. These results do however

serve to confirm that the average molecular bend angle does have an effect on the N_{TB} phase stability, and brings to light the interesting possibility of a “magic angle” at which the stability of the N_{TB} phase would be greatest, leading to possibilities in rational design of N_{TB} materials beyond the current, simplistic “bent” model. Obviously although the results presented are interesting it must be noted that they are obtained from mixed systems, in order to definitively confirm these findings it would be ideal to demonstrate similar properties for pure N_{TB} materials.

4.5.2. Mixture studies of compound **76** with a high HTP dopant

Despite several studies indicating that the N_{TB} phase exhibits a degree of local chirality^{70,72,80} there has been relatively little work into the effects of mixing chiral dopants into N_{TB} materials. Compound **76** (Figure 71), exhibits an enantiotropic N_{TB} phase and represented an ideal candidate to mix with a chiral dopant (**CD-1**) shown in Figure 72. This dopant was selected for its structural similarity to compound **76**, both compounds being apolar phenyl benzoate esters.

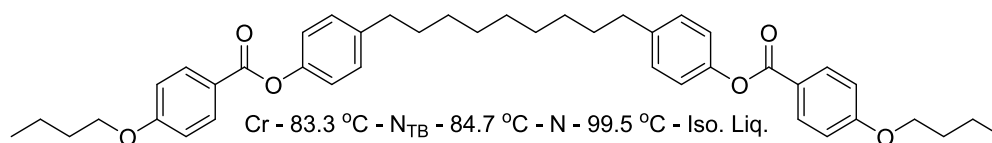


Figure 71: Structure and transition temperatures of compound **76**.

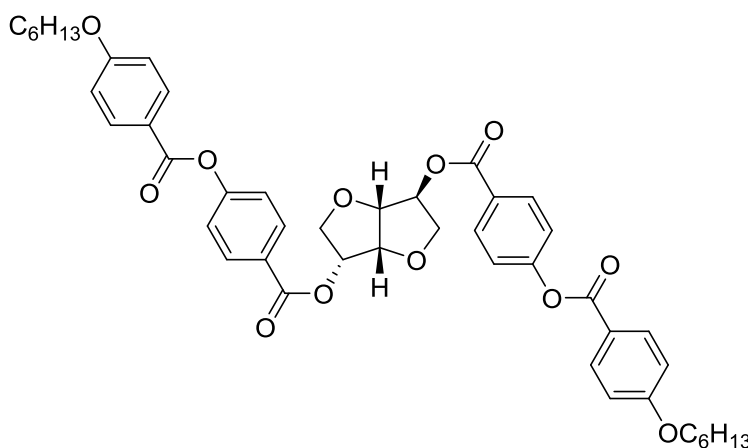


Figure 72: Molecular structure of chiral dopant **CD-1**.

A series of mixtures of increasing concentrations, ranging from 1-10 wt%, of **CD-1** in compound **76** were prepared (Table 19). These mixtures were analysed using POM, DSC and variable temperature XRD studies. Compound **76** and **CD-1** were found to be highly miscible across the range of concentrations used. The mesomorphic properties of the mixtures are summarised in a partial binary phase diagram in Figure 73, the tabulated data is available in an appendix to this thesis.

Mixture Number	Wt % CD-1 in Compound 76
M1	0.9
M2	2.1
M3	4.7
M4	5.2
M5	5.4
M6	5.5
M7	6.5
M8	7.1
M9	8.4
M10	9.8

Table 19: Composition and designation of mixtures of **compound 76** and **CD-1**.

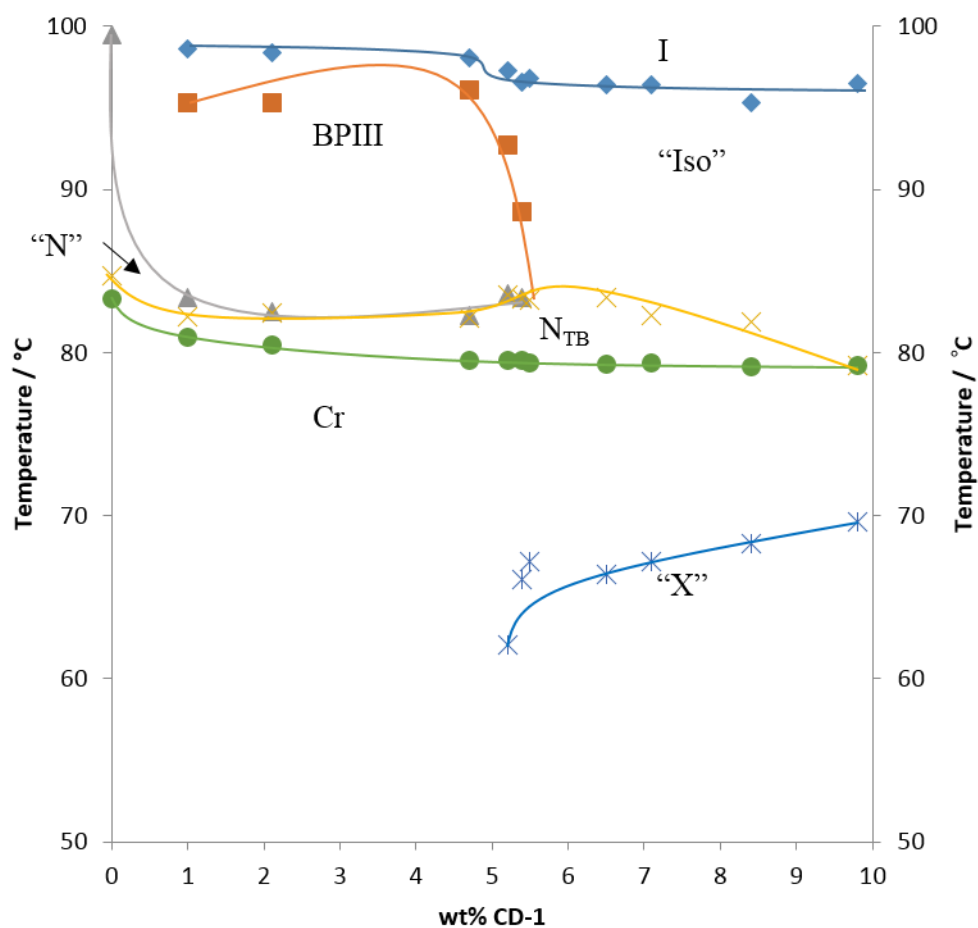


Figure 73: Partial phase diagram for binary mixtures of **compound 76** and **CD-1**.

At just 1 wt % of **CD-1** the nematic phase was suppressed from 99.5 °C in the pure compound to 83.4 °C, which represents a reduction in the temperature range of the nematic phase of approximately 15 °C in the neat material, to approximately 1 °C at 1 wt% of **CD-1**. The clearing point however did not fall and a wide temperature range blue phase, the optical texture of which is consistent with BPIII (Figure 74), was observed. Upon increasing the dopant concentration the blue phase temperature range remained almost unchanged, and was only observed to become suppressed at approximately 5-5.5 wt% of **CD-1**. Interestingly this also coincided with the observed elimination of the nematic phase. The formation of a blue phase in this case is consistent with published results showing that chiral bent materials, or bent core systems with induced chirality from a chiral dopant, show a tendency to form blue phases^{68,89}.

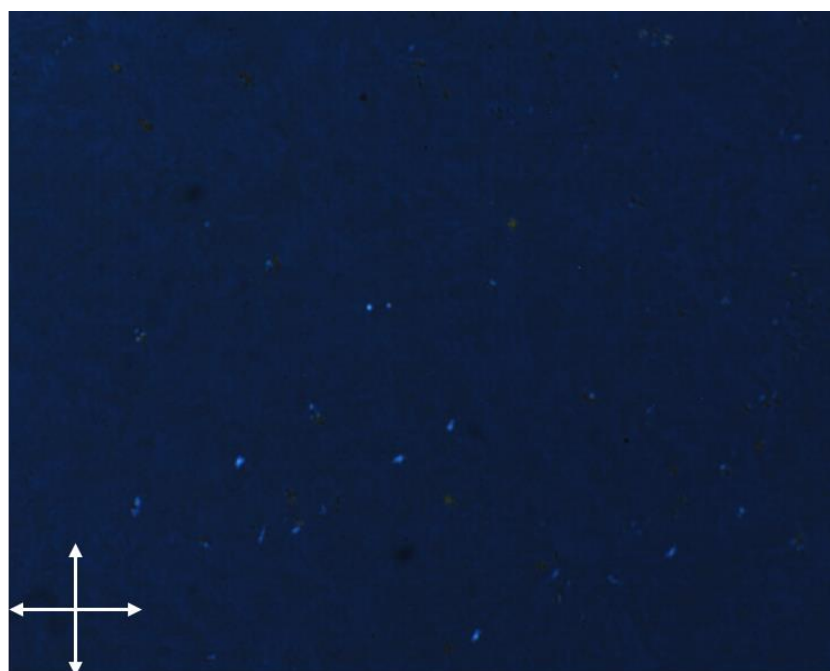


Figure 74: Photomicrograph of the BPIII texture of **M3** at 93 °C. Sample cooled at 0.1 °C min⁻¹. (x100)

Remarkably the thermal stability of the N_{TB} phase remained almost constant across the phase diagram. As a consequence this resulted in a direct transition from the isotropic liquid to the N_{TB} phase being observed from **M6** onwards. These mixtures represented the first time that the N_{TB} phase could be observed in its natural form rather than as a paramorphic texture formed from the nematic phase. Unlike the transition from the nematic phase which usually involves a straight transition front, N_{TB} phase nucleated in

the form of circular focal conic domains that developed radially from a central defect site (Figure 75). The overall texture, once fully developed maintained a strong similarity in terms of defects to the paramorphotic texture grown from the nematic.

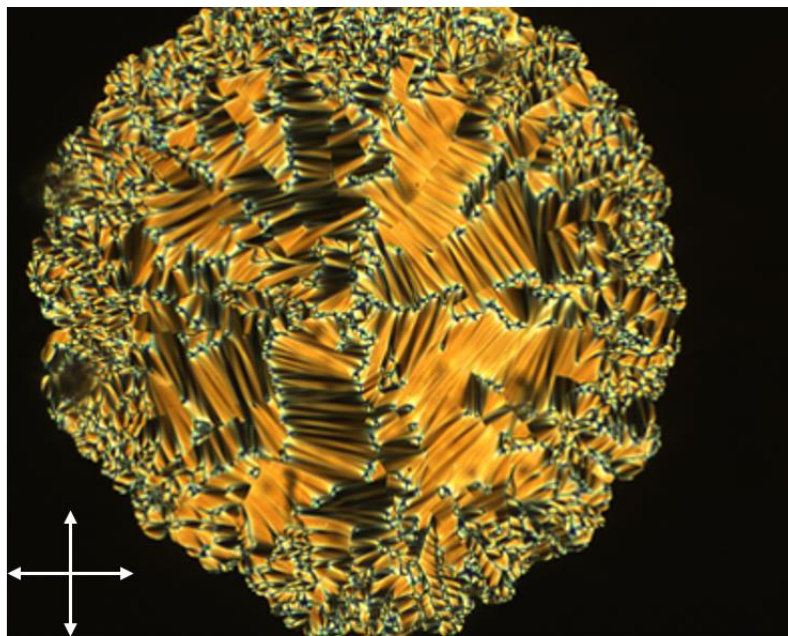


Figure 75: Photomicrograph of the Iso. Liq.- N_{TB} transition of **M10** at 80.3 °C. Sample was cooled at 0.1 °C min⁻¹.

An interesting phenomenon was observed during the slow cooling experiments for mixtures **M6-M10** whereby upon annealing the mixture 0.2-0.5 °C above the I- N_{TB} transition temperature for several hours a weakly birefringent texture was observed across the entire sample, see Figure 76. This texture appeared as large grey-blue, plate-like regions, which tended to nucleate individually and then coalesce into a mosaic texture. Despite appearing similar to BPII this phase exhibited no chiral response upon the rotation of the polarisers, the plate like texture is also similar to the natural texture of the smectic F phase, possibly indicating some degree of short-range hexagonal order. When further cooled, the transition from this phase to the N_{TB} occurred at the same temperature as the Iso. Liq.- N_{TB} transition under a normal cooling regime. It is interesting to note that this new phase was not observed with dynamic cooling which implies that the formation of this phase is kinetically, rather than thermodynamically controlled. When the platelet texture was subjected to mechanical shearing, the sample immediately reverted to the optically extinct texture of the isotropic liquid, requiring several hours of annealing to return to the mosaic texture.

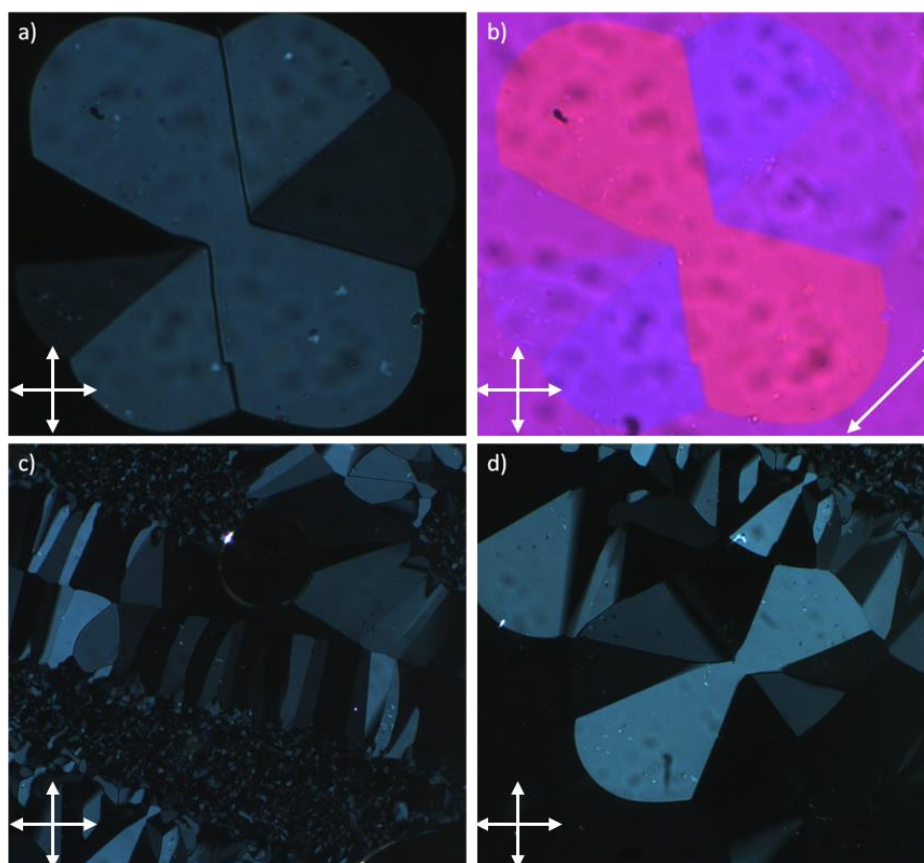


Figure 76: Photomicrographs of the platelet phase observed upon annealing **M10** at 80.6 °C. Photomicrograph (b) was taken with a quarter waveplate installed on the microscope. (x100)

DSC analysis of these mixtures (Figure 77) revealed an additional thermal event that did not coincide with any observations by POM. This transition was attributed to a liquid to liquid transition, and became broader with increasing **CD-1** concentration. This type of phenomenon is not unknown, and is sometimes observed for frustrated systems that exhibit TGB phases (analogies have been drawn to tangled and disentangled flux phases of type 2 superconductors⁹⁰). This result may imply that there are some possible similarities between the N_{TB} phase and these frustrated mesophases, or indeed in the mechanisms involved in assembling the phase from the isotropic liquid. Interestingly, the DSC traces for **M1-M5** show no peak corresponding to the BPIII observed via POM, which should occur between the liquid to liquid transition and the transition to the chiral nematic phase. While this is an unusual result it is not unheard of, previously published work has shown that, in the cases of chiral materials with low purity, which by definition

these mixtures are, that the DSC peak observed for the blue phase can broaden to the point of being difficult to observe⁹¹.

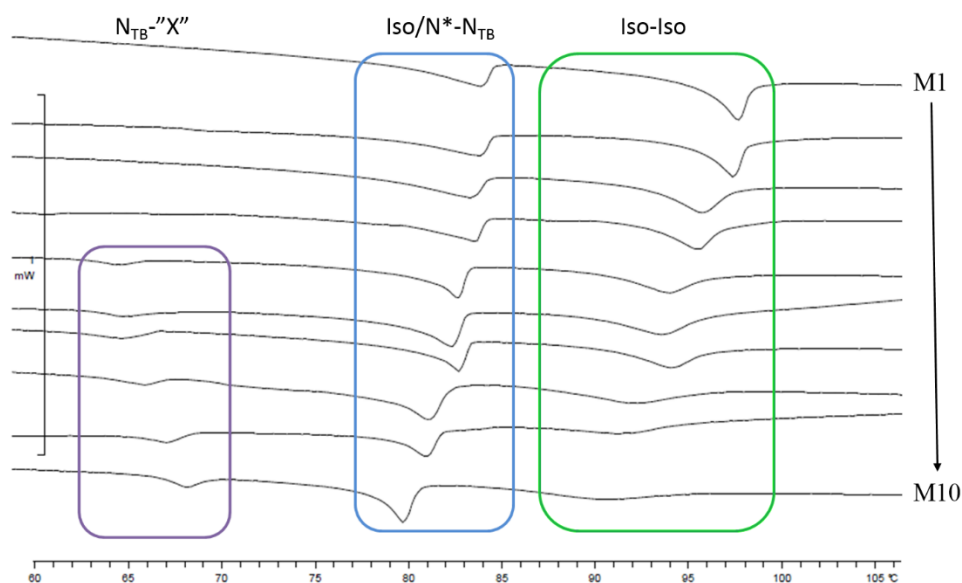


Figure 77: DSC traces (heat flow / mW vs. temperature / °C) on cooling for the mixtures of compound **76** and **CD-1**.

DSC analysis also revealed a second thermal event below the N_{TB} phase, well within the supercooling region of the crystal. In order to observe this phase (denoted as “X”) via POM rapid cooling was necessary, a sweeping transition front was observed correlating to the phase transition detected by DSC. The resulting paramorphic texture was similar to that of the N_{TB} phase, except there was a shift in the birefringence of the sample (Figure 78). Without observing the transition front the change was difficult to discern, a situation similar to the transition from the smectic A to hexatic B phase.

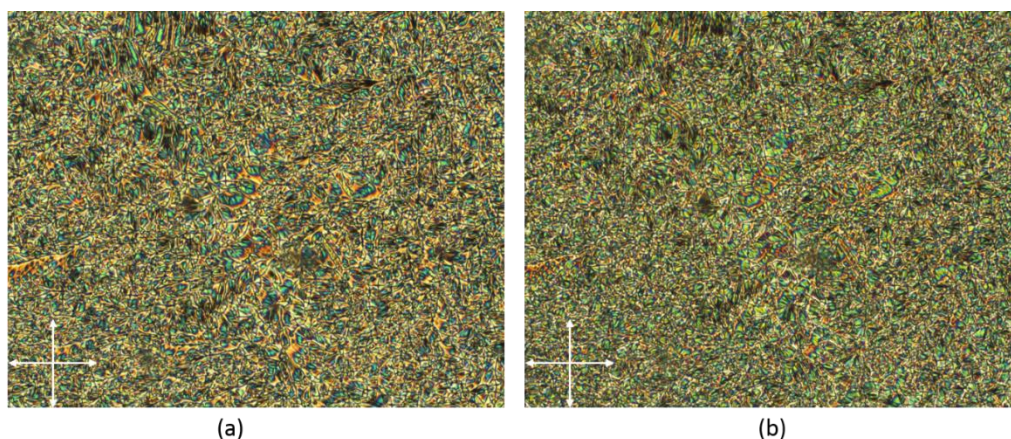


Figure 78: Photomicrograph of **M10** in the N_{TB} phase at 70.2 °C (a) and the "X" phase at 63.3 °C. Pictures obtained under rapid cooling (in excess of 10 °C min⁻¹). (x100)

Variable temperature DSC experiments were used to further investigate the thermodynamic versus kinetic nature of the phase transitions observed for mixture **M10** (Figure 79). The I- N_{TB} phase transition, as well as the N_{TB} -“X” phase transition were shown to occur at consistent temperature, although the signals for both peaks did become less intense, and sharper with decreasing cooling rate. This indicates that these phase transitions occur thermodynamically, which is consistent with traditional nematic and smectic behaviour. The Liq.-Liq. transition did not behave in a similar manner. Indeed the phase transition became broader with the decrease in cooling rate and the peak temperature drifted lower, indicating a kinetic element to this phase transition. One possible explanation for this unusual behaviour could be the formation of molecular aggregates within the liquid phase that do not interact over longer distances and hence do not exhibit the necessary order to form a definitive mesophase.

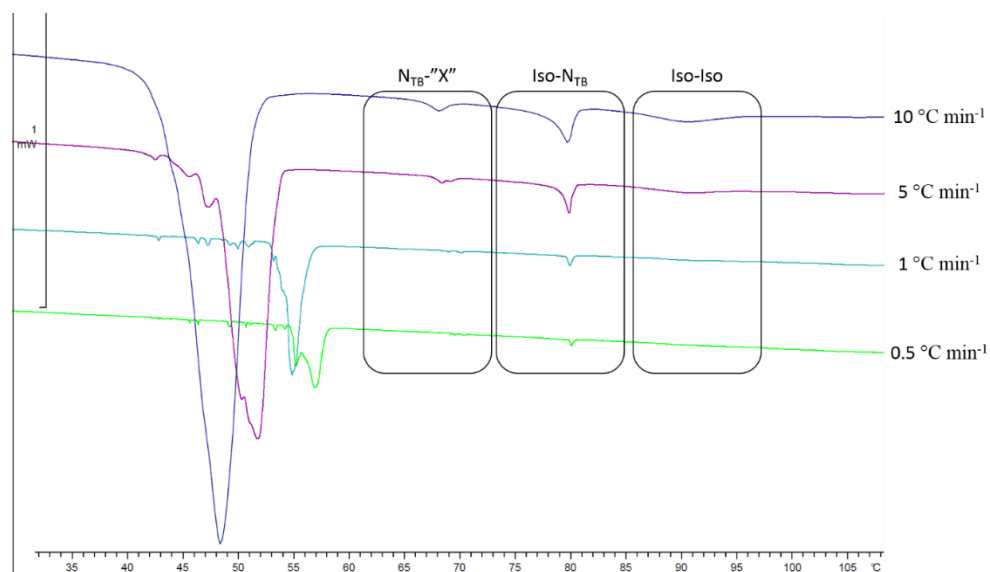


Figure 79: DSC traces (heat flow / mW vs. temperature / °C) on cooling for **M10** at variable cooling rates.

In order to further investigate the second isotropic phase, as well as the low temperature “X” phase, small angle X-Ray scattering studies were used to investigate mixture **M10**. This mixture was selected because as it exhibited the widest temperature range secondary isotropic phase as well as the highest N_{TB} -“X” transition temperature. The data obtained is summarised in Figure 80.

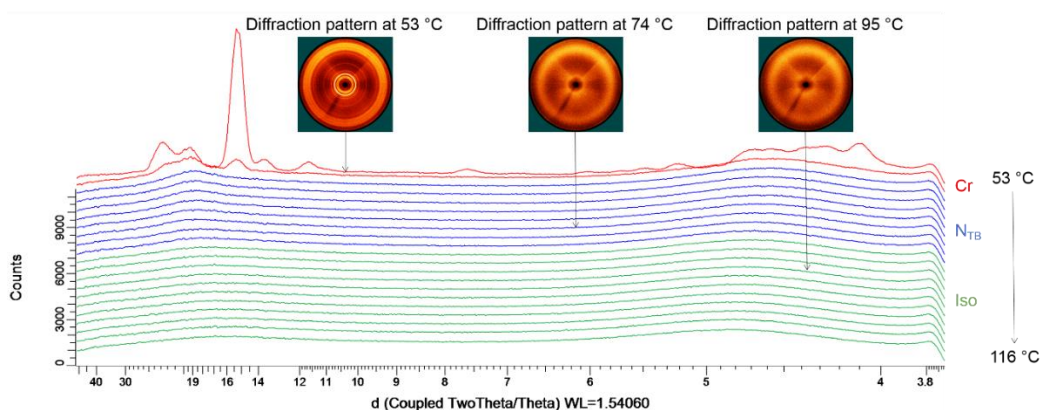


Figure 80: Two dimensional X-ray scattering patterns and a plot of d-spacing as a function of temperature for **M10**. Measurements takes every 3 °C from 116 to 54 °C.

The XRD experiments revealed that there was no discernible difference in the isotropic liquid and the optically extinct “Iso.” Phase. Both phases give rise to a broad, diffuse

diffraction in the small and wide angle regions. This eliminated the possibility that the optically extinct phase could be a cubic phase. Despite the low cooling rate no discernible peak was seen for the formation of the phase resembling BPII. At 71 °C a diffraction pattern typical of an unaligned N_{TB} phase was observed whereby a diffraction peak with higher intensity occurred in the small angle region and a diffuse peak in the wide angle region indicative of a liquid like ordering of chains was observed. When further cooled into the “X” phase there is very little discernible difference in the scattering pattern (Figure 81).

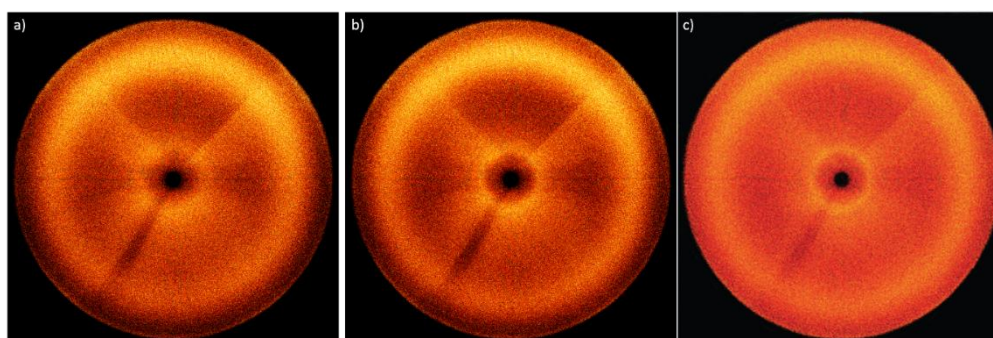


Figure 81: 2D XRD pattern for **M10** in a) the Iso. Liq. (95 °C), b) the N_{TB} phase (72 °C) and the "X" phase (62 °C).

Fitting the diffraction data from the small angle region using a 6-term Gaussian form reveals a subtle difference between the N_{TB} and the “X” phase, see Figure 82. Upon transition into the “X” phase the diffraction peak becomes slightly sharper and more intense than the peak in the N_{TB} phase. The weak intensity of the peak indicates the absence of lamellar ordering. The “X” phase must exhibit a similar level of order to the nematic and N_{TB} phases. A possible explanation for this is that the “X” phase is, in fact, just another deformation of the nematic phase similar to the N_{TB} phase, such as the splay-bend phase.

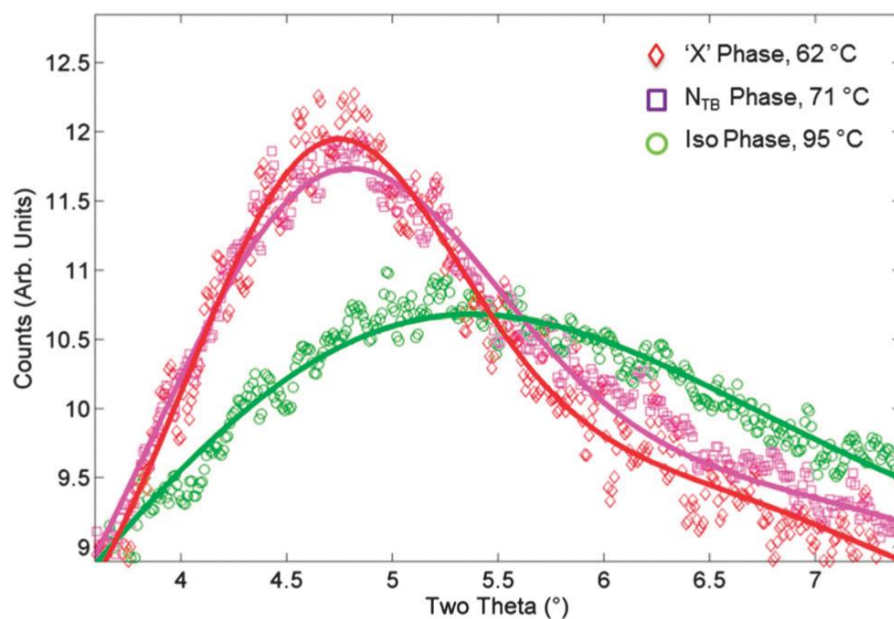


Figure 82: Enhanced plot of counts (arb. units) vs two theta (°) for **M10** in the isotropic, N_{TB} and "X" phases. The curves were fitted using a 6-term Gaussian distribution.

Resonant Soft X-ray Scattering (RSOXS) studies were carried out on both the neat compound **76** and on mixture **M10** in order to further probe the effect of the chiral dopant. In the neat material, upon heating the sample two sets of periodicities were observed, 8.6 nm in the crystal phase and 11.6-13.1 nm in the N_{TB} phase. These two values were separated by a clear discontinuous transition. Conversely, while a similar range of values were observed on cooling (≈ 12 -8.6 nm) there was a lack of a distinct transition between the two (Figure 83).

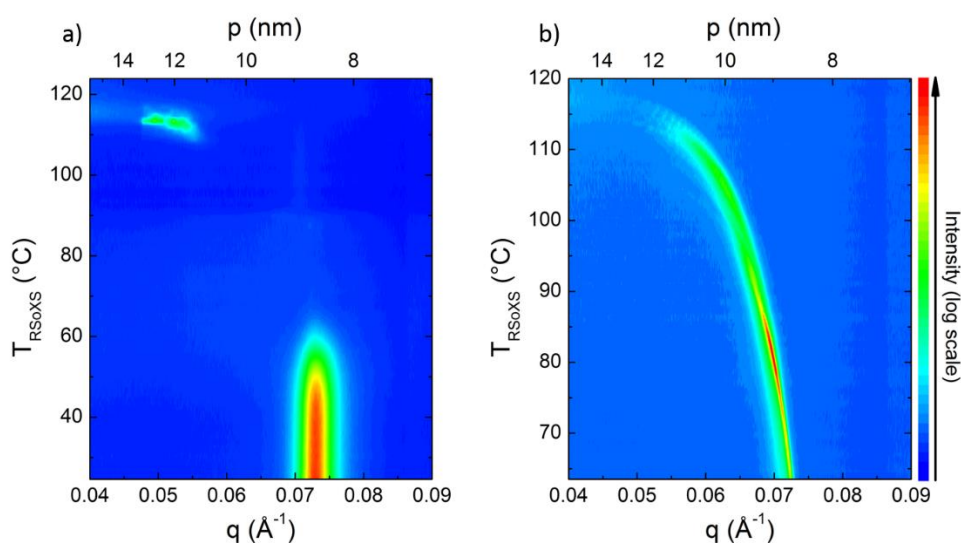


Figure 83: RSOXS plots for compound **76** on a) heating and b) cooling.

For **M10** the pattern observed upon cooling (Figure 84) was broadly similar, however the pitch of the N_{TB} phase at maximum temperature increases to ≈ 16 nm as opposed to 13 nm in the neat sample, decreasing to 9.4 nm with decreasing temperature. At 68 °C i.e. when the material enters the lower temperature “X” phase, a second peak appears at 8.8 nm, unlike the signal for the N_{TB} phase this peak is invariant with respect to temperature. This shows that there are two different periodicities in the “X” phase.

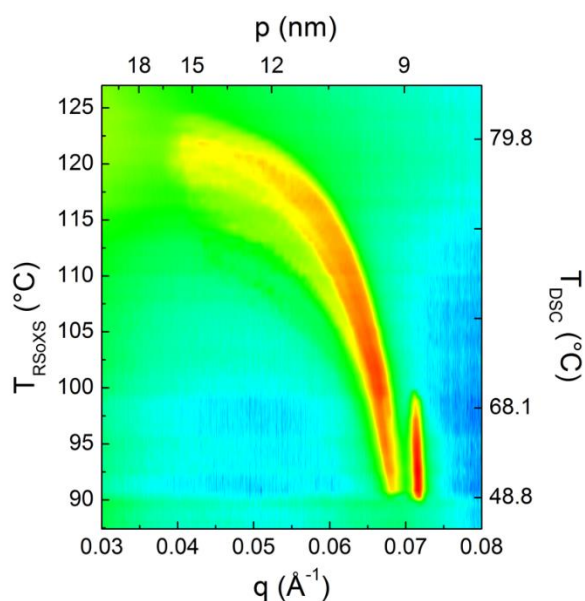


Figure 84: RSOXS plot of **M10** on cooling.

The effects of an electric field on the behaviour of compound **76** and its mixtures were also investigated. For the nematic phase of the neat compound a Fréedericksz transition was observed when the applied electrical field was both low frequency and low voltage (<1 Hz and <2 V μm^{-1}). Upon transition into the N_{TB} phase a texture consisting of a series of planar angled domains was observed with regions of light and dark attributed to domains of opposite twist in the N_{TB} helix. At low voltages the phase showed no response to the applied electric field, however when a low frequency, high voltage (<1 Hz and ≈ 20 V μm^{-1}) electrical field was applied these domains were observed to interconvert (Figure 85). These domains could also be interconverted by rotation of the sample by 3° .

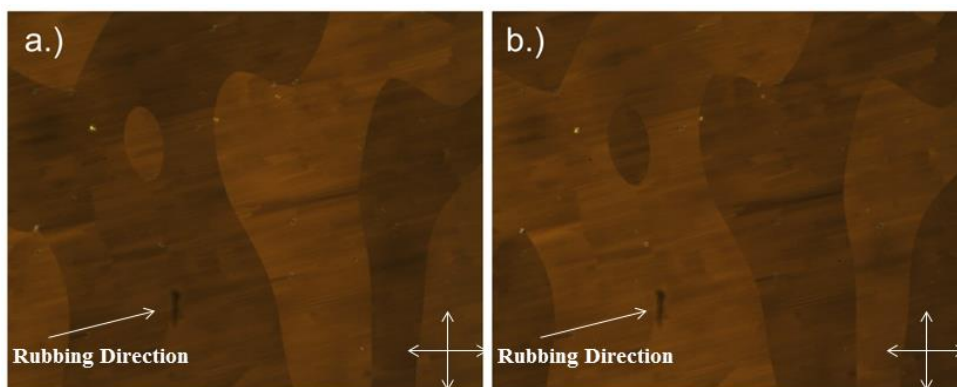


Figure 85: N_{TB} phase of compound **76** in a 5 μm cell with antiparallel buffed polyimide alignment layer. Sample subjected to an electric field (1Hz, 20 $\text{V } \mu\text{m}^{-1}$, square waveform) at 81 $^{\circ}\text{C}$. Sample cooled at 0.1 $^{\circ}\text{C } \text{min}^{-1}$ (x100)

M10 was annealed at 81-82 $^{\circ}\text{C}$ in a 5 μm antiparallel buffed polyimide cell in order to develop the platelet texture. The phase formed large domains which appeared to alternate between light and dark. Under an applied low frequency, medium voltage (<1 Hz and <12 $\text{V } \mu\text{m}^{-1}$) electric field the large domains were observed to interconvert with a switching angle of 10° which was significantly larger than the 3° switching angle of the N_{TB} phase (Figure 86).

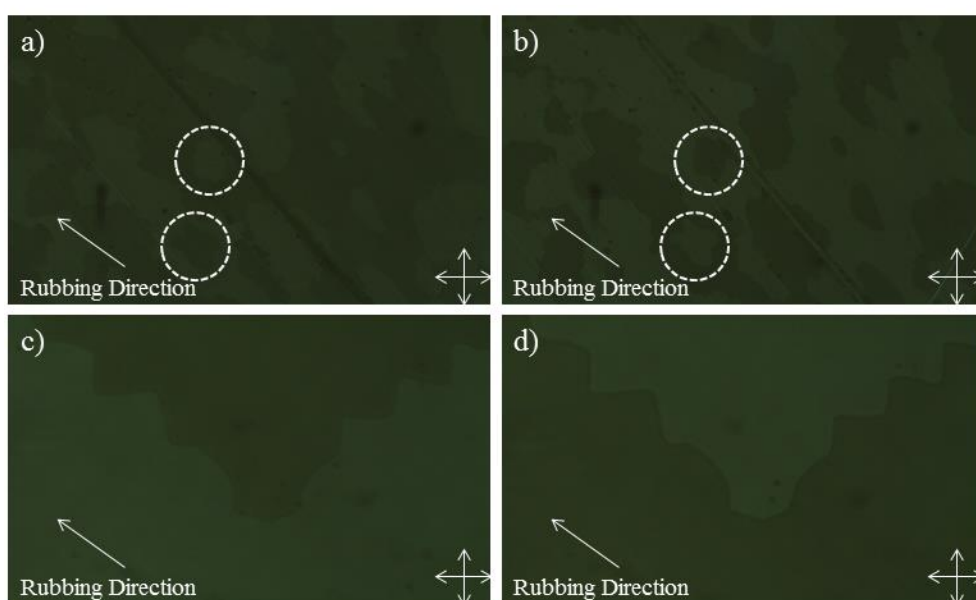


Figure 86: The "platelet" phase of **M10** under applied electrical field (1 Hz, 12 $\text{V } \mu\text{m}^{-1}$, square waveform) at 81 $^{\circ}\text{C}$ (a and b) and 81.5 $^{\circ}\text{C}$ (c and d).

Upon increasing voltage the switching behaviour was found to remain consistent up to and including voltages of $20 \text{ V } \mu\text{m}^{-1}$, however, even at medium voltages, increasing the frequency of the electric field above 33 Hz was observed to cause a transition to an optically isotropic phase. When the electrical field was removed the platelet phase was found to reform (Figure 87)

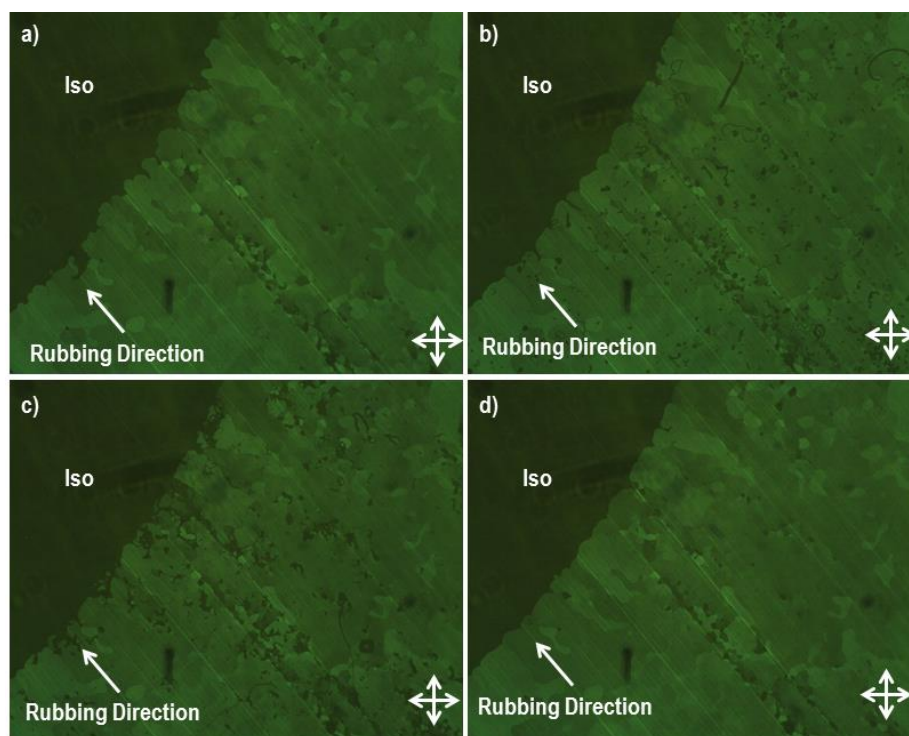


Figure 87: Domains observed upon annealing **M10** at $81.5 \text{ }^\circ\text{C}$ under (a) no field, (b) immediately after application of a 33 Hz, $12 \text{ V } \mu\text{m}^{-1}$ square waveform field, (c) immediately upon removal of the field and (d) 5 minutes after the field was removed. (x100)

The opposing domains shown in Figure 85 were absent in **M10**, upon cooling into the N_{TB} phase a texture comprised of blocky domains of dark striations separated by sharp, bright, angular lines (Figure 88). The absence of interconverting domains in this sample indicates that the introduction of a chiral dopant has eliminated one of the twist domains present in the neat N_{TB} material.

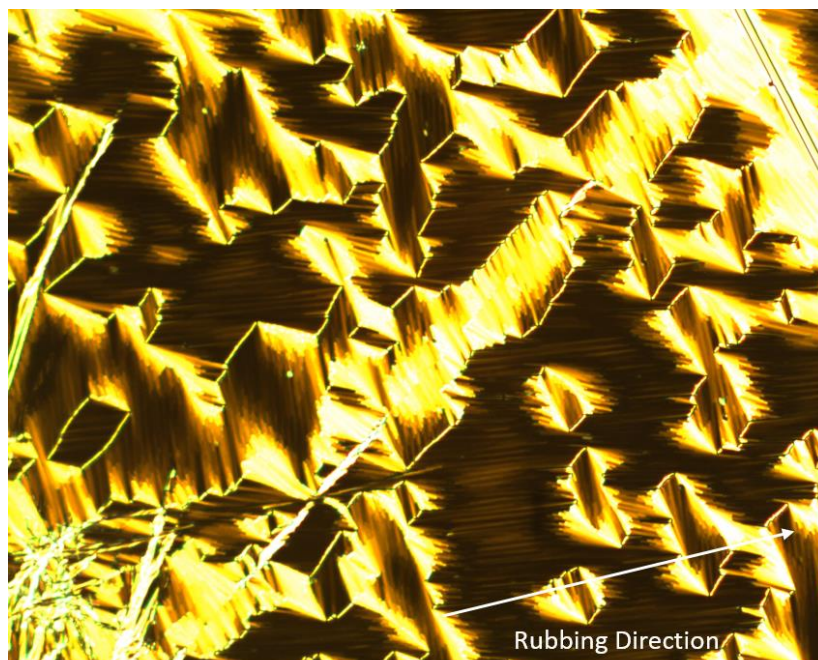


Figure 88: NTB phase of **M10** in a 5 μm cell with antiparallel buffed polyimide alignment layer at 79.5 $^{\circ}\text{C}$. (x100)

Conclusions

Compound **76** only exhibits enantiotropic N and N_{TB} phases. However, upon mixing compound **76** with the chiral dopant **CD-1**, novel mesophase behaviour was observed. Namely an isotropic liquid-isotropic phase transition akin to those found in frustrated systems such as TGB materials was observed in all mixtures up to 10 wt% **CD-1**. This may suggest a degree of similarity between the N_{TB} phase and the TGB phase, it is possible that these similarities only arise in the doped system due to the elimination of one of the twist domains with the introduction of a chiral dopant.

The emergence of an $I-N_{\text{TB}}$ transition at higher concentrations shows that a preceding nematic phase is not essential for the formation of the N_{TB} phase. The mixtures of **76** with **CD-1** allowed the natural texture of the N_{TB} phase as opposed to the paramorphic texture resulting from an $N-N_{\text{TB}}$ phase transition to be observed for the first time.

In mixtures containing higher concentrations of **CD-1** (5.5-10 wt%) annealing the mixture above the $\text{Iso}-N_{\text{TB}}$ transition temperature revealed a weakly birefringent phase consisting of plate like domains referred to as the “platelet” phase. The domains were found to be chirally unresponsive i.e. they did not display optical activity upon rotation of the polarisers. The phase did however, respond to an applied electric field; upon the

application of a low to moderate frequency electrical field (< 33 Hz) of any voltage ($1-20$ V μm^{-1}), alternating domains with a switching angle of 10° were observed. On application of higher frequency electric fields the phase transition shifted to a lower temperature and the mixture reverted to the optically extinct isotropic liquid phase. This behaviour was reversible with removal of the electric field followed by a short annealing period. XRD analysis ruled out both smectic and cubic phases but it is possible that the platelet phase is a form of modified blue-phase, in the same way that the N_{TB} phase itself is a modification of the generic nematic phase. DSC measurements taken of these mixtures show that the I-“Iso” phase transition occurs with an element of kinetic control. There is a possibility that the platelet phase and the second isotropic phase are related.

The “X” phase exhibited by **M6-M10** has thus far eluded definitive classification. Optically the phase is almost identical to the preceding N_{TB} phase, but a transition was observed by both POM and DSC analysis. The main problems with characterising this mesophase it is monotropic, occurring well into the supercooling range of the crystal. Although the optical texture and XRD data imply that this phase could be another modification of the nematic phase, such as the splay bend nematic, materials exhibiting this phase at more workable temperatures are necessary to fully characterise it.

Chapter 5: Conclusions

5. Conclusions.

One of the primary objectives of this research was to attempt to draw sets of structure property correlations between the mesomorphic behaviour of these materials and their gross molecular topology, to this end two broad families of materials were investigated. Bimesogens were investigated with respect to both the effect of the terminal group as well as the linking chain, and a series of so called “pseudo bent-core” materials were synthesised, in which the central unit was not as rigidly locked in a bent conformation as in normal bent-core liquid crystals.

For the pseudo bent-core materials the mesogenic behaviour was found to be primarily dependent on the angle between the two mesogenic units. This angle was found to be heavily controlled by the central group of the bisphenol core, ranging from a highly linear carbonyl linker to a highly bent 1,1-disubstituted cyclohexane. While the sterics of the core units were found to influence the liquid crystal properties somewhat, in that those materials with sterically bulky (SO_2 , $\text{C}(\text{CH}_2)_2$, $\text{C}(\text{C}_5\text{H}_{10})$) central groups exhibited no mesomorphic behaviour, in those materials that did exhibit liquid crystal phases a direct correlation could be drawn between the angle of the central core and the mesogenic properties. For those compounds linked by a carbonyl unit, which imparted the widest intermesogen angle (128°) of those studied, the phase behaviour was observed to be entirely nematic, consistent with rod-like materials. Upon moving to a methylene linker, which imparted a bend angle of 116.8° the phase behaviour underwent a drastic change. Instead of the nematic behaviour seen for the carbonyl linker the materials were found to exhibit a mesophase with a defect texture reminiscent of a smectic A phase, XRD observations confirmed this phase to be more ordered than a nematic, however the presence of two correlation lengths precluded its assignment as a smectic A. Rather, this phase was speculated to be some form of bilayer smectic phase, where the two correlation lengths correspond to the two layer spacings, or possibly a twisted smectic phase somewhat analogous to the N_{TB} phase observed in liquid crystal dimers, where the correlation lengths correspond to periodic distribution of molecular mass along the helical axis. This lamellar phase was also exhibited by the materials with a thioether central unit, the bend angle of which is the smallest of the mesogenic compounds at 105.7° . The phase behaviour of the thioether linked materials was predominantly monotropic, with the transition temperatures being significantly higher than those observed for the methylene core. This lends support to the assignment of the lamellar “X” phase as a twist-bend

deformation of the SmA phase, as the increase in the bend could serve as a stabilising factor for the formation of this structure.

One of the primary reasons for the synthesis and investigation of these materials was the search for new materials that exhibited the Dark Conglomerate phase, this was successful in that compounds **35** and **36** were both found to exhibit a phase which appeared optically extinct under normal light levels, but upon increasing the level of light was found to show a texture consisting of blue-grey blocky domains, consistent with previously published Dark Conglomerate materials. Of particular interest in terms of this phase is the observed XRD pattern; for both **35** and **36** upon transition from the preceding lamellar “X” phase or isotropic liquid an intense, sharp peak was observed in the diffraction pattern. For compound **35** this peak was several times larger than those observed for the “X” phase, with the peak observed for compound **36** showing a similar level of intensity. This implies that the phase is in possession of a large degree of molecular ordering comparable to that of a crystal lattice, yet the lack of any discernible peaks in the wide angle region indicates that this order is limited to the direction of the layer normal, with the layers themselves being disorganised. This degree of ordering was shown by compound **36**, which under ambient conditions was found to take in excess of one month to crystallise from the DC phase while on an untreated glass slide. When crystallisation was forced via low temperature DSC the peak was found to be unusually weak, implying that there is only a small change in the ordering between the DC phase and the crystalline solid.

For the bimesogens it was found that the terminal group had a significant effect on the mesomorphic properties of the material. It was found that conjugating terminal groups, such as nitrile, isothiocyanate and nitro serve to stabilise the phase behaviour, while non-conjugating groups such as fluoro and trifluoromethyl serve to destabilise it. This can be attributed to the propensity for the conjugating materials to align with the polar groups antiparallel to one another, owing to the alignment of the induced dipoles, this allows for the molecules to arrange into both the nematic and N_{TB} phases. Conversely for the compounds terminated by non-conjugating groups the dominating intermolecular force is the repulsion between the more negative terminal groups disrupting the molecular packing.

The compounds terminated by a nitro group provide an interesting insight into this effect as, while the nitro group is conjugating, the heptamethylene spaced nitro dimer exhibited

no mesomorphic properties. This exemplifies the effect discussed above as, while the nitro group is indeed a conjugating group, it also has a very strong dipole moment compared to the other polar terminal groups, thus the intermolecular repulsion dominates the quadrupolar attraction, destabilising the phase. In the nonamethylene spaced material however the nitro compound exhibited a monotropic nematic phase. This serves to demonstrate the effect of the spacer unit on phase behaviour, which will be discussed later.

When the polar, terminal group was replaced by an apolar aliphatic group the electronic effects of the chain are no longer the primary influence on the phase behaviour, instead the steric and conformational behaviour will dominate. In general for the apolar terminal groups there was a decrease in the observed melting and clearing points when compared to the polar terminated materials. This effect can be attributed to the flexibility of the aliphatic groups disrupting the molecules packing into a crystal lattice. This is supported by the general decrease in the melting point with increasing chain length. The alkyloxy chains showed a more stabilising effect on the N_{TB} phase than the alkyl chains, with all 3 of the alkyloxy terminated materials exhibiting the phase as opposed to only the propyl terminated alkyl material.

The second part of the investigation into bimesogens concerned the effects of the length and nature of the spacer unit on the mesogenic behaviour of the materials. To this end materials with a spacer length of 9, as well as materials with a spacer length of 7 but with the terminal methylene units replaced with oxygen atoms were synthesised. The ether-linked materials were found to exhibit only nematic phases and have vastly higher melting and clearing points. This is attributed to the more linear average shape of the molecule imparted by the ether links allowing the molecules to pack more effectively into the nematic and crystal phases. None of these ether linked materials exhibited the N_{TB} phase, a property that was again attributed to the more linear molecular geometry, as a bent structure is a necessity for the N_{TB} phase to form.

When two more methylene units were added to the spacer the general trends for the polar terminated materials were the same as those observed for the heptamethylene spacer, with the conjugating polar terminal groups promoting mesophase formation and the non-conjugating groups inhibiting it. The nitro terminated material in this series exhibited a monotropic nematic phase, this was attributed to the lowered melting point caused by the

lengthened spacer chain. This means there is less supercooling of the crystal required to cause the Iso.Liq.-N transition. For the non-polar terminated materials the trends again were similar to the heptamethylene spaced analogues, with the alkyloxy terminated compounds exhibiting more stable mesophases, in the nonamethylene spaced materials however all of the non-polar terminated compounds were liquid crystalline. This not only indicates that the lengthened methylene spacer serves to stabilise the mesophases but also allows for the trends in the relationship between the terminal chains and the phase behaviour to be investigated. A noticeable odd-even effect in terms of the transition temperatures with respect to the parity of the terminal chains. This is likely caused by the tendency of even spaced terminal chains to adopt more linear conformations, while those of odd parity are slightly more bent; this slight effect on the gross molecular topology causes the phases to be more stabilised in the materials with odd terminal chains.

The final family of bimesogens were synthesised to test whether increasing the length of the spacer of ether linked bimesogens would reduce the melting points to the degree where an N_{TB} phase would be exhibited. It had been shown by past research that breaking the symmetry in a bimesogen can stabilise the N_{TB} phase compared to symmetrical analogues, therefore a series of unsymmetrical bimesogens with an undecamethylenedioxy spacer were prepared, based on the molecular architecture of CBO11OCB. Of these compounds all were found, as expected, to exhibit nematic phases, of interest however were two which exhibited a monotropic N- N_{TB} phase transition. While both of these transitions occurred too far into the supercooling range of the crystal to allow for in depth analysis, the fact that these transitions occurred at all showed that the ether linked materials do have the potential to support the N_{TB} phase. The tendency toward significantly higher melting and clearing points in these materials can be attributed to the increase in flexibility allowing the molecule to pack and fold in such a way as to more effectively adopt crystal and nematic phases. The assumption of the all-*trans* conformer used in previous chapters for calculating intermesogen angles breaks down at longer spacer lengths. This is because the aromatic rings apply a degree of conformational lock to the units directly attached to them, with the degree of locking persisting over multiple spacer units. Due to this the shorter chains are less conformationally free, while in the longer spacers the central units of the chain have a much greater degree of rotational freedom, allowing the material to adopt more varied conformers and pack more effectively into phases. This is not unlike the effect observed in side chain liquid-crystal

polymers, in which at short spacer lengths the mesogenic behaviour is more tied to the properties of the polymer backbone, while at long spacers the properties of the mesogenic units and the polymer backbone decouple from one another.^{92,93}

Spurred on by the results obtained for the unsymmetrical bimesogens a series of mixture studies were carried out in order to determine the virtual N-N_{TB} transition temperatures of the pentamethylenedioxy linked compounds, as well as of the heptamethylene spaced compounds which did not exhibit the phase in their neat state. This was done by mixing these compounds with known N_{TB} material CB9CB. All of the compounds tested showed good miscibility with CB9CB, with the N_{TB} phase persisting to a high wt% of CB9CB in all cases. The resulting relationships between wt% of the compound and the Iso. Liq.-N and N-N_{TB} transition temperatures were extrapolated in a linear fashion to obtain the virtual transitions at 0 wt% CB9CB. The results showed that, in all cases the melting and clearing points showed a dramatic increase upon the insertion of ether linkages into the spacer chain; this was expected, as previous sections have outlined, due to the increased linearity of the molecule. Of particular interest however was the N-N_{TB} phase transition. Due to the necessity of a bent molecular architecture as part of the formation of the N_{TB} phase it would be expected that the increase in linearity would cause a significant destabilisation of the phase when compared to the methylene linked materials, this was not observed however, as the N-N_{TB} transition was broadly unaffected by the change, even rising in the case of some compounds. This indicates that the primary barrier to the ether linked dimers forming the N_{TB} phase is the large increase in the melting point caused by the ether linkage, rather than any destabilisation of the phase itself. This result, combined with the effects shown when increasing the spacer length, as well as reports of the N_{TB} phase occurring in materials with varied spacer structures, both more and less bent, indicates that the relationship between molecular bend and the incidence of the N_{TB} phase is not as simple as more bent equals a more stable phase, but rather may follow a bell curve like relationship, with an ideal angle for phase stability at the peak and the stability falling off at higher or lower values.

The N_{TB} phase has often been said to have a chiral superstructure, in order to investigate the effects of chirality on the N_{TB} phase one of the enantiotropic N_{TB} materials synthesised in this work (**76**) was doped with a chiral dopant. Even from low concentrations of the chiral dopant it was observed that the nematic range of compound **76** dropped to less than 1 °C, the clearing point however remained constant, with the N_{TB} phase being replaced

by a relatively wide temperature BPIII. This result was not unexpected as previously published results have shown that bent-core materials often form blue phases when mixed with a chiral dopant. What was of interest however was the lack of effect the addition of the dopant had on the N-N_{TB} phase transition. Across the entire range of concentrations the N-N_{TB} transition remained almost unchanged. This, combined with the elimination of the nematic and blue phases at 5.5 w% and up resulted in the mixture undergoing a direct I-N_{TB} phase transition, the first observed instance of this phase sequence. Mixtures with higher concentrations of chiral dopant also exhibited a lower temperature mesophase below the N_{TB} phase, with very similar optical texture and XRD pattern, the high degree of supercooling required to reach this phase rendered detailed characterisation difficult, however initial speculation is that this phase is another deformation of the nematic phase, such as the splay-bend nematic. A thermal event was observed in the DSC in between the Iso. Liq. and the succeeding phase observed by POM, this event had no corroborating change in the optical texture or XRD pattern. The lack of any observable superstructure lead to the assignment of this lower temperature state as a second liquid phase; this type of transition is often seen for frustrated systems such as TGB phases. The emergence of this transition could indicate that the addition of chiral dopant, and the resultant elimination of one of the possible twist directions can cause a similar degree of frustration, implying a degree of structural similarity between the N_{TB} and TGB phases. When the materials with high concentrations of chiral dopant (>5.5 wt%) were annealed just above the Iso.-N_{TB} transition temperature a weakly birefringent phase with an optical texture consisting of grey-blue plate like domains was observed to form. These domains appeared similar to those observed in BPII however they were chirally unresponsive, showing that this phase was not a Blue Phase. It is possible that this phase is a deformation of the Blue Phase in the same way that the N_{TB} phase is a deformation of the nematic, and that the liquid-liquid transition observed in the DSC is related to the mechanism of its formation.

The overarching goal of this research was to investigate the structure property relationships across multiple families of liquid crystals of unusual shape. This has been accomplished through the results obtained for both the pseudo-bent core materials and bimesogens. It is well known that true bent core materials have a propensity to form smectic phases and “banana” phases. When a small amount of flexibility is induced through the use of a bisphenol core the mesomorphic behaviour changes dramatically, and also becomes highly dependent on the nature of the linking unit of the bisphenol core.

In the case of these materials the more linear the material the more calamitic-like the phase behaviour becomes, as would be expected, however when the linking units are both bent, and have a degree of flexibility the phase behaviour shifts to be more prone to lamellar phases, as well as exhibiting the DC phase. This behaviour, specifically the occurrence of a possible twist-bend smectic phase, is likely because the increased flexibility allows for the molecules to twist slightly when packing into phases, as opposed to the firmly rigid cores of true bent-core compounds. Taking the flexibility to the extreme, by introducing a long, aliphatic spacer chain causes the phase behaviour to be much more consistent even when changing the nature of said spacer, with all of the bimesogens reported in this work exhibiting nematic and/or N_{TB} phases. This change is due to the conformational freedom of the spacer causing the molecules to be less prone to packing into organised layers such as the lamellar and DC phases observed in the pseudo bent-cores.

References

1. Singh, S. *Liquid Crystals: Fundamentals*. (World Scientific, 2002).
2. Neto, A. M. F. & Salinas, S. R. A. *The Physics of Lyotropic Liquid Crystals: Phase Transitions and Structural Properties*. (Oxford University Press, 2005).
3. Khoo, I. C. *Liquid Crystals: Second Edition*. (John Wiley & Sons, 2007).
4. Popa-Nita, V., Gerlic, I. & Kralj, S. The Influence of Disorder on Thermotropic Nematic Liquid Crystals Phase Behavior. *Int. J. Mol. Sci.* **10**, 3971–4008 (2009).
5. Collings, P. J. & Hird, M. *Introduction to Liquid Crystals*. (Taylor and Francis, 1997).
6. Goertz, V., Southern, C., Roberts, N. W., Gleeson, H. F. & Goodby, J. W. Unusual properties of a bent-core liquid-crystalline fluid. *Soft Matter* **5**, 463–471 (2009).
7. Demus, D. Plenary Lecture - 100 Years of Liquid-Crystal chemistry - Thermotropic Liquid-Crystals with conventional and unconventional molecular structure. *Liq. Cryst.* **5**, 75–110 (1989).
8. Goodby, J. W., Davis, E. J., Mandle, R. J. & Cowling, S. J. Nano-Segregation and Directed Self-Assembly in the Formation of Functional Liquid Crystals. *Isr. J. Chem.* **52**, 863–880 (2012).
9. Cowling, S. J., Davis, E. J., Mandle, R. J. & Goodby, J. W. Defect Textures of Liquid Crystals. in *Progress in Liquid Crystal Science and Technology, in Honor of Shunsuke Kobayashi's 80th Birthday* (eds. Kwok, H.-S., Naemura, S. & Ong, H. L.) 49–79 (World Scientific, 2013).
10. Vorlander, D. & Apel, A. Die Richtung der Kohlenstoff-Valenzen in Benzolabkömmlingen (II.). *Chem. Ber.* **65**, 1101 (1932).
11. Pelzl, G., Wirth, I. & Weissflog, W. The first 'banana phase' found in an original Vorländer substance. *Liq. Cryst.* **28**, 969–972 (2001).
12. Madsen, L. A., Dingemans, T. J., Nakata, M. & Samulski, E. T. Thermotropic Biaxial Nematic Liquid Crystals. *Phys. Rev. Lett.* **92**, 145505 (2004).
13. Acharya, B. R., Primak, A. & Kumar, S. Biaxial Nematic Phase in Bent-Core Thermotropic Mesogens. *Phys. Rev. Lett.* **92**, 145506 (2004).
14. Jang, Y. *et al.* Optical confirmation of biaxial nematic (N-b) phase in a bent-core mesogen. *Appl. Phys. Lett.* **95**, (2009).
15. Ortega, J., Folcia, C. L., Etxebarria, J., Gimeno, N. & Ros, M. B. Interpretation of unusual textures in the B₂ phase of a liquid crystal composed of bent-core molecules. *Phys. Rev. E* **68**, 11707 (2003).

16. Takezoe, H. & Takanishi, Y. Bent-core liquid crystals: Their mysterious and attractive world. *Japanese Journal of Applied Physics, Part 1: Regular Papers and Short Notes and Review Papers* **45**, 597–625 (2006).
17. Haddawi, S., Weissflog, W., Diele, S., Pelzl, G. & Baumeister, U. The binary system composed of a bent-core compound forming a B 7 phase and a nematogenic calamitic compound. *Liq. Cryst.* **37**, 1577–1585 (2010).
18. Chen, D. *et al.* Interface structure of the dark conglomerate liquid crystal phase. *Soft Matter* **7**, 1879 (2011).
19. Gimeno, N., Sánchez-Ferrer, A., Sebastián, N., Mezzenga, R. & Ros, M. B. Bent-core based main-chain polymers showing the dark conglomerate liquid crystal phase. *Macromolecules* **44**, 9586–9594 (2011).
20. Nagaraj, M. *et al.* Understanding the unusual reorganization of the nanostructure of a dark conglomerate phase. *Phys. Rev. E - Stat. Nonlinear, Soft Matter Phys.* **91**, (2015).
21. Niori, T., Sekine, T., Watanabe, J., Furukawa, T. & Takezoe, H. Distinct ferroelectric smectic liquid crystals consisting of banana shaped achiral molecules. *J. Mater. Chem.* **6**, 1231–1233 (1996).
22. Gorecka, E. *et al.* Ferroelectric phases in a chiral bent-core smectic liquid crystal: Dielectric and optical second-harmonic generation measurements. *Phys. Rev. E* **62**, R4524–R4527 (2000).
23. Link, D. R. *et al.* Spontaneous Formation of Macroscopic Chiral Domains in a Fluid Smectic Phase of Achiral Molecules. *Science (80-.)*. **278**, 1924 LP-1927 (1997).
24. Reddy, R. A. *et al.* Spontaneous Ferroelectric Order in a Bent-Core Smectic Liquid Crystal of Fluid Orthorhombic Layers. *Science (80-.)*. **332**, 72 LP-77 (2011).
25. Dantlgraber, G. *et al.* Chirality and Macroscopic Polar Order in a Ferroelectric Smectic Liquid-Crystalline Phase Formed by Achiral Polyphilic Bent-Core Molecules. *Angew. Chemie Int. Ed.* **41**, 2408–2412 (2002).
26. Henderson, P. A. & Imrie, C. T. Methylene-linked liquid crystal dimers and the twist-bend nematic phase. *Liq. Cryst.* **38**, 1407–1414 (2011).
27. Henderson, P. A., Niemeyer, O. & Imrie, C. T. Methylene-linked liquid crystal dimers. *Liq. Cryst.* **28**, 463–472 (2001).
28. Tripathi, C. S. P. *et al.* Nematic-nematic phase transition in the liquid crystal

- dimer CBC9CB and its mixtures with 5CB: A high-resolution adiabatic scanning calorimetric study. *Phys. Rev. E* **84**, (2011).
29. Mandle, R. J. *et al.* Apolar Bimesogens and the Incidence of the Twist-Bend Nematic Phase. *Chem. Eur. J.* **21**, 8158–8167 (2015).
 30. Date, R. W., Imrie, C. T., Luckhurst, G. R. & Seddon, J. M. Smectogenic Dimeric Liquid-Crystals - The preparation and properties of the α,ω -bis(4-normal-alkylanilinebenzylidene-4'-oxy)alkanes. *Liq. Cryst.* **12**, 203–238 (1992).
 31. Imrie, C. T. & Henderson, P. A. Liquid crystal dimers and higher oligomers: Between monomers and polymers. *Chem. Soc. Rev.* **36**, 2096–2124 (2007).
 32. Dozov, I. On the spontaneous symmetry breaking in the mesophases of achiral banana-shaped molecules. *Europhys. Lett.* **56**, 247–253 (2001).
 33. Ferrarini, A., Luckhurst, G. R., Nordio, P. L. & Roskilly, S. J. Understanding the unusual transitional behaviour of Liquid-Crystal Dimers. *Chem. Phys. Lett.* **214**, 409–417 (1993).
 34. Oswald, P. & Pieranski, P. *Nematic and Cholesteric Liquid Crystals*. (Taylor and Francis, 2005).
 35. Goodby, J. W. Chapter V: Symmetry and Chirality in Liquid Crystals. in *Handbook of Liquid Crystals Vol 1: Fundamentals* (eds. Demus, D., Goodby, J. W., Gray, G. W., Spiess, H. W. & Vill, V.) 115–133 (Wiley VCH, 1998).
 36. Goodby, J. W. Chirality in liquid crystals. *J. Mater. Chem.* **1**, 307 (1991).
 37. Dreher, R., Meier, G. & Saupe, A. Selective Reflection by Cholesteric Liquid Crystals. *Mol. Cryst. Liq. Cryst.* **13**, 17–26 (1971).
 38. van der Werff, L. *et al.* Thermochromic composite fibres containing liquid crystals formed via melt extrusion. *J. Mater. Sci.* **48**, 5005–5011 (2013).
 39. Gwag, K. C. H. and J. Y. and J. H. K. and J. S. High contrast reflective liquid crystal display using a thermochromic reflector. *J. Opt.* **17**, 25401 (2015).
 40. Smith, C. R., Sabatino, D. R. & Praisner, T. J. Temperature sensing with thermochromic liquid crystals. *Exp. Fluids* **30**, 190–201 (2001).
 41. Davis, E. J. & Goodby, J. W. Classification of Liquid Crystals According to Symmetry. in *Handbook of Liquid Crystals Volume 1* (eds. Goodby, J. W. *et al.*) 27–58 (Wiley VCH, 2014).
 42. Davis, E. J. & Goodby, J. W. Symmetry and Chirality in Liquid Crystals. in *Handbook of Liquid Crystals Volume 1* (eds. Goodby, J. W. *et al.*) 197–230 (Wiley VCH, 2014).

43. Musgrave, B., Lehmann, P. & Coles, H. J. A new series of chiral nematic bimesogens for the flexoelectro-optic effect. *Liq. Cryst.* **26**, 1235–1249 (1999).
44. Blatch, A. E., Coles, M. J., Musgrave, B. & Coles, H. J. Flexoelectric Liquid Crystal Bimesogens. *Mol. Cryst. Liq. Cryst.* **401**, 47–55 (2003).
45. Clarke, M. J., Blatch, A. E. & Coles, H. J. The effects of introducing ester linking groups on the flexoelectro-optic properties of symmetric bimesogens. *Mol. Cryst. Liq. Cryst.* **434**, 367–375 (2005).
46. Broughton, B. J., Clarke, M. J., Blatch, A. E. & Coles, H. J. Optimized flexoelectric response in a chiral liquid-crystal phase device. *J. Appl. Phys.* **98**, (2005).
47. Coles, H. J., Clarke, M. J., Morris, S. M., Broughton, B. J. & Blatch, A. E. Strong flexoelectric behavior in bimesogenic liquid crystals. *J. Appl. Phys.* **99**, (2006).
48. Ferrarini, A., Greco, C. & Luckhurst, G. R. On the flexoelectric coefficients of liquid crystal monomers and dimers: a computational methodology bridging length-scales. *J. Mater. Chem.* **17**, 1039–1042 (2007).
49. Atkinson, K. L. *et al.* Increasing the flexoelastic ratio of liquid crystals using highly fluorinated ester-linked bimesogens. *Phys. Chem. Chem. Phys.* **14**, 16377–16385 (2012).
50. Cestari, M., Frezza, E., Ferrarini, A. & Luckhurst, G. R. Crucial role of molecular curvature for the bend elastic and flexoelectric properties of liquid crystals: mesogenic dimers as a case study. *J. Mater. Chem.* **21**, 12303–12308 (2011).
51. Coles, H. J. & Pivnenko, M. N. Liquid crystal ‘blue phases’ with a wide temperature range. *Nature* **436**, 997–1000 (2005).
52. Blatch, A. E., Fletcher, I. D. & Luckhurst, G. R. Symmetric and non-symmetric liquid crystal dimers with branched terminal alkyl chains: Racemic and chiral. *J. Mater. Chem.* **7**, 9–17 (1997).
53. Wang, X. & Zhou, Q. *Liquid Crystalline Polymers*. (World Scientific).
54. Heggulustoy, C. M., Montani, R. S., Darda, M. B., Del Rosso, P. G. & Garay, R. O. Bent-shaped liquid crystal dimers. Influence of the direction of the oxybiphenylenecarboxyl groups on their mesomorphic behavior. *Arkivoc* 283–296 (2011).
55. Imrie, C. T. Non-symmetric liquid crystal dimers: How to make molecules intercalate. *Liq. Cryst.* **33**, 1449–1454 (2006).

56. Pandey, M. B., Dhar, R., Achalkumar, A. S. & Yelamaggad, C. V. Characteristic dielectric behaviour of the wide temperature range twist grain boundary phases of unsymmetrical liquid crystal dimers. *J. Physics-Condensed Matter* **19**, (2007).
57. Goodby, J. W. *et al.* A new molecular ordering in helical Liquid-Crystals. *J. Am. Chem. Soc.* **111**, 8119–8125 (1989).
58. Goodby, J. W. Twist grain boundary and frustrated liquid crystal phases. *Curr. Opin. Colloid Interface Sci.* **7**, 326–332 (2002).
59. Meyer, R. B. Structural Problems in Liquid Crystal Physics. in *Les Houches Summer School in Theoretical Physics, 1973. Molecular Fluids* (eds. Balian, R. & Weil, G.) 273–373 (Gordon and Breach, 1976).
60. Čopič, M. Nematic phase of achiral dimers spontaneously bends and twists. *Proc. Natl. Acad. Sci.* **110**, 15855–15856 (2013).
61. Cestari, M. *et al.* Phase behavior and properties of the liquid-crystal dimer 1'',7''-bis(4-cyanobiphenyl-4'-yl) heptane: A twist-bend nematic liquid crystal. *Phys. Rev. E* **84**, 31704 (2011).
62. Panov, V. P. *et al.* Spontaneous Periodic Deformations in Nonchiral Planar-Aligned Bimesogens with a Nematic-Nematic Transition and a Negative Elastic Constant. *Phys. Rev. Lett.* **105**, (2010).
63. Sekine, T. *et al.* Spontaneous helix formation in smectic liquid crystals comprising achiral molecules. *J. Mater. Chem.* **7**, 1307–1309 (1997).
64. Cestari, M. *et al.* Phase behavior and properties of the liquid-crystal dimer 1,7 - bis(4-cyanobiphenyl-4' - yl) heptane: A twist-bend nematic liquid crystal. *Phys. Rev. E* **84**, (2011).
65. Adlem, K. *et al.* Chemically induced twist-bend nematic liquid crystals, liquid crystal dimers, and negative elastic constants. *Phys. Rev. E* **88**, 8 (2013).
66. de Almeida, R. R. R., Zhang, C., Parri, O., Sprunt, S. N. & Jakli, A. Nanostructure and dielectric properties of a twist-bend nematic liquid crystal mixture. *Liq. Cryst.* **41**, 1661–1667 (2014).
67. Paterson, D. A. *et al.* Understanding the twist-bend nematic phase: the characterisation of 1-(4-cyanobiphenyl-4'-yloxy)-6-(4-cyanobiphenyl-4'-yl)hexane (CB6OCB) and comparison with CB7CB. *Soft Matter* **12**, 6827–6840 (2016).
68. Chen, D. *et al.* Chiral heliconical ground state of nanoscale pitch in a nematic liquid crystal of achiral molecular dimers. *Proc. Natl. Acad. Sci. U. S. A.* **110**,

- 15931–15936 (2013).
69. Imrie, C. T., Lu, Z., Picken, S. J. & Yildirim, Z. Oligomeric rod-disc nematic liquid crystals. *Chem. Commun.* 1245–1247 (2007). doi:10.1039/b614922g
 70. Beguin, L. *et al.* The Chirality of a Twist-Bend Nematic Phase Identified by NMR Spectroscopy. *J. Phys. Chem. B* **116**, 7940–7951 (2012).
 71. Zhang, Z. *et al.* Raman scattering studies of order parameters in liquid crystalline dimers exhibiting the nematic and twist-bend nematic phases. *J. Mater. Chem. C* **3**, 10007–10016 (2015).
 72. Hoffmann, A., Vanakaras, A. G., Kohlmeier, A., Mehl, G. H. & Photinos, D. J. On the structure of the N_x phase of symmetric dimers: inferences from NMR. *Soft Matter* **11**, 850–855 (2015).
 73. Vanakaras, A. G. & Photinos, D. J. A Molecular Theory of the Nematic-Nematic Phase Transitions in Mesogenic Dimers. *arXiv:1510.01265v1 [cond-mat.soft]* (2015).
 74. Gorecka, E. *et al.* Do the short helices exist in the nematic TB phase? *Liq. Cryst.* **42**, 1–7 (2015).
 75. Gray, G. W. & J.W., G. *Smectic Liquid Crystals: Textures and Structures.* (1985).
 76. Goodby, J. W. Phase Transitions: General and Fundamental Aspects. in *Handbook of Liquid Crystals Volume 1* (eds. Goodby, J. W. et al.) 59–76 (Wiley VCH, 2014).
 77. Frisch, M. J. *et al.* Gaussian 09, Revision D.01. *Gaussian 09, Revision D.01* (2009).
 78. Mandle, R. J. & Goodby, J. W. Does Topology Dictate the Incidence of the Twist-Bend Phase? Insights Gained from Novel Unsymmetrical Bimesogens. *Chem. – A Eur. J.* **22**, 18456–18464 (2016).
 79. Paterson, D. A., Abberley, J. P., Harrison, W. T., Storey, J. M. & Imrie, C. T. Cyanobiphenyl-based liquid crystal dimers and the twist-bend nematic phase. *Liq. Cryst.* 1–20 (2017). doi:10.1080/02678292.2016.1274293
 80. Chen, D. *et al.* Twist-bend heliconical chiral nematic liquid crystal phase of an achiral rigid bent-core mesogen. *Phys. Rev. E* **89**, (2014).
 81. Emsley, J. W., Lelli, M., Lesage, A. & Luckhurst, G. R. A Comparison of the Conformational Distributions of the Achiral Symmetric Liquid Crystal Dimer CB7CB in the Achiral Nematic and Chiral Twist-Bend Nematic Phases. *J. Phys.*

- Chem. B* **117**, 6547–6557 (2013).
82. Mandle, R. J., Archbold, C. T., Sarju, J. P., Andrews, J. L. & Goodby, J. W. The Dependency of Nematic and Twist-bend Mesophase Formation on Bend Angle. *Chem. Commun.* **6**, 36682 (2016).
 83. Greco, C., Luckhurst, G. R. & Ferrarini, A. Enantiotopic discrimination and director organization in the twist-bend nematic phase. *Phys. Chem. Chem. Phys.* **15**, 14961–5 (2013).
 84. Sebastian, N. *et al.* Dielectric, calorimetric and mesophase properties of 1''-(2',4-difluorobiphenyl-4'-yloxy)-9''-(4-cyanobiphenyl-4'-yloxy) nonane: an odd liquid crystal dimer with a monotropic mesophase having the characteristics of a twist-bend nematic phase. *Phys. Chem. Chem. Phys.* **16**, 21391–21406 (2014).
 85. Lopez, D. O. *et al.* Miscibility studies of two twist-bend nematic liquid crystal dimers with different average molecular curvatures. A comparison between experimental data and predictions of a Landau mean-field theory for the NTB-N phase transition. *Phys. Chem. Chem. Phys.* **18**, 4394–4404 (2016).
 86. Mandle, R. J. *et al.* Synthesis and characterisation of an unsymmetrical, ether-linked, fluorinated bimesogen exhibiting a new polymorphism containing the N-TB or 'twist-bend' phase. *Phys. Chem. Chem. Phys.* **16**, 6907–6915 (2014).
 87. Mandle, R. J., Voll, C. C. A., Lewis, D. J. & Goodby, J. W. Etheric bimesogens and the twist-bend nematic phase. *Liq. Cryst.* **43**, 13–21 (2016).
 88. Dunmur, D. A., Luckhurst, G. R., De La Fuente, M. R., Diez, S. & Pérez Jubindo, M. A. Dielectric relaxation in liquid crystalline dimers. *J. Chem. Phys.* **115**, 8681–8691 (2001).
 89. Hiremath, U. S. Synthesis and characterization of novel chiral dimers exhibiting highly frustrated liquid crystal phases. *Tetrahedron* **70**, 4745–4753 (2014).
 90. Goodby, J. W. *et al.* Liquid-crystalline Abrikosov flux phase with an antiferroelectric structure. *Chem. Commun.* 1149–1150 (2000).
doi:10.1039/B002941F
 91. Taborek, P., Goodby, J. W. & Cladis, P. E. Heat capacity peaks observed at the blue phase transitions in compounds of different purities. *Liq. Cryst.* **4**, 21–37 (1989).
 92. Finkelmann, H. & Rehage, G. Liquid Crystal Side Chain Polymers. *Adv. Polym. Sci.* **60/61**, 99–172 (1984).
 93. Finkelmann, H. & Wendorff, H. J. Structure of Nematic Side Chain Polymers. in

Polymeric Liquid Crystals (ed. Blumstein, A.) 295 (Plenum Press, 1985).

Glossary

Techniques

NMR	Nuclear Magnetic Resonance
ESI-MS	Electrospray Ionisation Mass Spectrometry
APCI-MS	Atmospheric Pressure Chemical Ionisation Mass Spectrometry
IR	Infra-Red
HPLC	High Performance Liquid Chromatography
TLC	Thin Layer Chromatography
POM	Polarised Optical Microscopy
DSC	Differential Scanning Calorimetry
SAXS	Small Angle X-ray Scattering
XRD	X-Ray Diffraction
NOESY	Nuclear Overhauser Effect Spectroscopy

NMR

s	Singlet
d	Doublet
t	Triplet
q	Quartet
quint	Quintet
sex	Sextet
m	Multiplet
δ	Chemical shift
ArH	Aromatic proton
CyHexH	Cyclohexyl proton

Chemical abbreviations

DCM	Dichloromethane
DMAP	Dimethylaminopyridine
EDAC	1-ethyl-3-(3-dimethylaminopropyl)carbodiimide
C(CH₂)₂	2,2-disubstituted propyl
C(C₅H₁₀)	1,1-disubstituted cyclohexane
MeCN	Acetonitrile
THF	Tetrahydrofuran
CDCl₃	Deuterated Chloroform
CB	Cyanobiphenyl
Units	
ppm	Parts per million
Hz	Hertz
g	Grams
mol	Moles
l	litres
wt%	Weight percent
°C	Degrees Celsius
m/z	Mass: charge ratio
J	Joules
Å	Ångströms (10 ⁻¹⁰ m)
V	volts

Liquid Crystals

I	Isotropic Liquid
Iso.	Isotropic
N	Nematic
N_{TB}	Twist-bend Nematic
SmA	Smectic A
SmC	Smectic C
Cryst.	Crystal
Hex.	Hexatic
TGB	Twist-grain Boundary
BP (I-III)	Blue Phase (I-III)
M.p.	Melting point

SI Prefixes

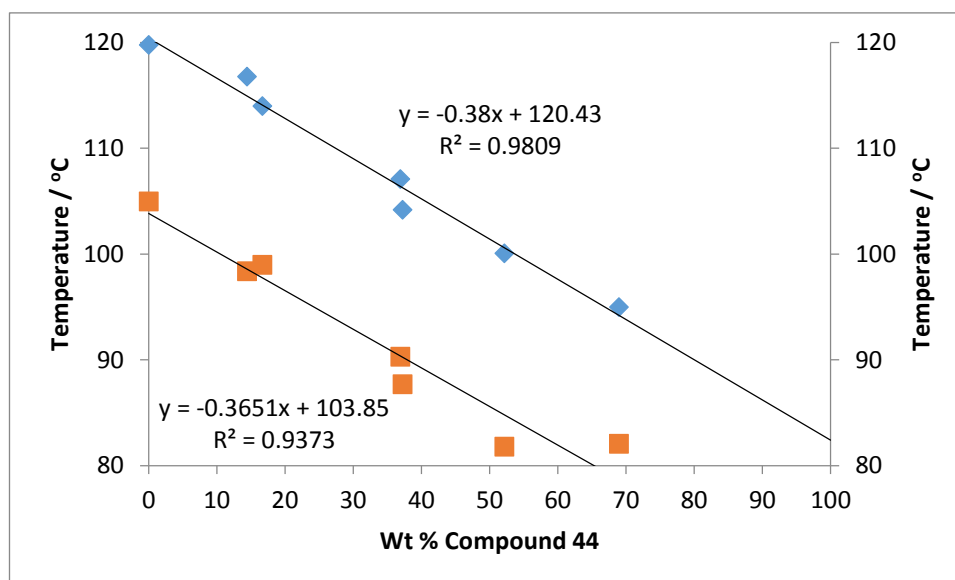
M	Mega (10^6)
k	Kilo (10^3)
c	Centi (10^{-2})
m	Milli (10^{-3})
μ	Micro (10^{-6})
n	Nano (10^{-9})
p	Pico (10^{-12})

Appendices

Appendix 1: Binary phase diagrams of compounds 44-65 with CB9CB

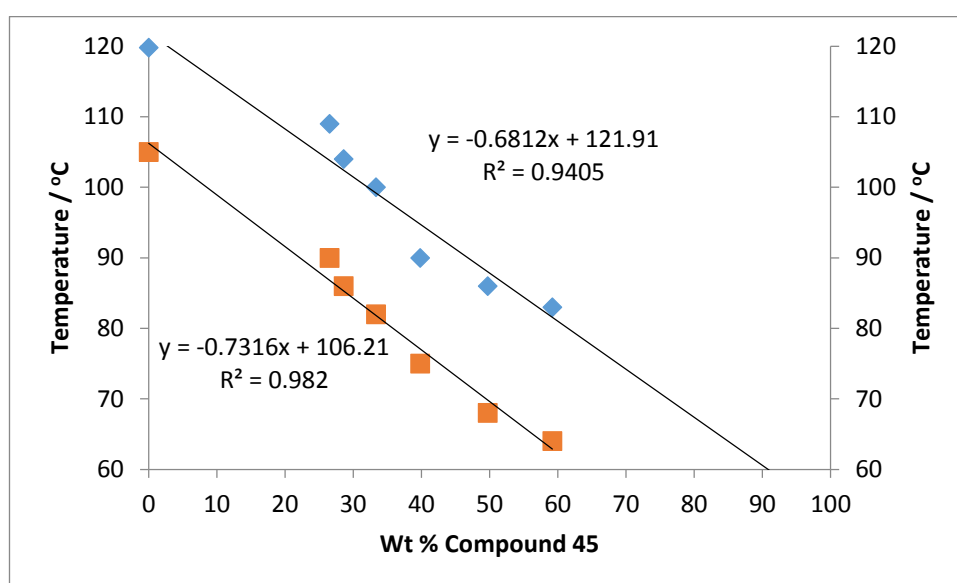
Compound 44

Mass (44) / mg	Mass CB9CB / mg	Total Mass / mg	Wt% (55)	I-N	N- N _{TB}
2.7	16	18.7	14	116.8	98.4
2.0	10	12	17	114.0	99
4.5	7.7	12.2	37	107.1	90.3
6.4	10.8	17.2	37	104.2	87.7
3.6	3.3	6.9	69	100.1	81.8
8	3.6	11.6	83	95	82.1



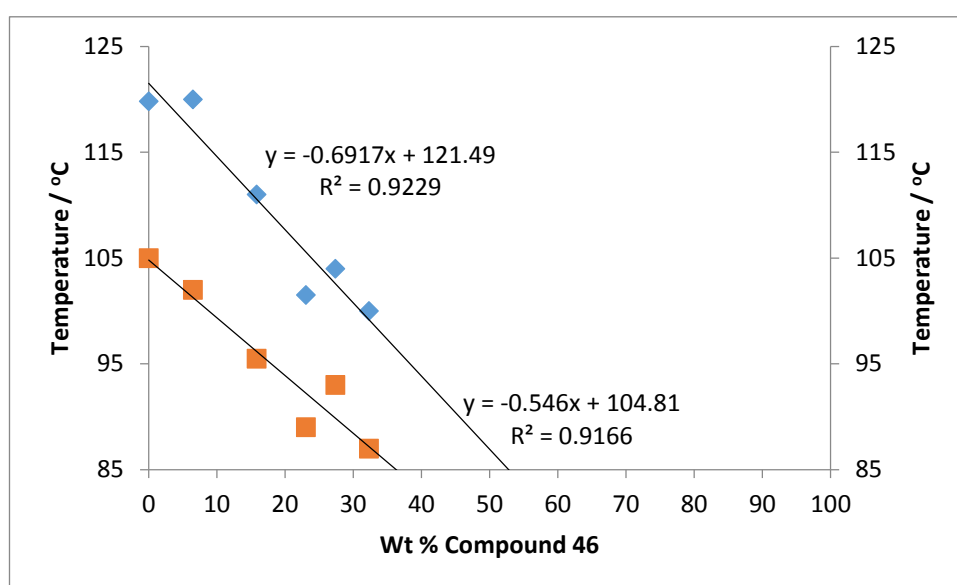
Compound 45

Mass (45) / mg	Mass CB9CB / mg	Total Mass / mg	Wt% (56)	I-N	N- NTB
3.9	10.8	14.7	27	109	90
3.8	9.5	13.3	29	104	86
3.8	7.6	11.4	33	100	82
4.1	6.2	10.3	40	90	75
8.6	8.7	17.3	50	86	68
7.4	5.1	12.5	59	83	64



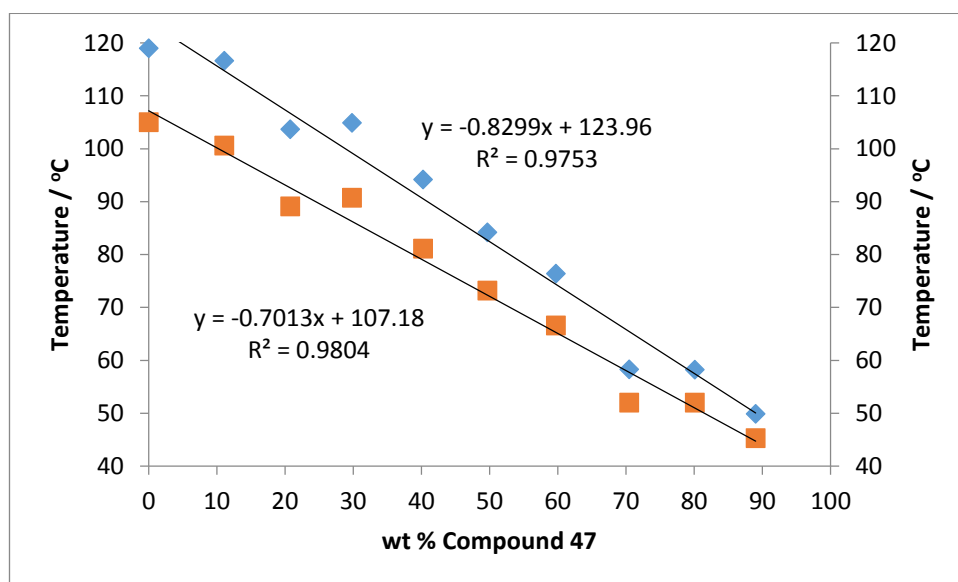
Compound 46

Mass (46) / mg	Mass CB9CB / mg	Total Mass / mg	Wt% (573)	I-N	N- N _{TB}
1.7	24.5	26.2	6	120	102
1.6	8.5	10.1	16	111	95.5
3.3	11	14.3	23	101.5	89
3.2	8.5	11.7	27	104	93
7.3	15.3	22.6	32	100	87



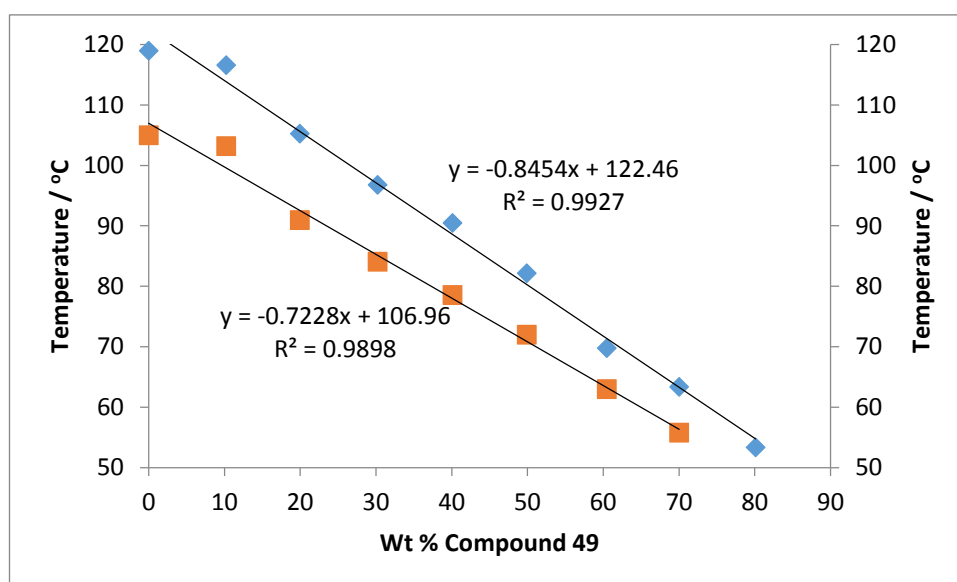
Compound 47

Mass (47) / mg	Mass CB9CB / mg	Total Mass / mg	Wt% (58)	I-N	N- NTB
1.15	9.21	10.36	11.10	116.6	100.6
2.09	7.97	10.06	20.78	103.7	89.1
3	7.06	10.06	29.82	104.9	90.7
4.07	6.05	10.12	40.22	94.2	81.1
5.06	5.13	10.19	49.66	84.2	73.2
6.09	4.11	10.2	59.71	76.4	66.6
7.04	2.95	9.99	70.47	58.3	52.0
8.16	2.03	10.19	80.08	58.2	52.0
9.01	1.11	10.12	89.03	49.9	45.3



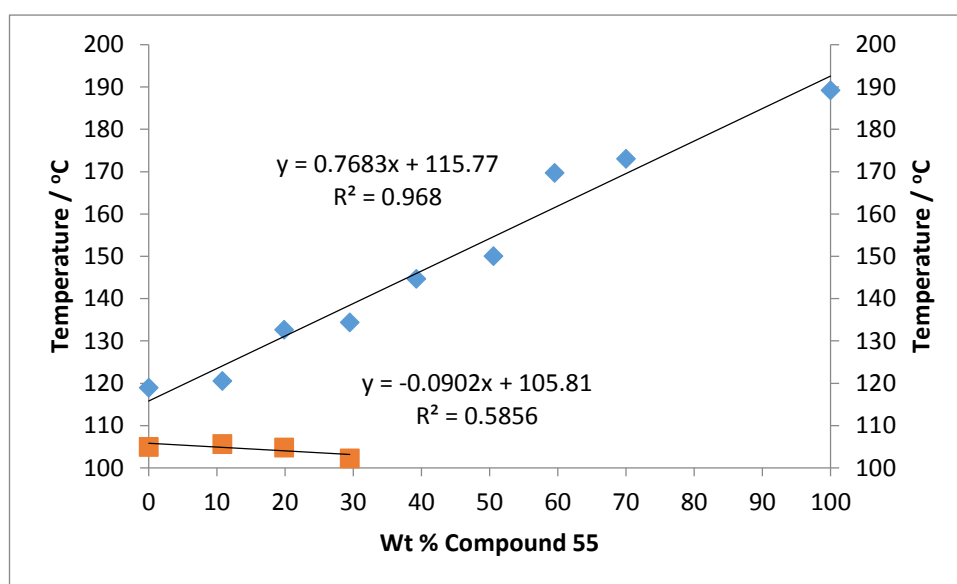
Compound 49

Mass (49) / mg	Mass CB9CB / mg	Total Mass / mg	Wt% (60)	I-N	N- N _{TB}
1.03	9.02	10.05	10.25	116.6	103.2
2.01	8.07	10.08	19.94	105.3	91
3.08	7.12	10.2	30.20	96.8	84.1
4.1	6.12	10.22	40.12	90.5	78.6
4.99	5.01	10	49.90	82.2	72
6.13	4.01	10.14	60.45	69.8	63
7.05	3.02	10.07	70.01	63.4	55.8
8.17	2.03	10.2	80.10	53.4	-



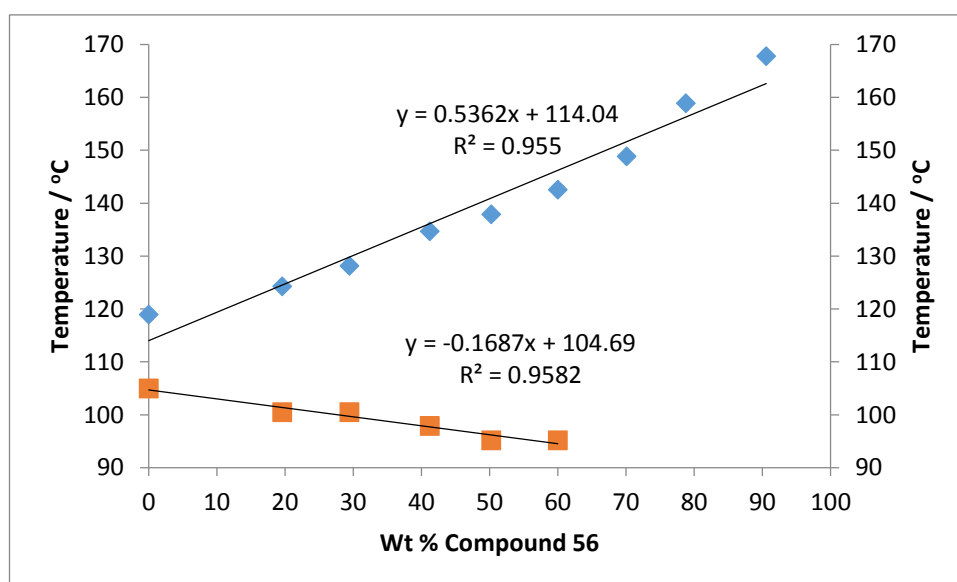
Compound 55

Mass (55) / mg	Mass CB9CB / mg	Total Mass / mg	Wt% (66)	I-N	N- N _{TB}
1.09	8.98	10.07	10.82	120.6	105.7
2	8.07	10.07	19.86	132.7	104.8
2.97	7.1	10.07	29.49	134.4	102.3
3.97	6.14	10.11	39.27	144.7	-
5.03	4.92	9.95	50.55	150.1	-
6.03	4.1	10.13	59.53	169.7	-
7.02	3.01	10.03	69.99	173.1	-



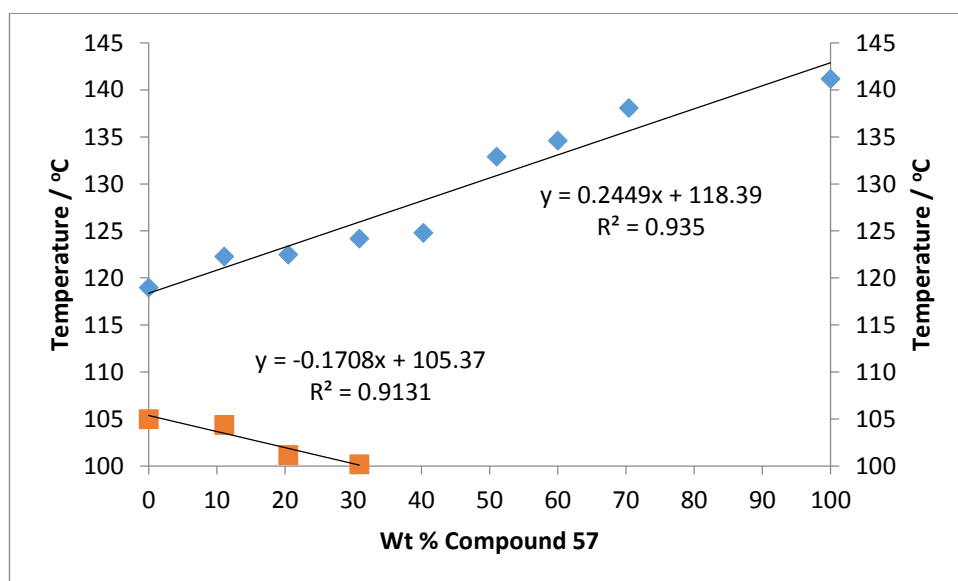
Compound 56

Mass (56) / mg	Mass CB9CB / mg	Total Mass / mg	Wt% (67)	I-N	N- N _{TB}
1.96	8.05	10.01	19.58	124.3	100.5
2.91	6.97	9.88	29.45	128.2	100.5
4.19	5.97	10.16	41.24	134.7	97.9
5.13	5.08	10.21	50.24	137.9	95.2
6.14	4.09	10.23	60.02	142.6	95.2
7.15	3.05	10.20	70.10	148.9	-
7.95	2.14	10.09	78.79	158.9	-
9.1	0.95	10.05	90.55	167.8	-



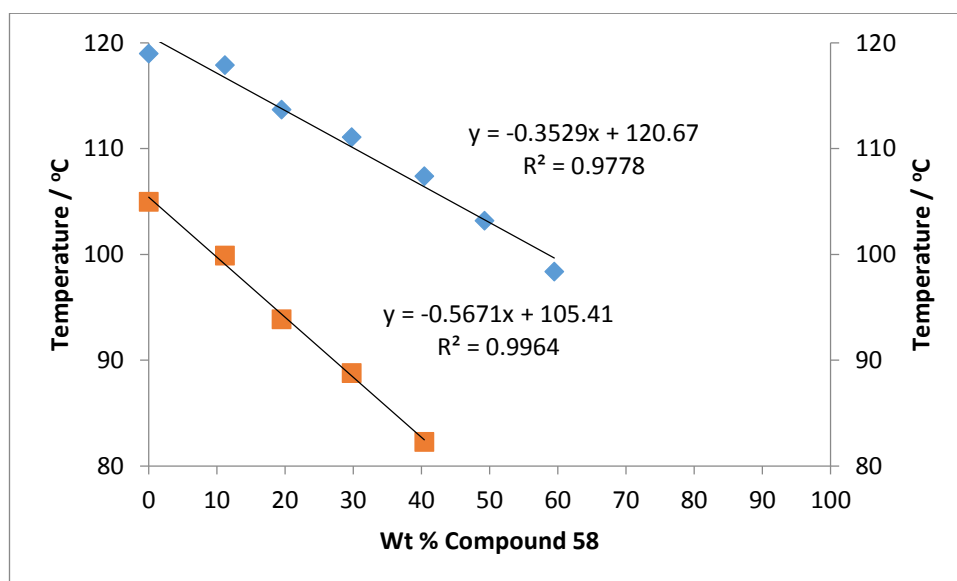
Compound 57

Mass (57) / mg	Mass CB9CB / mg	Total Mass / mg	Wt% (68)	I-N	N- N _{TB}
1.12	8.99	10.11	11.08	122.3	104.4
2.1	8.15	10.25	20.49	122.5	101.2
3.1	6.93	10.03	30.91	124.2	100.2
4.05	6.00	10.05	40.30	124.8	-
5.17	4.96	10.13	51.04	132.9	-
6.11	4.07	10.18	60.02	134.6	-



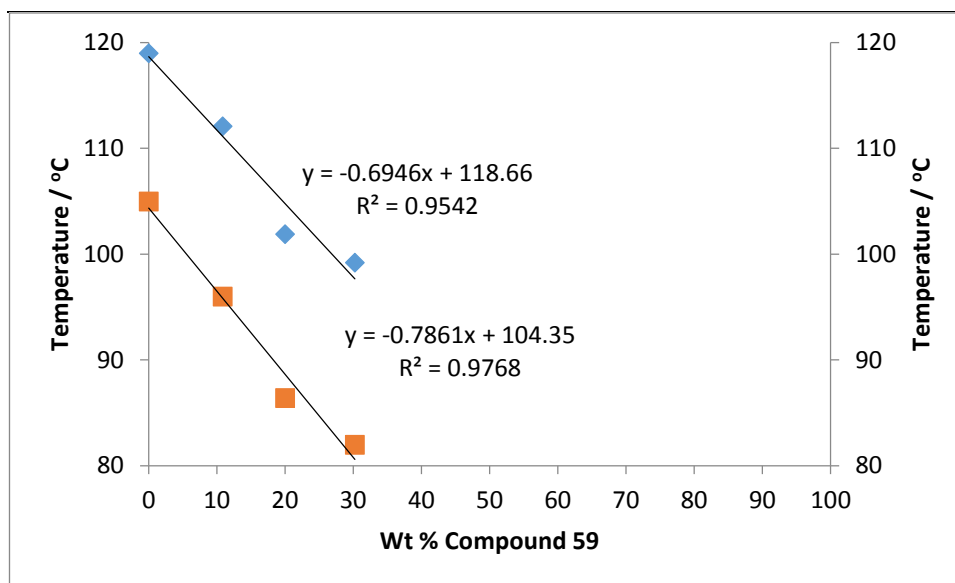
Compound 58

Mass (58) / mg	Mass CB9CB / mg	Total Mass / mg	Wt% (69)	I-N	N- N _{TB}
1.14	9.08	10.22	11.15	117.9	99.9
1.98	8.19	10.17	19.47	113.7	93.9
2.98	7.03	10.01	29.77	111.1	88.8
4.05	5.97	10.02	40.42	107.4	82.3
4.95	5.10	10.05	49.25	103.2	-
6.02	4.10	10.12	59.49	98.4	-



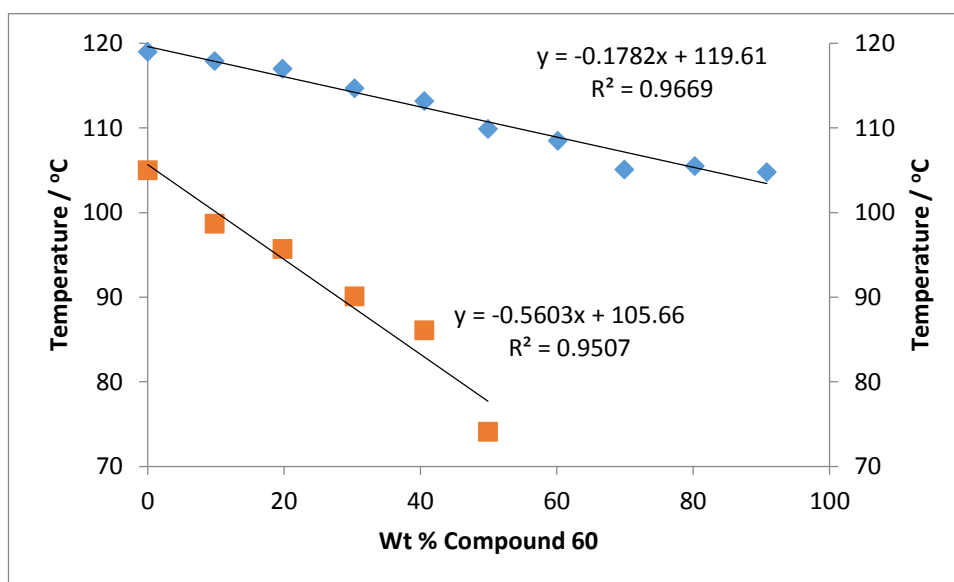
Compound 59

Mass (59) / mg	Mass CB9CB / mg	Total Mass / mg	Wt% (70)	I-N	N- N _{TB}
1.1	9.06	10.16	10.82677	112.1	96
2.03	8.11	10.14	20.01972	101.9	86.4
3.02	6.97	9.99	30.23023	99.2	82



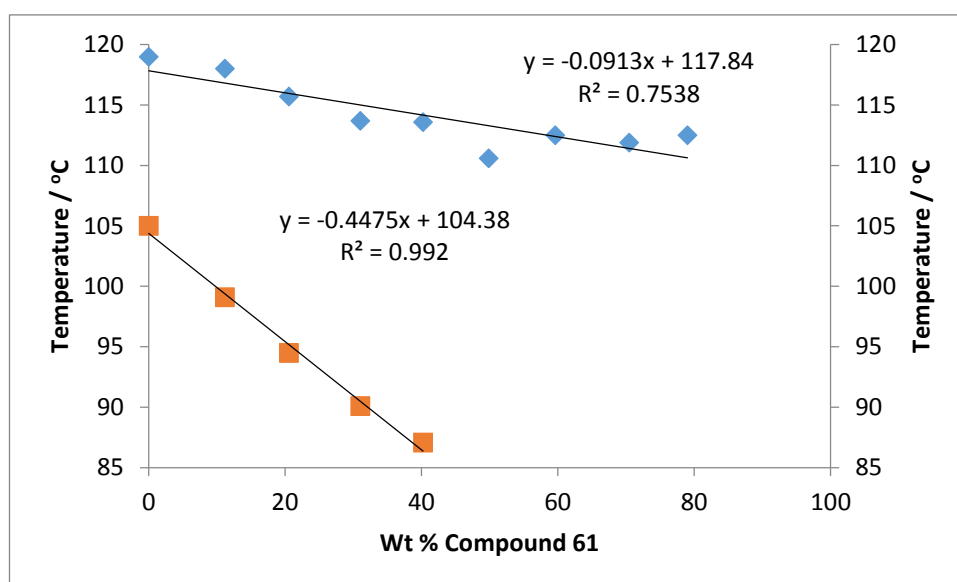
Compound 60

Mass (60) / mg	Mass CB9CB / mg	Total Mass / mg	Wt% (71)	I-N	N- N _{TB}
0.99	9.08	10.07	9.8311817	117.9	98.7
2.01	8.15	10.16	19.783465	117	95.7
3.11	7.14	10.25	30.341463	114.7	90.1
4.15	6.08	10.23	40.56696	113.2	86.1
5.03	5.05	10.08	49.900794	109.9	74.1
6.07	4.02	10.09	60.158573	108.5	-
7.17	3.09	10.26	69.883041	105.1	-
8.08	1.99	10.07	80.238332	105.5	-
9.05	0.92	9.97	90.772317	104.8	-



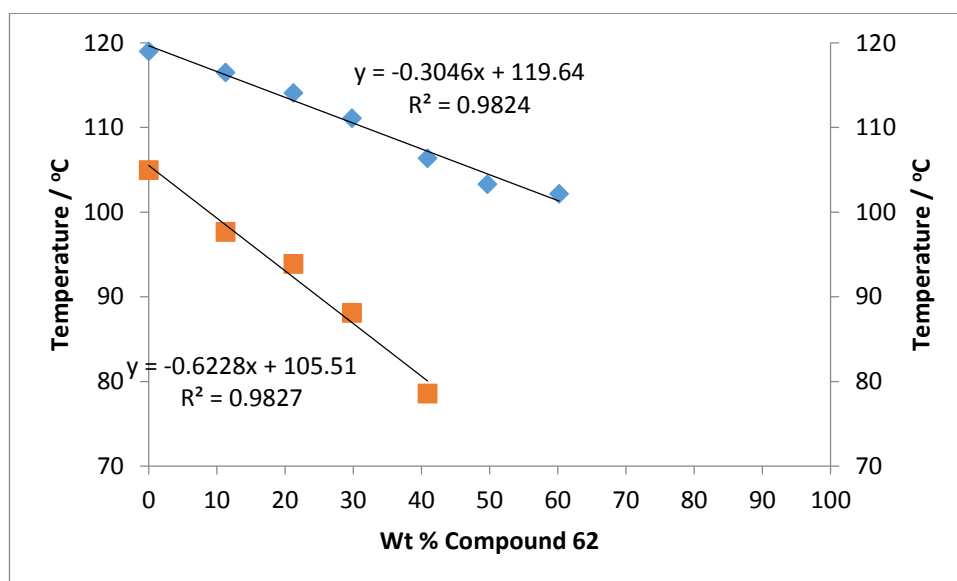
Compound 61

Mass (61) / mg	Mass CB9CB / mg	Total Mass / mg	Wt% (72)	I-N	N- N _{TB}
1.13	8.96	10.09	11.20	118	99.1
2.07	8.00	10.07	20.56	115.7	94.5
3.16	7.03	10.19	31.01	113.7	90.1
4.19	6.22	10.41	40.25	113.6	87.1
4.96	4.99	9.95	49.85	110.6	-
5.98	4.05	10.03	59.62	112.5	-
7.07	2.96	10.03	70.49	111.9	-
8.14	2.16	10.30	79.03	112.5	-



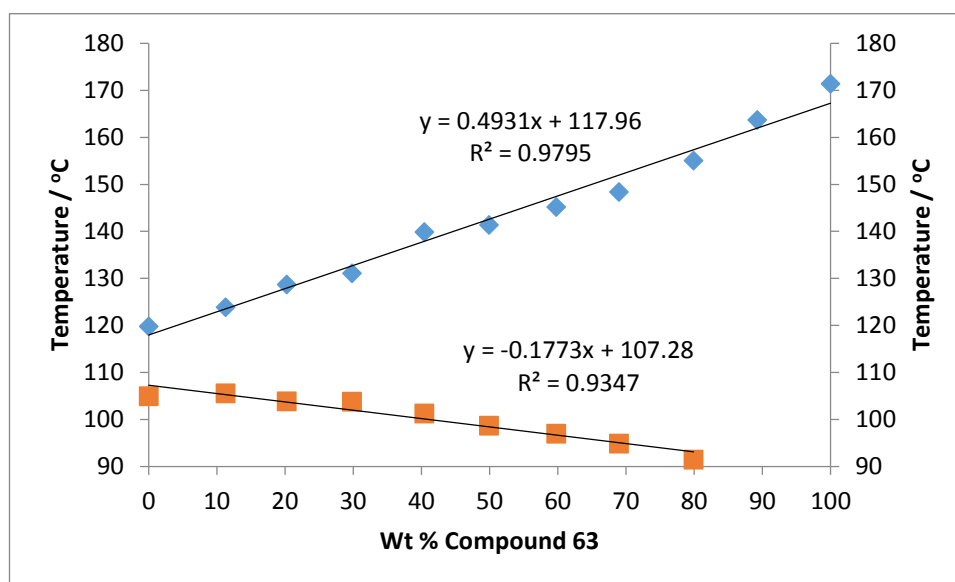
Compound 62

Mass (62) / mg	Mass CB9CB / mg	Total Mass / mg	Wt% (73)	I-N	N- N _{TB}
1.15	9.04	10.19	11.29	116.5	97.7
2.19	8.13	10.32	21.22	114.1	93.9
3.02	7.11	10.13	29.81	111.1	88.1
4.19	6.06	10.25	40.88	106.4	78.6
4.97	5.04	10.01	49.65	103.3	
6.17	4.08	10.25	60.20	102.2	



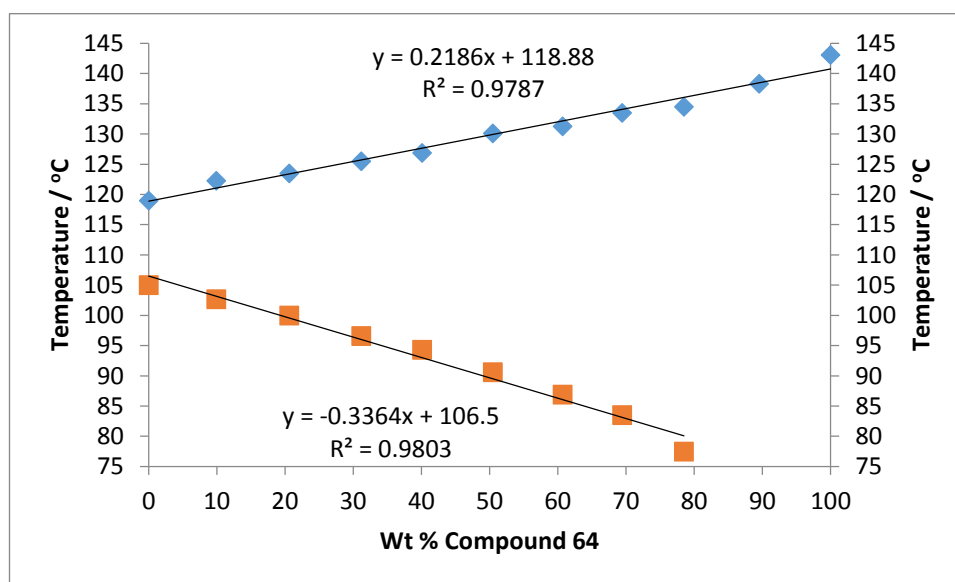
Compound 63

Mass (63) / mg	Mass CB9CB / mg	Total Mass / mg	Wt% (74)	I-N	N- N _{TB}
1	1.15	9.06	10.21	11.26	123.9
2	2.04	8.04	10.08	20.24	128.7
3	2.96	6.97	9.93	29.81	131.1
4	4.1	6.04	10.14	40.43	139.9
5	5.07	5.09	10.16	49.90	141.4
6	5.99	4.03	10.02	59.78	145.2
7	7	3.15	10.15	68.97	148.4
8	8.03	2.02	10.05	79.90	155.1
9	9.05	1.09	10.14	89.25	163.7



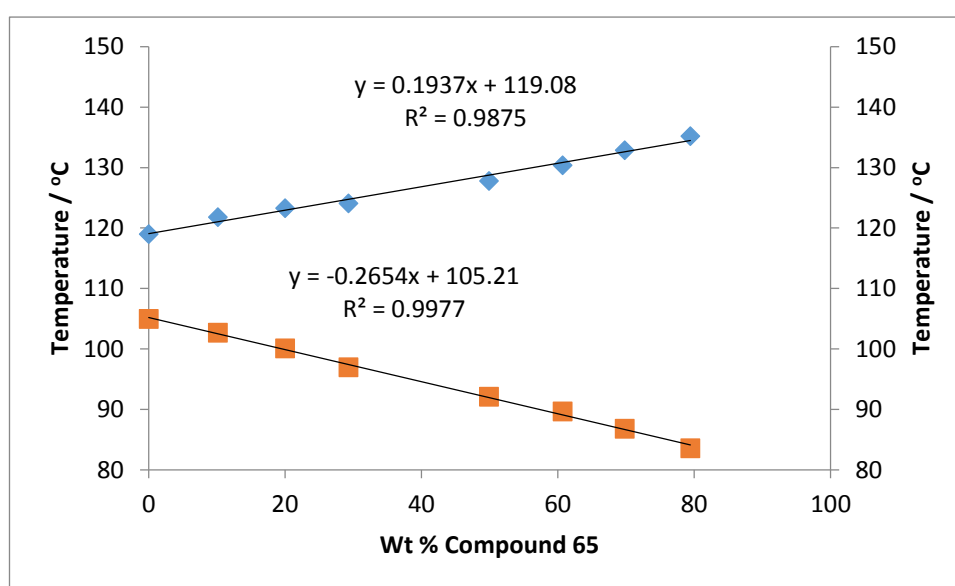
Compound 64

Mass (64) / mg	Mass CB9CB / mg	Total Mass / mg	Wt% (75)	I-N	N- N _{TB}
1.00	9.10	10.10	9.90	122.3	102.7
2.12	8.16	10.28	20.62	123.5	100
3.16	6.98	10.14	31.16	125.5	96.6
4.03	6.02	10.05	40.10	126.9	94.3
5.02	4.93	9.95	50.45	130.1	90.6
6.09	3.94	10.03	60.72	131.3	86.9
7.02	3.09	10.11	69.44	133.5	83.5
8.11	2.22	10.33	78.51	134.5	77.5
9.04	1.06	10.10	89.50	138.3	-



Compound 65

Mass (65) / mg	Mass CB9CB / mg	Total Mass / mg	Wt% (76)	I-N	N- N _{TB}
1.02	9.04	10.06	10.14	121.8	102.7
2.01	8.05	10.06	19.98	123.3	100.1
2.89	6.98	9.87	29.28	124.1	97.0
5.16	5.18	10.34	49.90	127.8	92.1
6.13	3.97	10.10	60.69	130.4	89.7
7.07	3.06	10.13	69.79	132.9	86.8
8.19	2.12	10.31	79.44	135.2	83.6



Appendix 2: Transitional behaviour of mixtures of compound 76 with CD-1 as presented in Figure 73

Mixture	Transition Temperatures / °C											
	Cr	“X”		N _{TB}	N*		BPIII		Iso.		I	
M1	• 80.9	-	-	• 82.2	• 83.4	• 95.3	• 98.6	•				•
M2	• 80.5	-	-	• 82.4	• 82.5	• 95.3	• 98.4	•				•
M3	• 79.5	-	-	• 82.1	• 82.3	• 96.1	• 98.1	•				•
M4	• 79.5	• 62.1		• 83.5	• 83.6	• 92.7	• 97.3	•				•
M5	• 79.5	• 66.1		• 83.3	• 83.4	• 88.6	• 96.6	•				•
M6	• 79.4	• 67.2		• 83.2	-	-	• 96.8	•				•
M7	• 79.3	• 66.4		• 83.4	-	-	• 96.4	•				•
M8	• 79.4	• 67.2		• 82.3	-	-	• 96.4	•				•
M9	• 79.1	• 68.3		• 81.9	-	-	• 95.3	•				•
M10	• 79.2	• 69.9		• 79.2	-	-	• 96.5	•				•